NASA Contractor Report 174776

ERROR REDUCTION PROGRAM

Final Report

Saadat A. Syed
Louis M. Chiappetta
A.D. Gosman

Contract NAS3-23686

January 11, 1985

NASA

1. Report No.	2. Government Accession No.	3. Recipient's Catalog No.
CR-174776		

4. Title and Subtitle	5. Report Date
Error Reduction Program - Final Report	April, 1985
	6. Performing Organization Code

7. Author(s)	8. Performing Organization Report No.
Saadat A. Syed, Louis M. Chiappetta and A. D. Gosman	PWA-5928-25
	10. Work Unit No.

9. Performing Organization Name and Address	11. Contract or Grant No.
United Technologies Corporation Pratt & Whitney, Engineering Division East Hartford, CT 06108	NAS3 - 23686
	13. Type of Report and Period Covered
12. Sponsoring Agency Name and Address	Final Report
National Aeronautics and Space Administration Lewis Research Center 21000 Brookpark Road, Cleveland, Ohio 44135	14. Sponsoring Agency Code

15. Supplementary Notes

NASA Program Manager: Russell W. Claus

16. Abstract

This report describes the details of a study, sponsored by the National Aeronautics and Space Administration to select, incorporate and evaluate the best available finite difference scheme to reduce numerical error in combustor performance evaluation codes.

The combustor performance computer programs chosen for this study were the two dimensional and three dimensional versions of Pratt & Whitney's TEACH code.

The criteria used to select schemes required that the difference equations mirror the properties of the governing differential equation, be more accurate than the current hybrid difference scheme, be stable and economical, be compatible with TEACH codes, use only modest amounts of additional storage, and be relatively simple.

The methods of assessment used in the selection process consisted of examination of the difference equation, evaluation of the properties of the coefficient matrix, Taylor series analysis, and performance on model problems. Five schemes from the literature and three schemes developed during the course of this study were evaluated.

This effort resulted in the incorporation of a scheme in 3D-TEACH which is usually more accurate than the hybrid differencing method and never less accurate.

17. Key Words (Suggested by Author(s))	18. Distribution Statement
Error Reduction, Numerical Error, Numerical Diffusion, Artificial Diffusion, Differencing Schemes, 3D Viscous Flow	

19. Security Classif. (of this report)	20. Security Classif. (of this page)	21. No. of pages	22. Price*
Unclassified	Unclassified		

FOREWORD

This document was prepared by the Engineering Division of the Pratt and Whitney Group of United Technologies Corporation, East Hartford, Connecticut, to describe the selection, incorporation, and evaluation of the best available finite difference scheme to reduce numerical error in the Combustor Performance evaluation codes. This task was accomplished under the National Aeronautics and Space Administration (NASA) sponsored Error Reduction Program, Contract NAS3-23686. The work was performed under the direction of NASA Project Manager, Mr. Russell W. Claus.

This report has been assigned the Contractor's report number PWA-5928-25.

TABLE OF CONTENTS

SECTION			PAGE
1.0	SUMMARY		1
2.0	INTRODUCTION		2
	2.1	OBJECTIVES	2
	2.2	APPROACH	3
	2.3	ORGANIZATION	3
3.0	BACKGROUND		4
	3.1	SOURCES OF ERROR IN PRESENT DESIGN CODES	4
		3.1.1 Assembly of Equations	4
		3.1.2 Physical Modeling	5
		3.1.3 Computer Solution	8
		3.1.4 Representation of Geometry	9
		3.1.5 Solution Algorithm	11
	3.2	UTILITY OF PRESENT DESIGN CODES	12
	3.3	REASONS FOR CONCENTRATING ON THE DIFFERENCING SCHEME FOR ACCURACY IMPROVEMENT	12
4.0	SELECTION OF MORE ACCURATE FINITE-DIFFERENCE SCHEMES		13
	4.1	CRITERIA OF ASSESSMENT	13
		4.1.1 Mirror Differential Equation Properties	13
		4.1.2 Accuracy	18
		4.1.3 Stability	19
		4.1.4 Economy	19
		4.1.5 Variable Storage Requirements	19
		4.1.6 Compatibility With Present Codes	16
		4.1.7 Complexity	20

TABLE OF CONTENTS (Continued)

SECTION		PAGE
4.2	METHOD OF ASSESSMENT	20
	4.2.1 Limitations of Method of Assessment	20
4.3	DESCRIPTION AND PRELIMINARY SCREENING OF CANDIDATE SCHEMES	21
	4.3.1 Central Difference Scheme (CDS)	21
	4.3.2 Upwind Difference Scheme (UDS)	22
	4.3.3 Agarwal Differencing Scheme (ADS)	23
	4.3.4 Quadratic Upwind Differencing Scheme (QUDS)	25
	4.3.5 Skew Upwind Differencing Scheme (SUDS)	26
	4.3.6 Cubic Spline Scheme (CSS)	28
	4.3.7 Glass and Rodi Hermitian Scheme (GRHS)	30
	4.3.8 Schemes Generated by Flux Blending	31
4.4	ACCURACY EVALUATION	36
	4.4.1 Truncation Error Analysis	36
	4.4.2 Description of Test Cases for Accuracy Assessment	40
	4.4.3 Results of Test Cases	45
4.5	STABILITY	54
4.6	COST EFFECTIVENESS	55
	4.6.1 Computing Times	55
	4.6.2 Computer Storage	57
4.7	COMPLEXITY AND COMPATIBILITY WITH EXISTING TEACH METHODOLOGY	58
4.8	PROGNOSTICATIONS FOR THREE DIMENSIONAL CALCULATIONS AND OTHER CONSIDERATIONS	58
4.9	CONCLUSIONS	59
4.10	SELECTION OF TWO DIFFERENCING SCHEMES	60

TABLE OF CONTENTS (Continued)

SECTION		PAGE
5.0	DERIVATION OF SELECTED SCHEMES FOR TEACH	61
5.1	THE BOUNDED SKEW-UPWIND DIFFERENCING SCHEME	61
5.1.1	Flux Form of the Equations of Motion	61
5.1.2	Calculation of the Fluxes	65
5.1.3	Calculation of the Coefficients for the Finite-Difference Form of the Equations of Motion	76
5.1.4	Boundary Conditions	77
5.1.5	The Bounding Scheme	87
5.2	THE QUDS DIFFERENCING SCHEME	91
5.2.1	Flux Form of the Equations of Motion	91
5.2.2	Calculation of the Fluxes	92
5.2.3	Calculation of the Coefficients for the Finite-Difference Form of the Equations of Motion	93
5.2.4	Boundary Conditions	94
5.3	COST OF QUDS AND BSUDS2	97
6.0	DISCUSSION OF TEST CASES	99
6.1	TWO-DIMENSIONAL LAMINAR FLOW TEST CASES	100
6.1.1	Flow Downstream of Rearward Facing Step	100
6.1.2	Swirling Flow Downstream of a Sudden Expansion	103
6.2	TWO-DIMENSIONAL TURBULENT FLOW TEST CASES	107
6.2.1	Turbulent Flow Downstream of a Rearward Facing Step	107
6.2.2	Coannular Nonswirling Turbulent Flow	111
6.2.3	Coannular Swirling Turbulent Flow	119

TABLE OF CONTENTS (Continued)

SECTION		PAGE
6.3	SUMMARY of 2D-TEST CASES	129
6.4	SELECTION OF DIFFERENCING SCHEME FOR 3D-TEACH	129
6.5	THREE-DIMENSIONAL TURBULENT FLOW TEST CASE	129
6.6	SUMMARY OF 3D-TEST CASE	148
6.7	SUMMARY OF TEST CASES	148
7.0	CONCLUDING REMARKS	150
8.0	RECOMMENDATIONS	152
APPENDIX A		158
APPENDIX B		217
Distribution List		243

1.0 SUMMARY

The National Aeronautics and Space Administration sponsored a program to select, incorporate and evaluate the best available finite difference scheme to reduce numerical error in combustor performance evaluation codes. This report describes the details of this study.

The combustor performance computer programs chosen for this study were the two dimensional and three dimensional versions of Pratt and Whitney's TEACH code.

The criteria used to select schemes required that the difference equations mirror the properties of the governing differential equation, be more accurate than the current hybrid difference scheme, be stable and economical, be compatible with TEACH codes, use only modest amounts of additional storage, and be relatively simple.

The methods of assessment used in the selection process consisted of examination of the difference equation, evaluation of the properties of the the coefficient matrix, Taylor series analysis, and performance on model problems. Five schemes from the literature and three schemes developed during the course of this study were evaluated. This initial evaluation resulted in the selection of the two most promising schemes, Quadratic Upwind Differencing Scheme (QUDS) and Bounded Skew Upwind Differencing Scheme Two (BSUDS2), for incorporation into 2D-TEACH for further evaluation. The accuracy and stability of these schemes were assessed by using laminar and turbulent flow test cases. These test cases, although two dimensional, contain important flow features found in gas turbine combustors. During the evaluation, it was found that QUDS was unstable and, hence, BSUDS2 was selected for incorporation into 3D-TEACH. This scheme was further evaluated by using a 3D-test case, modeling of a jet in cross flow.

This effort resulted in the incorporation of a scheme in 3D-TEACH which is usually more accurate than the hybrid differencing method and never less accurate. It is expected that overall improvement in accuracy resulting for complex flows will justify the increased cost of using this scheme. However, this study can only be considered as a first step in the process of developing the most suitable scheme for combustor performance codes. A number of questions have been generated as a result of this work and it is expected that answers to these questions will lead to further improvements in the accuracy and stability of the BSUDS2 scheme.

2.0 INTRODUCTION

2.1 OBJECTIVES

The main objective of the NASA-sponsored Error Reduction Program was to select, incorporate and evaluate the best available technique for the reduction of numerical diffusion in a 3D combustor performance evaluation code. The study focused on improvements in accuracy of computer programs of the TEACH (for Teaching Elliptic Axisymmetric Characteristics Heuristically) variety which were developed originally by Professor A. D. Gosman and co-workers of Imperial College, London, (e.g. Ref. 1) and are in general use.

The need for such a program can best be appreciated by comparing the numerical and exact solutions for the spreading of a passive scalar (dye in water for, example) in a simple flow field, Fig. 2-1. The differencing scheme used for this computation is the hybrid method which is used in almost all TEACH combustor codes. It can be seen that even for this simple flow situation, numerical (or artificial) diffusion generated by the differencing scheme greatly smears the profile. Numerical diffusion, especially in three-dimensional versions of TEACH, can become so large as to obscure the effects of the turbulance model in turbulent flow calculations. The accuracy of these codes becomes dependent on the number and distribution of nodes used in the finite-difference calculations; i.e., it is difficult to achieve a "grid-independent" solution. The number and distribution of grid nodes varies from user to user so that the results of parametric studies requiring more than variations in boundary conditions are questionable. This places a major restriction on the utilization of these codes for the design and development of practical combustors. Hence, there is a requirement for improving the accuracy of the differencing scheme presently embodied in these codes. This problem is addressed by the current program.

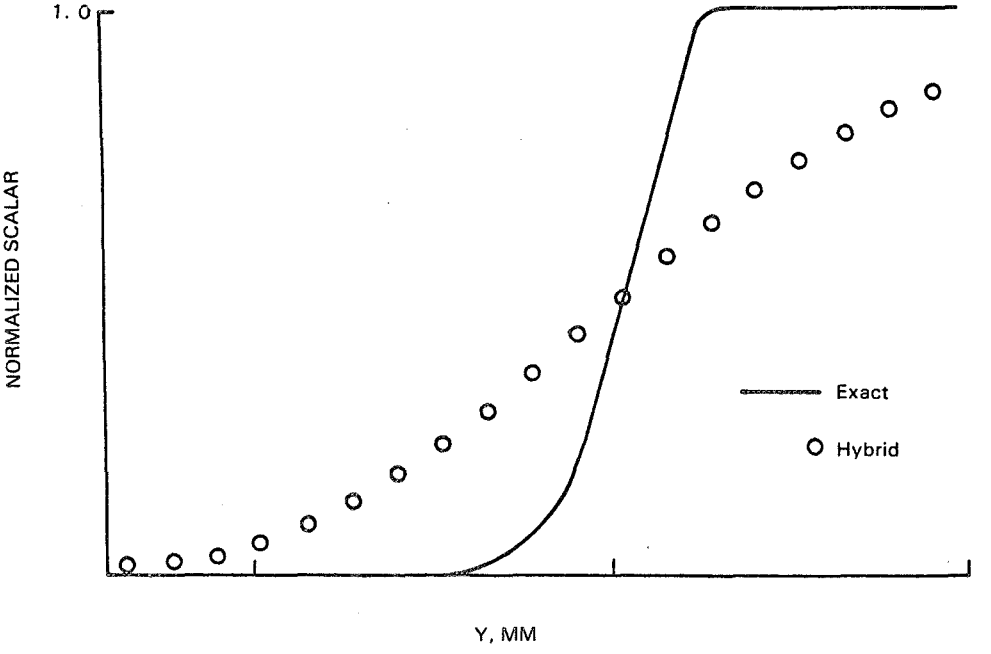

Convection and diffusion of a scalar step profile in constant property uniform inclined flow, cell peclect number, Pex = Pey = 60

Figure 2-1 Need for Error Reduction

2.2 APPROACH

The strategy adopted in this study was to select a number of candidate schemes and assess them for accuracy, solution stability, and overall cost-effectiveness. The accuracy assessment included consideration of the conservation and boundedness properties of the schemes, as well as conventional Taylor series error analyses and application to test cases. Solution stability was assessed heuristically by examining the properties of the coefficient matrix which each scheme generates. Cost-effectiveness was judged on the combined outcome of the foregoing assessments.

Based on this initial evaluation, two schemes were selected for incorporation into Pratt and Whitney's two-dimensional combustor performance code, 2D-TEACH (This computer program is the two-dimensional version of the three-dimensional code, 3D-TEACH, described in detail in Appendix B). The stability, accuracy and cost effectiveness of these two schemes were then examined by running a number of laminar and turbulent flow test cases. These test cases demonstrate typical flow features encountered in gas turbine combustors.

The more suitable of the two schemes was then incorporated into Pratt and Whitney's three-dimensional combustor performance code, 3D-TEACH (Appendix B). The improvement in accuracy of this scheme was evaluated for a test case modeling a row of jets in a cross flow and comparing the calculations against both experimental data and calculations performed using the hybrid differencing scheme.

2.3 ORGANIZATION

In Section 3 of this report a brief description of the sources of errors in the present combustor performance codes, 2D- and 3D-TEACH, is given and reasons for restricting attention in the present study to errors caused by the differencing scheme are explained. In Section 4 the procedure for selecting the two most promising schemes for incorporation into 2D-TEACH is described. This procedure involves selection of a number of schemes from the literature and evaluating their cost effectiveness by assessing their accuracy, stability, complexity, storage requirements and compatibility with 2D- and 3D-TEACH. In Section 5 implementation of the selected schemes into the TEACH codes is detailed and in Section 6 a description of the two- and three-dimensional test cases is given and the results of the computations are discussed. In Section 7, concluding remarks are given and in Section 8 recommendations for future work are presented.

3.0 BACKGROUND

An error reduction program in computational fluid mechanics faces the problem of selecting which of several errors are to be reduced since there are many sources of numerical error present in current design analysis codes. In this section, these error sources are described and the reasons for concentrating on errors due to the finite - difference method are given.

3.1 SOURCES OF ERROR IN PRESENT DESIGN CODES

The sources of error in present computer programs can be explained by referring to Figure 3-1 showing the four major steps of a typical computational procedure. In the following sections the errors introduced in each of these steps will be discussed with reference to the structure and models incorporated into the 2D and 3D-TEACH codes.

3.1.1 Assembly of Equations

In the first step, the governing partial differential equations are assembled. These consist of the Navier-Stokes equations for mass and momentum conservation, the energy equation, and the species transport equations together with additional auxiliary equations. The governing partial differential equations can be regarded as exact. The auxiliary equations, such as those used to represent various physical processes like chemical reaction, turbulence generation, etc., are generally only approximations in part because the relevant physical processes are known only approximately. In subsequent steps, other approximations (e.g., the finite-difference representation of the governing equations) introduce additional errors.

For example, the instantaneous value of a dependant variable, ϕ , in a turbulent reacting flow is usually taken as the sum of a time-mean value and a fluctuating value, a computational convenience, whose physical realism in increasingly questioned. When this definition is introduced into the Navier-Stokes equations and these are then time-averaged, further approximations to simplify the resulting Reynolds-averaged equations are introduced; specifically, fluctuations in laminar viscosity and density are often neglected.

As another example, infinitely-fast reaction rates are often assumed so that chemical reactions are represented by the one-step, irreversible reaction:

$$\text{Fuel} + \text{Oxidant} \rightarrow \text{Products} \qquad (3.1)$$

In this case, the combustion rate is assumed to be controlled by the turbulent mixing of eddies containing the reactants. From a chemical kinetics point of view, this reaction scheme is extremely crude and is relevant only in situations in which kinetics do not control the heat release rate. Fortunately, most of the gas turbine combustor operating envelop is in this category.

3.1.2 Physical Modeling

It has been established (Ref. 1) that a hierarchy of physical models exists. This hierarchy consists of models for:

- o Turbulence
- o Fuel-Spray Vaprization and Distribution
- o Combustion
- o Thermal Radiation

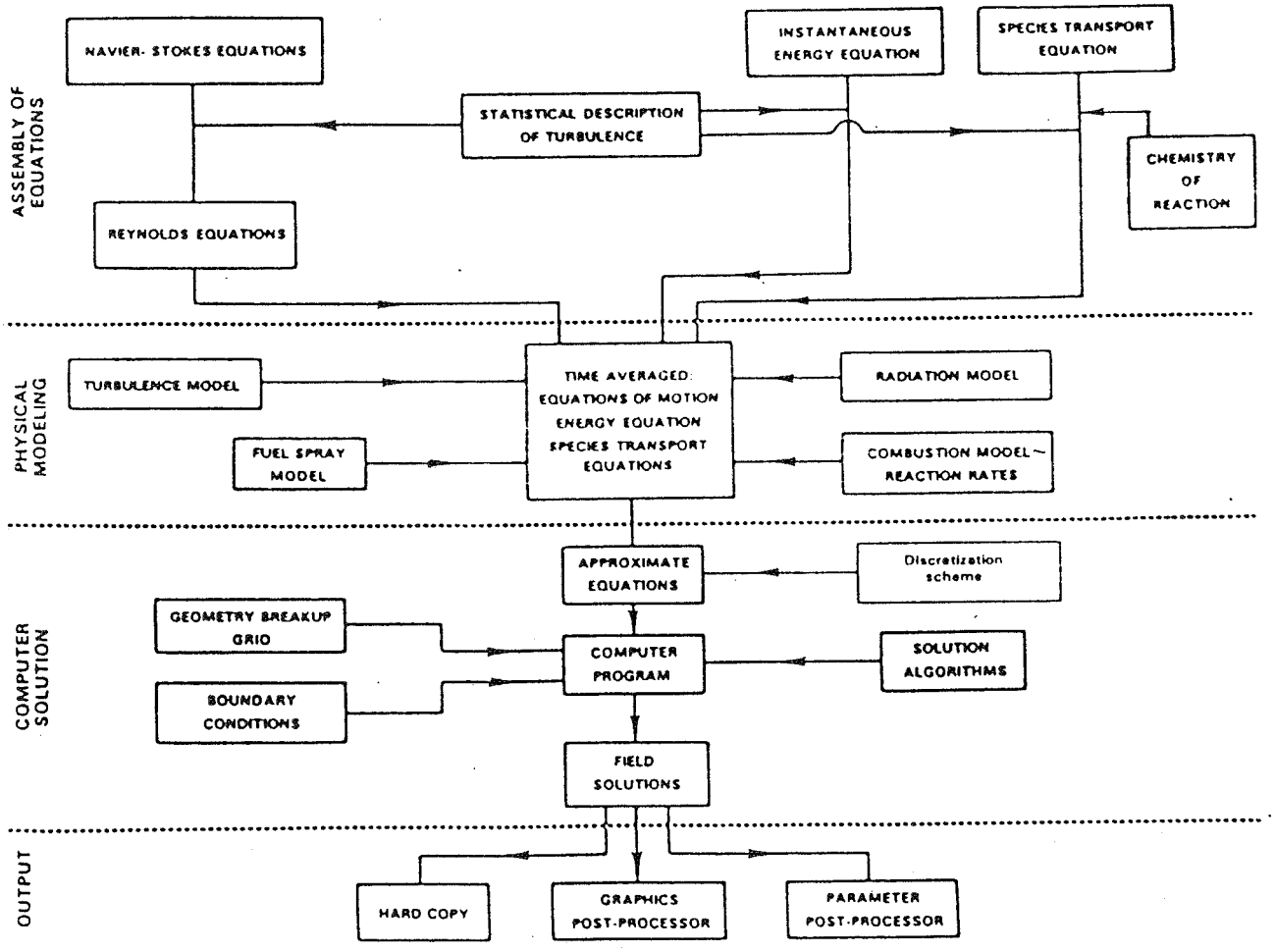

Figure 3-1 Flow Diagram of Computational Procedure

Clearly, there is little advantage to paying the computational cost of using, say, a radiation model of higher order accuracy than any of the models preceding it in the hierarchy.

The Reynolds averaged and other equations contain terms such as $\bar{\rho}\,\overline{u_j u_j}$ and $\bar{\rho}\,\overline{u_j m}$ where m is the mass fraction of chemical species "ℓ". Modeling is required to provide expressions for these correlations in terms of either known or calculable quantities.

Reynolds stresses can consist of two parts - a shear stress and a normal stress. The normal stress is obtained simply from the fluctuating dynamic pressures, while Boussinesq's analogy is used to relate the shear stress to the velocity gradient through an eddy viscosity μ_t. Thus variable density flow the Reynolds stresses can be expressed as:

$$-\bar{\rho}\,\overline{u_i' u_j'} = \mu_t \left(\frac{\partial \bar{u}_i}{\partial x_j} + \frac{\partial \bar{u}_j}{\partial x_i} - 2/3 \frac{\partial \bar{u}_k}{\partial x_k} \delta_{ij} \right) - 2/3\, \bar{\rho}\, K\, \delta_{ij} \tag{3.2}$$

where K is the turbulent kinetic energy and is defined as:

$$K = 1/2\ (\overline{u'^2} + \overline{v'^2} + \overline{w'^2})$$

The eddy viscosity, μ_t is obtained by dimensional arguments from the Prandtl- Kolmogorov definition,

$$\mu_t = \bar{\rho}\ \frac{C_\mu\ K^2}{\varepsilon} \tag{3.3}$$

where

ε = dissipation rate of K

The eddy viscosity is evaluated by means of transport equations for K and ε. using the familiar two-equation turbulence model.

Since the flow field is calculated using an effective turbulent eddy viscosity, it is computationally convenient to base the turbulent heat and mass transfer rates on effective thermal and mass eddy diffusivities.

In general, the eddy diffusivity is used to calculate the flux of a scalar by:

$$-\overline{u_i'\phi'} = \Gamma_{t,\phi} \frac{\partial \bar{\phi}}{\partial x_i} \tag{3.4}$$

where,

ϕ = scalar quantity such as temperature or species concentration
$\Gamma_{t\phi}$= turbulent eddy diffusivity for ϕ

The eddy diffusivity is found from the ratio of turbulent kinematic eddy viscosity ν_t to the turbulent Prandlt or Schmidt number, σ_t, for ϕ.

The turbulence model is a second order, mean-field closure to the equations. For the eddy viscosity approach, the two-equation model is the most general and sophisticated representation, and it is not computationally expensive. Sophistication comes from the use of differential equations to describe both the velocity scale and length scale to which the eddy viscosity can be related, rather than relying upon an a priori length scale specification as used in the mixing-length approach.

There are a number of limitations to the two-equations turbulence model. It is well known that the assumptions used to derive the turbulence kinetic energy dissipation rate (ε) equation are somewhat arbitrary. More importantly, use of the gradient diffusion idea itself has long been challenged. There are objections to the assumption that the Reynolds stresses depend on only the local mean rate of strain as well as to the assumption that the stresses are proportional to the local rate of strain. The "constant" of proportionality really depends on the ratio of local production and dissipation of turbulence energy, and this ratio is not actually a constant. A further weakness is the adoption of a single velocity scale at a point in the flow although it is known that this scale can vary from point to point. The implication of a single scale is that the turbulence is isotropic. Turbulent flows usually posses some degree of anisotropy and some flows (e.g. flows with swirl or with large streamline curvature in the streamwise direction) produce turbulence that is highly anisotropic. The velocity and length scales have to be the same order of magnitude as the mean field motion. This is only true for flows dominated by simple shear forces; buoyancy forces, for example, have separate scales. It is implied that the turbulent motions have a small scale compared to that over which the concentration of a diffusing quantity changes significantly, yet most of the larger eddies in a turbulent flow do not satisfy this condition whether they are coherent or not. Thus, material can be transported by vortical motion against the gradient of the scalar. Williams and Libby (Ref. 2) have called this process "counter-gradient diffusion," while Spalding has used the more descriptive phrase "pressure-gradient diffusion" (Ref. 3). By relying on local mean rates of strain consideration of the effect of flow history on turbulence structure is lost.

It can also be appreciated that there are levels of approximation that are, introduced into the averaging process that results in an enormous simplification for turbulence modeling. Similar approximations must be used for all the physical modeling used.

3.1.3 Computer Solution

When both the governing and auxiliary equations are assembled, they form a simultaneous set of non-linear partial differential equations and algebraic equations.

Numerical solution of the equation set is necessary. Conventional numerical methods available to solve equation sets of these types can be broadly divided into finite difference and finite element methods, although the dividing line is not distinct. Finite difference methods have a considerable background in the fluid dynamics area, and most solution approaches, including TEACH, utilize finite differences.

The finite difference analog of the differential equations is obtained by overlaying a computational mesh on the flow domain, and obtaining the basic finite difference form of the partial derivatives for every node of the mesh from a control volume approach (Ref. 4). The finite difference expressions, when substituted back into the differential equations, yield a set of linearized, algebraic equations for every node of the mesh. Thus, there are as many sets of equations as there are nodes in the calculation domain. These sets, along with the boundary conditions for the problem, can then be solved to give solutions for the entire flowfield.

The accuracy of a differencing scheme can be judged from the order of the terms of an equivalent Taylor Series that have been retained in the expansion. Unfortunately, the requirements of numerical stability are opposite to those of accuracy with respect to these terms. Achieving a balance between accuracy and stability can be particularly trying in the case of a chemically reacting flow because of the coupled nonlinearities which exist between the chemical and fluid mechanical processes. The spatial differencing of the convective terms of the conservation equations in an Eulerian coordinate system can result in numerical diffusion. Use of a higher order differencing scheme eliminates or significantly reduces this diffusion. However, the use of central-differencing method, for example, often produces oscillations in the solution that have no physical significance (Ref 5). The use of an upwind differencing, or donor cell, technique eliminates oscillations but introduces a diffusion-like term into the difference equations. Thus, while "numerical damping" suppresses oscillation, it leads to significant additional diffusion of the convected parameter. For flows with combustion, these parameters might be species concentration, temperature, etc. Unfortunately, diffusion of these quantities is responsible in a physical sense for flame propagation. Therefore, a severe restriction can be placed on the quality of quantitative prediction (Ref. 6).

It can be argued that use of upwind differencing in regions where convection strongly dominates streamwise diffusion is reasonable since the local upstream values of the field variables are swept downstream virtually unchanged, whereas in high-diffusion regions the form of the relatively small convection terms is not important. In regions where the two transport mechanisms are comparable, a switch to more accurate central differencing for convection or use of a suitably weighted combination of central and upstream differencing can be used.

This somewhat narrow view of complex flows has led to the appearance and use of a popular and successful hybrid central/upwind differencing scheme (Ref. 7). This scheme is currently used in TEACH codes. The method uses central differencing for convection and diffusion fluxes when the absolute value of the Peclet number for the control volumes existing about grid nodes is less than, or equal to, two: upwind differencing for convection fluxes and neglect of diffusion fluxes is used otherwise. Peclet number defines the relative importance of convective and diffusive transport and is numerically equivalent to a cell Reynolds number.

To use successfully the hybrid differencing scheme for complicated flows, care must be taken in establishing the computational grid upon which the calculations are performed. The approximations of the algebraic expressions used to represent the partial differential equations becomes asymptotically exact as the distance between the grid nodes is reduced. In the limit, the number of nodes can be increased until an asymptote to the solution of the differential equations is achieved. In practice, this increase is limited by computer storage and the cost of the calculation. However, it is not only the number of nodes that are used in determining the accuracy of a solution which is important, but also the distribution of those nodes within the flowfield to be determined (Refs. 8 , 9). This nodal distribution is important because whenever curvature of the flow in the streamwise coordinate direction exists, a truncation error arises in the solution (Ref. 10). In addition, there is also a problem in multidimensional flows of streamline-to-grid skewness (Ref. 11). With upwind differencing, these effects start to have a damaging effect on solution accuracy when the Peclet number exceeds two.

It has been concluded (Ref. 1) that the hybrid finite differencing scheme, although yielding physically realistic solutions in all circumstances, introduces excessive numerical diffusion for many two-dimensional flows and for all three-dimensional flows because presently available computer storage is generally not sufficient to permit local adjustment of the grids as described above. Thus, solution accuracy is presently controlled by the numerics rather than the hierarchy of physical modeling.

3.1.4 Representation of Geometry

A drawback of the present calculation methods based on TEACH-type computer programs is the lack of flexibility with respect to irregularly-shaped boundaries for the calculation domain. Therefore, the geometry is "discretized" to fit the coordinate system.

Figure 3-2 shows a typical modern, annular combustion chamber for an aircraft gas turbine engine. To calculate flows in such a combustor using a TEACH code means that curvilinear surfaces must be represented using "stair-steps." Figure 3-3 gives a two-dimensional (axisymmetric) example of such a representation.

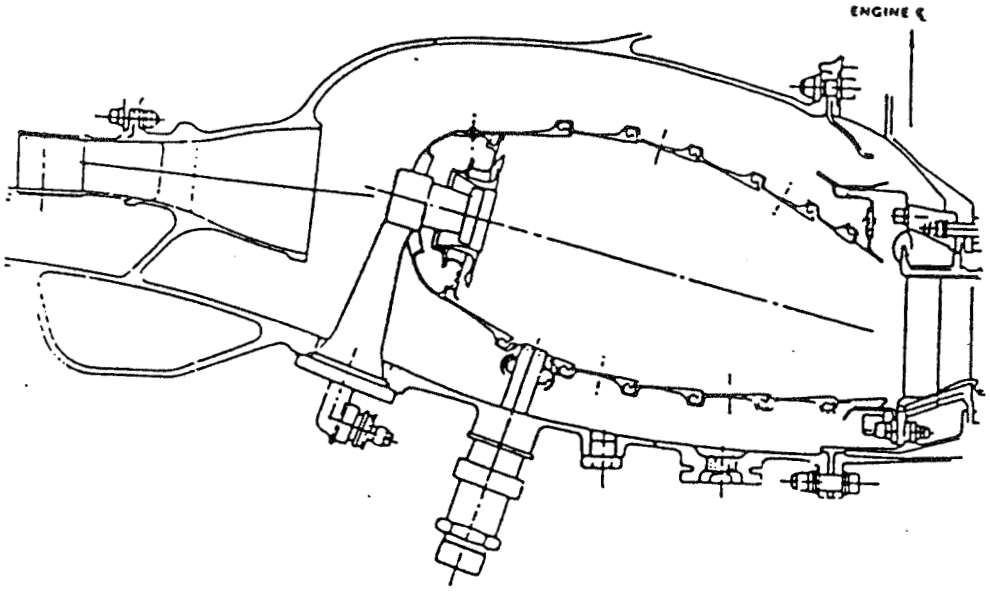

Figure 3-2 Cross Section of a Typical Modern Annular Combustion Chamber

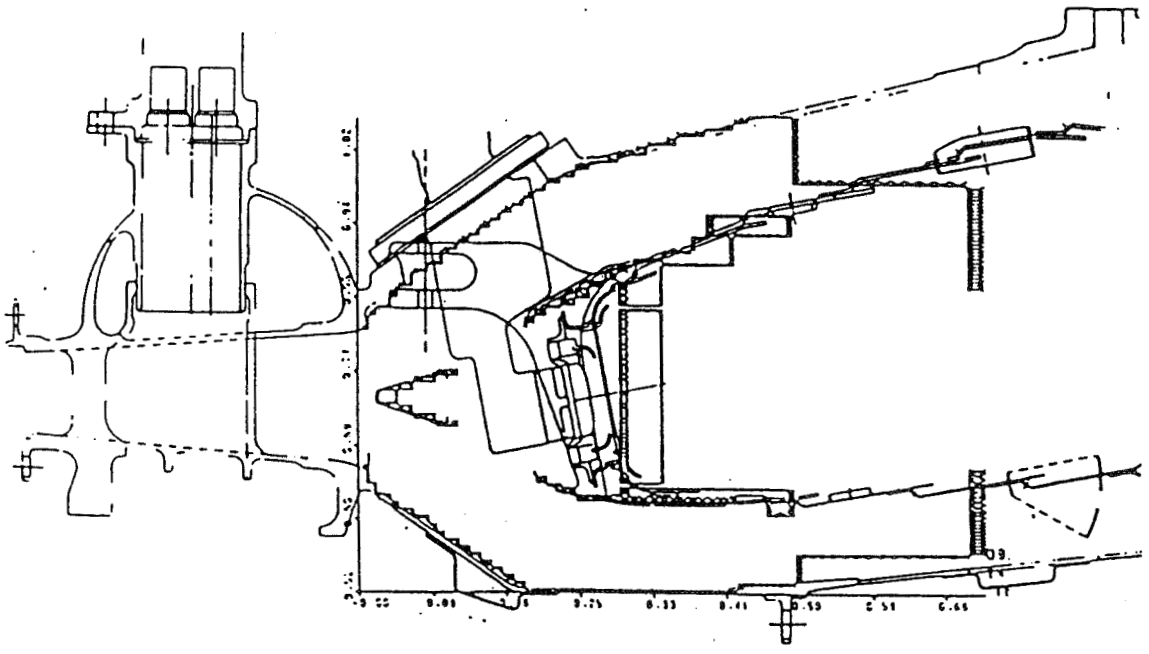

Figure 3-3 Stair-Step Representation of Actual Combustor Geometry

The use of stair-step geometries has a number of implications: First, surface areas are not correct. Thus, irrespective of physical modeling and numerical accuracy, calculation of wall shear stress and surface heat transfer rates can never be correct. Second, adequate representation of the geometry bounding the flow to be calculated usually requires more computer storage than is available on the present generation of computers. Mesh refining to control numerical diffusion is not therefore possible, and the calculated flowfield may be influenced incorrectly by the geometric representation.

3.1.5 Solution Algorithm

By their very nature, computational fluid dynamies (CFD) codes are large consumers of computer resources. The cost of a CFD calculation depends on the number of grid nodes, the number of equations to be solved at each node, and the rate of convergence produced by the solution algorithm. Generally, the number of nodes and equations are determined by the scope of the problem under investigation. If the convergence rate is too low, considerations of cost and economy may result in termination of the solution, even though the residuals in the relaxation process might still be high. An arbitrary limit is thus placed on solution accuracy by considerations of cost.

Low convergence rates in existing codes can occur, typically, if the calculation domain is large and has several entering streams so that the flowfield thereby contains a number of recirculation zones. In addition, an increased number of grid nodes is necessary to resolve adequately all the flow features. For such strongly elliptic flowfields, the weak coupling of the momentum and continuity equations through the SIMPLE (Semi-Implicit Method for Pressure-linked Equations) algorithm and the weakly implicit nature of the ADI (Alternating Direction Implicit) matrix solution procedure can result in low rates of convergence. In addition, such a flowfield can become physically marginally stable, nonstationary, or bistable in character, producing eddy-shedding, Coanda effects, separation, etc. A combination of entering flows could exist for which the presumed steady-state solution does not exist. The flow pattern may then change from iteration to iteration and the convergence rate may become unacceptably low. For nonstationary flows, divergence can result.

The equations to be solved can also present a convergence problem as, for example in reacting flows with the chemistry modeled using "stiff" exothermic reaction rate expressions. Similar problems arise in the turbulence equations (Ref. 12) when the equations are solved iteratively and uncoupled. Under such circumstances, severe under-relaxation is usually required to achieve convergence and the time to achieve a solution becomes unacceptably high.

The finite differencing used to approximate the partial differential equations generates the coefficient matrix for the equations. Matrix conditioning can influence convergence. If the coefficient matrix is always diagonally dominant, then any fast matrix solver may be used without difficulty. However, if diagonal dominance is lost, then the ADI method tends to be unstable; if the difference method produces negative coefficients, divergence usually results. Therefore, the solution accuracy depends not only on the order of the differencing scheme, but also on its compatability with the solution algorithm.

3.2 UTILITY OF PRESENT DESIGN CODES

From the above discussion, it appears that the numerical inaccuracies of present design codes limit their usefulness to the designer.

However, these codes are adequate for many engineering applications. The only practical engineering alernative is to conduct numerous experiments verifying a design. With the cost of fuel, materials and manpower increasing rapidly, this alternative is becoming an increasingly expensive proposition. Hence, even an approximate answer that eliminates some testing is acceptable. Although these codes lack quantitative accuracy, their qualitative accuracy has been demonstrated in a number of test cases. This qualitative accuracy allows an engineer to conduct parametric studies with confidence, allowing quick preliminary screening of design ideas. This ability is also useful in diagnosing and solving development problems. Once the problem is simulated with the code, it is then usually much quicker to develop an acceptable solution by using the computer than a rig.

3.3 REASONS FOR CONCENTRATING ON THE DIFFERENCING SCHEME FOR ACCURACY IMPROVEMENT

Several sources of error in the present design codes were described in Section 3.1. Although these codes are still useful for design purposes, improvement in quantitative accuracy will increase their utility. The question then has to be asked: how can the accuracy of these codes be improved. One strategy is to develop a new generation of codes that eliminate the statistical description of turbulence, introduce subgrid turbulence scaling and combustion models, reduce numerical diffusion, use a body fitted coordinate system, and use a faster solver than the ADI scheme. This strategy requires a long lead time because most of the models are in the development stage. In addition, it takes several years to turn a research code into a production code. This approach is best suited for a university and several universities are already working on different aspects of this strategy.

Another strategy to improve the present production codes in a relatively short period of time is to work on only one aspect of the problem. This strategy can yield only a limited improvement in accuracy when compared to the potential benefits of developing a new generation of combustor design codes; however, if only mature models are incorporated into the calculation procedure, the chances of success are large. It was shown in Section 3.1 that solution accuracy is presently controlled by numerics rather than the hierarchy of physical modeling. Hence, improvement in the differencing scheme is the first area that needs to be investigated and, if successful, will have an immediate impact on the accuracy of the code. There are several differencing schemes available in the literature that have been tested by a number of investigators and have shown promise in model problem studies of some simple flows. It is thought that these schemes have reached a level of maturity that they can now be tested in modeling more realistic flows. It was with these considerations in mind that NASA sponsored the Error Reduction Program to select, incorporate, and evaluate an improved-accuracy finite difference scheme in 3D-TEACH.

4.0 SELECTION OF MORE ACCURATE FINITE-DIFFERENCING SCHEMES

Having established in the previous section that improvements to the present finite-differencing scheme can yield significant benefits in the short term, the task then is to develop such improvements. During the development process, a number of constraints must be kept in mind:

1. The scheme is to be implemented in TEACH-type codes used to design gas turbine combustors; these codes are operated by engineers who are not necessarily expert in computational fluid mechanics. Hence, the scheme has to be robust, require no attention from the user, and yield results that are always physically plausible.

2. Since the selected scheme is to replace the hybrid scheme without any other changes being made to the code, it is important that the selected scheme be compatible with the other parts of the code such as the solution algorithm.

3. The scheme should be capable of computing accurately flows of the type that occur in a gas turbine combustor; thus, testing of candidate schemes must include some model problem studies representing realistic flowfields.

Several improved finite-difference schemes were selected from the literature and subjected to an initial screening process. Two schemes were then selected that were believed to be capable of calculating realistic gas turbine combustor flowfields, and were compatible with the present code. These two schemes were then incorporated into the 2D version of the TEACH code. After using the revised computer program to calculate several laminar and turbulent flow test cases containing important flow features common to gas turbine combustors, the more promising scheme was selected for use in the 3D version of TEACH. The initial screening process and selection of the two most promising schemes are described in this section.

4.1 CRITERIA OF ASSESSMENT

A scheme to be implemented into the present design codes should be not only more accurate than the present hybrid difference scheme but it should satisfy certain other criteria which are discussed below.

4.1.1 Mirror Differential Equation Properties.

Before any scheme is judged for accuracy, it is necessary to ensure that the approximation to the discretized equation mirrors certain key properties of the original differential equation. This discussion will be facilitated if a general discretized form of the equation to be solved is derived. The two-dimension form is presented, but similar remarks apply to the three-dimension case.

A prototype transport equation for a general scalar entity, ϕ, which may stand for a velocity component, temperature, concentration, turbulence energy, etc, can be written as:

$$\frac{\partial}{\partial x}\left(\rho u\phi - \Gamma\frac{\partial \phi}{\partial x}\right) + \frac{\partial}{\partial y}\left(\rho v\phi - \Gamma\frac{\partial \phi}{\partial y}\right) = S \tag{4.1}$$

where ρ and Γ are the density and diffusivity, respectively, S is the local volumetric source (sink) rate and u and v are the velocity components in directions x and y, respectively.

Integral forms of the above equations can be written for finite regions. If one integrates Equation 4.1 over the region defined by the dashed lines in Figure 4-1, one obtains:

$$\int_{y_s}^{y_n}\left(\rho u\phi - \Gamma\frac{\partial \phi}{\partial x}\right)\Bigg|_{x_w}^{x_e} dy + \int_{x_w}^{x_e}\left(\rho v\phi - \Gamma\frac{\partial \phi}{\partial y}\right)\Bigg|_{y_s}^{y_n} dx = \int_{y_s}^{y_n}\int_{x_w}^{x_e} S\,dx\,dy \tag{4.2}$$

where w, e, s and n denote the four surfaces of the region.

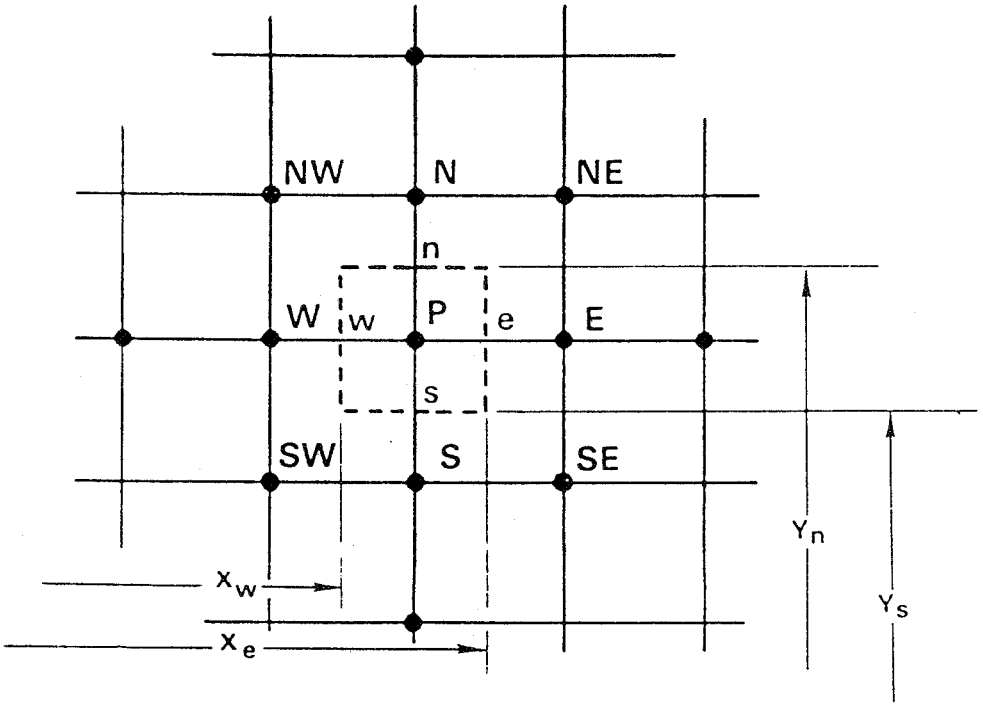

Figure 4-1 Region of Integration Defined by Grid Lines

Since the majority of the schemes examined are based on the integral analysis, (usually referred to as the "finite volume method" or "FVM", Ref 4) it will be useful to assemble and examine a relatively general form of discretized transport equation derived in this way. This analysis will follow the general lines of Gosman and Lai (1982)(Ref. 13). In the FVM, attention is focussed on the integrals of Equation 4.2, those on the left-hand side of which represent total transports by convection and diffusion through the cell face in question. If the transport through the w face is denoted by F_w. then:

$$F_w = \int_{y_s}^{y_n} (\rho u \phi - \Gamma \frac{\partial \phi}{\partial x}) \Big|_{x_w} dy \qquad (4.3)$$

which may be written, using the Mean Value Theorem (MVT) of the differential calculus, as:

$$F_w = [(\rho u \phi)_w - (\Gamma \frac{\partial \phi}{\partial x})_w] \Delta y \qquad (4.4)$$

where the subscript w now denotes an average along the cell face and $\Delta y = y_n - y_s$ is the face "area". A more compact and convenient expression is obtained through further use of the MVT to give:

$$F_w = C_w \phi_w - \Gamma_w \Delta y \, (\frac{\partial \phi}{\partial x})_w \qquad (4.5)$$

where $C_w = (\rho u)_w \Delta y$ is a convection coefficient; C_w and Γ_w are obtained by suitable averaging of the ρ, u, and Γ fields.

It is at this stage that the major approximations are introduced, the purpose of which is to relate ϕ_w and $(\partial\phi/\partial x)_w$ to ϕ values at the grid intersections or "nodes", which are labeled in the point-of-compass fashion as E, N, S, and W in Figure 4-1. Here it is assumed that ϕ_w is defined in terms of nodal values ϕ_i by:

$$\phi_w = \sum_w^i \alpha_w^i \phi_i \qquad (4.6)$$

where the α_w^i are weighting factors and Σ_w denotes summation over specified nodes in the vicinity of w. In a similar way $(\partial\phi/\partial x)_w$ will be approximated by:

$$\left(\frac{\partial \phi}{\partial x}\right)_w \simeq \left(\sum_{w+}^{i} \beta_{w+}^{i} \phi_i - \sum_{w-}^{i} \beta_{w-}^{i} \phi_i \right) / \Delta x \qquad (4.7)$$

where the β_w are further weighting factors, w^+ and w^- denote locations to the right and left of the cell face, respectively, and $\Delta x = x_p - x_w$. Insertion of the above expressions into Equation 4.5 finally yields:

$$F_w \simeq C_w \sum_w^i \alpha_w^i \phi_i - d_w \left(\sum_{w+}^{i} \beta_{w+}^{i} \phi_i - \sum_{w-}^{i} \beta_{w-}^{i} \phi_i \right) \qquad (4.8)$$

where $d_w = \Gamma_w \Delta y / \Delta x$

The discrete analogue of the integral transport Equation 4.2 is obtained using F_w from above and analogous formulae for the remaining F's and substituting into the equation:

$$F_w - F_e + F_s - F_n + S_u = 0.$$

Before this is done it will be useful for illustration purposes to specify a particular set of participating nodes, as this will allow the properties of the resulting equation to be more readily perceived. Here one chooses, for the w face, the "nearest-neighbor" set SW, W, NW, S, P and N (see Figure 4-1) which, together with analogous sets for the remaining three faces give rise to the "compact" nine-point molecule illustrated in the Figure 4-1. The resulting equation, when arranged into a substitution formula for ϕ_p, runs:

$$a_p \phi_p = \sum_w a_i \phi_i + S_u \tag{4.9}$$

where $\sum_w$ denotes summation over all eight nearest neighbors of P and:

$$a_p = C_e \alpha_e^p - C_w \alpha_w^p + C_n \alpha_n^p - C_s \alpha_s^p + d_e \beta_e^p + d_w \beta_w^p \tag{4.10}$$

$$a_W = (C_w \alpha_w^W + d_w \beta_w^W) + (C_s \alpha_s^W - C_n \alpha_n^W - d_n \beta_n^W - d_s \beta_s^W) \tag{4.11}$$

$$a_E = (-C_e \alpha_e^E + d_e \beta_e^E) + (C_s \alpha_s^E - C_n \alpha_n^E - d_n \beta_n^E - d_S \beta_S^E) \tag{4.12}$$

$$a_{NW} = C_w \alpha_w^{NW} - C_n \alpha_n^{nw} + d_w \beta_w^{NW} + d_n \beta_n^{NW} \tag{4.13}$$

$$a_{NE} = -C_e \alpha_e^{NE} - C_n \alpha_n^{NE} + dn\ \beta_n^{NE} \tag{4.14}$$

and

$$S_u = \int_{y_s}^{y_n} \int_{x_w}^{x_e} S\ dxdy \tag{4.15}$$

Several points about the above expressions are noteworthy. Firstly the "a" coefficients contain contributions from the fluxes from more than one cell face: for example, the a_w coefficient contains, in the first brackets, contributors from F_w and, in the second brackets, quantities relating to the intersecting faces s and n. Secondly, there are no obvious bounds on the coefficients: they may be positive, negative or zero. The significance of these observations will be explained below.

Having derived the general discretized form of the transport equation, the requirements that this equation has to meet to mirror the differential equation can be established. These requirements are discussed in the following sections.

4.1.1.1 Conservation

Equation 4.1 is, as already noted, an exact statement of the conservation of ϕ principle over the cell volume. Solutions of the discrete version (Equation 4.9) will obey this principle provided that the weighting factors α and β are uniquely defined at the cell boundaries, rather than at grid nodes for the reason that only the former practice will ensure that the fluxes are continuous across the cell boundaries.

4.1.1.2 Boundedness

It is well known that, in the absence of sources, solutions to Equation 4.1 will lie within bounds given by:

$$\min(\phi_B) < \phi < \max(\phi_B) \tag{4.16}$$

where ϕ_B denotes the boundary distribution. Sufficient conditions for the discrete solution to obey this "boundedness" principle are that:

- the coefficients a_p and a_i must all have the same sign, here taken without loss of generality to be positive, i.e.,

$$a_p,\ a_i \geq 0 \tag{4.17}$$

- the central coefficient must be the sum of its neighbors, i.e.,

$$a_p = \Sigma\ a_i \tag{4.18}$$

These ensure that when $Su = 0$, ϕ_p is simply the weighted mean of the neighboring ϕ, so no extraneous extreme can be produced.

The above conditions lead to further constraints on the weighting factors, which may be summarized, by reference to those relating to F_w, as follows:

- they must be non-negative, i.e.

$$\alpha_w,\ \beta_w \geq 0 \tag{4.19}$$

- the α_w must sum to unity, i.e.

$$\sum_w \alpha_w^i = 1 \tag{4.20}$$

- the β_w must obey the resolution:

$$\sum_{w^-} \beta_{w^-}^i = \sum_{w^+} \beta_{w^+}^i \tag{4.21}$$

Inspection of the coefficient definitions (Equations 4.10 - 4.14) reveals that obedience to the constraints of Equations 4.19 to 4.21 is not in itself sufficient to ensure that the conditions of Equations 4.17 and 4.18 will be satisfied. Infringement may occur from either the convection contributions (since the convective coefficients are unconstrained as to both magnitude and sign, apart from the overall mass continuity requirement) or from the diffusion contributions.

4.1.1.3 Transportation

The directional properties exhibited by fluid transport phenomena are well-known and are signaled in Equation 4.1 by the fact that, for $S = 0$, the equations become hyperbolic and streamlines become characteristics as the Peclet number, $\rho v L/\Gamma$, (where L is a typical length scale) tends to infinity. The implication for the discretization is that there are domains of influence and dependence requirements to be observed at each mesh point which, simply stated, entail that at large Peclet numbers information should be propagated along streamlines in the direction of the flow. Failure to observe this requirement can give rise to unstable solutions (nonphysical oscillations) because the coefficients can become negative.

4.1.2 Accuracy

Accuracy is the primary requirement of any scheme that proposes to reduce numerical diffusion. The scheme should be at least as accurate as the hybrid scheme in all situations, and more accurate in most situations.

The evaluation of the relative accuracies of different schemes is not a straight forward task. The ultimate test of a numerical scheme should be based on its ability to accurately calculate real flows. In the present context these flows should be of the type that occur in a gas turbine combustor. Unfortunately, such flows are complex, so analytical solutions are not available for comparison. Measurements in these flows are subject to large experimental inaccuracies. Moreover, these flows are turbulent, which means that the solution accuracy is clouded by the turbulence model being used.

Traditional means of evaluating accuracy of numerical schemes are available. For example, Taylor series analysis will give the order of the accuracy of any scheme. Since this analysis is only accurate in the limit when mesh spacing tends to zero, it is by no means clear that a higher-order scheme will necessarily yield results that are more accurate than a lower-order scheme on a mesh of finite size. Comparing solutions against model problems also has limited generality because model problems may not be able to represent adequately all the characteristics of the class of real flows for which the numerical scheme is to be developed.

The performance of a number of different numerical schemes can be evaluated by applying them to a single computational cell for different test cases. This method allows different schemes to be assessed quickly against each other, but has limited value because the conclusions are valid only for the particular test cases studied.

It is clear that any one approach alone is not sufficient to assess the accuracy of proposed schemes, and care should be taken in drawing general conclusions from any such single comparison. In this study, all of the above methods of accuracy assessment have been used in selecting the most accurate scheme.

4.1.3 Stability

Stability of a numerical scheme means that the computations using the scheme should be able to converge to a solution. The stability of a numerical scheme is, however, also related to the type of solution algorithm being used. For example, the present algorithm (an Alternating Direction Implicit-ADI- method using a Tridiagonal Matrix Algorithm-TDMA) requires that the coefficient matrix formed from the differencing be diagonally dominant. Any alternative differencing scheme for reducing numerical diffusion which generates a coefficient matrix in which this dominance is lost will be unstable if the present solution algorithm is used, regardless of the overall stability of the finite differencing used. However, a more robust solution algorithm in place of the ADI method may be able to converge to a solution with the same set of difference equations.

4.1.4 Economy

Any scheme, if it is to be used in production versions of present computer codes, should be economical to use when computing realistic flow problems. Economy is understood to mean that the computing time required when using the scheme should not be prohibitive. A scheme that yields a marginally more accurate solution but requires significantly greater computer time would not be cost effective. Computer codes requiring large computing times, usually increase the time required to complete a job; consequently, regular usage of the code is inhibited.

4.1.5 Variable Storage Requirements

Although the memory of present-day computers is extremely large, the number of variables required to be stored for a computer program that solves the equations for a two-phase turbulent, reacting, radiating flow using curvilinear coordinates can be very large, especially if the flow is three-dimensional and the geometry is complex. The storage capacity of even modern computers can be easily exceeded in such cases. Since the memory required is the product of the number of variables stored, the number of nodes in the mesh, and the number of nodes in the computational molecule, there is a trade-off between the variable storage requirements of a new scheme and the increase in accuracy that is achieved by using it.

With a more accurate scheme, a relatively coarse mesh may be used to achieve better accuracy compared to the existing scheme with a fine mesh. Therefore, a more accurate scheme may reduce the overall memory requirements even though the number of nodes in the computational molecule to be stored may have been increased.

4.1.6 Compatibility With Present Codes

If a scheme is compatible with the present program it requires less time to incorporate it into the code. The present study was limited to developing improved finite-difference schemes for TEACH-type codes. Therefore, it was essential that the proposed scheme be able to converge with the present solution algorithm.

4.1.7 Complexity

A simple scheme takes less time to incorporate into a code than a complex scheme. However, this is a one-time expense, and a complex scheme which is more accurate, economical and stable than a simple scheme is always to be preferred.

4.2 METHOD OF ASSESSMENT

It is clear from the above discussion that a differencing scheme has to meet several criteria before it can be considered for incorporation into the present design codes. It is also clear that traditional Taylor series analyses are not sufficient to assess the suitability of a given scheme. In this study, both model problem calculations and examination of the properties of the difference equations have been used to supplement the Taylor series analyses.

As explained in the previous section, examination of the weighting factors shows whether a certain discretized form is conservative or not. Inspection of the coefficients reveal whether the discretized equation satisfies the boundedness and transportational properties of the differential equation being approximated. Examination of the coefficient matrix gives a good indication whether it will be amenable to solution by the ADI method presently used in the design codes. As is well known, ADI methods work best when the coefficient matrix is diagonally dominant.

Model problem studies, in addition to assessing the accuracy of a given scheme, are useful in estimating its stability, cost effectiveness, complexity and variable storage requirements.

4.2.1 Limitations of Method of Assessment

The method of assessment described above is more general and informative than use of the Taylor series analysis method alone. Two limitations of the method of assessment should be noted, however. First, schemes more compatible with the present solver (the Alternating Direction Implicit method using a Tridiagonal Matrix Algorithm) have an advantage over those schemes that are less compatible; in principle, these schemes should be judged independently of the solver.. Second, the model problems used herein usually demonstrate the performance of a scheme for highly idealized flows possessing only a single flow complexity; these simple flows are used because analytical solutions are available. However, the practical performance of each scheme can only be assessed by computing more realistic flow situations.

In the next section, difference equations for the candidate schemes will be derived and their suitability will be assessed by examining the properties of the resulting equations.

4.3 DESCRIPTION AND PRELIMINARY SCREENING OF CANDIDATE SCHEMES

The following candidate schemes were assessed for incorporation into present design codes of the TEACH type.

1. Agarwal Differencing Scheme (ADS)
2. Quadratic Upwind Differencing Scheme (QUDS)
3. Skew Upwind Differencing Scheme (SUDS)
4. Cubic Spline Schemes (CSS)
5. Glass and Rodi Hermitian Scheme (GRHS)
6. Flux Blending Schemes

In the following sections the candidate schemes will be described. The descriptions will be brief for the most part, since many of the schemes are well known and have been presented elsewhere. The less-familiar flux blending approach will be developed in more detail. For the sake of brevity and ease of understanding, the equations will be presented for the special circumstances of flows in which u, v, ρ and Γ are uniform and positive, S=0, and the computing mesh is square with spacing Δ. The evaluation of the candidate schemes for their boundedness, transportation, and conservation properties will also be discussed in this section. Any improved accuracy scheme must satisfy these criteria for it to be considered as a candidate for incorporation into computational fluid mechanics codes.

4.3.1 Central Difference Scheme (CDS)

By way of illustration, and for later reference, the properties of the familiar CDS will be examined in the light of the framework described in Section 4.1.

The non-zero weighting coefficients for this are:

$$\alpha_w^p = \alpha_w^W = 1/2$$
$$\beta_w^p = \beta_w^W = 1 \qquad (4.22)$$

and likewise for α_e, β_e etc. These give

$$a_p = \Sigma a_i$$

where:

$$a_W = C_w \left(\frac{1}{2} + \frac{1}{P_{e_w}}\right) \quad , \quad a_S = C_s \left(\frac{1}{2} + \frac{1}{P_{e_s}}\right) \qquad (4.23)$$

$$a_E = C_e \left(-\frac{1}{2} + \frac{1}{Pe_e}\right) \quad a_N = C_n \left(-\frac{1}{2} + \frac{1}{P_{e_n}}\right)$$

$$a_{NW} = a_{SW} = a_{NE} = a_{SE} = 0$$

In the above equations, $P_{e_w} = C_w/d_w$.

These show that the scheme is conservative, but bounded only for $Pe_i < 2$. The cause of the latter limitation is failure to obey the transportation requirement (i.e., use of downstream ϕ values in the convective flux approximation).

For a one-dimensional problem, ϕ_p can be obtained by using equation 4.23. The result is:

$$\phi_p = \frac{1}{2}\left[\left(\frac{Pe}{2} - 1\right)\phi_E + \left(\frac{Pe}{2} + 1\right)\phi_W\right] \tag{4.24}$$

4.3.2 Upwind Difference Scheme (UDS)

In this scheme the β are identical to the above, but the α are given by the following expressions:

$$\alpha_w^W = \begin{cases} 1 , & C_w \geq 0 \\ 0 , & C_w < 0 \end{cases}$$

$$\alpha_w^P = \begin{cases} 0 , & C_w \geq 0 \\ 1 , & C_w < 0 \end{cases} \tag{4.25}$$

and the coefficients have the form:

$$a_P = \Sigma a_i$$

$$a_W = d_w \left[1 + \frac{1}{2}\left(\left|Pe_w\right| + Pe_w\right)\right]$$

$$a_E = d_e \left[1 + \frac{1}{2}\left(\left|Pe_e\right| - Pe_e\right)\right]$$

$$a_N = d_n \left[1 + \frac{1}{2}\left(\left|Pe_n\right| - Pe_n\right)\right]$$

$$a_S = d_s \left[1 + \frac{1}{2}\left(\left|Pe_s\right| + Pe_s\right)\right]$$

This scheme is seen to be both conservative and unconditionally bounded. Until recently it and the familiar Hybrid Differencing Scheme (HDS), which is an amalgam of CDS and UDS, were the only known schemes to possess these properties. The inaccuracy of these schemes at large Peclet numbers is well known, and the schemes that will be described in the following sections are intended to improve on this aspect. As will be seen, some of these schemes, in attempting to improve the accuracy, lose the essential qualities of the UDS and HDS schemes, namely conservation and boundedness.

4.3.3 Agarwal Differencing Scheme (ADS)

This scheme, which was developed by Agarwal (Ref. 14) employs the extended nine-point computational molecule shown in Figure 4-2. The scheme is of the finite-difference variety and evaluates the derivatives in the following way.

Convective Terms - These are expressed via Taylor series as:

$$\rho u \left(\frac{\partial \phi}{\partial x}\right)_p \simeq (\rho u)_p \frac{\phi_E - \phi_W}{2\Delta} - \left(\frac{\partial^3 \phi}{\partial x^3}\right)_p \frac{\Delta^2}{6} \tag{4.26}$$

in which $(\partial^3\phi/\partial x^3)_p$ is approximated in an upwind fashion by:

$$u > 0: \quad \frac{\partial^3 \phi}{\partial x^3} \simeq \frac{\phi_E - 3\phi_p + 3\phi_W - \phi_{WW}}{\Delta^3}$$

$$u < 0: \quad \frac{\partial^3 \phi}{\partial x^3} \simeq \frac{\phi_{EE} - 3\phi_E + 3\phi_p - \phi_W}{\Delta^3} \tag{4.27}$$

giving:

$$\rho u \left(\frac{\partial \phi}{\partial x}\right)_p = \left(\frac{\rho u}{6\Delta}\right)_p \left\{ \begin{array}{l} 2\phi_E + 3\phi_p - 6\phi_W + \phi_{WW}, \text{ for } u > 0 \\ -\phi_{EE} + 6\phi_E - 3\phi_p - 2\phi_W, \text{ for } u \leq 0 \end{array} \right\} \tag{4.28}$$

Diffusion Terms - These are evaluated in the usual central difference fashion, giving:

$$\Gamma \left(\frac{\partial^2 \phi}{\partial x^2}\right)_p \simeq \Gamma \left(\frac{\phi_E + \phi_W - 2\phi_p}{\Delta^2}\right) \tag{4.29}$$

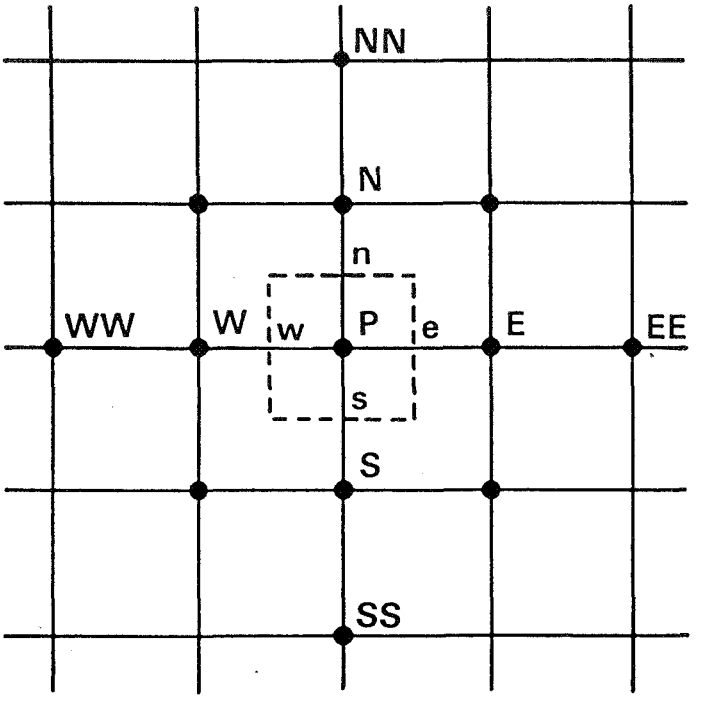

Figure 4-2 Extended Nine-Point Computational Molecule

Approximation of the y derivatives in a like fashion gives, after assembly, the following expressions for the non-zero coefficents of the discretized transport equation, for u, v> o:

$$
\begin{aligned}
a_E &= -\frac{1}{3} C_p + d \\
a_W &= C_p + d \\
a_{WW} &= -\frac{1}{6} C_p \\
a_p &= \frac{1}{2} C_p + 2d
\end{aligned}
\qquad (4.30)
$$

where $C_p \equiv (\rho u)_p \Delta$ and $d \equiv \Gamma/\Delta$

The following are comments on the ADS scheme.

1. This scheme is non-conservative, since Equation 4.27 does not guarantee continuity of convective flux between adjacent pairs of mesh points.

2. It is also not unconditionally bounded, because certain coefficients are either negative or can become so in some circumstances.

Concerning the latter point, Table 4-I gives the form of the coefficients for one-dimensional transport in terms of the ratio Pe = c/d, and their limiting values (after normalization by a_p) when this parameter tends to infinity. Also given is the absolute sum $\Sigma a_i/a_p$, which is a measure of the diagonal dominance of the coefficient matrix. Similar information is provided for the other schemes examined.

TABLE 4-I

ONE-DIMENSIONAL COEFFICIENTS AND THEIR LIMITING VALUES FOR INFINITE PE

						LIMIT PE $\to \infty$				
SCHEME	a_{WW}	a_W	a_E	a_{EE}	a_P	a_{WW}/a_P	a_W/a_P	a_E/a_P	a_{EE}/a_P	$\Sigma\lvert a_i/a_P\rvert$
ADS	$-\frac{Pe}{6}$	$Pe+1$	$-\frac{Pe}{3}+1$	0	$\frac{Pe}{2}+2$	$-\frac{1}{3}$	2	$-\frac{1}{6}$	0	$2\frac{1}{2}$
QUDS	$-\frac{Pe}{8}$	$\frac{7Pe}{8}+1$	$-\frac{3Pe}{8}+1$	0	$\frac{3Pe}{8}+2$	$-\frac{1}{3}$	$\frac{7}{3}$	-1	0	$3\frac{2}{3}$
UDS/ SUDS	0	$\frac{1}{2}(\lvert Pe\rvert + Pe)+1$	$\frac{1}{2}(\lvert Pe\rvert - Pe)+1$	0	$2+\lvert Pe\rvert$	0	1	0	0	1
CDS/ CSS	0	$\frac{1}{2}\left(\frac{Pe}{2}+1\right)$	$\frac{1}{2}\left(-\frac{Pe}{2}+1\right)$	0	1	0	∞	$-\infty$	0	∞

In the present instance it is clear that the negative coefficients are not insignificant in comparison to the positive ones and, moreover, the matrix is far from diagonally dominant. The expectation is therefore that problems of "nonphysical oscillations" and numerical instability may arise in generating solutions for this scheme. Since this scheme is not conservative and unbounded, it does not seem to be a promising scheme and was not considered further.

4.3.4 Quadratic Upwind Differencing Scheme (QUDS)

This scheme, which was proposed by Leonard (Ref. 15), is derived via the finite volume approach. It approximates the diffusion operator using conventional central differencing but uses upstream - biased quadratic interpolation to approximate the convective operator. For example, the term $(\rho u)_w \Delta \phi_w$ is evaluated as follows:

$$(\rho u)_w \Delta \phi_w = (\rho u)_w \Delta \begin{cases} -\frac{1}{8}\phi_{WW} + \frac{3}{4}\phi_W + \frac{3}{8}\phi_P \ , \ u > o \\ -\frac{1}{8}\phi_E + \frac{3}{8}\phi_W + \frac{3}{4}\phi_P \ , \ u \leqslant o \end{cases} \qquad (4.31)$$

The presence of the negative coefficients in the above is noteworthy, for it illustrates the point made earlier about the possibility of these arising when higher-order interpolation is employed. The adoption of these practices for the remaining terms gives, for $(u,v) \geq o$, the following non-zero coefficients:

$$\left.\begin{aligned} a_E &= -\frac{3}{8} C_x + d \\ a_W &= \frac{7}{8} C_x + d \\ a_N &= \frac{3}{8} Cy + d \\ a_{WW} &= -C_x/8 \\ a_{ss} &= -Cy/8 \\ a_p &= \frac{3}{8}(C_x + C_y) + 4d \end{aligned}\right\} \qquad (4.32)$$

where:

$$C_x = (\rho u \Delta)_w = (\rho u \Delta)_e$$

$$C_y = (\rho u \Delta)_n = (\rho u \Delta)_s$$

The following are comments on the QUDS scheme.

1. As already noted, this scheme is conservative.

2. However, it is not unconditionally bounded, as is indicated by the above and Table 4-I which also shows that it departs further from diagonal dominance than the ADS in the large Pe limit. Although this scheme is unbounded in its present form, it can be bounded using the bounding schemes to be described later. Hence this scheme will not be eliminated at present.

4.3.5 Skew Upwind Differencing Scheme (SUDS)

This is a finite volume scheme which was developed by Raithby (Ref. 16) and employs the compact nine-point computational molecule illustrated in Figure 4-1. In this scheme, the convective flux is obtained by employing upwind differencing along streamlines. The streamline direction is defined at each boundary by the velocity direction (Figure 4-3). The convected ϕ is obtained by back-projection of this vector until it intersects a grid line and then interpolation at the intersection point, the interpolation practice varying according to the sector in which the vector lies. By way of illustration, in the example of Figure 4-3, if the intersection lies between W and SW, linear interpolation is used. Thus:

$$\alpha_w^{SW} = \min\,(1\ ,\ Cy/2\ C_x)$$

$$\alpha_w^{W} = 1 - \alpha_w^{SW}$$

and all other α_w are zero. On the other hand, if intersection is between SW and S, $\alpha_w^{SW} = 1$ and all other α_w are zero.

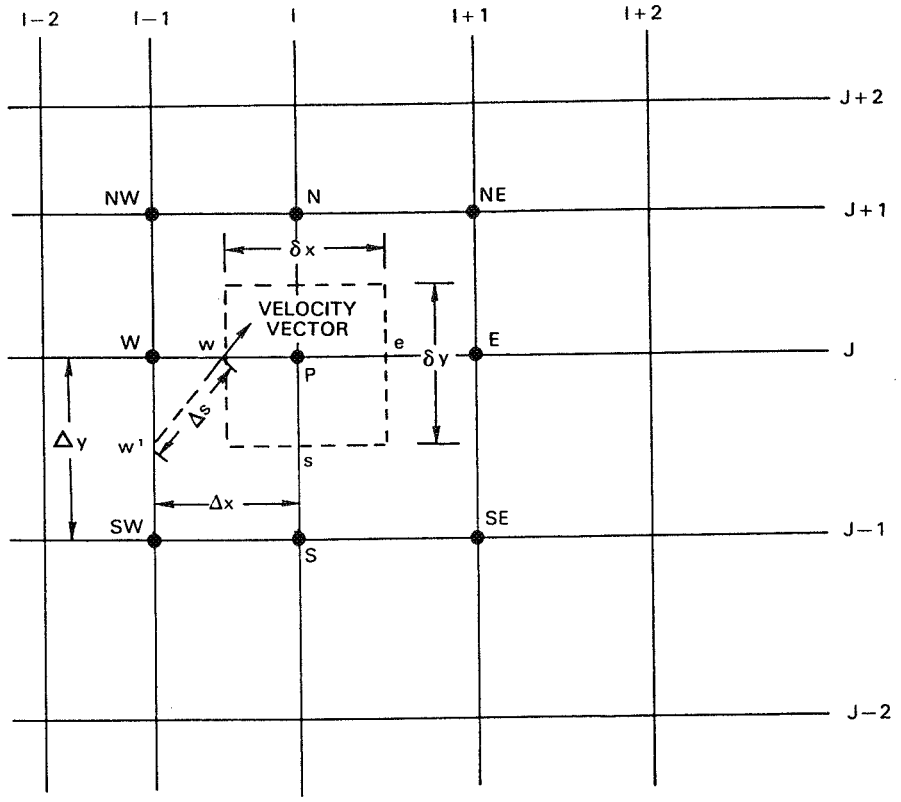

Figure 4-3 Control Volume for Skew Upwind Differencing for West Face of Control Volume and Positive Velocity Components

The above practices give rise, for the particular flow directions shown in Figure 4-3, to the following non-zero coefficient expressions:

$$\left.\begin{aligned} a_W &= d + C_x\,\alpha_w^W - C_y\,\alpha_n^W \\ a_E &= d \\ a_s &= d + C_y\,\alpha_s^S - C_x\,\alpha_e^S \\ a_N &= d \\ a_{sw} &= C_x\,\alpha_w^{SW} + C_y\,\alpha_s^{SW} \\ a_p &= \Sigma\, a_i \end{aligned}\right\} \qquad (4\text{-}33)$$

The following comments concern the SUDS scheme.

1. This scheme is conservative for reasons already explained.

2. It is not, however, unconditionally bounded because the net convective contributions to a_W and a_S can be of either sign. This condition is a consequence of the fluxes leaving through the n and e cell faces being linked to ϕ_W and ϕ_S, respectively.

3. The scheme reduces to the UDS when the mesh and flow are aligned, so in these circumstances it <u>is</u> bounded.

On the basis of the second comment it can be expected that the solutions produced by SUDS may exhibit "nonphysical oscillations" and may be difficult to obtain due to the matrix not being diagonally dominant. Although this scheme is not unconditionally bounded it will be retained for further accuracy evaluation because it can be bounded by the bounding schemes to be described later.

4.3.6 Cubic Spline Scheme (CSS)

The adjective "spline" will be used here to denote schemes based on assumed interpolation formulae whose coefficients are linked to nodal values of ϕ <u>and</u> one or more of its derivatives, ($\phi' = m$) and ($\phi'' = M$). A particular scheme will be examined briefly, namely the Cubic Spline Scheme (CSS), which has been employed by Rubin and Graves (Ref. 17), Vacca, Werle and Polak (Ref. 18) and Kumar (Ref. 19), among others. A cubic spline:

$$S = \sum_{i=0}^{3} a_i \, (x - x_s)^i$$

in the interval $x_{j-1} < x < x_j$, is a polynomial function which is continuous in ϕ, m and M such that:

$$S'' = M_{j-1} \frac{(x_j - x)}{\Delta} + M_j \frac{(x - x_{j-1})}{\Delta} \tag{4-34}$$

and hence, by integration:

$$S = M_{j-1} \frac{(x_j - x)^3}{6\Delta} + M_j \frac{(x - x_{j-1})^3}{6\Delta} + \left(\phi_{j-1} - M_{j-1} \frac{\Delta^2}{6}\right) \left(\frac{x_j - x}{\Delta}\right) + \left(\phi_j - M_j \frac{\Delta^2}{6}\right) \left(\frac{x - x_{j-1}}{\Delta}\right) \tag{4-35}$$

where $\Delta = x_j - x_{j-1}$. The M_j in the above equation are unknown, but can be related to the ϕ_j by requiring continuity of M_j at the matching of two splines, to give:

$$M_{j-1} + 4M_j + M_{J+1} = \frac{6}{\Delta^2} (\phi_{j-1} - 2\phi_j + \phi_{j+1}) \tag{4-36}$$

A similar derivation provides the following link between the m_j and ϕ_j.

$$m_{j-1} + 4\, m_j + m_{j+1} = \frac{3}{\Delta} (\phi_{j+1} - \phi_{j-1}) \tag{4-37}$$

The above, along with the functional relation between ϕ_j, M_j and m_j obtained by applying the differential equation to be solved at the nodal points, i.e.,

$$f (\phi_j, m_j, M_j) = 0 \tag{4-38}$$

produces three coupled sets of equations in the three unknowns. The resulting block 3 x 3 tridiagonal matrix requires in general an inversion procedure for solution, so the properties of the equations and the results they will produce are not so readily analyzed as were the earlier schemes considered here. However, the example application described below is a useful exception to this rule.

We consider the solution by the CSS of the 1-D convection-diffusion equation (designated in later sections as test Case OD1) for which the governing differential equation is, in the present notation:

$$\frac{Pe_\Delta}{\Delta} m_j - M_j = 0 \tag{4-39}$$

where $Pe_\Delta = \rho u \Delta / \Gamma$ is a Peclet number. This equation can be used to eliminate the M_j from Equation 4.36, thus:

$$\frac{P_{e\Delta}}{\Delta} (m_{j-1} + 4m_j + m_{j+1}) = \frac{6}{\Delta 2} (\phi_{j+1} - 2\, \phi_j + \phi_{j-1}) \tag{4.40}$$

The m_j can now be eliminated by combining Equations 4.37 and 4.40 to yield:

$$\frac{Pe_\Delta\, (\phi_{j+1} - \phi_{j-1})}{2} = \phi_{j+1} + \phi_{j-1} - 2\, \phi_j \tag{4-41}$$

or, in the "compass" notation and after rearrangement:

$$\phi_p = \frac{1}{2} \left(1 - \frac{Pe_\Delta}{2}\right) \phi_E + \frac{1}{2} \left(1 + \frac{Pe_\Delta}{2}\right) \phi_W \tag{4-42}$$

The above equation is identical to Equation 4.24 which was produced by three-point centered differencing.

The properties of the CDS are well-known and have been reviewed in Section 4.3.1. Briefly, the scheme is second order, positive and bounded provided that $Pe_\Delta < 2$. Above this value, diagonal dominance is lost, "nonphysical oscillations" occur, and the accuracy generally falls below that of lower order schemes. The available evidence about the CSS falls within this pattern; it should be noted that, in nearly all applications reported in the literature where the scheme has been successfully applied, the cell Peclet number Pe_Δ has been at or below the critical level in regions with steep gradients (Ref 4.5).

It would appear that the CSS is unlikely to be useful in the convection-dominated circumstances of interest in the present study; in some cases, it may be disadvantageous. Similar comments are likely to apply to higher order centered splines, the common deficiency being infringement of the transportation property. For convection-dominated flows, it may be useful to introduce the notion of an upwind-biased spline, as has been done in a preliminary way by Kumar (Ref. 19), but this is a matter for future research. No further consideration will therefore be given to the CSS in the remainder of this report.

4.3.7 Glass and Rodi Hermitian Scheme (GRHS)

This scheme, developed by Glass and Rodi (Ref. 20), uses a cubic interpolation polynomial instead of a cubic spline. This polynomial can be written in the following form in two dimensions.

$$\phi = \sum_{i=1}^{4} (a_i \phi_i + a_{x,i} m_{x,i} + a_{y,i} m_{y,i} + a_{xy,i} M_{xy,i}) \qquad (4.43)$$

where the a's are cubic polynomials in x and y, and m_x, m_y, and M_{xy} denote $\partial\phi/\partial x$, $\partial\phi/\partial y$ and $\partial^2\phi/\partial x\partial y$, respectively. This interpolation formula is employed in an explicit, time-marching method of characteristics calculation of convection whose essential features are listed below.

1. At each new time level, the characteristic line (i.e. particle path) passing through each grid node is traced back to the previous level from knowledge of the velocity field.

2. The value of ϕ at the intersection point of the characteristic with the old time level plane is determined using Equation 4.43 for each cell. This value is used to evaluate the convective flux.

3. The values of ϕ_j, m_j and M_j appearing in Equation 4.43 are determined at each mesh point by solving transport equations for them; those for M_j being derived through differentiation of the ϕ transport equation.

The novel character of this method complicates evaluation and comparison with the other schemes considered here. Also, this time-marching scheme is not compatible with the present steady-state formulation. It is acknowledged by its developers to be non-conservative (although they show that if the mesh is sufficiently fine to give good accuracy in ϕ, the conservation errors are also small). It is also not unconditionally bounded, but there is no obvious reason why the coefficients in Equation 4.43 cannot become negative. In addition, the usual stability limits on an explicit method apply, e.g., in one dimension:

$$\frac{u\delta t}{\Delta} < 1 \ , \ \frac{\Gamma_\Delta t}{\Delta^2} < \frac{1}{2} \tag{4.44}$$

The accuracy of the method, for the test cases examined by its developers, is markedly superior to those of CDS and UDS with which they were compared. It required about twice as much computing time as CDS and UDS on a given mesh, but on a time-for-given-accuracy basis it would undoubtedly prove better. These, however, were explicit calculations which invariably require substantially more time to reach the steady state than do implicit methods. The utility of the approach for the present purposes then depends on whether it can be implemented implicitly. This matter is beyond the scope of the present study, so the GRHS was also excluded from further consideration here.

4.3.8 Schemes Generated by Flux Blending

All of the otherwise desirable schemes that have been studied in this section suffer from the defect that the coefficients generated by these schemes are not unconditionally positive. Negative coefficients are not desirable from stability and boundedness considerations.

Hence, a method is needed that would either make the coefficients unconditionally positive or at least modify them so that the solution obtained remains within bounds. It is apparent that in the absence of this method all of the schemes studied so far will have serious flaws. There are only a few such methods available in the literature. A. D. Gosman (consultant to this program) and his co-workers at Imperial College, London, have been working on what are called Flux Blending Schemes. These schemes will be described in detail below.

4.3.8.1 The Flux Blending Strategy

The concept of flux blending was prompted by the "Flux Corrected Transport". (FCT) technique developed by Boris and Book (Ref. 21) and others, in the context of explicit time-marching techniques. The approach adopted here for implicit steady-state calculations was developed by Gosman and Lai (Ref. 13) and Gosman and Peric (Ref. 22) and differs from FCT in several important respects. It operates as follows: in the assembly of a flux-blended scheme, the flux F at each cell boundary is expressed as the weighted mean of a bounded (but perforce "low order") scheme, F^L and an unbounded, but higher order scheme, F^H, thus:

$$F = \gamma F^H + (1-\gamma) F^L \tag{4.45}$$

Here γ, the blending factor ($0<\gamma<1$) is uniquely defined at the cell boundary in question, so that the blended scheme is conservative. The other important requirement on γ is that it should be as large as possible, within the overriding constraint that the solution should be properly bounded.

Two alternative strategies have been developed for ensuring that the last named requirement is fulfilled (or nearly so). These strategies are listed below.

a) Strategy 1 - This strategy operates by choosing γ so as to suppress negative coefficients in the blended scheme: this, as was demonstrated earlier, is a sufficient condition for a bounded solution. This is the approach used by Gosman and Lai (Ref. 13).

b) Strategy 2 - This strategy, which was developed under the present contract, ensures that when negative coefficients occur, their contribution to the solution is below the level which would cause it to be out of bounds. This approach is more akin to the original FCT.

Each of these strategies has its advantages and disadvantages which are best brought out by examining the properties of some specific flux-blended schemes. Three of these will now be described, namely BSUDS1, which is a blend of the UDS and SUDS schemes based on strategy 1; BSUDS2, which blends the same schemes using strategy 2; and BQUDS, which uses the latter strategy to blend the UDS and QUDS.

4.3.8.2 The BSUDS1 Scheme

It is not difficult to show that if the UDS and SUDS fluxes are blended in the manner just described, the resulting non-zero coefficients for ($u, v \geq o$) are:

$$\left.\begin{aligned} a_W &= d + C_x\,(1 + \gamma_w\,\alpha_w^W - \gamma_w) - \gamma_n\,C_y\,\alpha_n^W \\ a_E &= d \\ a_S &= d + C_y\,(1 - \gamma_s\,\alpha_s^S) - \gamma_e\,C_x\,\alpha_e^S \\ a_N &= d \\ a_{SW} &= \gamma_w\,C_x\,\alpha_w^{SW} + \gamma_s\,C_y\,\alpha_s^{SW} \\ a_p &= \Sigma\, a_i \end{aligned}\right\} \qquad (4.46)$$

where the α are defined as before. Note that for the present, $\gamma_e = \gamma_w = \gamma_x$ and $\gamma_n = \gamma_s = \gamma_y$. The above coefficients bear a close similarity to those of the parent SUDS scheme, (c.f. Equation 4.33) but it is clear that in the present case it is always possible to avoid negative coefficients through appropriate specification of the γ's.

The determination of the appropriate γ field is however a non-trivial matter, for inspection of the expressions for a_W and a_S (the only coefficients which could become negative in the present circumstances) reveals that the values are interdependent; i.e. a_W and a_S contain both γ_x and γ_y as do certain of the other coefficients.

What has in fact emerged is an optimization problem of the following kind. Maximize the object function:

$$F(\gamma) = \gamma_1 + \gamma_2 \tag{4.47}$$

subject to the constraints that:

$$0 \leq \gamma \leq 1 \tag{4.48}$$

$$a_i = (e_i - f_i \gamma_{1,i} - g_i \gamma_{2,i}) > 0 \tag{4.49}$$

where $\gamma_{1,i}$ and $\gamma_{2,i}$ are the weighting factors appearing in a particular coefficient a_i and $(e_i - f_i \gamma_{1,i})$, and g_i are positive quantities deducible from the definition of that coefficient. For example,

$e_W = d + c_X$, $f_W = C_X (1 - \alpha_W^W)$; $g_W = C_y \alpha_n^W)$

Lai Ref. 23 used the 'Simplex' optimization method for this purpose and derived the following expressions for the optimum γ.

$$\gamma_y = \gamma_{1,i}^{opt} = 1 \tag{4.50}$$

$$\gamma_x = \gamma_{2,i}^{opt} = \begin{cases} 1, \text{ if } Pe_y > 2C_y/(C_x - C_y) \text{ and } 1 < \dfrac{C_x}{C_y} < 2 \\ 2(1/Pe_y + 1 - k_y) \quad \text{otherwise} \end{cases} \tag{4.51}$$

where: $K_y = \min (1, c_x/2 C_y)$

The follow are comments on the BSUDS1 scheme.

1. This scheme is conservative, has positive coefficients, and is unconditionally bounded.

2. In contrast to the FCT method, it operates only on the coefficients and makes no explicit reference to, or requires knowledge of, the solution bounds.

3. Because the resulting coefficient matrix is unconditionally diagonally dominant, numerical stability problems are minimized.

4. It has, however, two disadvantages: firstly, the positive coefficient requirement can be argued to be overly-stringent (i.e. it is a "sufficient" rather than a "necessary" condition for boundedness) and may lead to excessive blending of the low-order scheme; and secondly, it is only applicable when the computational molecules of the low and high order schemes coincide at those nodes where the latter produces negative coefficients. (In this respect the UDS and SUDS schemes are well-matched, for SUDS has positive coefficients at all but the principal nodes N, S, E and W). These disadvantages are overcome (at the expense of others) by the second blending strategy, which will now be described.

4.3.8.3 The BSUDS2 and BQUDS2 Schemes

As mentioned earlier, Blending Strategy 2 relaxes the positive coefficient requirement and replaces it with one of adherence to estimated bounds on ϕ. This gives rise to two distinct problems; one being to determine the bounds in a sufficiently general way, and the other to work out the appropriate γ values. This latter aspect will be dealt with first, on the assumption that the bounds are known.

The γ calculation is iterative and starts from an initial prescription of unity values everywhere. In the first stage of each iteration the γ values at all boundaries of a particular cell are taken to be equal when it is first considered. This allows the coefficients of the difference equation to be expressed in the following general way in the first iteration:

$$a_i = a_i' + \gamma a_i'' \tag{4.52}$$

$$(a_i' + \gamma \ a_i'') \phi_p = a_i'\phi_i + \gamma \ a_i''\phi_i \tag{4.53}$$

where a_i' contains those terms not depending on γ, and $\gamma a_i''$ contains the remainder. Let the solution to Equation 4.53 for given ϕ_i be ϕ_p and let the known lower and upper bounds, one of which will be imposed if ϕ_p lies outside them, be ϕ_{min} and ϕ_{max} respectively. It is then easy to show that if:

a) $\tilde{\phi}_p > \phi_{max}$ then

$$\gamma = \frac{\phi_{max}\Sigma a_i' - a\Sigma a_i'\phi_i}{\Sigma a_i''\phi_i - \phi_{max}\Sigma a_i'} \tag{4.54}$$

b) $\tilde{\phi}_p < \phi_{min}$ then

$$\gamma = \frac{(\Sigma a_i'\phi_i - \phi_{min}\Sigma a_i')}{\phi_{min}\Sigma a_i'' - \Sigma a_i''\phi_i} \tag{4.55}$$

if ϕ is within bounds, γ is simply left unchanged at the prevailing level.

It should be noted that these equations are valid only in the absence of sources and will be modified when sources are present (see Section 5.1.5).

The foregoing procedure produces a field of γ's which is non-unique, for in general, two values will have been calculated for each cell face. This is resolved in a second stage simply by taking the minimum of the two values in the knowledge that this is a "safe" practice, i.e., it will always maintain the bounds. This completes the iteration, after which $(a_i'')^m$ is replaced by $(\gamma a_i'')^{m-1}$ (where m is the iteration counter) in preparation for the next cycle.

There remains the non-trivial matter of how ϕ_{min} and ϕ_{max} are to be determined. This is the subject of continuing research, but quite encouraging results have been obtained by requiring that ϕ should be separately bounded by the prevailing neighboring ϕ_j along each grid line passing through P. In the model problem studies, this produces two estimates for the bounds, viz.,

$$(\phi_{min,\ max})_1 = \min,\ \max\ (\phi_E,\ \phi_W) \tag{4.56}$$

$$(\phi_{min,\ max})_2 = \min,\ \max\ (\phi_N,\ \phi_S) \tag{4.57}$$

and the practice is to calculate ϕ via Equations 4.56 and 4.57 for both and then take the minimum value. There are other alternatives to this scheme and this formulation is the one which was found useful for model problem studies. For the two and three dimensional codes, this formulation is replaced by another method of computing bounds on ϕ_p (see equations 5-54 and 5-55).

The application of this blending practice to SUDS and QUDS (for which the UDS has been used as the lower order scheme) is now a straightforward matter of deducing the appropriate expressions for the a_j' and a_j''. This has been done and is summarized in Table 4-II.

TABLE 4-II

COEFFICIENTS OF BQUDS AND BSUDS2 FOR THE CASE OF POSITIVE RADIAL AND AXIAL VELOCITIES

SCHEME	COEFFICIENTS ($u>0, v>0$)							
	a_E	a_W	a_N	a_S	a_{EE}	a_{WW}	a_{NN}	a_{SS}
BQUDS	$d_e - \frac{3}{8}\gamma_e C_e$	$d_w + C_w - \frac{2}{8}\gamma_w C_w + \frac{1}{8}\gamma_e C_e$	$d_n - \frac{3}{8}\gamma_n C_n$	$d_s + C_s - \frac{2}{8}\gamma_s C_s + \frac{1}{8}\gamma_n C_n$	0	$-\frac{1}{8}\gamma_w C_w$	0	$-\frac{1}{8}\gamma_s C_s$

SCHEME	COEFFICIENTS ($u>0, v>0$)							
	a_E	a_W	a_N	a_S	a_{NE}	a_{NW}	a_{SE}	a_{SW}
BSUDS2	d_e	$d_w + C_w - \gamma_w C_w(1-\alpha_w^W) - \gamma_n C_n \alpha_n^W$	d_n	$d_s + C_s - \gamma_s C_s(1-\alpha_s^S) - \gamma_e C_e \alpha_e^S$	0	0	0	$\gamma_w C_w \alpha_w^{SW} + \gamma_s C_s \alpha_s^{SW}$

Comments

1. The advantages of this blending procedure are that it is capable in principle of producing conservative and bounded solutions for any high-order scheme which is itself conservative, i.e. the "overlapping molecule" structures of the strategy 1 do not apply.

2. There are however several disadvantages as compared with strategy 1:

   a) The difference equations are now non-linear (i.e. the a_i's depend on the ϕ's through γ) even when the parent differential equation is not. Therefore, the cost and complexity of obtaining solutions increases. On the other hand, in many practical calculations the a_i are not constants anyway.

   b) The solution is only guaranteed to be bounded when the final result is obtained, so precautions must be taken to avoid the adverse consequences of overshoots at intermediate stages (see Appendix A-5).

   c) The coefficient matrix will not necessarily be diagonally dominant (although whatever lower-order blending is performed will increase diagonal dominance) so numerical stability problems may still arise.

   d) The uniqueness of the solution cannot be guaranteed due to the non-linearity of the equations and somewhat arbitrary although logical method of estimating the bounds. Studies thus far suggest that this is not a serious problem in practice.

Thus far, attention has been focused on the conservation and boundedness properties of the schemes chosen for evaluation. Based on this preliminary screening, three schemes, namely the ADS, the CSS and GRHS, were excluded from further evaluation; possible defects (negative coefficients) were identified in certain of the others. Recognition of these defects led to the development of flux blending schemes and these have been described in detail.

4.4 ACCURACY EVALUATION

This section contains a discussion of the accuracy evaluation of the remaining schemes.The consequences of the defects identified in the schemes in the previous section will also become apparent. The flux blending strategies will also be applied to some of the chosen schemes and their effect on the accuracy, stability and boundedness of these schemes will be studied by calculating some test cases.

4.4.1 Truncation Error Analysis

The formal Taylor Series Truncation Errors (TSTEs) of the schemes chosen in the previous section for further evaluation will now be presented and discussed. Since it is the accuracy of representation of the convective terms which is the critical issue, these TSTEs have been evaluated for the limiting case of purely convective transport. To facilitate interpretation of the results in terms of their numerical diffusion implications, the flow has been chosen to be uniform and parallel.

The truncation error expressions are given in different forms in Tables 4-III and 4-IV. For obvious reasons no entries appear for schemes based on the flux blending strategy 2, i.e. BSUDS2 and BQUDS2, but it can be assumed that the associated TSTEs will be strongly biased towards the higher-order component of the blend. Evidence to this effect can be seen in the TSTE for BSUDS1, discussed below. Although ADS has been eliminated from consideration, it is included in this discussion because it turns out to be the most accurate scheme based on TSTE analyses and reinforces the argument against using only Taylor series analyses for accuracy evaluation.

TABLE 4-III

TRUNCATION ERRORS FOR THE CONVECTIVE TERMS OF THE UDS, SUDS, BSUDS1, QUDS AND ADS FOR A UNIFORM FLOW AND SQUARE MESH: CARTESIAN COORDINATE VERSIONS

SCHEME	TRUNCATION ERROR
UDS	$\frac{1}{2}\rho\Delta\left(u\frac{\partial^2\phi}{\partial x^2}+v\frac{\partial^2\phi}{\partial y^2}\right)$
SUDS	$\frac{1}{2}\rho\Delta\left[u\frac{\partial^2\phi}{\partial x^2}+v\frac{\partial^2\phi}{\partial y^2}+2v\left(\frac{1}{2}+k\right)\frac{\partial^2\phi}{\partial x\partial y}\right];\ k=\min\left(1,\frac{u}{2v}\right)$
BSUDS1	$\frac{1}{2}\rho\Delta\left[u\frac{\partial^2\phi}{\partial x^2}+v\frac{\partial^2\phi}{\partial y^2}+2v\frac{\partial^2\phi}{\partial x\partial y}\right]$
QUDS	$-\frac{1}{24}\rho\Delta^2\left[u\frac{\partial^3\phi}{\partial x^3}+v\frac{\partial^3\phi}{\partial y^3}\right]$
ADS	$-\frac{1}{12}\rho\Delta^3\left[u\frac{\partial^4\phi}{\partial x^4}+v\frac{\partial^4\phi}{\partial y^4}\right]$

The entries of Table 4-III express the TSTE's in the original Cartesian coordinates (x, y) and the corresponding velocity components (u, v) in which they were derived. However it is more instructive to transform them into the "streamline" coordinates (s,n), where s and n are measured along and normal to the streamlines, respectively. Table 4-IV contains the transformed versions, certain terms of which are singled out for attention by enclosing them in square brackets. These forms involve derivatives in the streamline direction which, in the present convection-dominated circumstances, will be negligible in the absence of sources, thus, it can be argued, it is the remaining terms, involving cross-stream derivatives, which are the principal source of error, (provided of course that the TSTE is truly representative of the error, a point which will be discussed later).

According to Table 4-IV the hierarchy of the various schemes is as follows: 1) UDS, SUDS and BSUDS1-1st order; 2) QUDS - second order; 3) ADS- third order, where the "order" refers to the exponent on the mesh spacing Δ. If, as in many finite difference analyses "order" is erroneously taken to be synonymous with "accuracy", then the ADS would stand out as superior to the other schemes and the UDS, SUDS and BSUDS1 would be collectively dismissed as having the same low accuracy. This interpretation is now widely recognized as being misleading and evidence to support this view will be given here.

TABLE 4-IV

TRUNCATION EXPRESSIONS OF TABLE 4-III, TRANSFORMED INTO (s, n) STREAMLINE COORDINATES

SCHEME	TRUNCATION ERROR
UDS	$\frac{1}{2}\rho\lvert V\rvert\Delta\left\{\frac{\sqrt{2}}{2}\sin(2\theta)\sin(\pi/4+\theta)\frac{\partial^2\phi}{\partial n^2}+\left[(\cos^3\theta+\sin^3\theta)\frac{\partial^2\phi}{\partial s^2}+\sin(2\theta)(\sin\theta-\cos\theta)\frac{\partial^2\phi}{\partial s\partial n}\right]\right\}$
SUDS	$\frac{1}{2}\rho\lvert V\rvert\Delta\left\{\frac{1}{2}\sin(2\theta)(\cos\theta-2\sin(\theta K)\frac{\partial^2\phi}{\partial n^2}+\left[\cos^3\theta+\sin^3\theta+\sin\theta\sin(2\theta)\ (\tfrac{1}{2}+K)\frac{\partial^2\phi}{\partial s^2}\right.\right.$ $\left.\left.+\ (\sin(2\theta)(\sin\theta-\cos\theta)+2\sin\theta\cos(2\theta)(\tfrac{1}{2}+K)\frac{\partial^2\phi}{\partial s\partial n}\right]\right\}$; $K=\min(1,\frac{1}{2}\frac{u}{v})$
BSUDS1	$\frac{1}{2}\rho\lvert V\rvert\Delta\left\{\frac{\sqrt{2}}{2}\sin(2\theta)\ \sin(\pi/4-\theta)\frac{\partial^2\phi}{\partial n^2}+\left[(\cos^3\theta+\sin^3\theta+\sin\theta\sin(2\theta)\frac{\partial^2\phi}{\partial s^2}\right.\right.$ $\left.\left.\left((\sin(2\theta)(\sin\theta-\cos\theta)+2\sin\theta\cos(2\theta)\right)\frac{\partial^2\phi}{\partial s\partial n}\right]\right\}$
QUDS	$\frac{-1}{24}\rho\lvert V\rvert\Delta^2\left\{\frac{1}{4}\sin(4\theta)\frac{\partial^3\phi}{\partial n^3}+\left[(\cos^4\theta+\sin^4\theta)\frac{\partial^3\phi}{\partial s^3}-\frac{3}{2}\sin(4\theta)\frac{\partial^3\phi}{\partial s^2\partial n}+\frac{3}{2}\sin^2(2\theta)\frac{\partial^3\phi}{\partial s\partial n^2}\right]\right\}$
ADS	$\frac{-1}{12}\rho\lvert V\rvert\Delta^3\left\{\frac{1}{2}\sin2\theta(\sin^3\theta+\cos^3\theta)\frac{\partial^4\phi}{\partial n^4}+\left[(\cos^3\theta+\sin^3\theta)\frac{\partial^4\phi}{\partial s^4}+2\sin(2\theta)(\sin^3\theta-\cos^3\theta)\frac{\partial^4\phi}{\partial s^3\partial n}\right.\right.$ $\left.\left.+\frac{3}{2}\sin^2(2\theta)\cos\theta+\sin\theta)\frac{\partial^4\phi}{\partial s^2\partial n^2}+\sin^2(2\theta)(\cos\theta-\sin\theta)\frac{\partial^4\phi}{\partial s\partial n^3}\right]\right\}$

It is conventional to interpret those TSTE's which contain second derivatives, e.g. $\partial^2\phi/\partial x^2$, $\partial^2\phi/\partial y^2$, $\partial^2\phi/\partial n^2$ as being diffusion-like, by analogy with the "real" diffusion terms in the full transport Equation 4.1. This analogy allows a numerical diffusion coefficient Γ_{num} to be defined as the ratio:

$$\Gamma_{num} = TSTE/(\partial^2\phi/\partial x^2) \qquad (4.59)$$

and evaluated for schemes having TSTE's of this kind. These comprise the first-order UDS, SUDS and BSUDS1. Table 4-V gives the numerical diffusivity formulae, which are all of the general form

$$\Gamma_{num} = \rho \Delta |v| f(\theta) \tag{4.59}$$

TABLE 4-V

NUMERICAL DIFFUSIVITY EXPRESSIONS FOR UDS, SUDS AND BSUDS1 IN STREAMLINE COORDINATES

SCHEME	Γ_{num}
UDS	$\frac{\sqrt{2}}{4}\rho\Delta\|\vec{V}\|\sin(2\theta)\sin(\pi/4+\theta)$
SUDS	$\frac{1}{4}\rho\Delta\|\vec{V}\|\sin(2\theta)[\cos(\theta)-2\sin(\theta k)]$; $k \equiv \min\left(1, \frac{u}{2v}\right)$
BSUDS1	$\frac{\sqrt{2}}{4}\rho\Delta\|\vec{V}\|\sin(2\theta)\sin(\pi/4-\theta)$

where $|v| = (u^2 + v^2)^{1/2}$ and $\theta = \tan^{-1}(u/v)$ are, respectively, the magnitude of the resultant velocity and the angle which it makes with the mesh. The function $f(\theta)$ is dimensionless and is plotted in Figure 4-4 for each of the schemes mentioned. The plot is terminated at $\phi = 45^\circ$ because the functions are all symmetrical about this angle. It can be seen that i) the levels and variations of Γ_{num} produced by the three schemes are quite different, indicating that their "order" is an incomplete indicator of their relative performance; ii) the SUDS is substantially better than the UDS, and BSUDS1 is between the two, but strongly biased towards the former; and iii) whereas Γ_{num} for the UDS increases monotonically from zero at $\theta = 0$ to a maximum at $\theta = 45^\circ$, the other schemes have their maxima at intermediate angles and have zeros at the two extremes. On the basis of these results and the mode of operation of BSUDS2 it can be conjectured that it would probably fall between SUDS and BSUDS1.

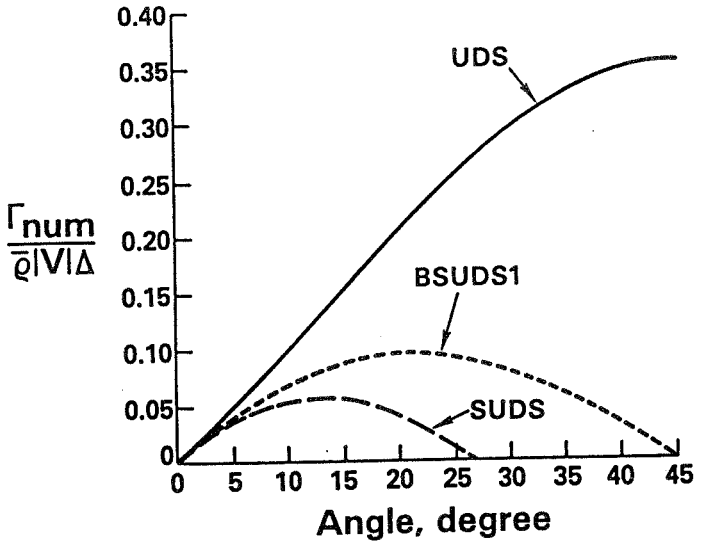

Figure 4-4 Comparison of Numerical Diffusivities for Discretization Schemes

As a final comment, it should be noted that, while the TSTE's of the ADS and QUDS are not diffusion-like and therefore do not permit the evaluation of a Γ_{num}, it is not correct to imply that they will not produce numerical smearing or other unfavorable effects; this will be shown in the test cases described in Section 4.4.3.

4.4.2 Description of Test Cases for Accuracy Assessment

The test cases chosen here to evaluate the discretization schemes are ones for which it is possible to obtain exact solutions to the governing equations. The cases fall into two classes according to whether they are one- or two-dimensional. Within the latter there is a further sub- division according to whether "single-cell" or "field" calculations are performed. In the first-named kind, a single computational molecule is considered and is analyzed using the difference equation by inserting the exact analytical values for the neighboring ϕ and comparing the result with the exact ϕ. The fact that an algebraic formula is obtained for the ϕ error is convenient for analysis, but the approach has the disadvantage of not showing the error propagation and accumulation effects that often occur in practical calculations. Hence, "field" tests, in which calculations are performed over a representative computing mesh with the exact values imposed at the boundaries only, were also included.

In this section, all of the test cases are described. Results of the model problem studies based on these test cases are discussed in Section 4.4.3. Unless otherwise stated, these test cases pertain to situations in which ρ, u, v and are everywhere uniform (which means that the flow is everywhere uniform and parallel). The computing mesh has square cells of side Δ. It should be noted that most schemes were not applied to all test cases: Table 4-VI shows the various combinations examined.

TABLE 4-VI

SUMMARY OF THE COMBINATIONS OF DISCRETIZATION SCHEME AND TEST CASE EXAMINED

	Model problem								
Scheme	OD1	OD2	OD3	TDF1	TDF2	TDF3	TDF4	TDS1	TDS2
QUDS	✓	✓	✓	✓	✓	✓	✓	✓	
SUDS				✓	✓	✓	✓	✓	✓
BSUDS1				✓		✓	✓	✓	✓
BSUDS2				✓	✓				
BQUDS	✓	✓		✓	✓				
UDS		✓		✓	✓	✓	✓	✓	✓

4.4.2.1 One-Dimensional Cases

These represent solutions to the one-dimensional transport equation.

$$\frac{d\phi}{dx^*} - \frac{1}{Pe_L}\frac{d^2\phi}{dx^{*2}} = S^* \qquad (4.60)$$

where $x^* = x/L$, $Pe_L = \rho uL/\Gamma$, $S^* = SL\rho u$ and L is a characteristic length. The following test cases were examined:

(a) Convection and diffusion in absence of source, Test Case (OD1).

Here $S^* = 0$ and the boundary conditions $\phi = 0, 1$ at $x^* = 0, 1$ are imposed to give:

$$\phi = \frac{\exp (Pe_L x^*) - 1}{\exp (Pe_L) - 1} \tag{4.61}$$

(b) Convection with no diffusion and linear source, Test Case (OD2).

This is similar to case OD1 above, but the source S^* is now a piecewise-linear distribution. This test case was also employed by Leonard (Ref. 15) in his presentation of the QUDS scheme. The exact solution is of the form;

$$\phi = \phi_0 + a (x^* - x_0^*) + b (x^* - x_0)^2 \text{ , for } x^* \geq x_0^* \tag{4.62}$$

where x^* is the starting point of the source and a and b are constants linked to its level and gradient.

(c) Convection with no diffusion and plane source (OD3).

For this case Pe is assumed to be infinitely large, $S^*=1$ at $x^*=0.2$ and is zero elsewhere, and $\phi = 0$ at $x^*=0$. The solution is:

$$\phi = 0 \text{ , } x^* < 0.2$$
$$\phi = 1 \text{ , } x^* > 0.2$$

4.4.2.2 Two-Dimensional Cases

For these test cases, solutions are obtained to the two-dimensional transport equation,

$$\rho u \frac{\partial \phi}{\partial x} + \rho v \frac{\partial \phi}{\partial y} - \Gamma \left(\frac{\partial^2 \phi}{\partial x^2} + \frac{\partial^2 \phi}{\partial y^2}\right) = 0 \tag{4.63}$$

for the different circumstances described below. These cases will be denoted by "TD" with a suffix S or F to indicate whether they were used for single cell or field evaluations, respectively.

(a) Convection in Absence of Diffusion

Three cases are considered for the convection of a prescribed distribution ϕ (n), where n is the coordinate normal to the streamlines. In two of the cases the flow is uniform and parallel, Figure 4-5, but in the third case, the streamline pattern corresponds to irrotational plane stagnation flow (Figure 4-6) in which the ϕ are found to be rectangular hyperbolae, i.e.

$$\phi = xy \tag{4.64}$$

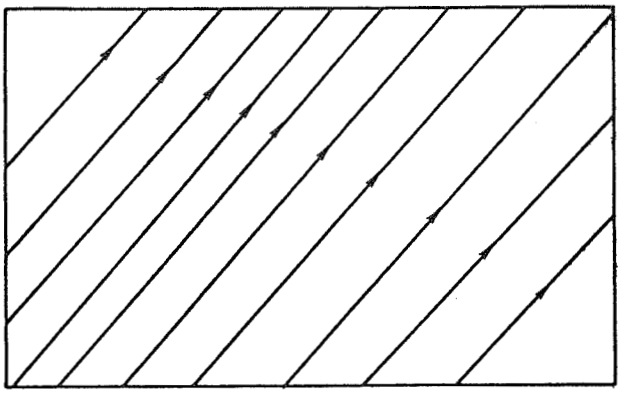

Figure 4-5 Uniform and Parallel Flow

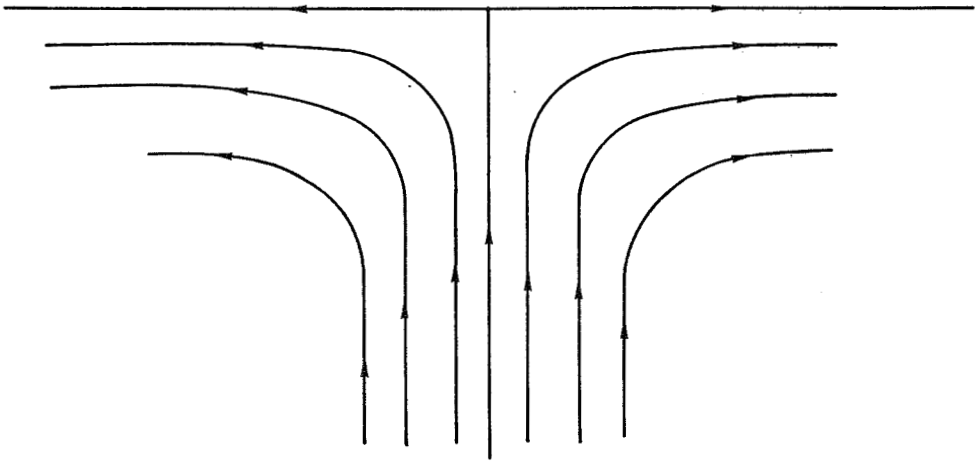

Figure 4-6 Inviscid Plane Stagnation Flow

In all cases the exact solution is simply $\partial\phi/\partial S = 0$ where S is the streamline coordinate: thus on each streamline ϕ is constant and equal to its initial value.

(i) Single Cell Calculation of Convection of a Gaussian Distribution in Uniform Flow (TDS1) - Here $\phi(n) = \exp(-1/2\ (n\Delta^*)^2)$ where $\Delta^* = \Delta/\sigma$, σ is the standard deviation of the Gaussian, and n is measured from the streamline passing through node P, Figure 4-7.

(ii) Field Calculation of Convection of a Step Function in Uniform Flow (TDF1) - In this case

$$\phi(n) = 0 \text{ , for } n < n_s$$
$$1 \text{ , for } n \geq n_s \qquad (4.65)$$

where n_s denotes a selected reference streamline.

(iii) Field Calculation of Convection of a Square Wave Function in Irrotational Plane Stagnation Flow (TDF2)

$$\phi(n) = 1 \text{ for } n_{s1} \leq n \leq n_{s2}$$
$$= 0 \text{ otherwise} \qquad (4.66)$$

where n_{s1} and n_{s2} denote reference streamlines.

(b) Field Calculations of Convection and Diffusion of Initial Step Profile in Uniform Flow (TDF3)

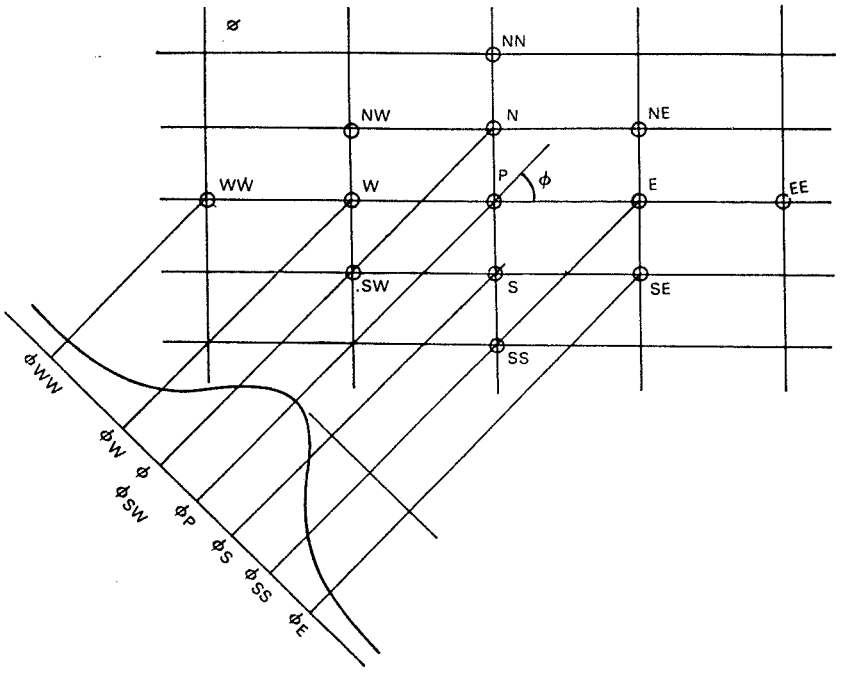

Figure 4-7 Single Cell Calculation of Convection of a Gaussian Distribution

This case is similar to TDF1 but now cross-stream diffusion is allowed to modify the initial step profile as it proceeds downstream. The exact solution is:

$$\phi(\Delta, n) = \frac{1}{2}\left[1 + \text{erf}\left[\frac{1}{2} n \, (Pe/\Delta)^{\frac{1}{2}}\right]\right]$$

where erf is the error function.

(c) Scalar Transport in Jet Flow Field (TDF4)

In this particular case the flow field is non-uniform, being that of a self-preserving laminar plane jet. The associated velocity field and the corresponding self-preserving scalar field, for the case where the jet is initially "heated", are given by Schlicting (Ref. 24) and will not be quoted here. In the test calculations the exact velocities are imposed throughout the grid in such a way as to ensure that the discrete mass conservation requirement is obeyed at each cell; the exact ϕ values are imposed at the boundaries in the usual fashion.

(d) Single Cell Calculation of Convection and Diffusion of ϕ with Initial Linear Distributions (TDS2)

In this case the linear ϕ distributions are imposed at the boundaries. The solution for ϕ_p is given by Castro (Ref. 25) and is in the form of an infinite series.

4.4.3 Results of Test Cases

The results of some of the test calculations will now be presented under the headings of the different schemes which have been tested. In many instances the predictions of the UDS are included to provide an indication of the improvements which have been achieved.

4.4.3.2 The QUDS and SUDS

The QUDS results for the single-cell test Case TDS1 (convection of a Gaussian distribution) will be examined first: they are displayed in Figure 4-8a, showing ϕ_p plotted against the angle between the flow and the grid, for various values of the ratio Δ^* of the mesh spacing to the standard deviation.

Evidently at any given Δ^* there is agreement with the exact solution (given by $\phi_p = 1$, for all θ) at $\theta = 0$, but a finite and increasing error emerges for angles up to 45°, indicating that numerical smearing is occurring. The UDS results of Figure 4-8b show similar behavior, but the errors are considerably larger.The single-cell test case results for SUDS are shown in Figure 4-8c. This figure indicates maximum error levels comparable to those obtained using QUDS, but they occur for SUDS at angles of around 15°. This is in contrast to QUDS which gives large errors at the larger angles. The latter behavior is in conformity with the numerical diffusivity characteristics displayed earlier in Figure 4-4.

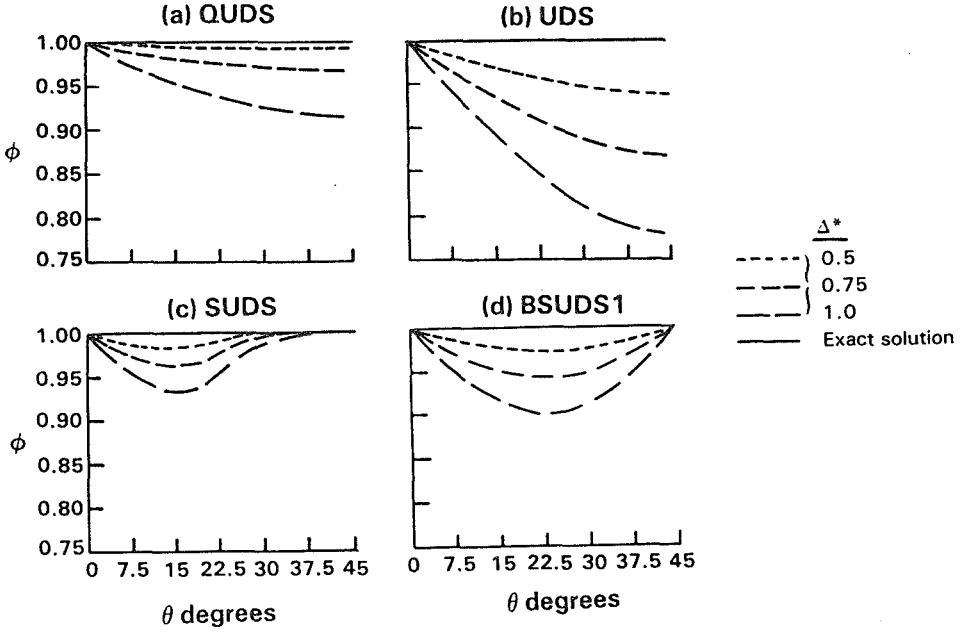

Figure 4-8 Comparison of QUDS, UDS and SUDS for Test Case TDS1

Figure 4-9 shows a plot of the error with Δ^* and indicates that the error decreases more rapidly for the QUDS than it does for the UDS as the mesh is refined. The slopes of the lines are 3 and 1, respectively, in conformity with the indications of the TSTE analysis of Table 4-III for the UDS but not apparently for QUDS which the analysis indicates to be second order; for a Gaussian distribution, the leading error term for QUDS is zero (i.e. $\partial\phi^3/\partial x^3 = 0$) whereas the next highest term in the error series is non zero. Note also that the line representing SUDS in Figure 4-9, has the same slope as that of QUDS (the fact that it lies below the QUDS result is of lesser significance, since it is merely due to the SUDS error being small at the flow angle 30° for which the results are plotted) indicating that in the present instance SUDS behaves like a third order scheme. This apparent conflict with the truncation error analysis can be explained by the fact that leading terms of the error series are in the present case small in comparison to the higher order ones. The results of Figure 4-9 show the inadequacy of using truncation error analysis alone in determining the accuracy of various schemes.

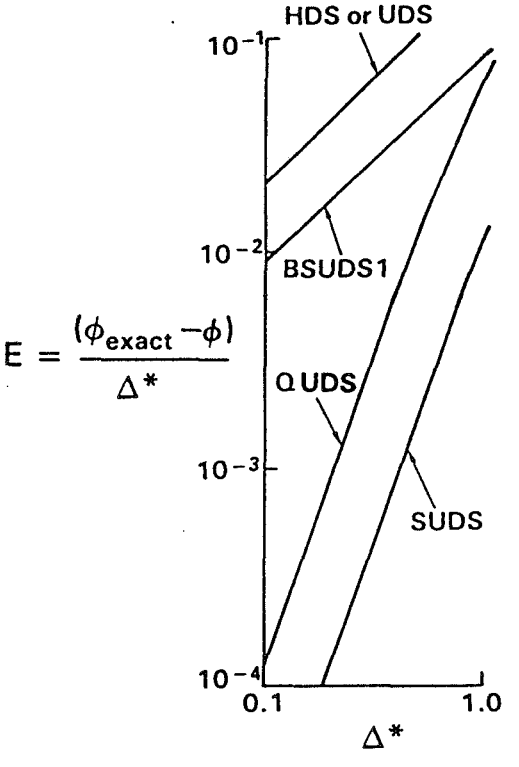

Figure 4-9 Error as a Function of Mesh Spacing for Test Case TDS1 for Various Schemes for Flow Angle of 30°

For the field calculations, Figure 4-10 shows the QUDS predictions and exact solutions for the convection and diffusion of a step profile (Case TDF3) for an overall Peclet number of 50 and for various θ. The results are displayed in terms of the ϕ profiles along the vertical mid-plane of a 9 x 9 grid and show the much-reduced smearing error of QUDS as compared with UDS as θ is increased (it is nonetheless finite and increases with θ). Also shown are the undesirable undershoots and overshoots of the higher-order QUDS scheme. Examination of the SUDS field calculations for Case TDF3, also shown in Figure 4-10, confirms the general characteristics already described but also illustrates the fact that, like QUDS, this scheme can produce unbounded behavior when ϕ gradients are steep: in this instance the peak excursions of the two schemes are comparable. QUDS would better preserve the slope of the exact solution at angles up to 30° but beyond this SUDS is clearly superior. Indeed, a general trend can be noted in which a given scheme either produces a bounded solution of reduced slope or an unbounded solution of correct slope.

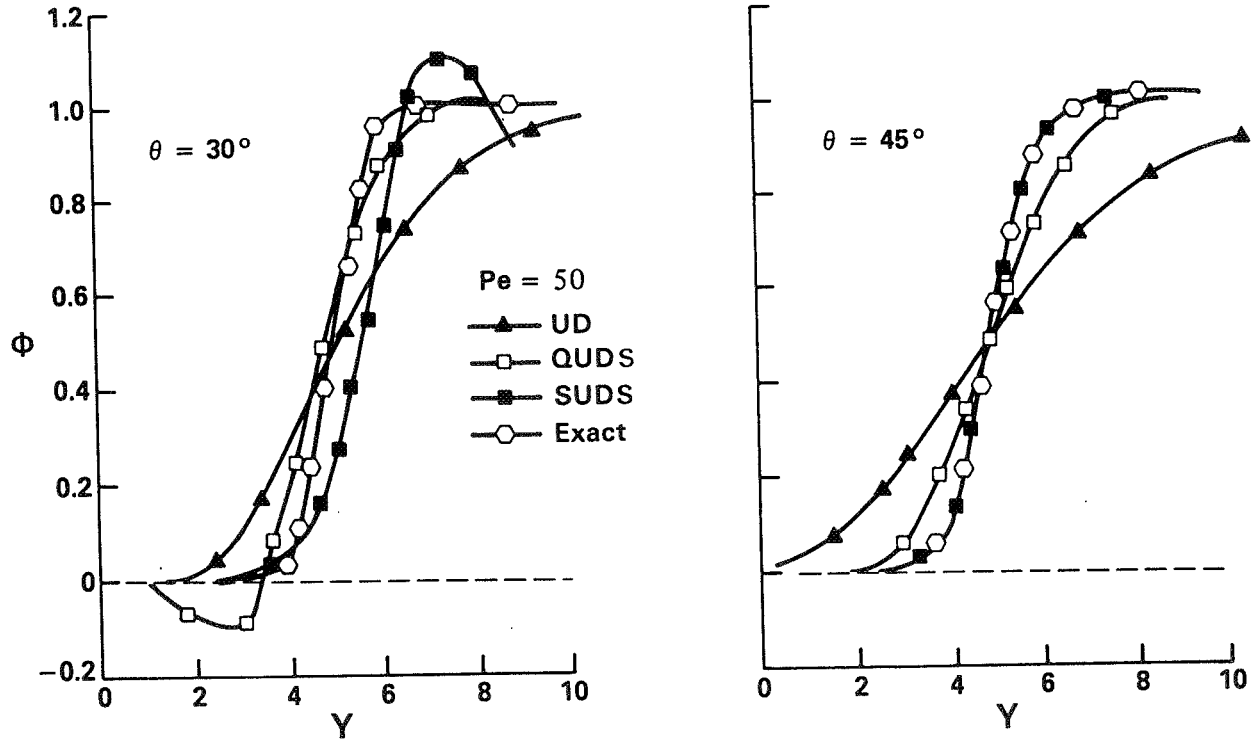

Figure 4-10 Comparison of QUDS and SUDS Schemes for Test Case TDF3

A similar evaluation applies to the results for infinite Peclet number (TDF1) when SUDS results (Figure 4-11) are compared with the QUDS results (Figures 4-12). However, at larger angles the SUDS profiles exhibited more severe oscillations than those generated by QUDS.

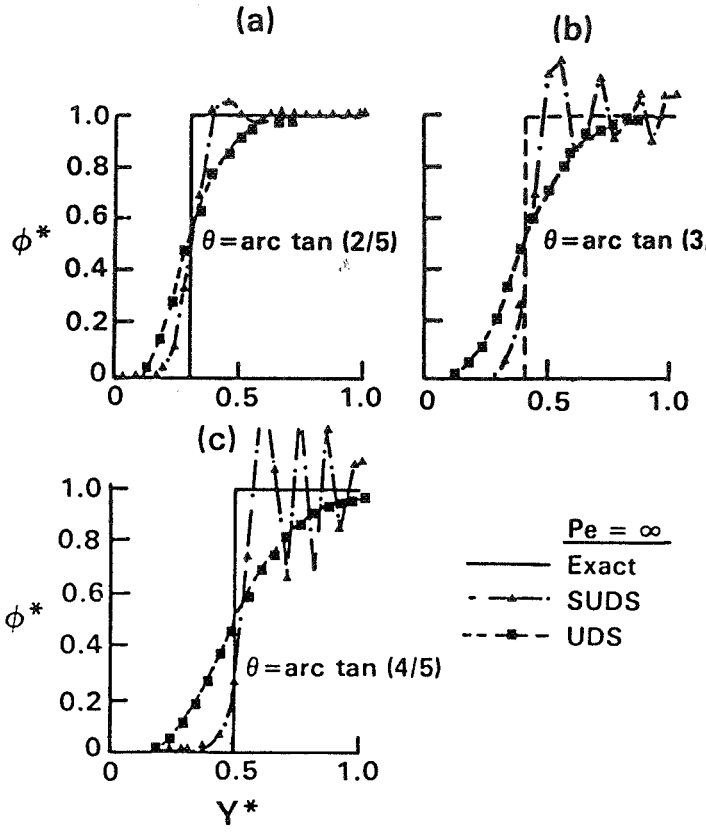

Figure 4-11 SUDS Calculations for TDF1 for Various Flow Angles

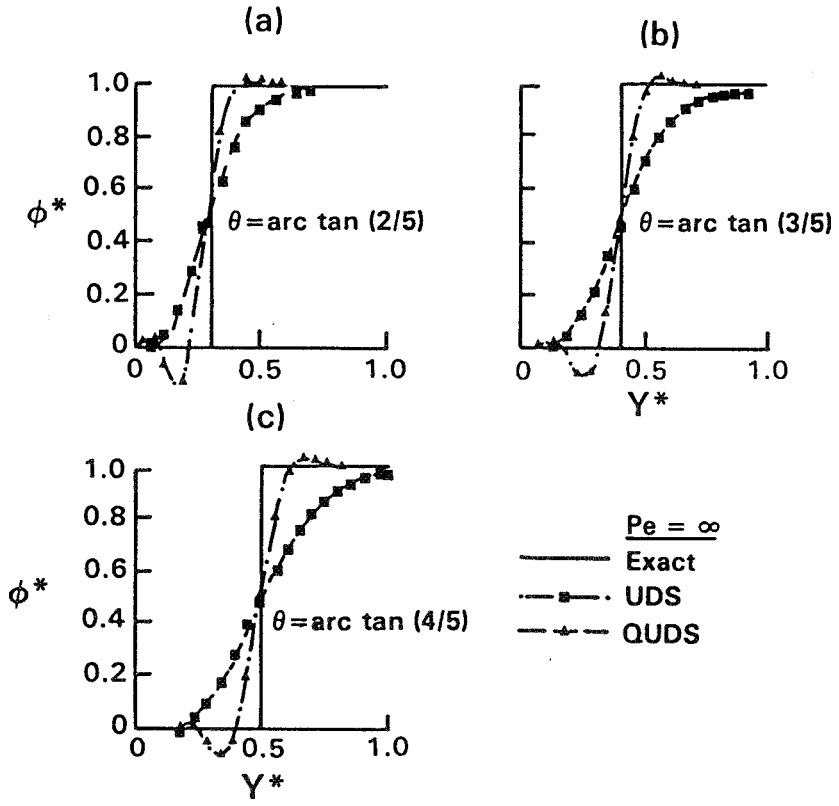

Figure 4-12 QUDS Calculations for TDF1 for Various Flow Angles

The comparisons for the convection of a square wave in a irrotational stagnation flow field (TDF2) are shown in Figure 4-13 in terms of the ø profile across the outlet boundary of the calculation domain, which is identical with the inlet distribution. The QUDS predictions are considerably better than those of the UDS but exhibit significant undershoots and overshoots. The SUDS predictions for Case TDF2 can also be seen in Figure 4-13 and compared with the QUDS results in the diagram. On balance there is little to recommend either scheme: both reproduce the square wave to a similar extent, albeit without maintaining the proper bounds. SUDS maintains the wave amplitude better while introducing a phase error (the prediction is shifted to the left relative to the exact solution) whereas the reverse is true with the QUDS.

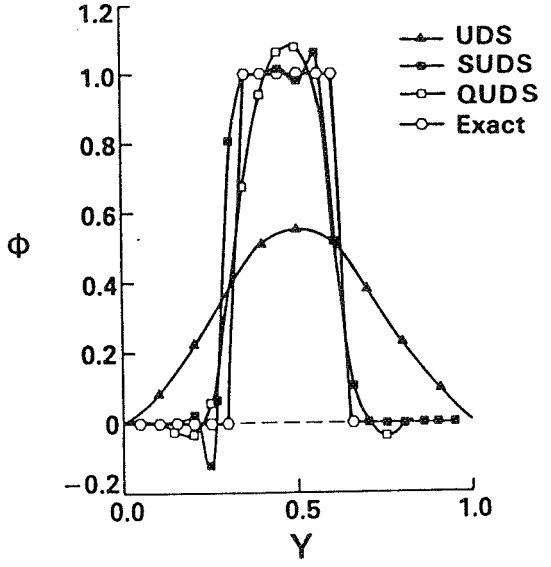

Figure 4-13 Comparison of QUDS and SUDS Schemes for Test Case TDF2

The results obtained using QUDS and SUDS to compute the scalar transport in a laminar jet flow (TDF4) are shown in Figure 4-14, where the profiles along the vertical mid-plane are plotted. In this case the QUDS solutions remain within expected bounds (probably due to the smoothness of the ø profile) and are more accurate than those of the UDS at both angles; however, QUDS exhibits substantial diffusion-like errors at the largest angle ($\theta = 45^{\circ}$). SUDS, like QUDS, maintains the proper bounds because the ø gradients are less severe. In familiar pattern, QUDS is better at small angles and SUDS is better at large angles.

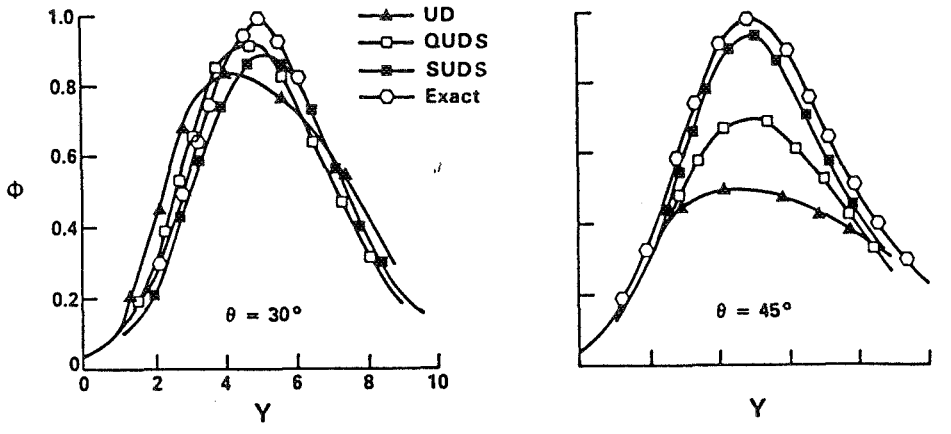

Figure 4-14 Comparison of QUDS and SUDS Schemes for Test Case TDF4

The comparison of QUDS and SUDS can be summarized in the following manner: both schemes suffer from boundedness problems when conditions with regard to the cell Peclet number, flow angle relative to the mesh, and gradients in ϕ are large. QUDS is more accurate for smaller flow angles while SUDS is more accurate for larger flow angles.

4.4.3.3 Flux-Blended Schemes

In this section the performance is examined for BSUDS1 (which was derived by blending UDS and SUDS to maintain positive coefficients) and for BSUDS2 and BQUDS2, (where the blending criterion is the preservation of local bounds on the solution).

(a) One-Dimensional Tests

Since in one-dimensional flow, the UDS and SUD are identical, calculations were performed only using BQUDS2 and the results are displayed in Figures 4-15 (Case OD1) and 4-16 (Case OD2). In both cases, it can be seen that oscillations have been suppressed and the proper bounds maintained; moreover, these results were obtained with steep gradients in the dependent variable.

(b) Two-Dimensional Tests

A comparison of the BSUDS2 and BQUDS2 solutions for TDF1 of Figure 4-17 shows that both exhibit similar characteristics as those exhibited by BQUDS2 for the one-dimensional test cases. The tendency in all cases is to maintain the proper bounds without introducing excessive numerical diffusion; this is indicated by the fact that in flow regimes where the original QUDS and SUDS solution were within bounds (Figures 4-11 and 4-12), those solutions are virtually unchanged except from some "rounding" of the profile corners. Again BQUDS2 seems to be more accurate at small angles whereas BSUDS2 is more accurate at large ones.

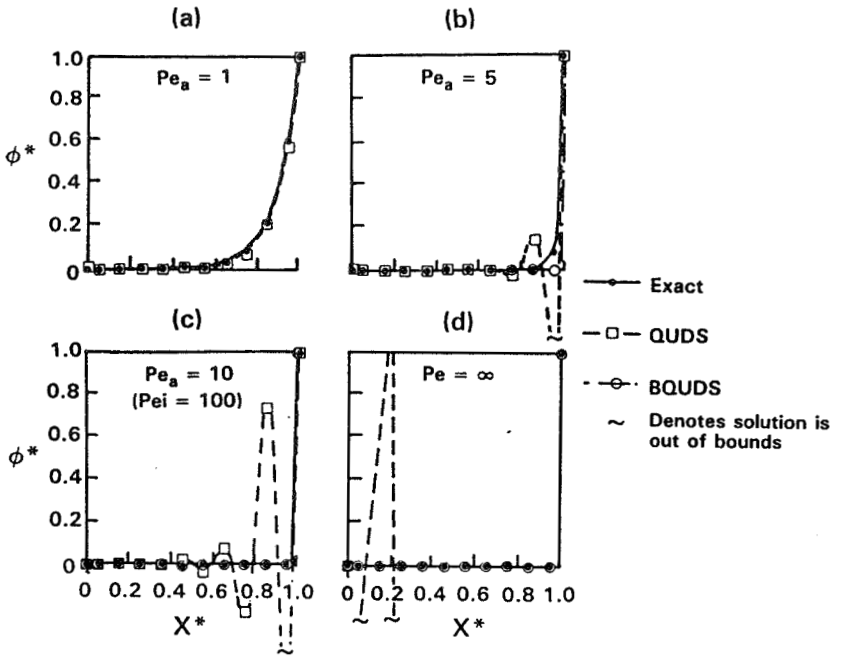

Figure 4-15 Comparison of Bounded and Unbounded QUDS Schemes for Test Case OD1

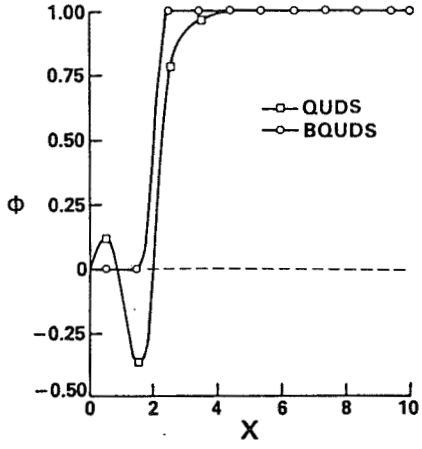

Pure convection of a Scalar with plane source in one-dimensional flow

Figure 4-16 Comparison of Bounded and Unbounded QUDS Schemes for Test Case OD2

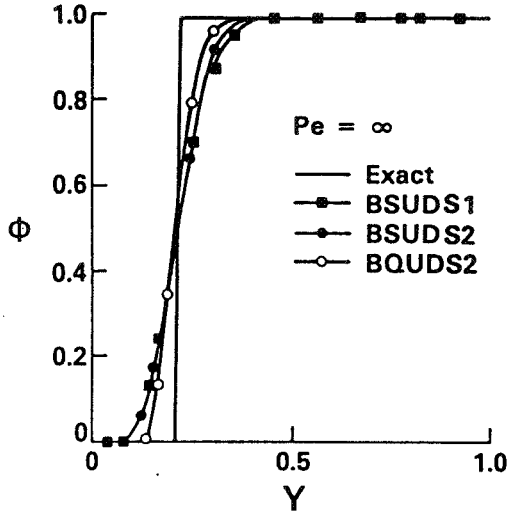

Pure convection of Scalar profile in a uniform flow field

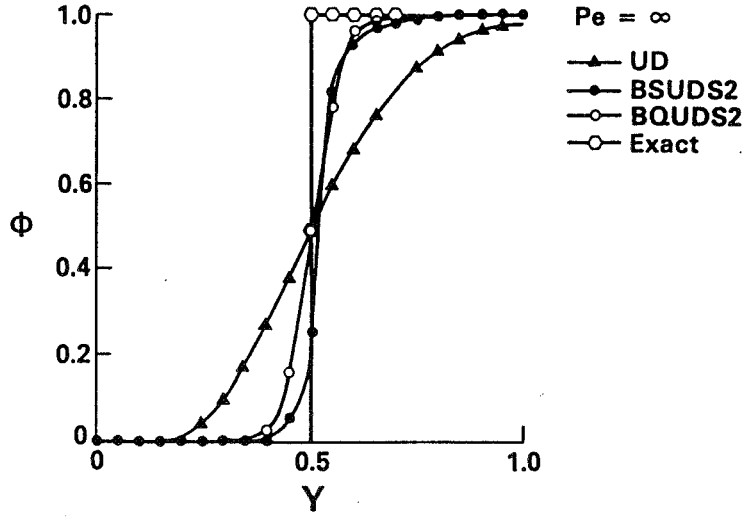

Pure convection of a Scalar profile in a uniform flow field

Figure 4-17 Comparison of BSUDS2 and BQUDS2 Schemes on Test Case TDF1

The performance of BSUDS2 and BQUDS2 for model problem TDF2, Figure 4-18, is similar to their unbounded counterparts, Figure 4-13, except that the unrealistic over and undershoots have been suppressed.

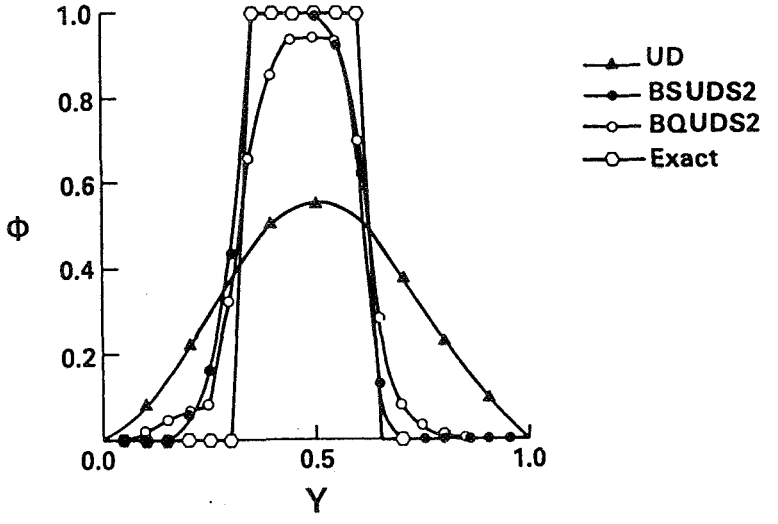

Figure 4-18 Comparison of BSUDS2 and BQUDS2 Schemes on Test Case TDF2

The performance of the alternative blending approach, as embodied in BSUDS1, will now be examined. In this instance results are available for the two single cell cases and are included for Case TDS1 in Figure 4-9 and the accompanying error plot of Figure 4-10. According to the first two figures the BSUDS1 errors lie between those of the UDS and SUDS, with a bias in Figure 4-9 towards the latter as expected from the numerical diffusivity analysis (Figure 4-1). Results for TDS2 are similar and are not shown.

The field calculations for Case TDF3 appear in Figure 4-19 and confirm that BSUDS1 does not exhibit the SUDS overshoots. It has been found that the BSUDS1 solution tends to lie closer to SUDS than to UDS, especially at the larger θ, due to the fact that the negative coefficients of SUDS reach their peak magnitudes at the smaller angles.

The BSUDS1 calculations for the jet case (TDF4) they differed very little from those of SUDS at all angles, presumably because the negative coefficients of the latter contribute little to the solution due to the smaller gradients there. These calculations are not shown.

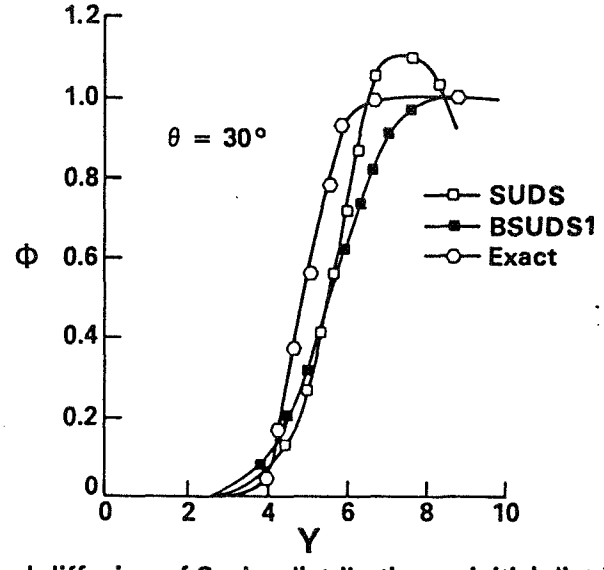

Figure 4-19 Comparison of SUDS and BSUDS1 Schemes on Test Case TDF3

It is concluded that the bounding schemes can suppress overshoots and undershoots successfully. The loss in accuracy, or increase in numerical diffusion, for Bounding Scheme 2 seems to be negligible for the test cases considered. Bounding Scheme 1 does introduce numerical diffusion but it is still far more accurate than UDS. BQUDS2 seems to be more accurate at small flow angles whereas BSUDS2 seems to be more accurate at large flow angles.

4.5 STABILITY

Within the context of the present tests, no instability problems were encountered with the SUDS and BSUDS1 schemes. For the latter, this behavior is expected since the associated coefficient matrix is always diagonally dominant. Although the SUDS matrix does not possess this property, the departures were evidently not so great as to prevent convergence. However, it should be noted that other users have reported such problems. Some problems were overcome by using better grids and modifying under-relaxation factors.

Convergence problems were encountered during the development of Bounding Scheme 2. These instabilities were traced to the failure to insure that, for a given set of blended coefficients, a reasonable approximation is obtained for the corresponding ϕ field; otherwise, the method of estimating the local solution bounds cannot operate properly. This problem, which should really be attributed to the properties of the equation solver employed rather than to the discretization method, was solved by arranging an inner iteration cycle in which, for given coefficients, the residual error of the ϕ solution was always reduced to a preset level. Once this was done, no further problems were encountered.

The calculations using the QUDS scheme were prone to instability, whether the Tridiagonal Matrix Algorithm (TDMA) or the Pentadiagonal Matrix Algorithm (PDMA) were used in the ADI solution procedure. No such problems were encountered in 1D calculations with PDMA since it then acts as a direct solver. It was found that the instabilities could be suppressed through the use of conventional under-relaxation (typical factors being 0.5-0.6) but, as will be seen in the next section, the rather large number of iterations required suggests that stability is still marginal. BQUDS2 also suffered from this problem, but to a slightly lesser extent.

An important implication of the foregoing findings is that better solution algorithms are needed for QUDS-type schemes to make them fully cost-effective. It was hoped that the PDMA might provide the answer, since it uses for all of the ϕ values along a grid line to which it is applied. That this expectation was not realized may be due either to the fact that linkages also exist on two neighboring lines on each side or to the occurrence of negative coefficients at the principal and outlying nodes. It is interesting to note that the more stable SUDS generates a more compact 9-diagonal matrix; although negative coefficients may occur, these occur only at the principal nodes.

4.6 COST EFFECTIVENESS

The measure of cost effectiveness of the schemes used here is examined in terms of their computing time and storage requirements, however, since current trends in computer technology indicate that increased storage is becoming more plentiful and inexpensive, the emphasis in the cost-effectiveness calculation is on computing time.

Strictly speaking, the comparison between schemes should be on an equal accuracy basis, i.e. tests should be performed on each scheme with different grids to obtain a pre-specified level of error. However because this is time-consuming and also because the differences between the predictions of the "higher order" schemes on a given grid are generally much smaller than those between any other scheme and UDS, the results for calculations using the same grid will be compared. This comparison gives only a first estimate of the cost of using alternative schemes regardless of accuracy. Additional cost information is provided for the schemes incorporated into the 2D and 3D versions of TEACH for the more realistic test cases discussed in Section 6.

4.6.1 Computing Times

A representative set of computing times is shown in Table 4-VII. These pertain to calculations for Case TDF2 on the 9 x 9 grid, and were obtained on a CDC Cyber 174 machine: however it is not the absolute times which are of interest, but rather their relation to the baseline figures for UDS which are also shown.

Table 4-VII shows the following: (i) the time required for a single assembly of all coefficients, T_{coeff}; (ii) the time required for a single application of the ADI solver, T_{solver}, this turns out to be almost the same for both TDMA and PDMA versions; (iii) the total number of outer iterations performed, N_{outer}, which is also equal to the total number of coefficient assemblies; (iv) the total number of inner iterations performed, N_{inner}, which is equal to the total number of ADI passes; and finally (v) the total CPU time, excluding compilation and initialization. It should be noted that N_{inner} and N_{outer} are identical for all but the BSUDS2 and BQUDS2 schemes; for these two, it was necessary to ensure that the inner loop be executed to a preset

residual tolerance rather than for a preset number of ADI sweeps (specified as unity for all other schemes).

TABLE 4-VII

COMPARISON OF COMPUTING TIMES AND NUMBER OF ITERATIONS REQUIRED FOR CALCULATIONS OF CASE TDF2 ON 9 X 9 MESH

Scheme	Coeff assembly time	Solver time	No. of outer-iter	No. of inner-iter	CPU time
UDS	1.0	1.0	1.0	1.0	1.0
SUDS	7.0	1.0	1.0	1.0	1.5
QUDS	6.0	1.0	14 - 20	14 - 20	10 - 15
BSUDS1	8.0	1.0	1	1	1.5
BSUDS2	8.0	1.0	2 - 3	5 - 6	4 - 5
BQUDS2	7.5	1.0	7 - 13	65 - 160	32 - 69

- Inefficiency of BQUDS2 is due to the solver (TDMA) which is not compatable

Some interesting general features emerge from this table. Firstly, the variations between the coefficient assembly times for "higher-order" schemes are small in relation to the increase over the UDS figure, the ratio over the latter being in the range 6-8. Secondly, T_{coeff} and T_{solver} are roughly the same, excluding those for the UDS; and thirdly, QUDS and BQUDS2 clearly require substantially more outer iterations than the others.

Turning now to detailed comparisons, it is clear that SUDS and BSUDS1 are the most cost-effective for the present applications due to the smaller number of iterations (inner and outer) required; the CPU time increase over that for UDS is only 50 percent. The additional cost of the first flux-blending procedure is evidently insignificant.

The next most cost-effective method is BSUDS2, which requires 3 times the SUDS/BSUDS1 CPU time, due to the increased number of iterations required for convergence; however, BSUDS2 is measurably more accurate than SUDS or BSUDS2.

QUDS and BQUDS2 are considerably more expensive, requiring respectively 2-3 and 6-14 times the BSUDS2 CPU time. The additional expenditure is due to the increased values of N_{outer}. For BQUDS2, there is the additional cost due to the substantial level of N_{inner}.

It should be emphasized that, although the results in Table 4-VII are representative of the present tests, the poor performance for QUDS, BQUDS2 and BSUDS2 is due in large measure to the unsuitability of the solvers employed.

TABLE 4-VIII

SUMMARY OF ADDITIONAL STORAGE REQUIREMENTS
OVER THOSE OF THE UDS

SCHEME	NO. OF ADDITIONAL 2D ARRAYS	QUANTITIES STORED
SUDS	4	a_{NW}, a_{SW}, a_{NE}, a_{SE}
QUDS	4	a_{WW}, a_{SS}, a_{NN}, a_{EE}
BSUDS1&2 BQUDS2	6	AS ABOVE, PLUS $\gamma_{e/w}$ AND $\gamma_{n/s}$

4.6.2 Computer Storage

For 2D applications, none of the schemes examined generates unacceptable additional storage requirements over those of UDS. Table 4-VIII indicates the number of additional two-dimensional arrays required. In the case of SUDS and QUDS, the increase is equal to the number of additional "neighbor" coefficients, i.e., 4. The flux blended versions require two additional arrays to store the γ values for each coordinate direction. Assuming that there is a choice between savings in CPU time, code complexity and savings in storage, savings in CPU time, code complexity will take precedence.

4.7 COMPLEXITY AND COMPATIBILITY WITH EXISTING TEACH METHODOLOGY

The evaluation of complexity is necessarily subjective, but if the schemes examined were so ranked, they might appear as follows, with complexity increasing from left to right:

	ADS		
UDS,	SUDS	, BSUDS1,	BSUDS2
	QUDS		BQUDS2

In no case can it be said that any particular scheme is difficult to comprehend and implement, although the possibilities for error are obviously greater as one moves away from the simplicity of UDS. Perhaps the major pitfalls lie in the imposition of the boundary conditions, which require particular care with schemes like QUDS, SUDS and their bounded counter parts. This difficulty is common to all higher-order schemes.

Concerning compatibility with TEACH, it is sufficient to note that all of the tests reported herein were performed with versions of this code employing the same basic methodology. Some minor problems were encountered, such as those due to the extra row of external nodes at boundaries when QUDS and BQUDS2 were implemented, but these were more tedious than difficult. Of course, the solvers which have been employed are not particularly well suited to QUDS, but the modular structure of the code readily allows a better solver to be used.

4.8 PROGNOSTICATIONS FOR THREE DIMENSIONAL CALCULATIONS AND OTHER CONSIDERATIONS

Before the final evaluation is made it is important to consider two further aspects which have not been examined in detail in the studies described thus far, namely:

(a) The suitability of the various schemes for three-dimensional applications.

(b) Experience of application of the schemes to flow field calculations.

Both the SUDS and QUDS (and bounded versions thereof) have computational "molecules" of equal size in 2D, i.e. each comprises 9 nodes; in 3D, the SUDS molecule increases to 27 nodes, whereas the QUDS size is only 13 nodes. Thus QUDS possesses a nearby two-fold advantage in coefficient assembly time and storage requirements.

Also, it should be noted that Bounding Scheme 1 is inapplicable to the SUDS in 3D, due to the fact that the coefficients of the non-principal, or "corner" nodes, may become negative. (Bounding Scheme 2 is of course still applicable).

Relatively few applications have been reported using SUDS and QUDS in flow field calculations. Fewer still have been made using BSUDS1 and none using BSUDS2 or BQUDS2.

The studies of greatest relevance here are those of Castro (Ref. 25), Leschzeiner and Rodi (Ref. 26), Han, Launder and Humphrey (Ref. 27), Leschzeiner and Launder (Ref. 28) and Lai (Ref. 23). Their findings may be summarized as follows:

i) No major problems were reported in solving the SUDS-based equations, but difficulties were encountered in obtaining solutions when QUDS was used. The exception is the recent work of (Ref. 27) where a particular arrangement of the coefficient matrix was found which produced stable ADI solutions in comparable numbers of iterations to those for the UDS calculations of the same problem.

ii) The accuracies of the SUDS and QUDS results were similar in most instances, with the notable exception of the test problem of laminar flow in a square cavity with a sliding wall. Here SUDS was scarcely better than UDS, whereas QUDS was markedly superior to both.

iii) BSUDS1 has been shown by Lai (Ref. 23) and Benadecker et al (Ref. 29) to perform satisfactorily as regards convergence and to be markedly more accurate than UDS (again with the exception noted in (i) above).

The poor performance of SUDS referred to in paragraph ii) was attributed by Lai (Ref. 23) to the failure of this scheme to account properly for the effects of pressure gradients, which act like "sources" in the momentum equations and are particularly important in the cavity problem. This deficiency, which did not appear to manifest itself in other problems involving strong pressure gradients, arises because SUDS tries to preserve velocity, rather than total pressure, along streamlines.

4.9 CONCLUSIONS

1) Of the schemes examined, BSUDS2 and BQUDS2 appear to offer the most promise for 3D applications.

2) The cost-effectiveness of QUDS and BQUDS2 is currently impaired by the lack of an efficient and reliable solver. Once a suitable solver is found, then the accuracy and compactness of the 3D computational molecule of these schemes is likely to render them superior to SUDS and its derivatives.

3) The ADS, although of higher formal order than SUDS and QUDS, is non-conservative, and has been rejected for this reason.

4) Spline schemes of the conventional centered variety like the CSS appear to be susceptible to severe overshoot problems and are also non-conservative. For these reasons they are not recommended at their present stage of development. Similar comments apply to the GRHS Hermitian scheme.

5) The flux-blending strategies for eliminating overshoots seem ideally suited for implicit calculations and are likely to see further development and application.

4.10 SELECTION OF TWO DIFFERENCING SCHEMES

No scheme seems to have emerged from this evaluation with a clear-cut margin of superiority over the others. SUDS offers a more favorable matrix structure from the solver point of view, especially when bounded as in BSUDS1/2. On the other hand, it has not performed well in isolated instances and it does generate a large computational molecule in 3D.

QUDS has performed well in flow field applications as regards accuracy (although it too produced some isolated poor results in the present scalar transport tests). Further, it has the compelling attraction of a comparatively small 3D molecule. Although the basic scheme can produce significant overshoots, it seems amenable to bounding by the flux blending strategy 2. The main argument against QUDS is the lack of a wholly suitable solver.

Both QUDS and SUDS, bounded and unbounded, show a flow angle dependence regarding their accuracy. QUDS seems to be more accurate at small angles whereas SUDS has a greater advantage at large angles. It should be noted that either of these two schemes will be an improvement over the hybrid differencing scheme at any angle.

Thus, SUDS and QUDS were selected for evaluation in the two-dimensional version of TEACH. Although it was desirable to implement them with flux blending, it was not essential for testing these schemes in realistic flows as required in this contract. The unbounded version of QUDS was selected since it could be coded relatively quickly in TEACH and permit extensive testing of the method. BSUDS1 and BSUDS2 were also selected since they offered accuracy improvements comparable to those obtainable using QUDS, nonphysical oscillation could be avoided using flux-blending, and the computational molecule was reasonably compatible with the current solver. Based on the results of the test cases, it was anticipated that BSUDS2 would be more accurate than BSUDS1. It has been noted, however, that BSUDS1 is not suitable for use in the 3D-TEACH code.

5.0 DERIVATION OF SELECTED SCHEMES FOR TEACH

In this section, the details of the derivations for the two improved finite-difference methods incorporated into the two-dimensional version of TEACH are presented. In Section 5.1, the derivation for the skew-upwind differencing scheme using the second bounding method (BSUDS2) is given. In Section 5.2, the derivation for the Quadratic Upwind Differencing Scheme (QUDS) is given. BSUDS2 was also selected for use in the three dimensional version of TEACH. The extension of the material in Section 5.1 for use in the 3D-TEACH computer program is presented in Appendix B.

5.1 THE BOUNDED SKEW-UPWIND DIFFERENCING SCHEME

In this section, the bounded skew-upwind differencing scheme is described. First, a brief review of the flux form of the equations of motion is presented. Second, a detailed description of the finite-difference form of the flux contribution to a representative face of a typical control volume is given; the derivation of the flux contributions to the other faces is then outlined. Third, the resulting coefficients for the finite-difference equations representing the total flux (and sources) are presented. Fourth, the results of applying the boundary conditions are shown in a manner consistent with the foregoing flux representation. Fifth, the bounding scheme for the coefficients is detailed.

5.1.1 Flux Form of the Equations of Motion

The equations of motion for both laminar flow and (time-averaged) turbulent flow can be written in similar fashion for all of the dependent variables:

$$\frac{\partial}{\partial x}(\rho u \phi) + \frac{1}{r^{\delta}}\frac{\partial}{\partial r}(r^{\delta}\rho v \phi) = \frac{\partial}{\partial x}\left(\Gamma_{\phi}\frac{\partial \phi}{\partial x}\right) + \frac{1}{r^{\delta}}\frac{\partial}{\partial r}\left(\Gamma_{\phi r}\delta\frac{\partial \phi}{\partial r}\right) + S_{\phi} \qquad (5.1)$$

where $\delta = 0$ for two-dimensional (planar) flow and $\delta = 1$ for axisymmetric flow. The variable ϕ represents any of the dependent variables (e.g., the velocity components u, v, w, mixture fraction, turbulence kinetic energy and turbulence energy dissipation). The exchange coefficient, Γ_{ϕ}, represents the sum of both laminar and turbulent contributions and is interpreted as the effective viscosity for ϕ = u, v, w, the effective diffusivity for ϕ = mixture fraction, etc. S_{ϕ} is a generalized source term.

Equation (5.1) is integrated over a control volume appropriate for each dependent variable ϕ and, after some manipulation, the finite-difference equivalent form of Equation (5.1) is obtained. The control volumes are defined using an orthogonal grid formed by the intersection of coordinate lines in both the axial and radial coordinate direction. For planar (two-dimensional) problems, a unit thickness and uniform properties in the direction normal to the plane of the grid are assumed. The intersection of the grid lines form the

grid nodes at which all flow properties except the axial (u) and radial (v) velocities are calculated; i.e., all scalars and the tangential velocity component (w) for swirling flows. The axial velocity is calculated using a second grid with grid nodes located midway between the scalar grid nodes in the axial direction and coincident with the scalar grid nodes in radial position. The radial velocity is calculated using a third grid with grid nodes located midway between the scalar grid nodes in the radial direction and coincident with the scalar grid nodes in axial position. Directions in the grids are identified as north, south, east and west. The grid system for the scalars is shown in Figure 5-1. The positions of the u and v storage locations (grid systems) relative to the scalar grid are shown in Figure 5-2.

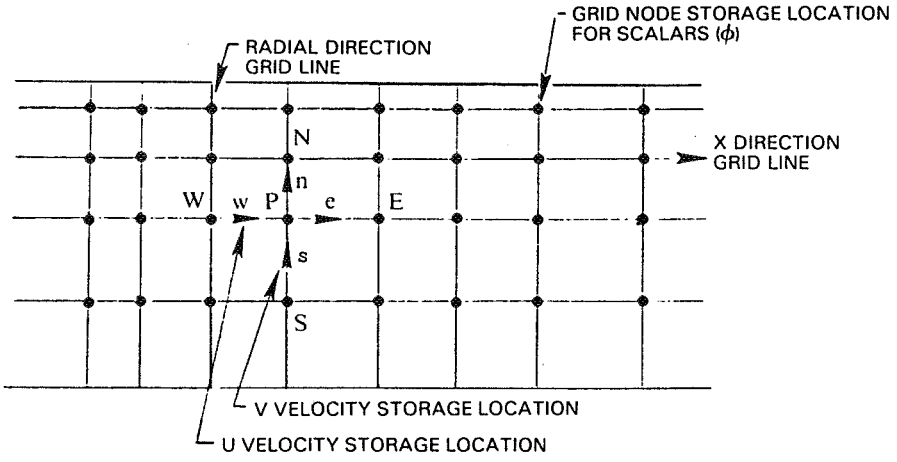

Figure 5-1 Grid System for Scalars

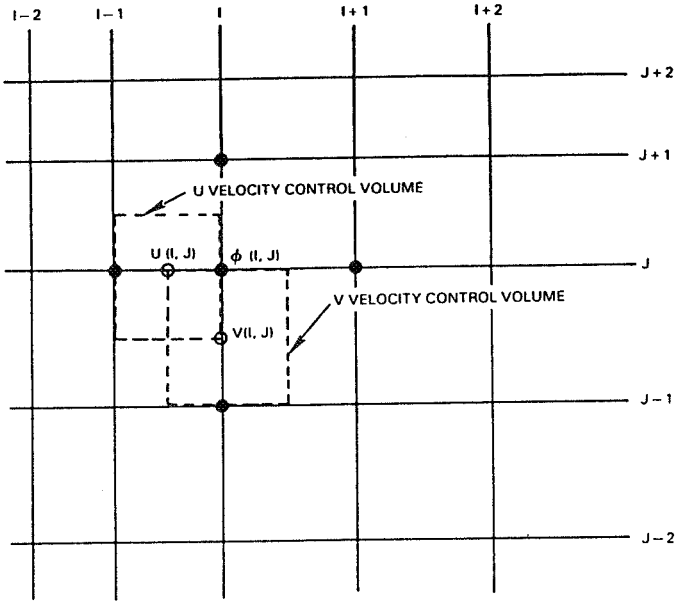

Figure 5-2 Storage Locations for Axial (U) and Radial (V) Velocities Relative to Scalar (¢) Grid System

Control volumes for each scalar and the tangential velocity are defined by planes located midway between the scalar grid nodes, as shown in Figure 5-3. Normal velocity components, therefore, lie along the boundaries of the control volumes. Generally, boundaries for the u or v control volumes include scalar grid-lines and are not necessarily located midway between velocity grid lines.

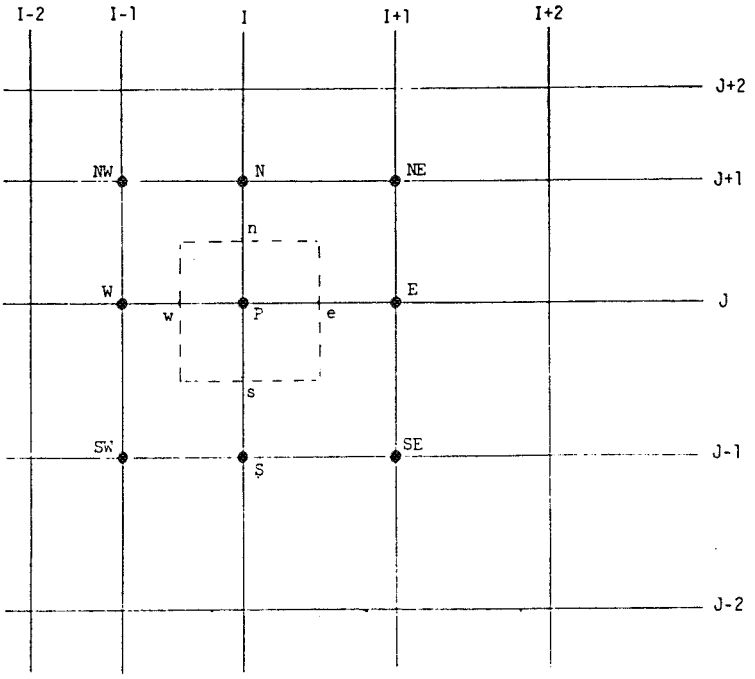

Figure 5-3 Scalar Control Volume

The finite-difference form of Equation (5.1) is derived by integrating this equation over the appropriate control volume. For the scalars and the tangential velocity component, the grid systems defined above provide some computational convenience. Since the u and v velocities are stored midway between the scalar grid nodes, the convective fluxes from the north, south, east and west faces can be calculated without recourse to averaging any of these velocities. Also, the pressure gradient driving the flow can be computed without averaging pressures.

In performing the integration over the control volume for each term in Equation (5.1), the mean-value theorem is employed and the source term is linearized in the vicinity of the center of the control volume (point P). After some manipulation, the finite-difference form of Equation (5.1) is obtained.

$$C_E\phi_e - C_W\phi_w + C_N\phi_n - C_S\phi_s = D_E(\phi_E - \phi_P) - D_W(\phi_P - \phi_W) + D_N(\phi_N - \phi_P) - D_S(\phi_P - \phi_S) + (S_u + S_P\phi_P) \tag{5.2}$$

where C_E, C_W, etc. are "convective coefficients" as defined below

$$\begin{aligned} C_E &= (\rho u)_e a_e \\ C_N &= (\rho v)_n a_n \\ C_W &= (\rho u)_w a_w \\ C_S &= (\rho v)_s a_s \end{aligned} \tag{5.3}$$

and $a_n = a_S$, $a_W = a_e$ are the areas of the faces of the control volume.

The "diffusion" coefficients are given by

$$\begin{aligned} D_E &= \left(\frac{\Gamma\phi}{\Delta x}\right)_e a_e \\ D_N &= \left(\frac{\Gamma\phi}{\Delta y}\right)_n a_n \\ D_W &= \left(\frac{\Gamma\phi}{\Delta x}\right)_w a_w \\ D_S &= \left(\frac{\Gamma\phi}{\Delta y}\right)_s a_s \end{aligned} \tag{5.4}$$

and $(\Delta x)_e$ is the distance between points P and E, etc. (e.g., see Figure 5-3).

It is important to note that Equation (5.2) applies to all of the dependent variables although the appropriate grid must be used in each case to define the geometric parameters used in the calculation. Also, Equation (5.2) applies to all of the difference procedures considered in the program since each scheme is simply an alternative method for defining (interpolating for) the dependent variable at the faces of the control volume (e.g., ϕ_e, ϕ_w, ϕ_n, ϕ_s). However, the diffusion terms are always represented by central differences.

It is convenient to define a total flux for each face of the control volume as the sum of a convective flux and a diffusive flux such that:

$$F_e - F_w + F_n - F_s = S_u + S_P\phi_P \tag{5.5}$$

where

$$\begin{aligned} F_e &= C_E\phi_e - D_E\,(\phi_E - \phi_P) \\ F_w &= C_W\phi_w - D_W\,(\phi_P - \phi_W) \\ F_n &= C_N\phi_n - D_N\,(\phi_N - \phi_P) \\ F_s &= C_S\phi_s - D_S\,(\phi_P - \phi_S) \end{aligned} \tag{5.6}$$

In the following section, the skew differencing procedure will be used to calculate the values of the dependent variables at the faces of the control volume. As a result, Equation (5.5) will include not only the values of ϕ at the "normal," or main, grid node locations (E, W, N, S and P) but also at the corner locations (NE, SE, NW, and SW). The finite-difference form for Equation (5.5) will be shown to be:

$$\begin{aligned} A_P\phi_P = {} & A_E\phi_E + A_W\phi_W + A_N\phi_N + A_S\phi_S + A_{NE}\phi_{NE} + A_{SE}\phi_{SE} \\ & + A_{NW}\phi_{NW} + A_{SW}\phi_{SW} + S_U + S_P\phi_P \end{aligned} \tag{5.7}$$

5.1.2 Calculation of the Fluxes

Recall that the equation of motion, Equation (5.1), can be written in terms of fluxes to each face of the control volume, Equation (5.5). In this section, a procedure will be described to calculate fluxes, F_e, F_w, F_n, and F_s. The derivation of F_w, the flux to the west face of a typical scalar control volume, is given in detail. The derivation of the other fluxes and of the fluxes for the u and v velocity components are outlined.

Consider the control volume shown in Figure 5-4. At present, it is assumed that the velocity vector is oriented as shown; i.e., the u and v components are non-negative. The flux to the west face is given by:

$$F_w = C_W\phi_w - D_W\,(\phi_P - \phi_W) \tag{5.8}$$

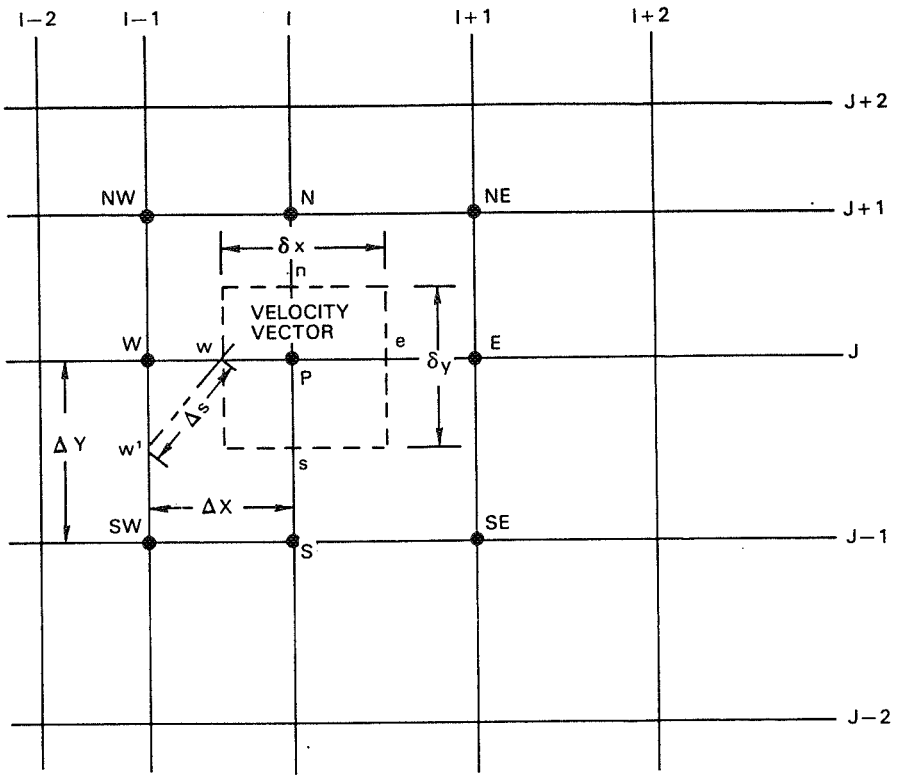

Figure 5-4 Control Volume for Skew-Upwind Differencing for West Face of Control Volume and Positive Velocity Components

For central-differencing (CD), the value of the dependent variable at the west face, ϕ_W, is given by linear interpolation between ϕ at the W and P grid nodes.

$$\phi_w = (1 - \alpha_w)\ \phi_W + \alpha_w \phi_P \tag{5.9}$$

where the interpolating factor is

$$\alpha_w = \frac{X_w - X_W}{X_P - X_W} \tag{5.10}$$

In the 2D-TEACH computer program, $\alpha = 0.5$ for each face of the control volume for each scalar variable and the tangential velocity component since the control volume faces are located midway between scalar grid nodes. For the axial and radial velocity components, however, the α for each face may assume other values. The central difference form of the flux at the west face is then:

$$\frac{F_{w_{CD}}}{D_W} = \left[P_{e_w} (1 - \alpha_w) + 1 \right] \phi_W + (\alpha_w P_{e_w} - 1)\ \phi_P \tag{5.11}$$

where the Peclet number at this face is given by:

$$P_{e_w} = C_W / D_W \tag{5.12}$$

The upwind difference (UD) form for the flux at the west face is obtained by setting a_W to zero and neglecting the diffusion term:

$$\frac{F_{W_{UD}}}{D_W} = P_{e_w} \phi_W \tag{5.13}$$

Equation (5.8) is also the starting point for the skew upwind differencing (SUD) scheme. The value of ϕ at the west face of the control volume, ϕ_W is determined by extrapolating the velocity vector upstream to the point w' which lies along the grid line connecting the west and southwest nodes (see Figure 5-4) to give·

$$\phi_{w'} = (1 - k_w)\, \phi_W + k_w\, \phi_{SW} \tag{5.14}$$

where the skew interpolation factor is the ratio of the vertical distance between w' and SW to the vertical distance between W and SW:

$$k_w = \frac{1}{2} \frac{V_w}{U_w} \frac{\Delta x}{\Delta_y} \tag{5.15}$$

For very large flow angles (skewing) relative to the coordinate directions, k_W will exceed unity and w' will be defined in terms of ϕ at the SW and S nodes. However, it is known that this approach can yield negative coefficients at the corner nodes (NW, SW, NE, SE) which can in turn produce oscillations in the solution. To assure that the coefficients for the corner nodes are non-negative, then:

$$k_w = \max\left(1.0,\ \frac{1}{2} \left|\frac{V_w}{U_w}\right| \frac{\Delta x}{\Delta_y}\right) \tag{5.16}$$

The use of absolute values in Equation (5.16) permits this equation to be used to define k_W for all velocity components at the west face.

In his original development of the skew upwind differencing approximation, Raithby (Ref. 11) assumed that $\phi_W = \phi_{W'}$. Thus,

$$\frac{F_{W_{SUD}}}{D_W} = P_{e_w} \phi_{w'} - (\phi_P - \phi_W) \tag{5.17}$$

It is desirable to use the central difference procedure for small values of the grid Peclet number and the skew upwind differencing method for large values of the grid Peclet number. It is also desirable that these two formulations produce a continuous transition at the transition Peclet number, which in the present case is:

$$P_{e_w}^{*} = \frac{1}{\alpha_w} \tag{5.18}$$

For the scalar grid system used in the 2D-TEACH computer program, Pe* = 2. At the transition Peclet number, the central difference result (Equation 5.11) is:

$$\frac{F_{w_{CD}}}{D_w} = \frac{\phi_w}{\alpha_w} \tag{5.19}$$

while the skew upwind differencing method (Equation 5.17) yields:

$$\frac{F_{w_{SUD}}}{D_w} = \frac{\phi_{w'}}{\alpha_w} - (\phi_P - \phi_W) \tag{5.20}$$

Noting the definition given by Equation (5.14), it is clear that these two results are not equal.

The fluxes at the transition Peclet number can be made equal by noting (contrary to the assumption made by Raithby) that ϕ_w and $\phi_{w'}$ are related by:

$$\phi_{w'} = \phi_w - \left(\frac{\partial \phi}{\partial s}\right)_w \Delta s + \ldots \tag{5.21}$$

so that Equation (5.17) becomes

$$\frac{F_{w_{SUD}}}{D_w} = P_{e_w}\phi_w - P_{e_w}\left(\frac{\partial \phi}{\partial s}\right)_w \Delta s - (\phi_P - \phi_W) \tag{5.22}$$

Writing the central difference result in terms of the flux definition, Equation 5.8, then:

$$\frac{F_{w_{CD}}}{D_w} = P_{e_w}\phi_w - (\phi_P - \phi_W) \tag{5.23}$$

Clearly, these two fluxes will be equal at the transition Peclet number if a correction, $Pe_w^* (\partial\phi/\partial s)_w \Delta s$, is added to the skew upwind differencing flux, Equation 5.17, to obtain:

$$\frac{F_{w_{SUD}}}{D_w} = P_{e_w}\phi_{w'} + P_{e_w}^* \left(\frac{\partial\phi}{\partial s}\right)_w \Delta s - (\phi_P - \phi_W) \tag{5.24}$$

The derivative $(\partial\phi/\partial s)_w$ can be computed by:

$$\frac{\partial\phi}{\partial s} = \frac{\phi_W - \phi_{w'}}{\Delta s} \tag{5.25}$$

Then, using Equation (5.9), (5.14) and (5.18), Equation (5.24) becomes

$$\frac{F_{w_{SUD}}}{D_w} = P_{e_w}\phi_W - (P_{e_w} - P_{e_w}^*)\, k_w\, (\phi_W - \phi_{SW}) \tag{5.26}$$

At the transition Peclet number, the fluxes calculated by central differencing (Equation 5.19) and skew upwind differencing (Equation 5.26) are equal.

It will be recalled that the above result for the skew upwind differencing flux at the west face of the control volume was derived for non-negative values of the axial and radial velocities. Similar results can be derived for other combinations of u and v by consistent application of the process leading to Equation (5.26). The result is a general expression for the flux as calculated using skew upwind differencing:

$$\begin{aligned}\frac{F_{w_{SUD}}}{D_w} = {} & P_{e_w}\left[\sigma_w^u \phi_W + (1 - \sigma_w^u)\,\phi_P\right] \\ & - (P_{e_w} - P_{e_w}^*)\, k_w \left[\sigma_w^u \left\{\phi_W - \sigma_w^v \phi_{SW} - (1 - \sigma_w^v)\,\phi_{NW}\right\}\right. \\ & \left. + (1 - \sigma_w^u)\left\{\phi_P - \sigma_w^v \phi_S - (1 - \sigma_w^v)\,\phi_N\right\}\right]\end{aligned} \tag{5.27}$$

The parameters, σ_w^u and σ_w^v, are switches that indicate the direction of the components of the local flow velocities.

$$\sigma_w^u = \frac{1}{2}\left(1 + \frac{U_w}{|U_w|}\right) \tag{5.28}$$

$$\sigma_w^v = \frac{1}{2}\left(1 + \frac{V_w}{|V_w|}\right) \tag{5.29}$$

Each of these parameters has a value of unity if the velocity component is positive (or, by convention, non-negative) and zero if it is negative. The transition Peclet number is now given by the general result.

$$P_{e_w}^* = \frac{1}{\sigma_w^u - (1 - \alpha_w)} \tag{5.30}$$

In the hybrid differencing procedure, the more accurate central differencing formulation (Equation 5.11) is used when the Peclet number is less than the transition value while the less accurate, but stable, upwind differencing result (the generalization of Equation (5.13))

$$\frac{F_{w_{UD}}}{D_w} = P_{e_w}\left[\sigma_w^u \phi_W + (1 - \sigma_w^u)\phi_P\right] \tag{5.31}$$

is used when the Peclet number is greater than the transition value. Originally, it was believed that a similar hybrid procedure could be developed for skew upwind differencing with Equation (5.11) used for $Pe < Pe^*$ and Equation (5.27) used for $Pe > Pe^*$. However, this approach proved to be unworkable since some of the coefficients derived from this hybrid formulation for use in Equation (5.7) could be negative. As an alternative, a flux blending scheme (to be described in Section 5.1.5) is used in which a weighted average of the upwind differencing and the skew upwind differencing fluxes is used. The weighting (blending) factor, γ, is chosen in such a way as to assure boundedness. The bounded skew-upwind differencing (BSUD) flux is defined by:

(5.32)

$$\frac{F_{w_{BSUD}}}{D_w} = \gamma_w F_{w_{SUD}} + (1 - \gamma_w) F_{w_{UD}}$$

with the weighting factor restricted to the range, $0 \leq \lambda_w \leq 1$. As a consequence of this definition:

$$\frac{F_{w_{BSUD}}}{D_w} = P_{e_w} [\sigma_w^u \phi_W + (1 - \sigma_w^u) \phi_P] - (P_{e_w} - P_{e_w}^*) \gamma_w k_w \left[\sigma_w^u \left\{ \phi_W - \sigma_w^v \phi_{SW} - (1 - \sigma_w^v) \phi_{NW} \right\} + (1 - \sigma_w^u) \left\{ \phi_P - \sigma_w^v \phi_S - (1 - \sigma_w^v) \phi_N \right\} \right] \quad (5.33)$$

Finally, a bounded skew hybrid differencing (BSHD) formulation can be defined as:

$$\frac{F_{w_{BSHD}}}{D_w} = \lambda_w F_{w_{CD}} + (1 - \lambda_w) F_{w_{BSUD}} \quad (5.34)$$

where λ_w is permitted to assume only two values: $\lambda_w = 1$ for central differencing ($Pe < Pe^*$) and $\lambda_w = 0$ for bounded skew-upwind differencing ($Pe > Pe^*$). Equations (5.33) and (5.34) are the basic working relationships used to determine the flux at the west face of the control volume. The contributions of the flux to each of the coefficients in Equation (5.7) can be immediately identified by using Equations (5.33) and (5.34) in Equation (5.5).

Equations analogous to Equation (5.33) can be derived for the other three faces of the control volume in exactly the same manner as employed above. However, the results can be obtained by inspection as follows.

The east face flux is obtained by translating the nodal subscripts eastward such that:

West Subscript		East Subscript
W	becomes	P
P	becomes	E
SW	becomes	S
NW	becomes	N
S	becomes	SE
N	becomes	NE

Of course, the lower case subscript "w" becomes "e."

The south face flux is obtained from the west flux (Equation 5.33) by rotating the nodal subscripts counterclockwise through 90 degrees.

West Subscript		East Subscript
W	becomes	S
SW	becomes	SE
NW	becomes	SW
S	becomes	E
N	becomes	W
u	becomes	σ^v
$1 - \sigma^u$	becomes	$1 - \sigma^v$
σ^v	becomes	$1 - \sigma^u$
$1 - \sigma^v$	becomes	σ^u

The north face flux is derived by translating the south flux result northward.

South Subscript		North Subscript
S	becomes	P
P	becomes	N
SE	becomes	E
SW	becomes	W
E	becomes	NE
W	becomes	NW

The results of the manipulations are summarized in Tables 5-I through 5-III.

TABLE 5-I

DEFINITION OF BOUNDED SKEW HYBRID DIFFERENCING FLUXES

West

$$\frac{F_{w_{BSHD}}}{D_W} = \lambda_w F_{w_{CD}} + (1 - \lambda_w) F_{w_{BSUD}}$$

East

$$\frac{F_{e_{BSHD}}}{D_E} = \lambda_e F_{e_{CD}} + (1 - \lambda_e) F_{e_{BSUD}}$$

South

$$\frac{F_{s_{BSHD}}}{D_S} = \lambda_s F_{s_{CD}} + (1 - \lambda_s) F_{s_{BSUD}}$$

North

$$\frac{F_{n_{BSHD}}}{D_N} = \lambda_n F_{n_{CD}} + (1 - \lambda_n) F_{n_{BSUD}}$$

TABLE 5-II

CENTRAL DIFFERENCING FLUXES

West

$$\frac{F_{w_{CD}}}{D_W} = \left[P_{e_w} (1 - \alpha_w) + 1 \right] \phi_W + \left(\alpha_w P_{e_w} - 1 \right) \phi_P$$

East

$$\frac{F_{e_{CD}}}{D_E} = \left[P_{e_e} (1 - \alpha_e) + 1 \right] \phi_P + \left(\alpha_e P_{e_e} - 1 \right) \phi_E$$

South

$$\frac{F_{s_{CD}}}{D_S} = \left[P_{e_s} (1 - \alpha_s) + 1 \right] \phi_S + \left(\alpha_s P_{e_s} - 1 \right) \phi_P$$

North

$$\frac{F_{n_{CD}}}{D_N} = \left[P_{e_n} (1 - \alpha_n) + 1 \right] \phi_P + \left(\alpha_n P_{e_n} - 1 \right) \phi_N$$

TABLE 5-III

BOUNDED SKEW-UPWIND DIFFERENCING FLUXES

West

$$\frac{F_{w_{BSUD}}}{D_W} = Pe_w \left[\sigma_w^u \phi_W + (1 - \sigma_w^u) \phi_P\right] - (Pe_w - Pe_w^*) \gamma_w k_w$$
$$\left[\sigma_w^u \left\{ \phi_W - \sigma_w^v \phi_{SW} - (1 - \sigma_w^v) \phi_{NW} \right\} \right.$$
$$\left. + (1 - \sigma_w^u) \left\{ \phi_P - \sigma_w^v \phi_S - (1 - \sigma_w^v) \phi_N \right\} \right]$$

East

$$\frac{F_{e_{BSUD}}}{D_E} = Pe_e \left[\sigma_e^u \phi_P + (1 - \sigma_e^u) \phi_E\right] - (Pe_e - Pe_e^*) \gamma_e k_e$$
$$\left[\sigma_e^u \left\{ \phi_P - \sigma_e^v \phi_S - (1 - \sigma_e^v) \phi_N \right\} \right.$$
$$\left. + (1 - \sigma_e^u) \left\{ \phi_E - \sigma_e^v \phi_{SE} - (1 - \sigma_e^v) \phi_{NE} \right\} \right]$$

South

$$\frac{F_{s_{BSUD}}}{D_S} = Pe_s \left[\sigma_s^v \phi_S + (1 - \sigma_s^v) \phi_P\right] - (Pe_s - Pe_s^*) \gamma_s k_s$$
$$\left[\sigma_s^v \left\{ \phi_S - (1 - \sigma_s^u) \phi_{SE} - \sigma_s^u \phi_{SW} \right\} \right.$$
$$\left. + (1 - \sigma_s^v) \left\{ \phi_P - (1 - \sigma_s^u) \phi_E - \sigma_s^u \phi_W \right\} \right]$$

North

$$\frac{F_{n_{BSUD}}}{D_N} = Pe_n \left[\sigma_n^v \phi_P + (1 - \sigma_n^v) \phi_N\right] - (Pe_n - Pe_n^*) \gamma_n k_n$$
$$\left[\sigma_n^v \left\{ \phi_P - (1 - \sigma_n^u) \phi_E - \sigma_n^u \phi_W \right\} \right.$$
$$\left. + (1 - \sigma_n^v) \left\{ \phi_N - (1 - \sigma_n^u) \phi_{NE} - \sigma_n^u \phi_{NW} \right\} \right]$$

5.1.3 Calculation of the Coefficients for the Finite-Difference Form of the Equations of Motion

The finite-difference form of the equations of motion, (e.g., Equation (5.7)) can be derived directly from the flux information presented in Tables 5-I through 5-III and the sign conventions determined from Equation (5.5). The resulting expressions will contain the unknown blending factor, γ. The blending strategy requires that the terms in the equations for the coefficients most responsible for producing negative coefficients be isolated so that appropriate values for γ can be determined. Furthermore, the coefficients for the control volumes adjacent to the physical boundaries of the flow may require modification to incorporate the effect of the boundary conditions. Thus, to simplify manipulation and modification, some additional notation will be defined.

Let the center of the control volume (point P) be located at the Ith axial position and Jth radial position. The flux contributions (the components of the total flux) to the east face are denoted as E1(I,J), E2(I,J), E3(I,J) and the flux contributions to the north face are denoted as N1(I,J) N2(I,J), N3(I,J). These flux contributions are defined as follows.

Central Differencing

$$\begin{aligned} E1(I,J) &= D_E - \alpha_e C_E \\ E2(I,J) &= E1(I,J) + C_E \\ E3(I,J) &= 0 \end{aligned} \tag{5.35}$$

$$\begin{aligned} N1(I,J) &= D_N - \alpha_n C_N \\ N2(I,J) &= N1(I,J) + C_N \\ N3(I,J) &= 0 \end{aligned} \tag{5.36}$$

Bounded Skew-Upwind Differencing

$$\begin{aligned} E1(I,J) &= (\sigma_e^u - 1)\, C_E \\ E2(I,J) &= E1(I,J) + C_E \\ E3(I,J) &= k_e (C_E - P^*_{e_e} D_E) \end{aligned} \tag{5.37}$$

$$\begin{aligned} N1(I,J) &= (\sigma_n^v - 1)\, C_N \\ N2(I,J) &= N1(I,J) + C_N \\ N3(I,J) &= k_n (C_N - P^*_{e_n} D_N) \end{aligned} \tag{5.38}$$

The use of central versus bounded skew-upwind differencing is determined by the value of the Peclet number at each face. The parameters C_E, D_E, α_e, k_e, . . . are local values; the subscripts (I,J) have been omitted in the interest of readability. The corresponding flux contributions at the west face are given immediately by E1(I-1,J), E2(I-1,J), E3(I-1,J) and the flux contributions at the south face are N1(I,J-1), N2(I,J-1), N3(I,J-1).

The coefficients of the finite-difference form of the equations of motion may then be defined in terms of these flux contributions. The results are presented in Table 5-IV. The coefficient Ap can be shown to be equal to the sum of the other eight coefficients when use is made of the mass continuity restriction:

$$C_E - C_W + C_N - C_S = 0 \tag{5.39}$$

The boundary conditions (Section 5.1.4) and the blending scheme (Section 5.1.5) can be applied directly to the flux contributions so that the results shown in Table 5-IV are general.

5.1.4 Boundary Conditions

The boundary conditions are applied to the flux contributions as defined by Equations (5.35) through (5.38) so that the set of coefficients (e.g., Table 5-IV) for each dependent variable is the same throughout the computational domain. This consistency simplifies the application of both (1) the algorithm for solving the set of simultaneous equations for each variable and (2) the bounding procedure (see Section 5.1.5).

5.1.4.1 Scalars

A typical control volume for a scalar variable is shown in Figure 5-5 (which is based in part on Figure 5-1). It will be recalled that the axial velocities are stored midway between the scalar gridlines in the axial direction; therefore, the axial velocities are stored at the midpoints of the east and west faces of the scalar control volume. Similarly, the radial velocities are stored at the midpoints of the north and south faces of the scalar control volumes.

The extreme physical boundaries of the flow are located midway between the most extreme gridline and its nearest neighboring gridline in each direction. The gridlines are numbered from I=1 through I=NI in the axial direction and from J=1 through J=NJ in the radial direction. Thus, the interior nodes are numbered from I=2 through NI-1 in the axial direction and from J=2 through NJ-1 in the radial direction. In the following discussion, the boundary conditions are applied to the various faces of the control volume for an interior node (I,J), as shown in Figure 5-5, to produce modified east-west flux contributions (E1, E2, E3) or north-south flux contributions (N1, N2, N3) for use in calculating the coefficients of the finite-difference equations for the scalars (e.g., Table 5-IV). In the process of introducing the effects of the boundary conditions for the interior nodes, it will be seen that some of the flux contributions at adjacent nodes are also affected.

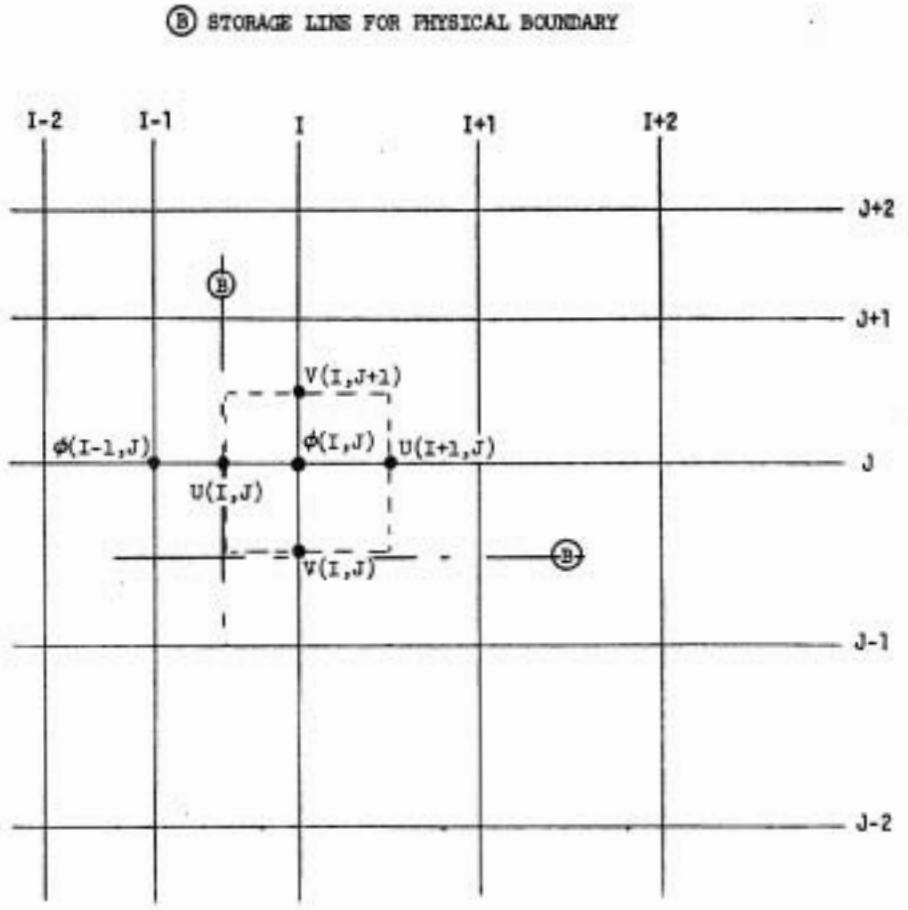

Figure 5-5 Grid System Showing Scalar Control Volume Near Physical Boundaries

TABLE 5-IV

CO-EFFICIENTS OF THE FINITE-DIFFERENCE EQUATIONS

$$A_W(I,J) = E2(I-1,J) - \gamma_w \left[\sigma_e^u E3\right]_{I-1,J}$$
$$+ \gamma_s \left[(1 - \sigma_n^v)\, \sigma_n^u N3\right]_{I,J-1}$$
$$- \gamma_n \left[\sigma_n^v \sigma_n^u N3\right]_{I,J}$$

$$A_E(I,J) = E1(I,J) + \gamma_e \left[(1 - \sigma_e^u) E3\right]_{I,J} + \gamma_s \left[(1 - \sigma_n^v)(1 - \sigma_n^u) N3\right]_{I,J-1}$$
$$- \gamma_n \left[\sigma_n^v (1 - \sigma_n^u) N3\right]_{I,J}$$

$$A_S(I,J) = N2(I,J-1) - \gamma_s \left[\sigma_n^v N3\right]_{I,J-1} + \gamma_w \left[(1 - \sigma_e^u)\, \sigma_e^v E3\right]_{I-1,J}$$
$$- \gamma_e \left[\sigma_e^u \sigma_e^v E3\right]_{I,J}$$

$$A_N(I,J) = N1(I,J) + \gamma_n \left[(1 - \sigma_n^v) N3\right]_{I,J} + \gamma_w \left[(1 - \sigma_e^u)(1 - \sigma_e^v) E3\right]_{I-1,J}$$
$$- \gamma_e \left[\sigma_e^u (1 - \sigma_e^v) E3\right]_{I,J}$$

$$A_{SW}(I,J) = \gamma_w \left[\sigma_e^u \sigma_e^v E3\right]_{I-1,J} + \gamma_s \left[\sigma_n^u \sigma_n^v N3\right]_{I,J-1}$$

$$A_{SE}(I,J) = \gamma_s \left[\sigma_n^v (1 - \sigma_n^u) N3\right]_{I,J-1} - \gamma_e \left[(1 - \sigma_e^u)\, \sigma_e^v E3\right]_{I,J}$$

$$A_{NW}(I,J) = \gamma_w \left[\sigma_e^u (1 - \sigma_e^v) E3\right]_{I-1,J} - \gamma_n \left[(1 - \sigma_n^v)\, \sigma_n^u N3\right]_{I,J}$$

$$A_{NE}(I,J) = -\gamma_e \left[(1 - \sigma_e^u)(1 - \sigma_e^v) E3\right]_{I,J} - \gamma_n \left[(1 - \sigma_n^v)(1 - \sigma_n^u)\right] N3_{I,J}$$

NOTE: The blending factors γ_w, γ_e, γ_s and γ_n are the factors appropriate for the (I,J) node as determined by the procedure discussed in Section 5.1.5.

There are four types of boundary to be considered:

(1) specified wall,
(2) specified inlet,
(3) axis of symmetry,
(4) unspecified opening.

The application of these boundary conditions to modify the flux contributions used to determine the finite-difference coefficients for a node (I-1,J) having a physical boundary on the west face of its control volume will be described in detail. The modifications to the coefficients due to the other physical boundaries are similar and will be summarized.

West Boundary

For the specified wall boundary condition, the velocity normal to the wall at the west boundary (the west face of the control volume for the node (I,J)) is zero; velocity components in the radial or tangential direction may be nonzero (e.g., a moving wall). The zero normal (u) velocity, which for this case is stored at the axial location of the west boundary, results in the use of the central difference formulae for the flux contributions, E1, E2 and E3, for the west face of the node (I,J). These flux contributions are computed and stored as east face contributions for the node (I-1,J), see Equation (5.35). Specifically, for a specified wall located at the west face of the control volume for the node (I,J):

$$\begin{aligned} E1(I-1,J) &= DE(I-1,J) \\ E2(I-1,J) &= E1(I-1,J) \\ E3(I-1,J) &= 0 \end{aligned} \qquad (5.40)$$

For a specified wall, the value of the scalar at the wall may be either known (e.g., turbulence kinetic energy = 0) or unknown (e.g., temperature). Since the variation of the scalar from its wall value to the value at the node (I,J) is generally non-linear, it is prudent in every case to decouple the wall values from the system of equations. The influence of the wall can be reflected by using appropriate wall functions to compute the source terms for the scalars. From Table 5-IV, it can be seen that the known or unknown wall values of the scalar can be excluded if the coefficients A_W, A_{SW}, A_{NW} are zero for the node (I,J). These coefficients depend upon the values of:

a) E2 (I-1,J)
b) E3 (I-1,J)
c) N3 (I,J) - N3 at the north face of the control volume for node (I,J)
d) N3 (I,J-1) - N3 at the south face of the control volume for node (I,J)

Inspection of the coefficients listed in Table 5-IV indicates that N3(I,J) is excluded automatically unless the axial and radial velocities are positive at the north face, and N3(I,J-1) is excluded unless the axial velocity is positive and the radial velocity is negative at the south face of the control volume for the node (I,J).

The necessary modifications can be summarized as follows.

$$\begin{aligned} &E1(I-1,J) = 0 \\ &N3(I,J) = 0 \\ &N3(I,J-1) = 0 \end{aligned} \tag{5.41}$$

It follows immediately from Equation (5.40) that:

$$\begin{aligned} &E2(I-1,J) = 0 \\ &E3(I-1,J) = 0 \end{aligned} \tag{5.42}$$

and therefore, A_W, A_{SW}, and A_{NW} will be zero for the node (I,J).

For a specified opening, the value of the scalar is known at the west face of the control volume for the node (I,J). In general, the cell Peclet number is greater than the transition value whenever the boundary represents a specified opening. Therefore, the flux contributions E1, E2 and E3 at the node (I-1,J) are computed using the skew upwind differencing formulae, Equation (5.37). However, since the boundary is coincident with the west face of the control volume for the node (I,J), there is no skewing of the flow at this face and, therefore, E3(I-1,J) is set to zero.

The determination of the coefficient A_W for the node (I,J) also requires the computation of the north face and south face flux contributions, N3(I,J) and N3(I,J-1), respectively. Since the specified opening is coincident with the west face of the control volume for the node (I,J) and since this face is located midway between the nodes (I-1,J) and (I,J), it is necessary to double the value of the skewing interpolation factors used to compute N3(I,J) and N3(I,J-1); i.e.,

$$\begin{aligned} k_n &= \max\,(2*k_n,\ 1.0) \\ k_s &= \max\,(2*k_s,\ 1.0) \end{aligned} \tag{5.43}$$

where the values of k_n and k_s on the right-hand side of Equation (5.43) are calculated in accordance with the normal distance between gridlines I-1 and I.

If the west face of the control volume for the node (I,J) is an axis of symmetry, then the flux normal to this face is zero. By definition, the unknown values of the scalar at the nodes (I-1,J) and (I,J) are equal; the gradient of the scalar normal to the axis vanishes. Thus, an axis of symmetry is mathematically identical to a specified wall boundary condition with zero gradient (source) at the wall. The modifications to the flux contributions are given by Equations (5.42) and (5.43).

For an unspecified opening, it is assumed that (1) the flow is exiting through the opening, (2) the streamlines are parallel in the vicinity of the opening, and (3) the cell Peclet number exceeds the transition value. Determination of the coefficient A_W, A_{SW}, and A_{NW} for the node (I,J) requires the calculation of the flux contributions E2(I-1,J), E3(I-1,J), N3(I,J) and N3(I,J-1). By the third assumption, the skew upwind differencing formulae,

Equations (5.37) and (5.38), are used. By the second assumption, E3(I-1,J), N3(I,J) and N3(I,J-1) are zero. By the first assumption, the flow direction switch o^u at the node (I-1,J) is zero so that E2(I-1,J) is zero. Thus these assumptions are equivalent to:

$$\begin{aligned} &E2(I-1,J) = 0 \\ &E3(I-1,J) = 0 \\ &N3(I,J) = 0 \\ &N3(I,J-1) = 0 \end{aligned} \tag{5.44}$$

and it follows that A_W, A_{SW}, and A_{NW} for the node (I,J) vanish. Thus, the unknown values of the scalars at the unspecified opening are decoupled from the system of equations.

It is seen that the modifications to the flux contributions for the specified wall, axis of symmetry, and unspecified opening boundary conditions are identical and, therefore, the coefficients A_W, A_{SW}, and A_{NW} for the node (I,J) vanish for these boundary conditions.

East Boundary

If the east face of the control volume for the node (I,J) is a physical boundary, it is necessary to modify the flux contributions E1(I,J), E3(I,J), N3(I,J) and N3(I,J-1) used to determine the coefficients A_E, A_{SE}, and A_{NE} for the node)I,J). For reasons similar to those given in the discussion of the west boundary, in the case of the specified wall, axis of symmetry, or unspecified opening boundary conditions, it is necessary that:

$$\begin{aligned} &E1(I,J) = 0 \\ &E3(I,J) = 0 \\ &N3(I,J) = 0 \\ &N3(I,J-1) = 0 \end{aligned} \tag{5.45}$$

so that A_E, A_{SE}, and A_{NE} for the node (I,J) are zero. For the specified opening, it is sufficient that:

$$\begin{aligned} &E3(I,J) = 0 \\ &k_n = \max\,(2*k_n,\ 1.0) \\ &k_s = \max\,(2*k_s,\ 1.0) \end{aligned} \tag{5.46}$$

The last two conditions guarantee that the flux contributions N3(I,J) and N3(I,J-1) are calculated correctly.

South Boundary

If the south face of the control volume for the node (I,J) is a specified wall, an axis of symmetry, or an unspecified opening, then it is necessary that:

$$\begin{aligned} &N2(I,J-1) = 0 \\ &N3(I,J-1) = 0 \\ &E3(I-1,J) = 0 \\ &E3(I,J) = 0 \end{aligned} \tag{5.47}$$

so that the coefficients A_S, A_{SW}, and A_{SE} vanish. For a specified opening, it is necessary that:

$$\begin{aligned} &N3(I,J-1) = 0 \\ &k_w = \max\ (2*k_w,\ 1.0) \\ &k_e = \max\ (2*k_e,\ 1.0) \end{aligned} \tag{5.48}$$

The last two conditions assure that E3(I-1,J) and E3(I,J) are computed properly.

North Boundary

If the north face of the control volume for the node (I,J) represents a specified wall, an axis of symmetry, or an unspecified opening, then it is necessary that:

$$\begin{aligned} &N1(I,J) = 0 \\ &N3(I,J) = 0 \\ &E3(I-1,J) = 0 \\ &E3(I,J) = 0 \end{aligned} \tag{5.49}$$

so that the coefficients A_N, A_{NW}, and A_{NE} vanish. For a specified opening, it is necessary that:

$$\begin{aligned} &N3(I,J) = 0 \\ &k_w = \max\ (2*k_w,\ 1.0) \\ &k_e = \max\ (2*k_e,\ 1.0) \end{aligned} \tag{5.50}$$

The last two conditions guarantee that E3(I-1,J) and E3(I,J) are calculated correctly.

5.1.4.2 Axial Velocity

A typical control volume for the axial velocity, u, is shown in Figure 5-6. The indices I and J refer to the scalar grid system. The index I' refers to the axial velocity grid system; note that this index varies between I'=2 and NI. The east and west faces of the axial velocity control volumes are coincident with the vertical scalar gridlines. The axial storage locations of physical boundaries are the same as the axial locations of the axial velocities; the inverse is, of course, not true. The radial locations of the u

velocity and scalar control volumes are identical. The radial velocity, v, is stored (effectively) at the corners of the u-velocity control volume. The system of simultaneous equations for the axial velocity field describes the axial velocity distribution from I'=3 to NI-1 and J=2 to NJ-1. However, the coefficients for this system of equations require the determination of some flux contributions along the gridlines I'=2 to I'=NI-1 and J=1 to J=NJ-1.

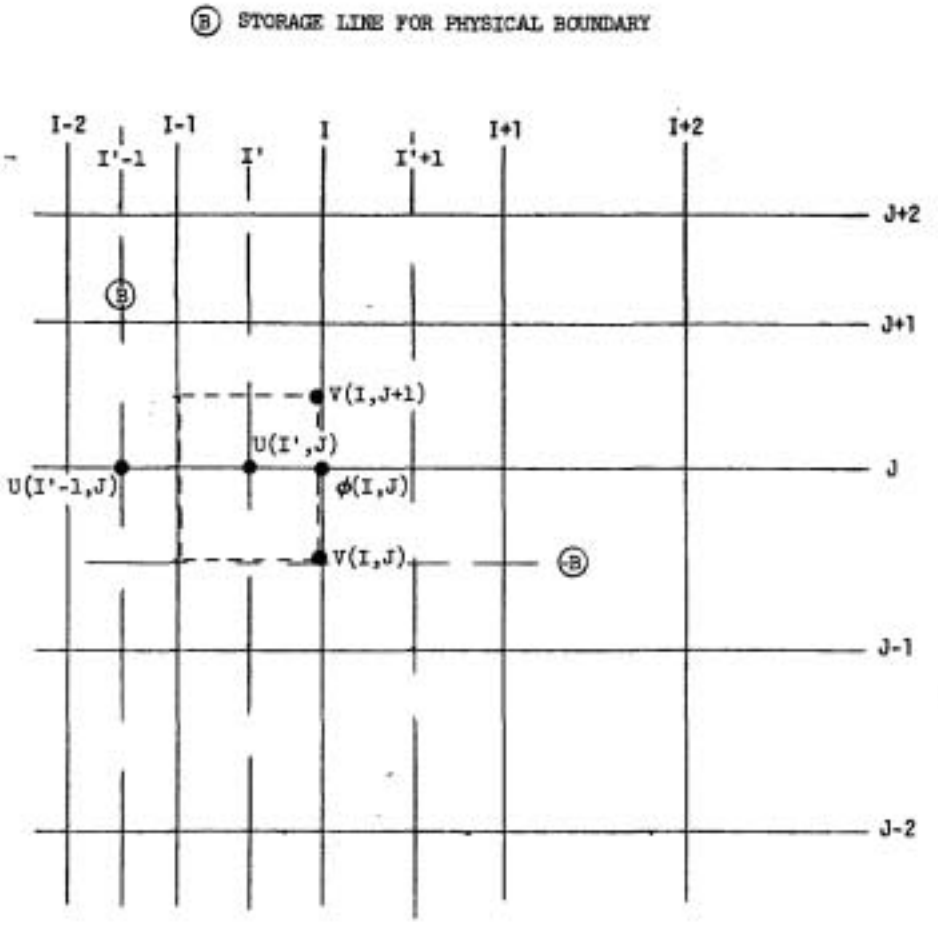

Figure 5-6 Scalar and U-Velocity Grid Systems Showing U-Velocity Control Volume Near Physical Boundaries

West Boundary

If a physical boundary is located to the west of the axial velocity control volume for the node (I',J), then the physical boundary is located along the gridline, I'-1. If the physical boundary represents either a specified wall or an axis of symmetry, then u(I'-1,J) is zero; if it represents a specified opening, then u(I'-1,J) is a known, specified value. If the physical boundary represents an unspecified opening, then it is assumed that the velocity u(I'-1,J) is known from the previous iteration using a special procedure described below. In every case, it is seen that the axial velocity is known at the node (I'-1,J). Therefore, the axial velocity at the west face of the control volume for the node (I',J) can be computed in the same manner as is used for any axial velocity interior node.
The radial velocities for the west face of the control volume are stored at the corners of the axial velocity control volume (see Figure 5-6). Therefore the radial velocity at the center of the west face can be interpolated directly from these data. Thus, one can obtain the values of u and v and the flux contributions can be computed using Equation (5.35) or (5.37) in the usual manner. Thus, it is seen that the application of the boundary conditions at the node (I,J) requires no modification to the computation of E1, E2 and E3 provided that the correct axial velocities are stored at the node (I'-1,J).

In the discussion on scalar variables, it was stated that, at an unspecified opening, it is assumed that (1) the flow is exiting through the opening, (2) the streamlines are parallel in the vicinity of the opening, and (3) the cell Peclet number exceeds the transition value. These assumptions are also made for the determination of the axial velocity at an unspecified opening. It is possible to estimate the axial velocity at the node (I'-1,J) using these assumptions together with the mass conservation restriction for the total mass flow rate and a relationship for the axial velocity distribution at an unspecified opening based upon the second assumption and conservation of radial momentum. Since this procedure is not peculiar to the bounded skew hybrid differencing procedure but is part of the general procedures used for all finite-difference schemes in the TEACH computer program, it will not be described in this section. The procedure produces an estimate for the axial velocity at the node (I'-1,J) for the unspecified opening boundary condition using the solution obtained from the previous iteration.

East Boundary

If a physical boundary is located immediately to the east of the axial velocity control volume for the node (I'J), then the physical boundary is located along the gridline, I'+1. The various boundary conditions affect the value of the axial velocity u(I'+1,J) in a manner similar to that described for the west boundary.

South Boundary

The radial positions of the scalar and axial velocity grid systems are the same. Therefore, if the south face of the axial velocity control volume for the node (I',J) is also a physical boundary, then the modifications of the flux contributions are similar to those made for the scalar with a physical boundary along its south face, Equation (5.47) or (5.48). In the present case, the storage location for the radial position of the axial velocity is always coincident with the radial position of the axial velocity control volume. Therefore, the skewing interpolation factors, k_w and k_e, are always increased in accordance with Equation (5.48).

If the physical boundary at the south face of the axial velocity control volume represents a corner, then in accordance with the definition of the location of the physical boundaries relative to the scalar grid system, the corner extends to the midpoint of the south face. Therefore, the axial (U_s) and radial (V_s) velocities used at this face to compute the flux contributions are determined from a weighted average of velocities for the specified wall and an appropriate flow boundary condition.

North Boundary

If a physical boundary is located along the north face of the axial velocity control volume for the node (I',J), then the boundary conditions are used to modify the flux contributions in a manner similar to that used for the south boundary. The treatment for a corner is also similar.

5.1.4.3 Radial Velocity

A typical control volume for the radial velocity, v, in the vicinity of the physical boundaries is shown in Figure 5-7. The indices I and J refer to the scalar grid system. The index J' refers to the radial velocity system; note that this index varies between J'=2 and NJ. The axial location of the v and scalar control volumes are identical. The axial velocity is stored (effectively) at the corners of the v-velocity control volume. The system of equations for the radial velocity field describes the radial velocity distribution for I=2 to NI-1 and J'=3 to NJ-1. However, the coefficients for the system of equations require the determination of some flux contributions along the gridlines I=2 to NI-1 and J'=2 to NJ-1.

Because of the symmetry of the notation describing the axial and radial velocity distribution, the modifications to the parameters used to compute the flux contribution coefficients of the finite-difference equations for the radial velocity follow immediately from the discussion of the scalar and axial velocity boundary conditions.

5.1.4.4 Tangential Velocity

The axial and radial locations of the gridlines for the tangential velocity, w, and the scalars are identical. It then follows that the boundary conditions are treated in a similar manner so the modifications discussed earlier in the case of the scalars apply to the tangential velocity as well.

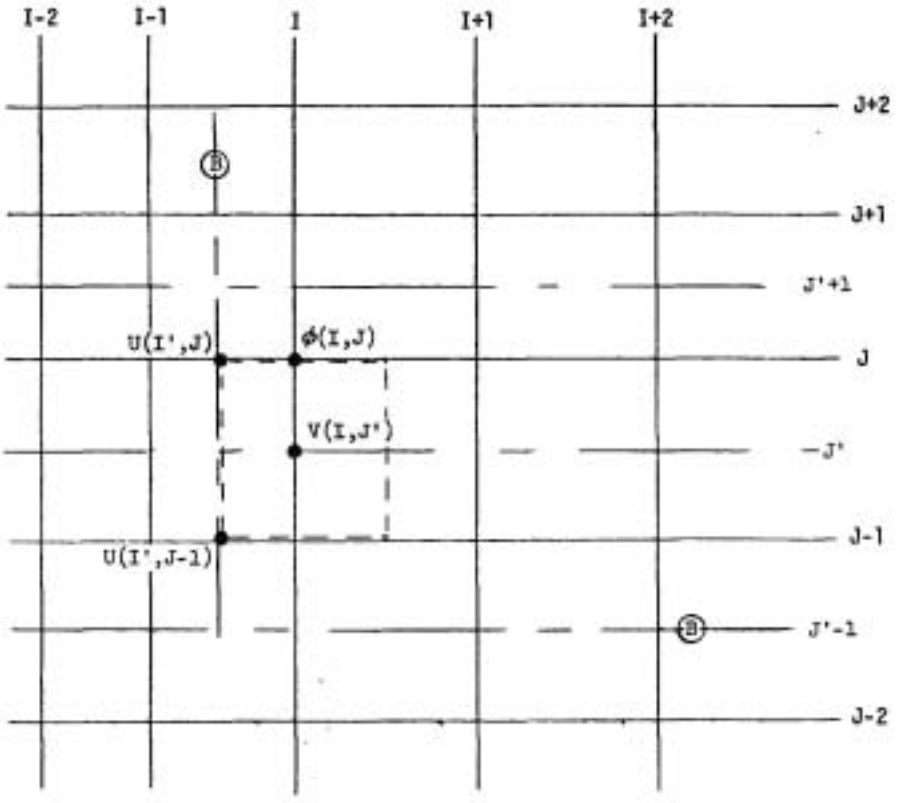

Figure 5-7 Scalar and V-Velocity Grid Systems Showing V-Velocity Control Volume Near Physical Boundaries

5.1.5 The Bounding Scheme

The calculation of the bounded skew-upwind differencing fluxes and, therefore, the determination of the coefficients to the finite-difference form of the equations of motion, require that the blending factor, γ, be determined. The blending factor specifies the respective contributions of the flux computed using skew and upwind differencing. For example, at the west face of the typical control volume, Equation (5.32) states:

$$\frac{F_{w_{BSUD}}}{D_w} = \gamma_w F_{w_{SUD}} + (1 - \gamma_w) F_{w_{UD}} \tag{5.51}$$

The coefficients including the local blending factor are listed in Table 5-IV.

It is possible to show that the corner coefficients (A_{SW}, A_{SE}, A_{NW}, A_{NE}) are unconditionally non-negative. For example, consider the coefficient A_{SW}:

$$A_{SW}(I,J) = \gamma_w [\sigma^u_e \sigma^u_e E3]_{I-1,J} + \gamma_s [\sigma^u_n \sigma^u_n N3]_{I,J-1} \tag{5.52}$$

Both γ_W and γ_S are restricted to the range $0 \leq \gamma \leq 1$. If both the axial and radial velocities at the west face of the control volume are positive, then both σ_e^u and σ_e^v at this location are unity; in any other case, either (or both) are zero. For positive u and v velocities, the flux contribution E3(I-1,J) at the west face is positive. Therefore, the west face flux contribution to A_{SW} is always non-negative. The same reasoning, when applied to the south face, leads to a similar conclusion. Therefore, A_{SW} is unconditionally non-negative. The other corner coefficients are treated in the same manner.

Now, consider the four main coefficients (A_W, A_E, A_S, A_N). From Table 5-IV:

$$A_W(I,J) = E2(I-1,J) - \gamma_W \left[\sigma_e^u E3\right]_{I-1,J} + \gamma_S \left[(1-\sigma_n^v)\, \sigma_n^u N3\right]_{I,J-1} - \gamma_n \left[\sigma_n^v \sigma_n^u N3\right]_{I,J} \qquad (5.53)$$

From the definitions of the flux contributions, Equations (5.35) through (5.38), it is evident that:

(1) E2(I-1,J) is positive if the axial velocity is positive and it is zero otherwise;

(2) σ_e^u and E3 at the west face (I-1,J] are positive if the axial velocity is positive but σ_e^u is zero if u is negative;

(3) from the definitions of E2 and E3 and the fact that $\gamma_W \leq 1$, it is therefore concluded that the first two terms in Equation (5.53) must yield a non-negative result;

(4) the third term is zero unless u is positive and v is negative at the south face, in which case, it is negative;

(5) the fourth term is non-positive because the term within the brackets is always non-negative.

Therefore, it is possible that the coefficient A_W is negative.

It is desirable that all of the coefficients of the finite-difference form of the equations of motion (Equation (5.7)) be non-negative for in this case the value of the dependent variable ϕ at the node P is simply a weighted average of the values of ϕ at the surrounding nodes exclusive of the somewhat complicating effects of local sources. A bounding scheme is a procedure to limit the values of the coefficients of the finite difference equations in such a manner as to produce this physically realistic result. Its principal computational advantage is to exclude under- and overshoots of the solution during the iterative procedure. These oscillations can produce severe numerical instability.

The bounding procedure used herein is based upon the following sequence.

(1) For each iteration, the solution for the distribution of the dependent variable ϕ is obtained using the blending factors γ determined during the previous iteration; the blending factors are set to unity for the first iteration.

(2) For each point P in the variable field, the maximum and minimum values for ϕ are determined from the neighbors:

$$\phi_{max}=\max\ (\phi_N,\ \phi_S,\ \phi_E,\ \phi_W,\ \phi_{NE},\ \phi_{NW},\ \phi_{SW},\ \phi_{SE}) \tag{5.54}$$

$$\phi_{min}=\min\ (\phi_N,\ \phi_S,\ \phi_E,\ \phi_W,\ \phi_{NE},\ \phi_{NW},\ \phi_{SW},\ \phi_{SE}) \tag{5.55}$$

It should be noted that the effects of sources are not included explicitly in calculating ϕ_{max} or ϕ_{min} since the explicit result is difficult to perform while avoiding double counting of the source effect. However, the effect of sources on the neighbors is accounted for implicitly because the difference equations being solved include these sources. In any case, the results obtained will be no worse than to force the use of upwind differencing by making $\gamma = 0$ at the node where a peak in the profile of the variable being considered is occurring.

It should also be noted that one or more ϕ may be excluded from the determination of ϕ_{max} or ϕ_{min} when the control volume under consideration is adjacent to certain types of physical boundaries. For example, if the x-axis is an axis of symmetry, then ϕ_S is excluded since it is identical to ϕ_P and its use could yield an inappropriate range of permissible values.

(3) If $\phi_{min} < \phi_P < \phi_{max}$, then the local value of the blending factor is unaltered from its current value. However, if ϕ_P is outside of this range, then a new value of γ must be determined. For this purpose each of the coefficients in Table 5-IV is written in the form:

$$A_k = A_k' + \gamma A_k'', \quad k = N,\ S,\ NE,\ SE\ \ldots \tag{5.56}$$

where it has been assumed that the blending factors for each of the faces of the local control volume are equal. Then Equation (5.7) can be written as:

$$\phi_p \left[\Sigma A_k' + \gamma \Sigma A_k''\right] - S_p\phi_p = \Sigma A_k'\phi_k + \gamma \Sigma A_k''\phi_k + S_u \tag{5.57}$$

Now, if $\phi p < \phi_{min}$, then from this equation,

$$\gamma > \frac{\Sigma A_k'\phi_k - \phi_{min} \Sigma A_k' + S_u + S_p\phi_{min}}{\phi_{min} \Sigma A_k'' - \Sigma A_k''\phi_k} \tag{5.58}$$

but if $\phi p > \phi_{max}$, then

$$\gamma < \frac{\Sigma A_k'\phi_k - \phi_{max} \Sigma A_k' + S_u + S_p\phi_{max}}{\phi_{max} \Sigma A_K'' - \Sigma A_k''\phi_k} \tag{5.59}$$

Of course, in practice the value of γ is determined by use of the appropriate equality for Equation (5.58) or Equation (5.59).

(4) In this fashion, the local value of $\gamma(I,J)$ is determined. The coefficients in Table 5-IV are then recomputed using the blending factors and the new distribution of ϕ is determined. For each face of the control volume at the point (I,J), there are two values of γ as determined for the two control volumes sharing the common face. Thus, a sufficient condition for assigning local values of the blending factors is given by:

$$\begin{aligned} \gamma_w &= \min\left[\gamma\ (I-1,J),\ \gamma\ (I,J)\right] \\ \gamma_e &= \min\left[\gamma\ (I,J),\ \gamma\ (I+1,J)\right] \\ \gamma_s &= \min\left[\gamma\ (I,J-1),\ \gamma\ (I,J)\right] \\ \gamma_n &= \min\left[\gamma\ (I,J),\ \gamma\ (I,J+1)\right] \end{aligned} \tag{5.60}$$

This procedure for determining the blending factors effectively limits the value of the dependent variable range to values of its principal neighbors. However, it is still possible that some of the main coefficients will be negative. More restrictive schemes can be formulated (e.g., blending strategy 1) that guarantee that all coefficients of the finite-difference equations are non-negative but these procedures achieve this result by reducing the blending factor toward zero; the greater relative contribution of upwind differencing in this case produces larger amounts of numerical diffusion. Thus, the selection of a blending scheme represents a compromise between the undesirable effects of numerical instability and numerical diffusion.

5.2 THE QUDS DIFFERENCING SCHEME

In this section, the QUDS (for Quadratic Upwind Differencing Scheme) is described. This finite differencing method was developed by Leonard (Ref. 30 and 31) and is based upon interpolating for the value of the dependent variable at each face of the control volume by using a second-degree (quadratic) polynomial biased toward the upwind direction as discussed below. The interpolated value is used to calculate the convective term in the governing equation for the dependent variable while central differencing is used to approximate the diffusion term. No bounding procedure was used with QUDS in the current program.

5.2.1 Flux Form of the Equations of Motion

It will be recalled from the discussion of the skew-upwind differencing scheme that the flux form of the governing equation is:

$$F_e - F_w + F_n - F_s = S_u + S_p\phi_p \tag{5.61}$$

where the fluxes are calculated using:

$$\begin{aligned} F_e &= C_E\phi_e - D_E(\phi_E - \phi_p) \\ F_w &= C_W\phi_w - D_W(\phi_p - \phi_W) \\ F_n &= C_N\phi_n - D_N(\phi_N - \phi_p) \\ F_s &= C_S\phi_s - D_S(\phi_p - \phi_S) \end{aligned} \tag{5.62}$$

Then using quadratic interpolation for ϕ_e, ϕ_w, ϕ_n, ϕ_s and referring to Figure 5-8, it can be shown that the finite-difference form of Equation (5.61) is:

$$\begin{aligned} A_p\phi_p = {} & A_E\phi_E + A_W\phi_W + A_N\phi_N + A_S\phi_S + A_{EE}\phi_{EE} + A_{WW}\phi_{WW} + A_{NN}\phi_{NN} \\ & + A_{SS}\phi_{SS} + S_u + S_p\phi_p \end{aligned} \tag{5.63}$$

5.2.2 Calculation of the Fluxes

In this section, the calculation of the values of the dependent variable at the faces of the control volume shown in Figure 5-8 is described. The derivation of F_w, the flux at the west face of a typical scalar control volume, is given in detail. The derivation of the other fluxes is outlined.

Recall that the flux to the west face is given by:

$$F_w = C_w\phi_w - D_w(\phi_P - \phi_W) \tag{5.64}$$

In its original form, QUDS required the use of a general second-degree polynomial for the calculation of ϕ_w (see Ref. 31):

$$\phi_w = c_0 + c_1x + c_2x^2 + c_3y + c_4y^2 + c_5xy \tag{5.65}$$

However, it is argued in Ref. 31 that it is generally unnecessary to consider interpolation in the transverse direction so that for ϕ_w (and, similarly for ϕ_e):

$$\phi = c_0 + c_1x + c_2x^2 \tag{5.66}$$

while for ϕ_n or ϕ_s:

$$\phi = c_0 + c_1y + c_2y^2 \tag{5.67}$$

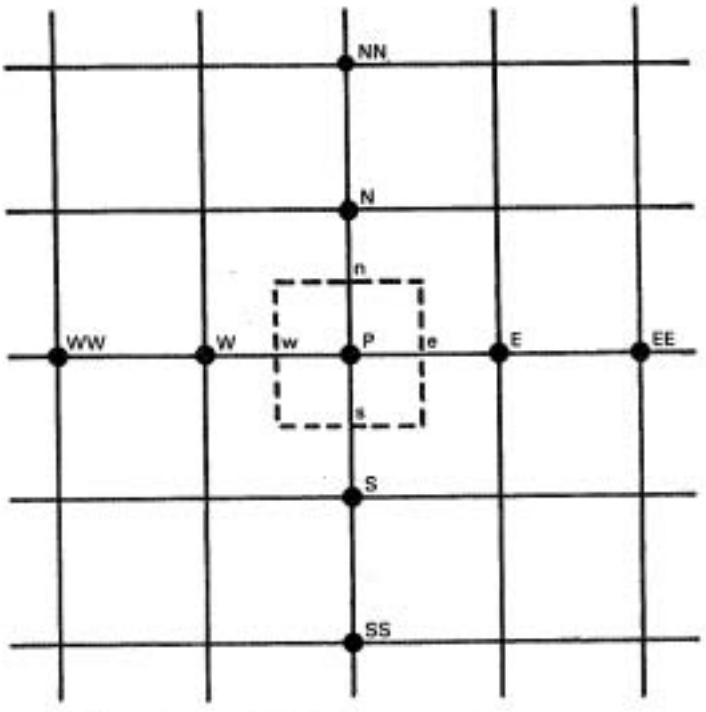

Figure 5-8 Control Volume for the QUDS Scheme

In calculating ϕ_w, the mathematically equivalent but more convenient quadratic form is used.

$$\phi = c_0 + c_1(x - x_P) + c_2(x - x_p)(x - x_W) \tag{5.68}$$

Consider the situation for positive axial velocity u in which case the values of ϕ at the grid nodes P, W and WW are used to evaluate c_0, c_1, and c_2; that is, the calculation of ϕ_w, designated ϕ_w^+ in this case, is biased toward the upwind node at X_{WW}. Then:

$$\phi_w^+ = \phi_p + \frac{\phi_W - \phi_p}{X_W - X_p}(X_w - X_p) + \left[\frac{\phi_{WW} - \phi_p}{X_W - X_p} - \frac{\phi_W - \phi_p}{X_W - X_p}\right] \frac{(X_w - X_p)(X_w - X_W)}{X_{WW} - X_W} \tag{5.69}$$

For the case when the axial velocity is negative, the coefficients in Equation (5.68) are calculated using the values of ϕ at the grid nodes W, P and E (that is, biased upwind from the west face) so that:

$$\phi_w^- = \phi_p + \frac{\phi_W - \phi_p}{X_W - X_p}(X_w - X_p) + \left[\frac{\phi_E - \phi_P}{X_E - X_p} - \frac{\phi_W - \phi_p}{X_W - X_p}\right] \frac{(X_w - X_p)(X_w - X_W)}{X_E - X_W} \tag{5.70}$$

Defining a flow velocity direction switch in the same manner as that used in the bounded skew-upwind differencing procedure, the value of ϕ at the west face becomes:

$$\phi_w = \sigma_w^u \phi_w^+ + (1 - \sigma_w^u) \phi_w^- \tag{5.71}$$

The value of ϕ at the other faces of the control volume is calculated analogously. For the east face, the values of ϕ at the grid nodes W, P and E are used when the axial velocity is positive and the values at the grid nodes P, E and EE are used when the axial velocity is negative. Since the interpolation for the south and north face is formally identical to that for the west and east face, respectively, the expression for ϕ_s (or ϕ_n) can be obtained directly from ϕ_w (or ϕ_e).

5.2.3 Calculation of the Coefficients for the Finite-Difference Form of the Equations of Motion

The finite-difference form of the equations of motion (e.g., Equation (5.63)) can be obtained by inserting the expressions for ϕ_e, ϕ_w, ϕ_s, and ϕ_n into Equation (5.62) and applying Equation (5.61). From equations like (5.69) and (5.70), it can be seen that all ϕ_i, $i \neq P$, occur as the difference between ϕ_i and ϕ_p. Hence, the coefficient of ϕ_p in Equation (5.63) becomes:

$$A_p = \sum_{i \neq P} A_i + C_E - C_W + C_N - C_S - S_P \tag{5.72}$$

However, the mass continuity restriction requires that:

$$C_E - C_W + C_N - C_S = 0 \tag{5.73}$$

so that:

$$A_p = \sum_{i \neq p} A_i \quad - S_p \tag{5.74}$$

The equations for the coefficients of Equation (5.63) are presented in Table 5-V. It should be noted that these coefficients are expressed as much as possible in a manner consistent with that used for the bounded skew-upwind differencing method. The mneumonic devices used in implementing QUDS into TEACH differ from the current nomenclature because implementation of QUDS was initiated prior to the derivation of the equations for BSUDS2.

5.2.4 Boundary Conditions

In QUDS, boundary conditions are applied directly to the finite-difference coefficients listd in Table 5-V. There are four types of boundary conditions used in the present analysis:

(1) specified wall,
(2) specified inlet,
(3) axis of symmetry
(4) unspecified opening.

The discussion presented in this section relies heavily on remarks made earlier in Section 5.1.4 for the bounded skew-upwind differencing procedure.

5.2.4.1 Scalars

When calculating for the flux on a face of a control volume, adjustments are made if this face is near a boundary. For the west face, adjustments are made for the situations shown in Figure 5-9.

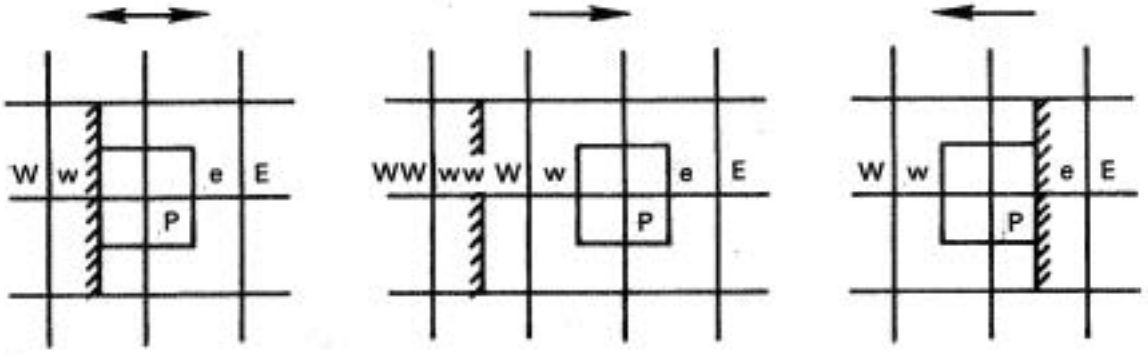

Case 1: West face boundary

Case 2: West-sest face boundary, flow positive

Case 3: East face boundary, flow negative

Figure 5-9 Axial Velocity Boundary Condition Application

TABLE 5-V

COEFFICIENTS OF THE FINITE-DIFFERENCE EQUATIONS FOR QUDS

$$A_W = C_W(1-\alpha_w) + D_W - C_W\alpha_w(1-\alpha_w)\frac{X_P-X_W}{X_E-X_W} + \sigma_w^u C_W\alpha_w(1-\alpha_w)\frac{X_P-X_W}{X_E-X_W}\frac{X_E-X_{WW}}{X_W-X_{WW}}$$
$$+ \sigma_e^u C_E\alpha_e(1-\alpha_e)\frac{X_E-X_P}{X_P-X_W}\frac{X_E-X_P}{X_E-X_W}$$

$$A_E = -C_E\alpha_e + D_E + C_E\alpha_e(1-\alpha_e)\frac{X_E-X_P}{X_E-X_W} - (1-\sigma_e^u)C_E\alpha_e(1-\alpha_e)\frac{X_E-X_P}{X_E-X_W}\frac{X_{EE}-X_W}{X_{EE}-X_E}$$
$$- (1-\sigma_w^u)C_W\alpha_w(1-\alpha_w)\frac{X_P-X_W}{X_E-X_P}\frac{X_P-X_W}{X_E-X_W}$$

$$A_S = C_S(1-\alpha_s) + D_S - C_S\alpha_s(1-\alpha_s)\frac{Y_P-Y_S}{Y_N-Y_S} + \sigma_s^v C_S\alpha_s(1-\alpha_s)\frac{Y_P-Y_S}{Y_N-Y_S}\frac{Y_N-Y_{SS}}{Y_S-Y_{SS}}$$
$$+ \sigma_n^v C_N\alpha_n(1-\alpha_n)\frac{Y_N-Y_P}{Y_P-Y_S}\frac{Y_N-Y_P}{Y_N-Y_S}$$

$$A_N = -C_N\alpha_n + D_N + C_N\alpha_n(1-\alpha_n)\frac{Y_N-Y_P}{Y_N-Y_S} - (1-\sigma_n^v)C_N\alpha_n(1-\alpha_n)\frac{Y_N-Y_P}{Y_N-Y_S}\frac{Y_{NN}-Y_S}{Y_{NN}-Y_N}$$
$$- (1-\sigma_s^v)C_S\alpha_s(1-\alpha_s)\frac{Y_P-Y_S}{Y_N-Y_P}\frac{Y_P-Y_S}{Y_N-Y_S}$$

$$A_{WW} = -C_W\sigma_w^u\alpha_w(1-\alpha_w)\frac{X_P-X_W}{X_P-X_{WW}}\frac{X_P-X_{WW}}{X_W-X_{WW}}$$

$$A_{EE} = C_E(1-\sigma_e^u)\alpha_e(1-\alpha_e)\frac{X_E-X_P}{X_{EE}-X_P}\frac{X_E-X_P}{X_{EE}-X_E}$$

$$A_{SS} = -C_S\sigma_s^v\alpha_s(1-\alpha_s)\frac{Y_P-Y_S}{Y_P-Y_{SS}}\frac{Y_P-Y_S}{Y_S-Y_{SS}}$$

$$A_{NN} = C_N(1-\sigma_n^v)\alpha_n(1-\alpha_n)\frac{Y_N-Y_P}{Y_{NN}-Y_P}\frac{Y_N-Y_P}{Y_{NN}-Y_N}$$

These boundaries can be any of the following types: a) Specified opening, b) Unspecified opening, c) Specified wall, and d) Axis. Separate treatment is required for each of these types. In the following sections, these boundaries are considered for each of the cases described above.

Case 1

If the boundary is a specified wall, axis, or an unspecified opening, the nodes W and WW are decoupled from the system of equations and the influence of the wall is incorporated into the finite-difference equations using the source terms; hence, A_W and A_{WW} are set equal to zero. For a specified inlet, the value of ϕ is known and is effective at the west face, hence, A_{WW} is set equal to zero. However, because central differencing is used, D_W (the diffusion through the west face), is calculated as if ϕ was located a full node away. Therefore, one extrapolates to get ϕ_W from ϕ_W, ϕ_P, and ϕ_E. The resultant extra terms are incorporated into the source terms.

Case 2

The west face for the west node is coincident with a boundary and the velocity on the west face is eastward. In this case, the value of ϕ_{WW} must be approximated. For an axis of symmetry, this value should be the same as ϕ_W. For an unspecified opening, the assumption that the flow is parallel to the gridlines in the region of the opening again suggests that ϕ at the west-west node should be set equal to ϕ at the west node. For a specified wall, the ϕ_{WW} node is set equal to ϕ_W because for scalar variables the gradient in ϕ near the wall is assumed to be zero. For a specified opening, the known value on the boundary is used, and an extrapolation can be used so that ϕ_{WW} is a function of ϕ_{WW}, ϕ_W, and ϕ_P. In all cases, the resultant extra terms are incorporated into the source terms.

Case 3

For flow westward through the west face when the east face is a boundary, the approximation for ϕ_W uses ϕ_E at the east node rather than on the east face. For an axis of symmetry, unspecified opening, or specified wall, the treatment is analogous to Case 2 and ϕ_E is set equal to ϕ_e. For a specified opening, an extrapolation of ϕ_W, ϕ_P, and ϕ_E is used to approximate ϕ_e. As in case 2, all resultant extra terms are incorporated into the source terms.

Since the computational molecule used in QUDS is more extensive than that used for SUDS, there are a number of additional special cases that must be considered in modifying the coefficients of the finite-difference equations in the vicinity of the boundaries. These modifications are too tedious to examine here, and the interested reader should consult the computer program developed during this effort.

5.3 COST OF QUDS AND BSUDS2

In Table 5-VI, the CPU time required to assemble the coefficients of the finite-difference equations relative to that required when using the hybrid differencing method are shown for BSUDS2 and QUDS as implemented in the 2D-TEACH computer code used in this contract. BSUDS2 requires considerably more CPU time to assemble coefficients than does QUDS. Since QUDS is unbounded, its coefficients can be calculated as needed (i.e., "in line"). For BSUDS2, these coefficients must be computed and stored prior to application of the bounding strategy; then, the coefficients must be bounded in a process that requires nearly as much CPU time as that required for computing them in the first instance. Since the solver requires only about 30 percent of the total CPU time for any of the schemes, the total cost of using BSUDS2 is nearly twice that of QUDS. These time requirements do not include the effect of the time required to achieve a converged solution using hybrid, bounded skew, or quadratic differencing. This effect varies from problem to problem. In some cases, QUDS required more iterations to achieve convergence; in other cases, BSUDS2 required more iterations. In general, both BSUDS2 and QUDS required more iterations to converge than did hybrid differencing. In Section 6 detailed convergence information for all test cases is given.

The storage requirements for BSUDS2 and QUDS are also different (Table 5-VII). BSUDS2 requires 20 extra two-dimensional storage arrays where QUDS requires no additional arrays, in part because BSUDS2 was bounded whereas QUDS was not. However, BSUDS2 can also be programmed in such a way as to require less storage, but only at the cost of reduced speed and increased complexity of the code. Since 2D-TEACH is a large code, the percentage increase in storage is not significant.

In 3D-TEACH, BSUDS2 also requires twice as much CPU time as does hybrid differencing per iteration. Since the number of coefficients which have to assembled in 3D are three times as many as 2D-TEACH, it can be seen that 3D-TEACH has been coded much more efficiently than has 2D-TEACH. The storage requirements of BSUDS2 are increased significantly when compared to 2D-TEACH; that is 53 additional 3D-storage arrays are required. Since 3D-TEACH analyzes less physically complex flows (apart from flow dimensionality) than 2D-TEACH analyzes, the storage requirement goes up by a factor of two.

TABLE 5-VI

COST OF IMPROVED ACCURACY

Time

Scheme	Coefficient Assembly Time [iteration x node]	Solar [iteration x node x sweep
HYBRID	1.0 * (0.07m sec)	1 * (0.015m sec)
BUSDS2	2.3	1
QUDS	1.3	1

*Normalized to HYBRID

TABLE 5-VII

COST OF IMPROVED ACCURACY

Storage

Scheme	Number of Extra Arrays Used	Storage Increase (percent)
BSUDS2	20	13
QUDS	0	0

6.0 DISCUSSION OF TEST CASES

Two classes of test cases were used to demonstrate the accuracy improvement of the computer programs used in this contract. The first class consists of a set of highly idealized cases for which the exact results are known. This class was used (1) to verify that the computer programs were substantially free of programming errors and (2) to determine by numerical experiment the properties of selected mathematical features of the program. This first class of test cases was used in conjunction with the model problem studies and is described in Section 4.0. The present discussion is limited to describing the results obtained using the second class of test cases.

The need for the second class of test cases arises because in the first type of problems the flow field was assumed to be uniform and properties such as density and viscosity were constant. In addition, the mesh was uniform and cell aspect ratio was unity. None of these conditions exists when analyzing real combustor flows; hence, conclusions reached after running the first class of problems can become invalid when real combustor flows are calculated. It is therefore essential to check the selected schemes in situations which are simple enough in geometry to be modeled exactly by 2D-TEACH and 3D-TEACH and yet be representative of 3D-combustor calculations. In addition to satisfying the above criterion, these test cases have to meet the conditions used to select bench mark experiments suitable for verifying CFD codes (Ref. 1). These conditions are listed below.

1) Minimum necessary flow dimensionality. For the two dimensional version of TEACH, experiments in which the flows can be represented as two-dimensional were selected. Three-dimensional flow situations were used only when specifically testing the three-dimensional version of the program.

2) Well-behaved flows. Flows in which instabilities, periodicity, or changes in gross behavior occur as flow conditions change were avoided. For example, flows were not used in which the location of reattachment points of separated flow regions could undergo significant shifts as Reynolds number is changed over the range of interest.

3) Known boundary conditions. Experiments were selected for which entrance (and exit) flow profiles could be specified as completely as possible. For turbulent flows, initial profiles of turbulence intensity and integral length scale were sought.

4) Extensive instrumentation. Attempts were made to find flow mapping experiments in which nonintrusive techniques were used to characterize flows throughout the chamber volume.

As the test cases selected originally were run using both the baseline and revised versions of the computer program, it became apparent that additional test cases were needed. For example, the accurate prediction of turbulent flows requires the use of both a good numerical scheme and a sufficiently accurate turbulence model. Current turbulence models require further

development and their use may produce errors that cannot be separated from those produced by alternative numerical procedures. Therefore, two laminar flow cases were also selected for analysis; however, one of these cases was not based upon experimental data.

The turbulent flow test cases were based on experiments discussed in References 1, 32, and 33. In general, none of the test cases satisfies completely all of the criteria noted previously. In some cases, one or more important inlet profile is not reported; in these cases, the unknown inlet conditions have been assumed or extrapolated from downstream results. However, all of the test cases do contain flow features representative of those found in modern gas turbine engine combustors.

The test cases used were:

1) Laminar flow over a rearward facing step (2D)
2) Laminar flow with swirl in a sudden expansion (2D)
3) Turbulent flow over a rearward facing step (2D)
4) Coannular turbulent flow in a sudden expansion (2D)
5) Coannular turbulent swirling flow in a sudden expansion (2D)
6) Row of turbulent jets in turbulent crossflow (3D)

6.1 TWO-DIMENSIONAL LAMINAR FLOW TEST CASES

Two laminar flow cases were used. The first consisted of the flow downstream of a rearward facing step. The second consisted of the swirling flow downstream of a sudden expansion. These cases were run to assess the performance of the alternative finite-difference schemes independently of the turbulence model.

6.1.1 Flow Downstream of Rearward Facing Step

The laminar flow downstream of a rearward facing step was computed using the three finite-difference schemes considered herein; the baseline hybrid method - HYBRID, the second bounded skew-upwind differencing scheme - BSUDS2, and the quadratic upwind differencing scheme - QUDS. The flow geometry is shown in Figure 6-1. The inlet Reynolds number was assumed to be 250, the inlet axial velocity profile was taken as uniform, and the inlet vertical velocity was assumed to be zero. The test case was run using four uniform, and successively finer, meshes designated TOPHAT1, TOPHAT2, TOPHAT3 and TOPHAT4. Mesh size parameters and computed flow reattachment points are presented in Table 6-I. It is seen that the mesh size is halved in each direction for each subsequent mesh. Representative computed streamlines are shown in Figure 6-2.

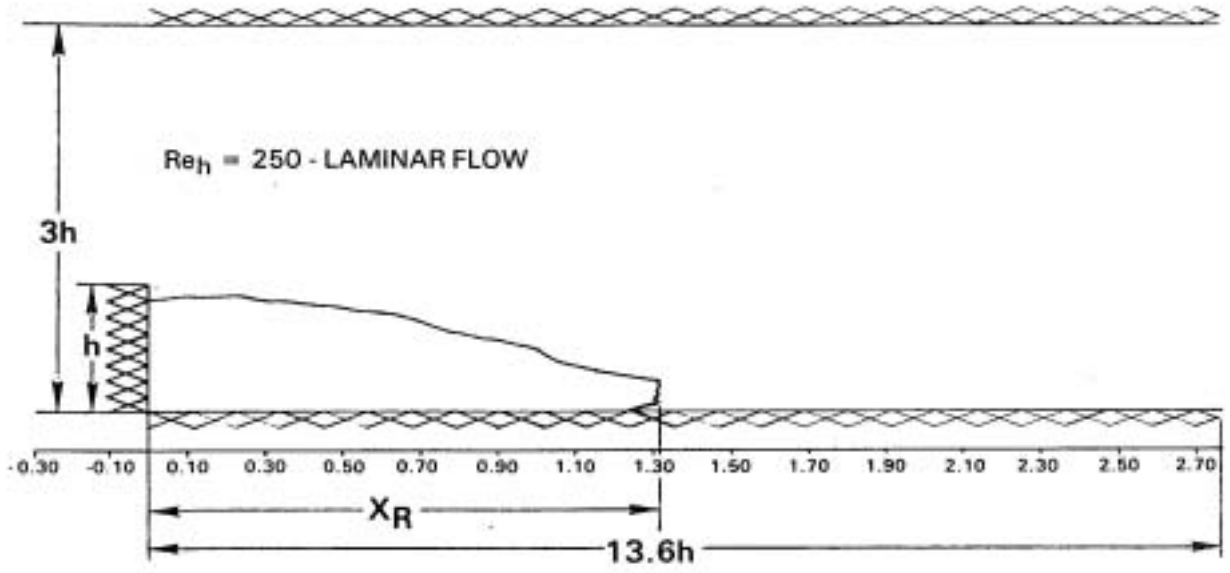

Figure 6-1 Laminar Flow Over a Rearward Facing Step with Uniform Inlet Velocity Profile - Stagnation Streamline

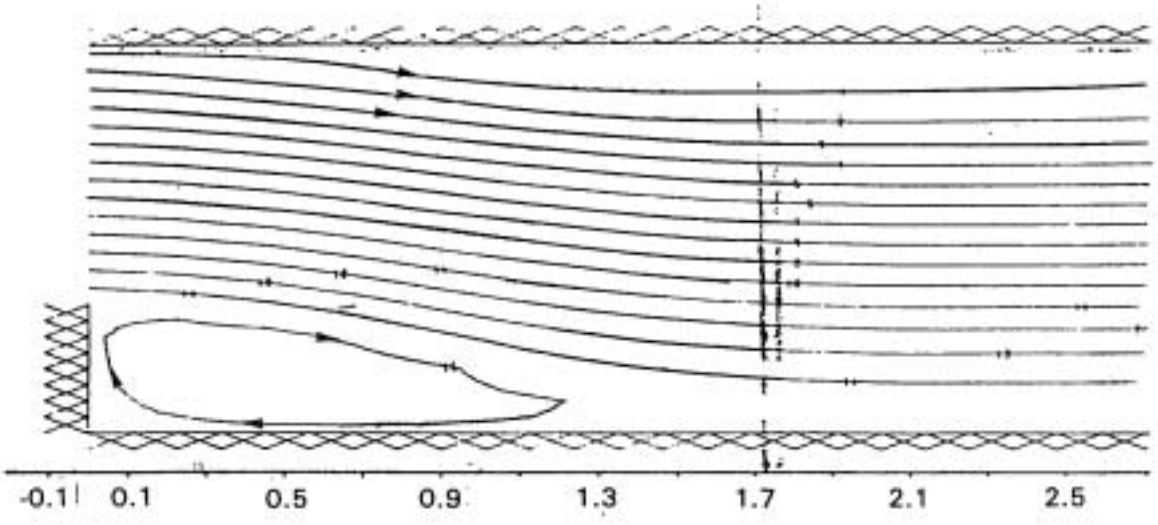

Figure 6-2 Representative Streamlines for Flow Over a Rearward-Facing Step

TABLE 6-I

COMPUTED REATTACHMENT LENGTHS FOR VARIOUS DIFFERENCING SCHEMES FOR THE FIRST LAMINAR FLOW TEST CASE

		Reattachment Length, X_R/h		
Case	Grid	HYBRID	QUDS	BSUDS2
TOPHAT1	10 x 6	2.5	5.32	2.2
TOPHAT2	20 x 12	3.14	5.25	3.95
TOPHAT3	40 x 24	4.52	5.35	5.78
TOPHAT4	78 x 48	5.53	5.75	5.98

The variation of computed reattachment length with total number of grid nodes (the product of the number of nodes in each direction) is shown in Figure 6-3. Also shown is the experimentally determined value of 6.3 reported by Durst (Ref. 32) for this flow. It can be seen from Figure 6-3 that, for the coarsest mesh, HYBRID and BSUDS2 have comparable accuracy that is considerably worse than that of QUDS. The predicted reattachment length using QUDS is not too sensitive to the number of grid nodes used. As the mesh is refined, the accuracy of BSUDS2 increases rapidly and becomes somewhat superior to that of QUDS. It appears that all of the methods give essentially the same asymtotic value as the mesh is refined. For mesh densities normally used in two-dimensional flow calculations (i.e., ~1000 nodes), BSUDS2 and QUDS perform about equally well and both are superior to the HYBRID method. It should be noted that this assessment is specific to the type of flow calculated in this test case and is probably dependent on the Reynolds number of the flow.

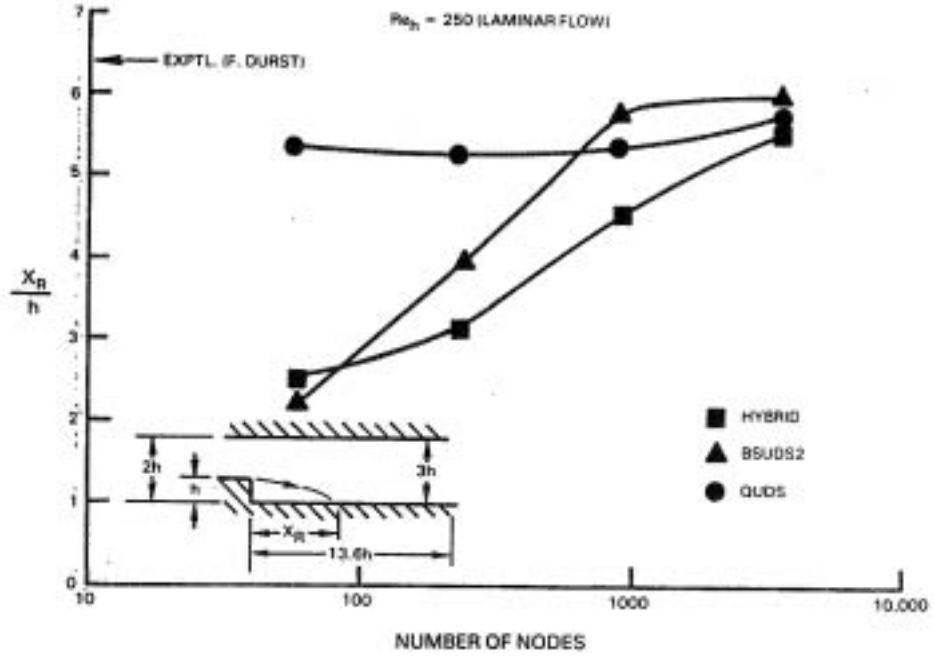

Figure 6-3 Computed Reattachment Length Using Different Finite Difference Schemes.

From Figure 6-3, it can be seen that the computed reattachment point is always less than the measured value. It is possible that the underprediction of reattachment length indicates that a grid-independent result has not yet been achieved. More likely, this slight (~4 percent) error is due to the uniform axial velocity inlet profile used in the calculations since the experimental inlet profiles were not available from Reference 32.

6.1.2 Swirling Flow Downstream of a Sudden Expansion

The second laminar flow test case consisted of the swirling flow downstream of a sudden expansion in flow area. The Reynolds number for this flow was 450. The inlet tangential velocity was assumed to be equal to the axial velocity to give a vane angle of 45 degrees and a swirl number of 0.66. The expansion ratio, which is defined as the ratio of the outer radius, R, to the inner radius, r, was 3.0. The flow field was terminated by a sudden contraction with a contraction ratio of 3.0. Uniform profiles of axial and tangential velocity were specified as the inlet boundary conditions. There are no experimental measurements available for this case. The geometry and flow conditions are given in Figure 6-4. This test case was run using three uniform meshes designated COARSE, FINE, and XFINE, and described in Table 6-II. The computed streamlines shown in Figure 6-4 make it obvious that it is difficult to characterize such flows using a single parameter such as reattachment length. At a given station, the velocity profiles change significantly with a relatively insignificant change in the length of the recirculation zones.

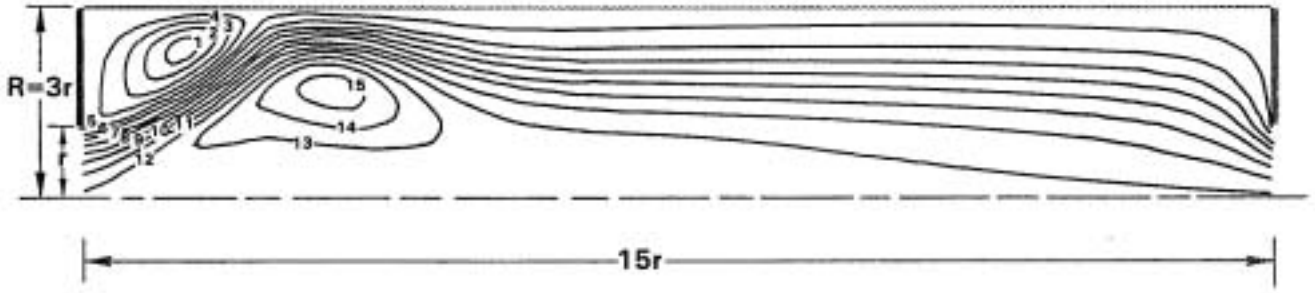

Figure 6-4 Flow in a Sudden Expansion with Swirl; Re = 450, Swirl No. = 0.66, Vane Angle = 45-degree.

TABLE 6-II

MESH DENSITIES FOR THE SECOND LAMINAR FLOW TEST CASE

Case	Grid
COARSE	20 x 10
FINE	40 x 20
XFINE	78 x 40

Figure 6-5 shows the stagnation streamlines computed using the COARSE mesh. It can be seen that the solutions produced by the three finite-difference schemes differ significantly from each other, although two basic recirculation zones are being calculated by all of the methods. The results for BSUDS2 show a distinct lobed central recirculation region while the results for QUDS show that a lobe is just beginning to form. The results for HYBRID show no lobed region. For the FINE mesh, Figure 6-6, hybrid differencing still does not show a lobed region but detailed inspection of the computed velocity profiles shows that further mesh refinement may lead to a lobed region. Computed stagnation streamlines using the finest mesh, XFINE, are shown in Figure 6-7. It can be seen that the shape of the recirculation region calculated using BSUDS2 has changed the least. The central recirculation region calculated using QUDS now shows a larger inner bubble which indicates that for even finer meshes QUDS may also produce the lobed recirculation bubble being computed by BSUDS2. Results for HYBRID still do not show break-up of the central recirculation region, but a comparison of the velocity profiles for FINE and XFINE meshes indicates that further mesh refinement will lead to break-up.

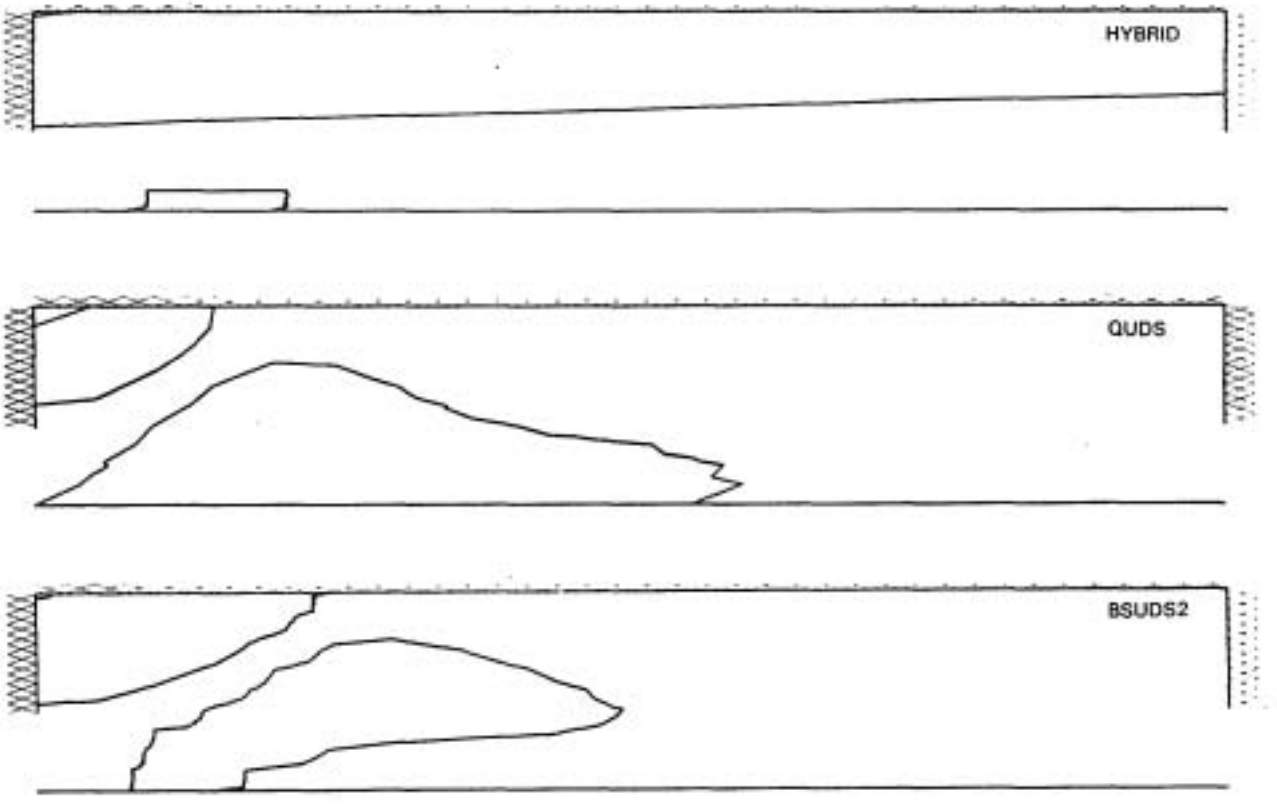

Figure 6-5 Stagnation Streamlines for Second Laminar Flow Test Case on 20 x 10 Mesh.

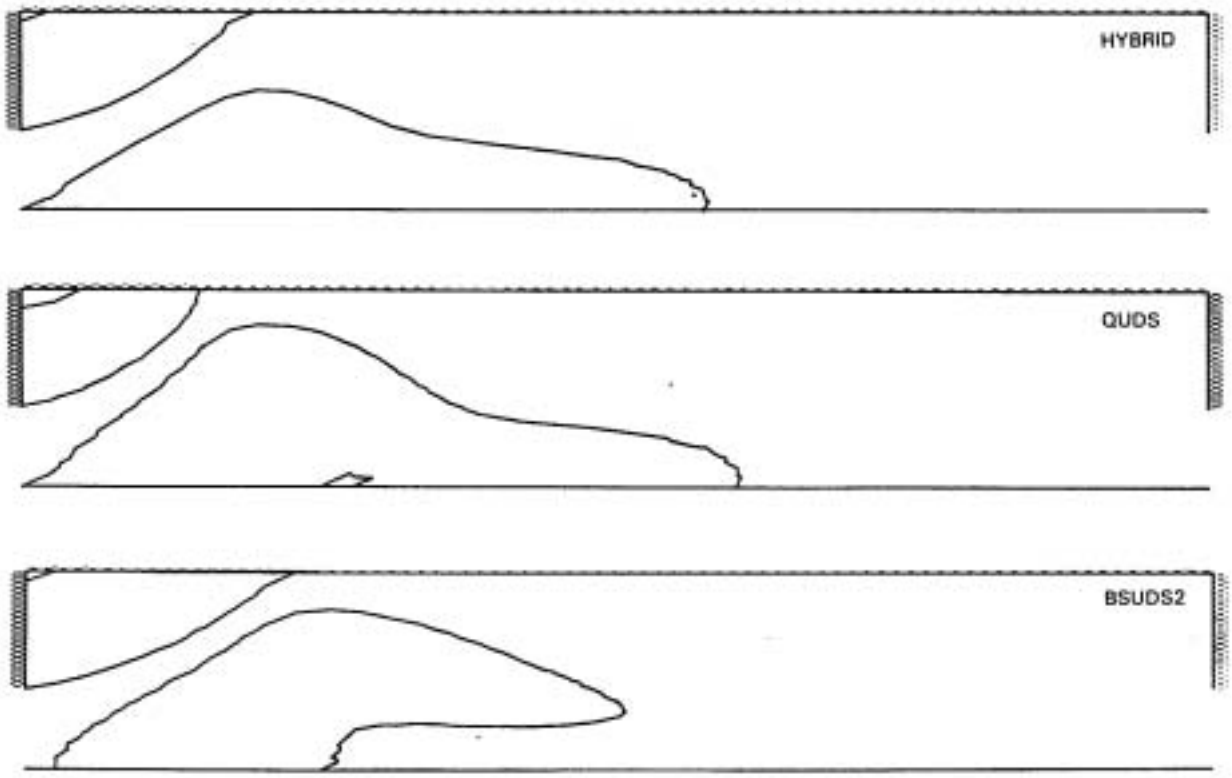

Figure 6-6 Stagnation Streamlines for Second Laminar Flow Test Case on 40 x 20 Mesh.

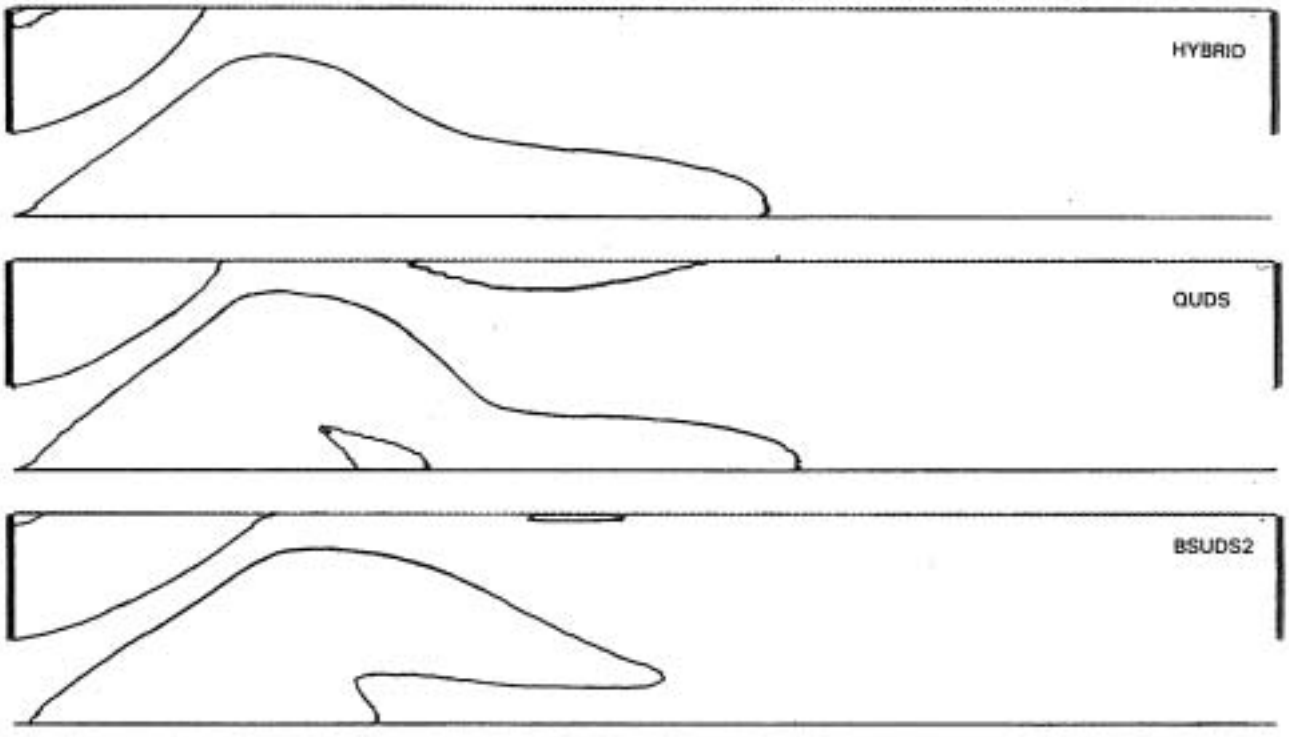

Figure 6-7 Stagnation Streamlines for Second Laminar Flow Test Case on 78 x 40 Mesh.

From the above, it can be concluded that the results for BSUDS2 are probably nearer to a mesh-independent solution than the results using either HYBRID or QUDS, although it appears that the use of QUDS will produce a mesh-independent solution more quickly than HYBRID. The implication of this conclusion is that, for this flow situation, the BSUDS2 results appear to be more accurate than the QUDS results.

It is interesting to note that lobed recirculation zones have been observed in experiments for similar swirl numbers and geometries in turbulent flow (Ref. 31) as shown in Figure 6-8. It can be seen that it is the back-pressure effect due to the downstream contraction that produces the lobed feature.

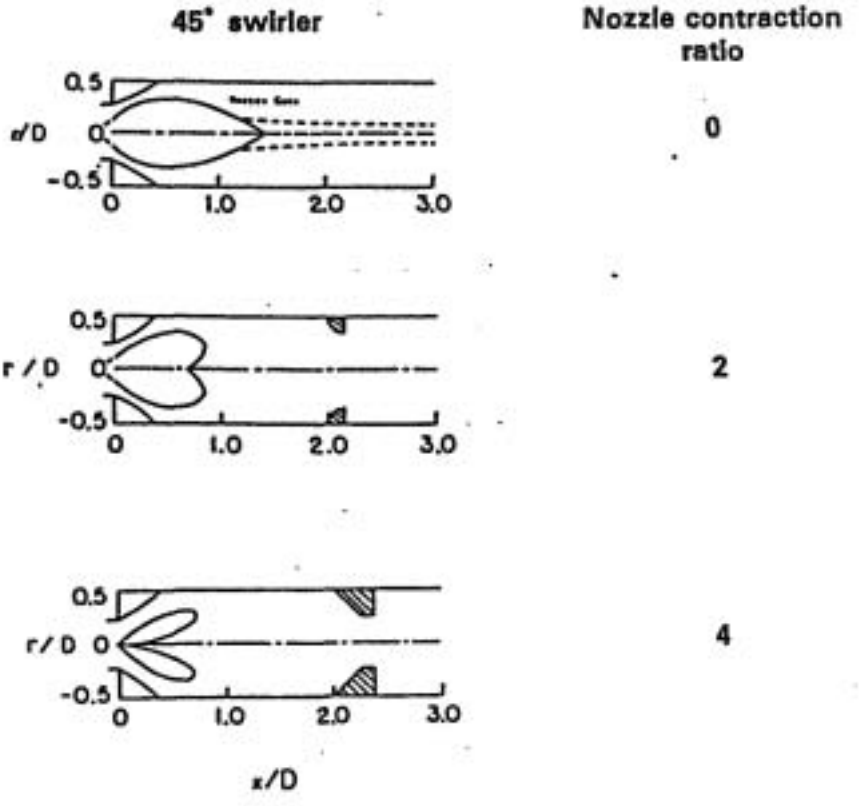

Figure 6-8 Experimentally Observed Lobed Recirculation Regions in Turbulent Flow - Yoon and Lilly (Ref. 33)

The results of the second laminar flow test case are in apparent contradiction with those of the first test case, because in the first test case QUDS was more accurate than BSUDS2. Perhaps one explanation is the flow angle. The flow angle in the first test case, Figure 6-2, seems to be smaller than the flow angle of the second test case, Figure 6-4. It was found during the model problem studies, Section 4.0, that the accuracy of these schemes was flow angle dependent and probably the flow angles of the above two cases are such that one favors QUDS and the other BSUDS2.

6.2 TWO-DIMENSIONAL TURBULENT FLOW TEST CASES

Three two-dimensional turbulent flow test cases were run using the baseline and revised computer programs. The first test case consisted of the analysis of the flow downstream of a rearward facing step. The second considered the coannular nonswirling, axisymmetric flow downstream of a sudden enlargement in flow area. The third case used swirling flow in the same flow geometry as the second case.

6.2.1 Turbulent Flow Downstream of a Rearward Facing Step

The first test case consisted of the analysis of the flow downstream of a rearward-facing step. Extensive data have been reported for this configuration in Reference 33. This experiment has been used by several workers to assess the accuracy of their flow field models and it has been designated as Stanford Case 421.

The geometry of the test section used in the experiment reported in Reference 32 is shown in Figure 6-9; the vertical scale has been exaggerated for clarity. The flow region from a point 4 step heights upstream of the step (where suitable data for initial conditions were obtained) to a point 20 step heights downstream of the step (well beyond the location of the reattachment point) was analyzed. In Figure 6-9, this region is delineated by the dashed lines.

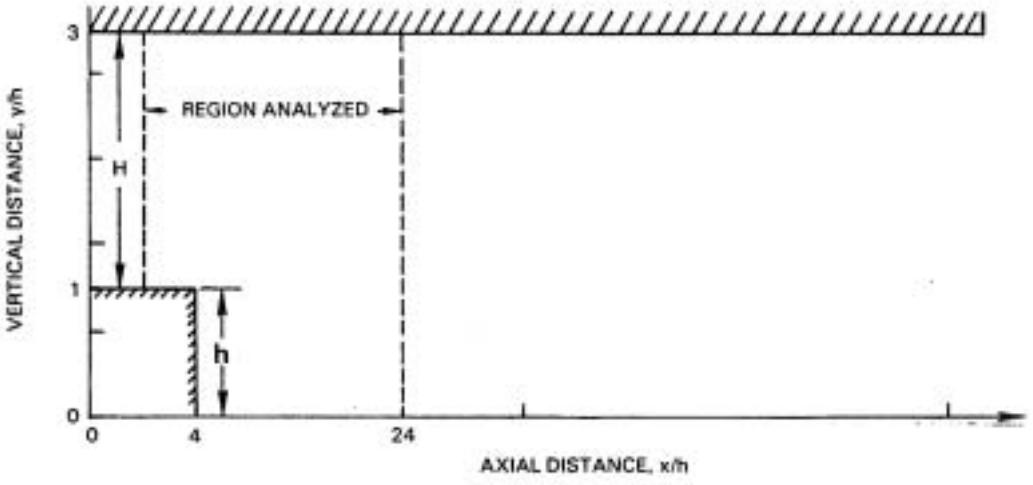

Figure 6-9 Geometry of Test Section for Flow Over a Rearward-Facing Step - First Turbulent Flow Test Case

Initial conditions for the baseline case are shown in Table 6-III and are based on test conditions reported in Reference 34. The initial boundary layer was approximated in a step-wise manner as indicated in Table 6-III.

TABLE 6-III

INITIAL CONDITIONS FOR CASE 421

Mean Velocity	18.32 m/sec
Temperature	41.2 C
Pressure	101.35 KN/m^2
Boundary Layer Thickness	8.4 mm
Turbulence Intensity (u'/u)	.003

Axial Velocity Profile - Assumed

u = 9.16 m/sec,	$1.0 \leq y/h < 1.0336$
u = 13.74 m/sec,	$1.0336 \leq y/h < 1.0736$
u = 18.32 m/sec,	$1.0736 \leq y/h \leq 3.0$

The turbulence energy dissipation rate was calculated from the expression

$$\varepsilon = 3.0K^{3/2}/H$$

where K is the turbulence kinetic energy and H is the height of the channel. The experimentally-determined reattachment point was located at 7 ± 1 step-heights from the step.

Three cases, each using a different grid system, were calculated using the baseline computer program for the conditions shown in Table 6-III. The pertinent grid information is given in Table 6-V and the grid set up for three cases is explained below. The first case used the relatively coarse grid shown in Figure 6-10 and the grid has been designated as COARSE; in Figure 6-10, the vertical scale has been exaggerated for clarity. A second case was then run using a grid obtained by nearly doubling the number of grid lines in each direction; this grid has been designated as FINE. Based on the results obtained for these two cases, a third case was run in which the number of vertical grid lines was approximately the same as that used in FINE, but the distribution of both horizontal and vertical grid lines was changed to reduce the Peclet number distribution in the vicinity of both the step and the reattachment point; this grid has been designated as ADJUSTED. In the baseline code, the finite-difference approximation to the governing flow equations uses central differencing for Peclet numbers less than 2 and upwind differencing for Peclet numbers greater than 2. Errors due to numerical diffusion are associated with the use of upwind differencing. The Peclet number distribution for the horizontal (east-west) direction for ADJUSTED is shown in Figure 6-11. It can be seen that, even for this dense mesh, the Peclet number is in the range from 2 to 10 for a relatively large portion of the separated flow region. Since the streamlines are at an angle to the grid in this region, numerical diffusion is still present. (The high Peclet number zone, Peclet > 10, outside of this region has little influence on the computed results because the streamlines are almost parallel to the mesh.) The Peclet number distribution for the vertical (north-south) direction is shown in Figure 6-12 and indicates that central differencing is used for the convective terms in the vertical direction throughout the separation zone; thus, the calculated results should be relatively free of errors due to the finite-difference approximation for these terms.

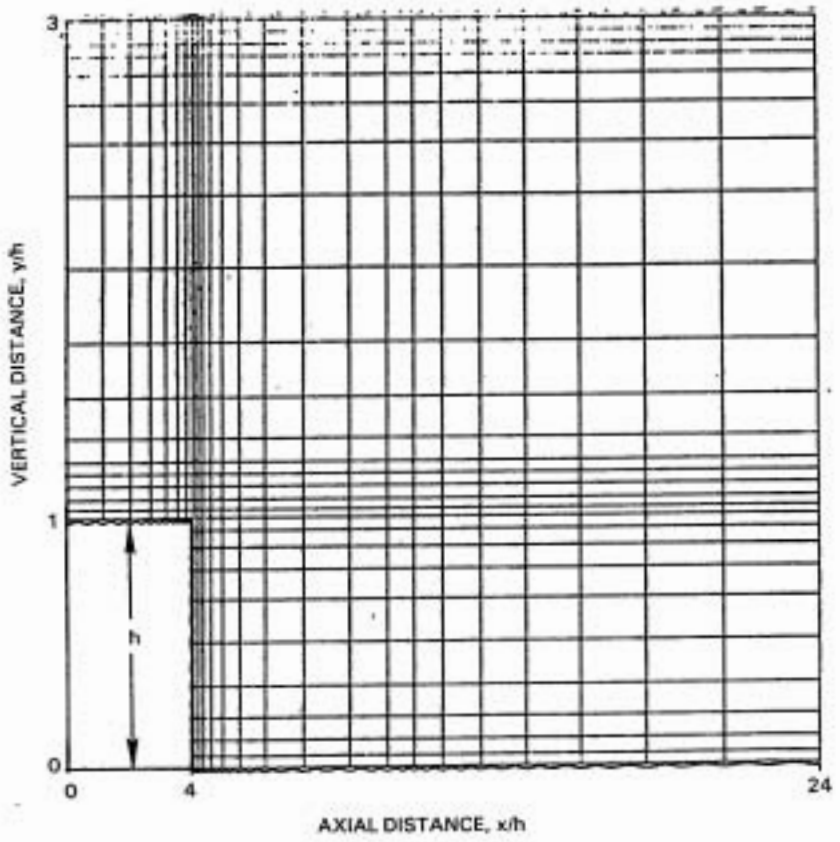

Note: (X and Y axis are not on same scale)

Figure 6-10 Grid System for Stanford Case 421-COARSE.

The calculated and measured reattachment points are presented in Table 6-IV. Use of either of the alternative grid systems (that is, FINE or ADJUSTED) resulted in a substantial improvement in the accuracy of the predicted location. As the results in Table 6-IV show, ADJUSTED is reasonably free from numerical diffusion. Further mesh refinement is required to make the calculation completely free of numerical diffusion, but the number of nodes needed to eliminate diffusion was beyond the storage capability of the computer used in this program.

TABLE 6-IV

CALCULATED AND MEASURED REATTACHMENT POINTS
(h = step height)

Measured (mean value) $X_R/h = 7$

Calculated:	Case	Reattachment Length, X_R/h HYBRID	BSUDS2	QUDS
	COARSE	5.2	5.4	5.5
	FINE	5.7	5.9	Unstable
	ADJUSTED	5.8	5.8	Unstable

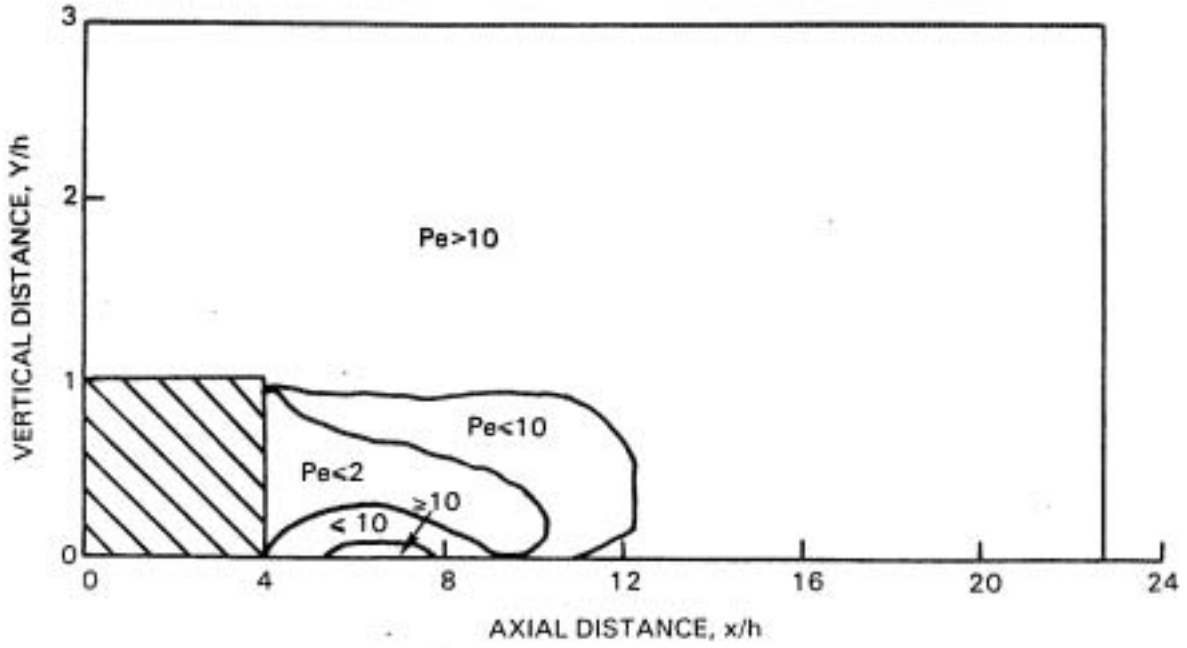

Note: (X and Y axis are not on same scale)

Figure 6-11 East-West Peclet Number Distribution for Stanford Case 421-ADJUSTED Using HYBRID Differencing (Pe = Peclet Number)

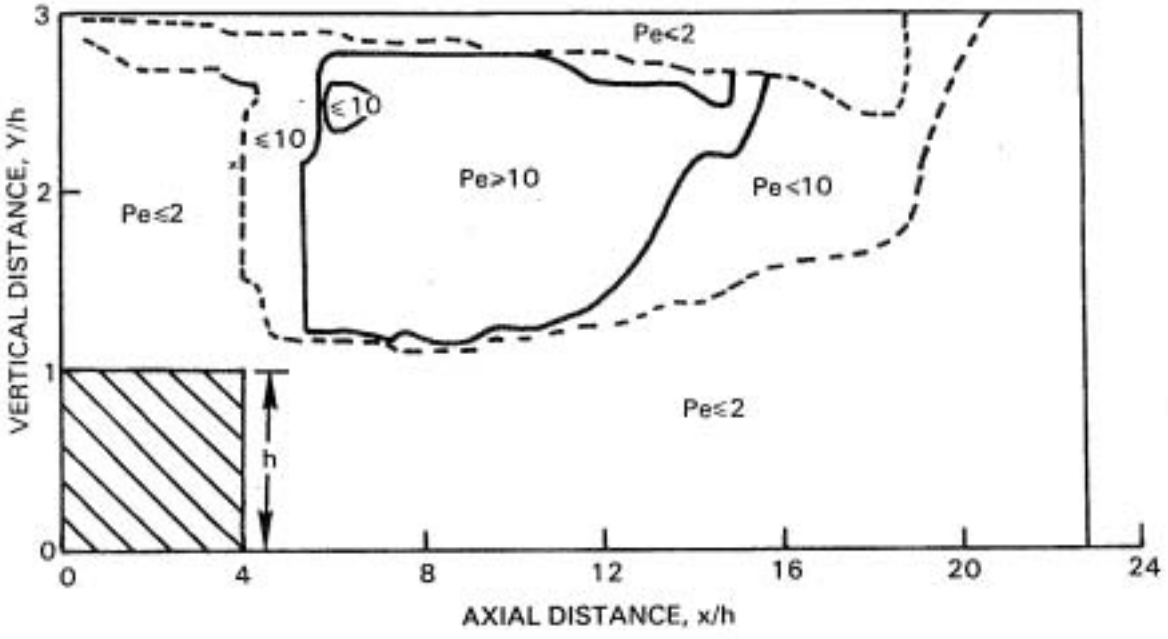

Note: (X and Y axis are not on same scale)

Figure 6-12 North-South Peclet Number Distribution for Stanford Case 421-ADJUSTED Using HYBRID Differencing (Pe = Peclet Number)

For completeness, additional information about the grid system used and the number of iterations required to achieve convergence is summarized in Table 6-V.

TABLE 6-V

ADDITIONAL GRID SYSTEM INFORMATION

Case	Number of Grid Lines		Number of Iterations to Convergence	
	X-Direction	Y-Direction	HYBRID	BUSDS2
COARSE	26	29	308	253
FINE	50	56	780	538
ADJUSTED	74	53	1515	993

The first test case was then run using the BSUDS2 finite-difference method. The grids and flow conditions were identical to those used with the baseline computer program using hybrid differencing. In fact, the same input files were used to run both the HYBRID and BSUDS2 cases. The calculated reattachment points are presented in Table 6-IV where it can be seen that BSUDS2 is slightly more accurate than hybrid differencing for both the COARSE and FINE meshes. However, the improvement in accuracy is not as large as suggested by the model problem studies, Section 4.0, and laminar test case 1. For the ADJUSTED mesh, the reattachment point given by HYBRID and BSUDS2 is the same. It is curious to note that the reattachment length with the ADJUSTED grid decreases slightly as compared to the FINE grid.

Since the ADJUSTED grid was designed for HYBRID to give more accurate results, it is not surprising that this grid has become somewhat inefficient for BSUDS2. The number of iterations to achieve convergence is less for the BSUDS2 than for the HYBRID method. However, since BSUDS2 requires the calculation of more finite-difference coefficients than HYBRID, total computation time may be greater when BSUDS2 is used.

Results of running the above test case with QUDS are also given in Table 6-IV. For the coarse grid, it can be seen that the trend shown in laminar test case 1 is followed. QUDS is marginally better than BSUDS2 and HYBRID. However, the difference in accuracy is not as large as it was in the laminar flow test cases. For finer grids, QUDS becomes unstable. This behavior was expected, because as discussed in Section 4.0, QUDS is not compatible with the solver presently incorporated in TEACH.

6.2.2 Coannular Nonswirling Turbulent Flow

The computer programs were applied to the analysis of the coaxial nonswirling flow downstream of a sudden enlargement in flow area, as reported by Johnson and Bennett in Reference 35. The flow is admitted into a 61 mm radius tube by two concentric annuli. The inner annulus has an exit radius of 12.5 mm, and the outer annulus has an exit radius of approximately 15.3 mm. The experimental apparatus is shown in Figure 6-13. The flow in both annuli is water.

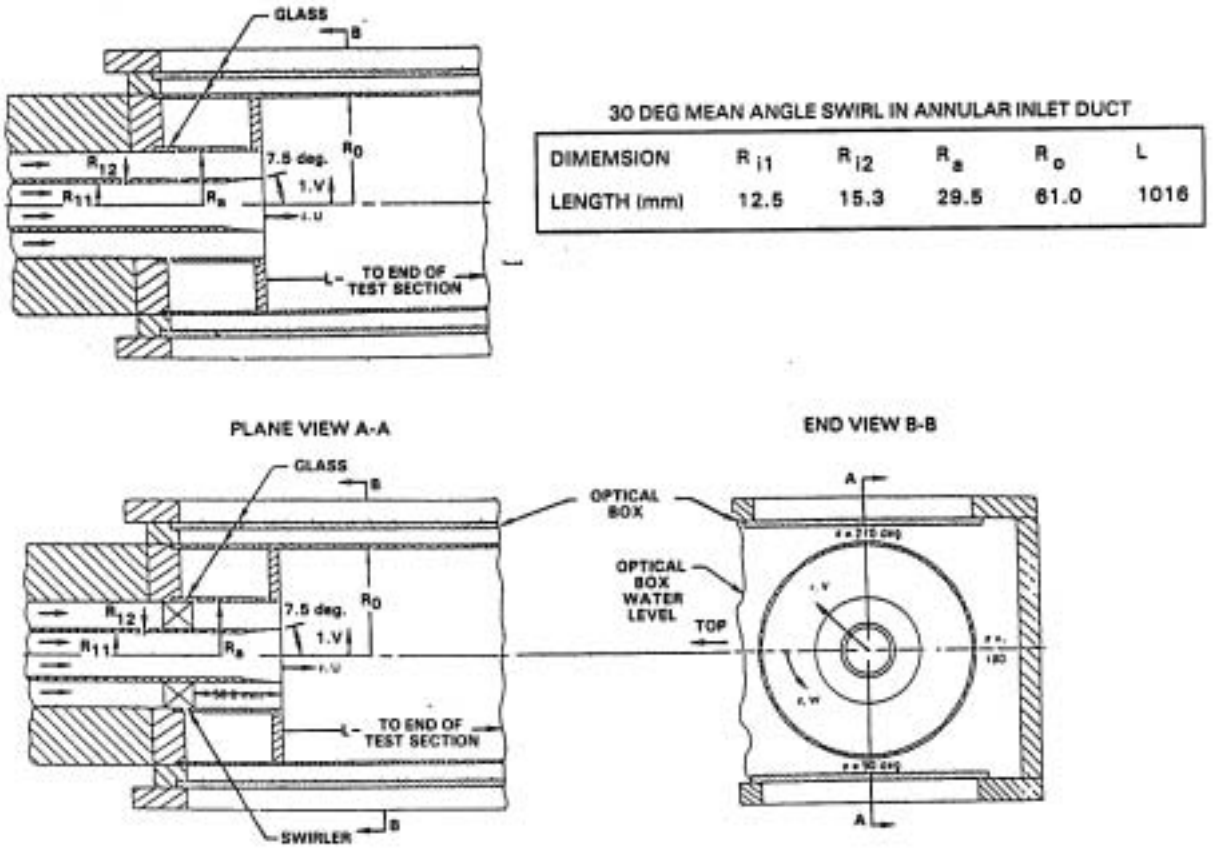

30 DEG MEAN ANGLE SWIRL IN ANNULAR INLET DUCT

DIMEMSION	R_{i1}	R_{i2}	R_s	R_o	L
LENGTH (mm)	12.5	15.3	29.5	61.0	1016

Figure 6-13 Second Test Case - Co-axial jets with and without swirl

The tube dividing the two annuli is tapered to a sharp edge at the exit of the annular region (that is, at the entrance of the sudden enlargement region). Very limited data are currently available at the end of the annular region. Hence, the following assumptions were made to establish the boundary conditions for the inlet.

Upstream of the annular jet, measured profiles of axial velocity were provided. Turbulence energy was calculated from measured turbulence intensity assuming isotropic turbulence. Since no measurements were available for the length scale, the following expression was used for the calculation of dissipation rate:

$$\varepsilon = (3.0\ K^{3/2})/D_h$$

where D_h is the hydraulic diameter.

Experimental information on the boundary conditions for the central jet were provided at a station 12.7 mm downstream of the expansion. Measurements could not be made at the expansion plane itself due to lack of optical access. It was therefore decided to use the information provided at 12.7 mm to estimate the conditions at the sudden expansion, in the following manner:

- Axial Velocity - From the measurement of peak velocity at the 12.7 mm station and the flow Reynolds number, a fully developed turbulent pipe flow profile was calculated which was then adjusted to give the correct mass flow rate.

- Turbulence Energy - The measured value of the turbulence energy on the centerline at 12.7 mm, normalized by the centerline axial velocity at this point, was used to provide a limiting boundary value of turbulence energy at the inlet, assuming that this ratio remained constant:

$$K/u^2 = 0.005$$

Turbulence energy dissipation rate was calculated in the same manner as it was calculated for the annular jet.

Global values of the initial conditions are presented in Table 6-VI. The axial velocity profile for the inner annulus was specified in accordance with the velocity distribution calculated using the analyses mentioned above.

TABLE 6-VI

INITIAL CONDITIONS FOR NONSWIRLING FLOW TEST CASE
(Based on Reference 35)

	Inner Flow	Outer Flow
Mean Velocity, m/sec	0.596	1.74
Mass Flow Rate, kg/sec	0.648	0.55
Temperature, °C	15.6	15.6
Turbulence Intensity (u'/u)	0.057	0.036

Three cases, each using a different grid system, were calculated for the conditions shown in Table 6-VI. The first case used the relatively fine grid shown in Figure 6-14 and has been designated EXTRA FINE grid. The second case used a grid with the same vertical definition as that shown in Figure 6-14 but with approximately one-half the number of axial nodes; this case has been designated FINE grid. The third case used approximately one-half the number of nodes in each direction, relative to the grid shown in Figure 6-14 and has been designated COARSE grid. The vertical scale in Figure 6-14 has been exaggerated for clarity.

A comparison of the measured and calculated centerline axial velocity distribution is shown in Figure 6-15 for the coarse grid. It can be seen that in the initial region the results do not agree well with the data regardless of the differencing scheme used.

Figure 6-16 shows the comparison for the FINE grid. Since QUDS was unstable for this mesh, only HYBRID and BSUDS2 calculations are shown. It can be seen that there is virtually no difference between the two calculations. However, it cannot be said that a mesh independent solution has been obtained because east-west cell Peclet numbers are large even for this grid, Figure 6-17. North-south cell Peclet numbers, Figure 6-18, are well within limits. Calculations with the EXTRA FINE grid did not show any further improvement and hence are not shown.

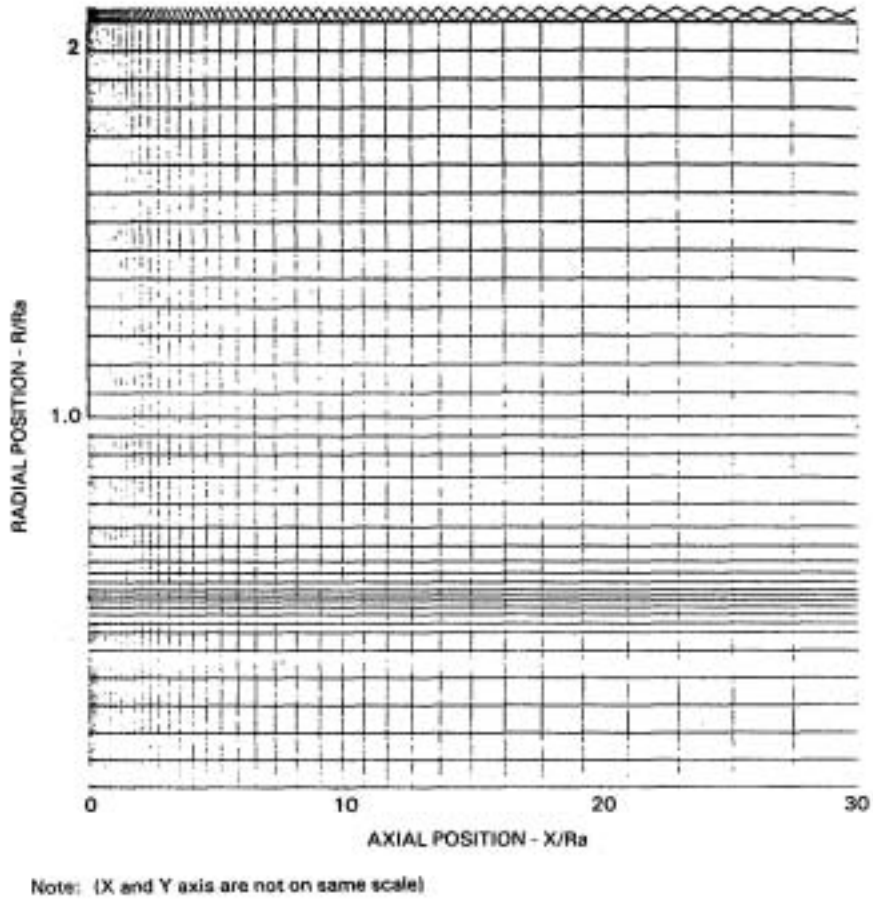

Figure 6-14 Grid System for Second Turbulent Flow Test Case - Extra Fine Grid (R_{T2} = 15.3mm)

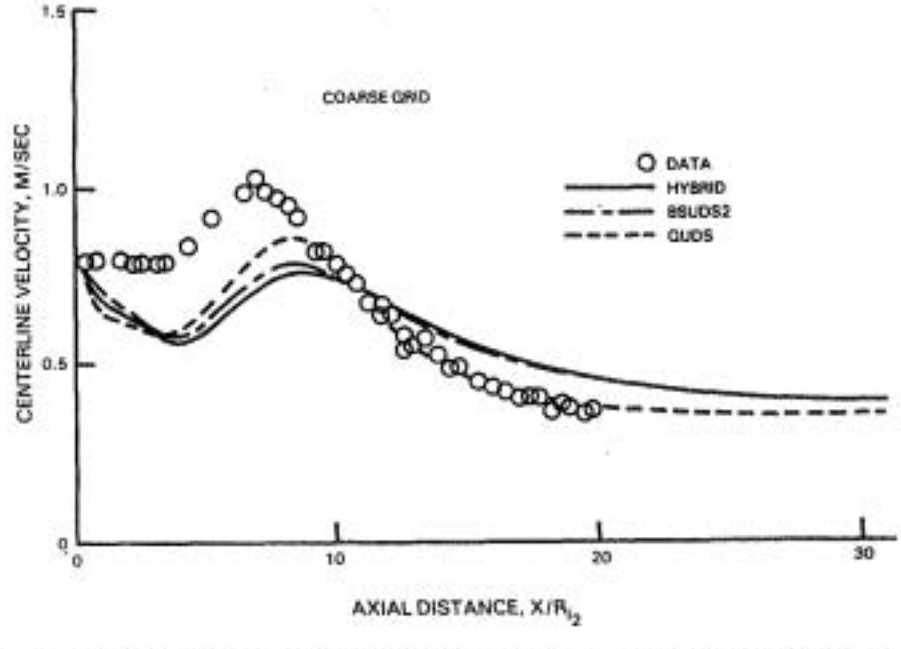

Figure 6-15 Axial Velocity Distribution - Second Turbulent Flow Test Case

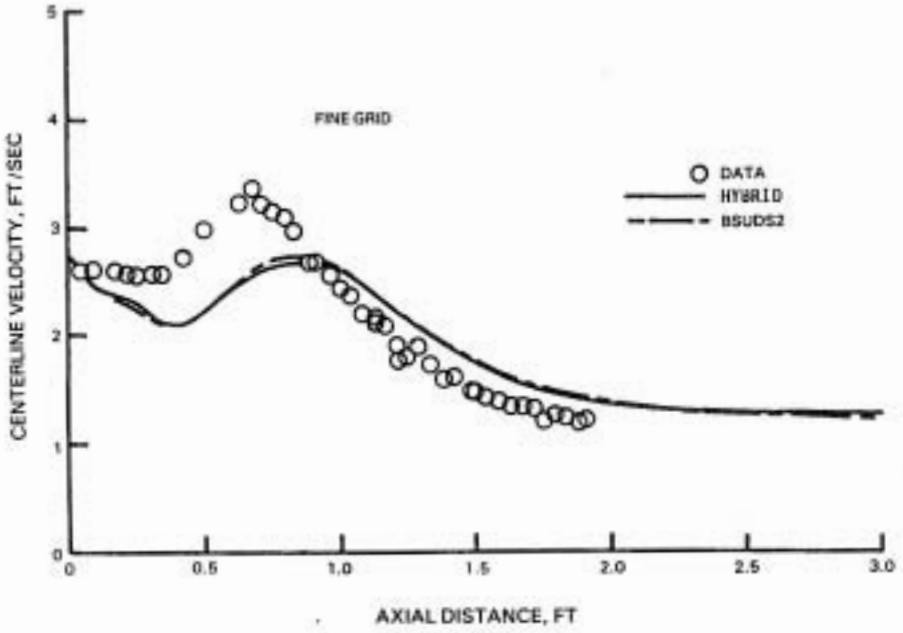

Figure 6-16 Axial Velocity Distribution - Second Turbulent Flow Test Case

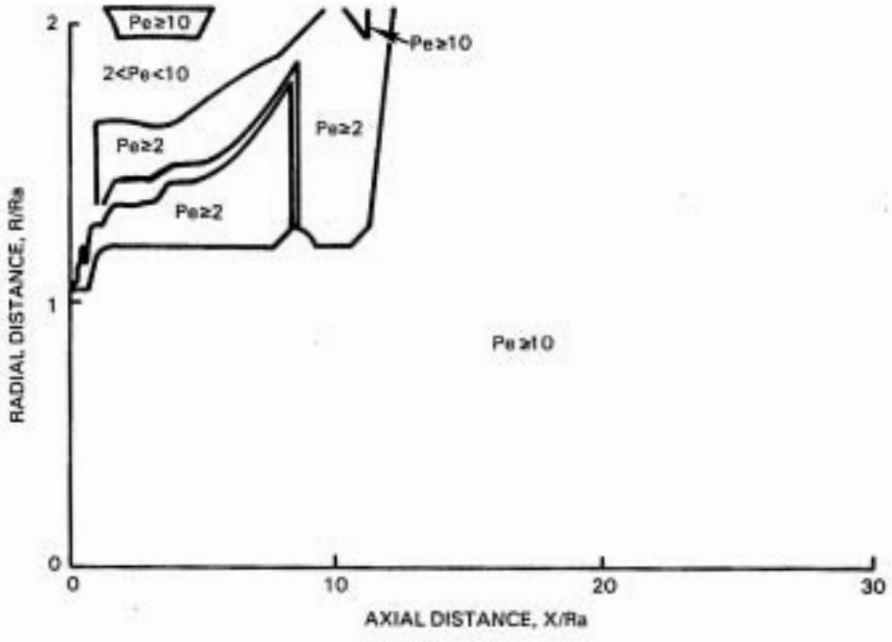

Note: (X and Y axis are not on same scale)

Figure 6-17 East-West Peclet Number Distribution for Second Turbulent Flow Test Case; Pe = Peclet Number.

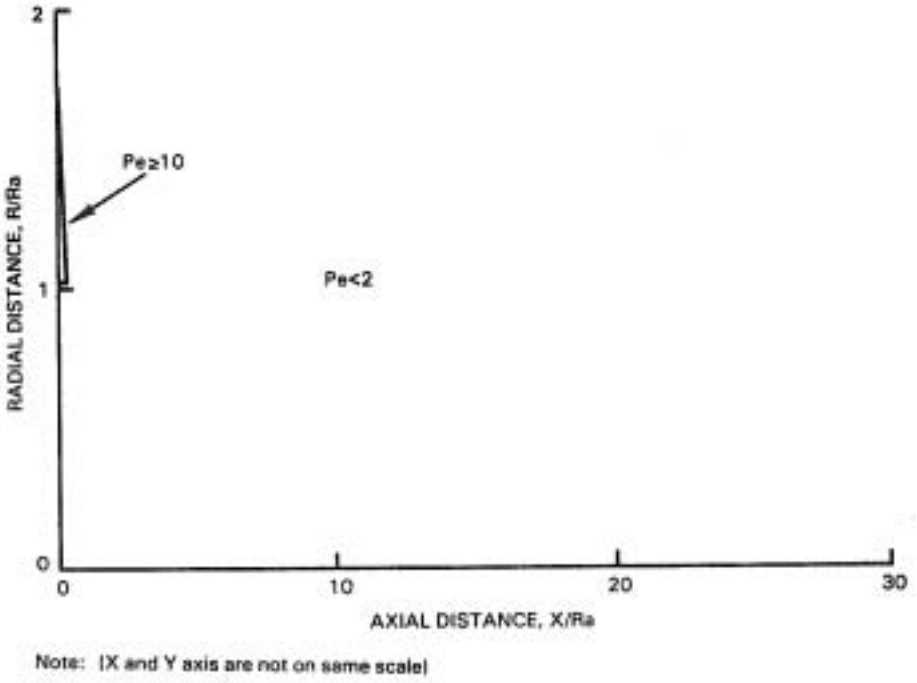

Figure 6-18 North-South Peclet Number Distribution for Second Turbulent Flow Test Case; Pe = Peclet Number.

Figure 6-19 shows the calculated streamlines for the case. This figure also shows the three stations at which comparisons of the radial profiles of the mixture fraction and axial velocity were made. These comparisons are shown in Figures 6-20 and 6-21 for the coarse grid and in Figures 6-22 and 6-23 for the FINE grid. It can be seen that the agreement with the experiment is reasonable even for the coarse grid, and mesh refinement does not result in further improvements. The apparent good agreement is somewhat misleading because comparison of the centerline profiles had shown quite a significant discrepancy between the data and calculations. Also, as was found in the first turbulent flow test case, the accuracy of hybrid differencing is almost as good as that of BSUDS2 and QUDS, and emphasizes the need to investigate further this behavior.

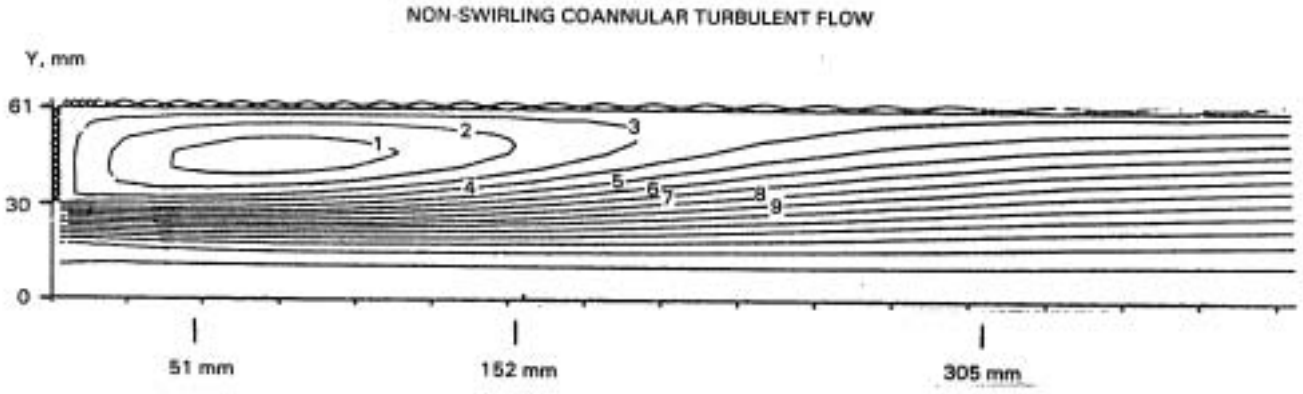

Figure 6-19 Stations at Which Comparisons of Radial Profiles Were Made

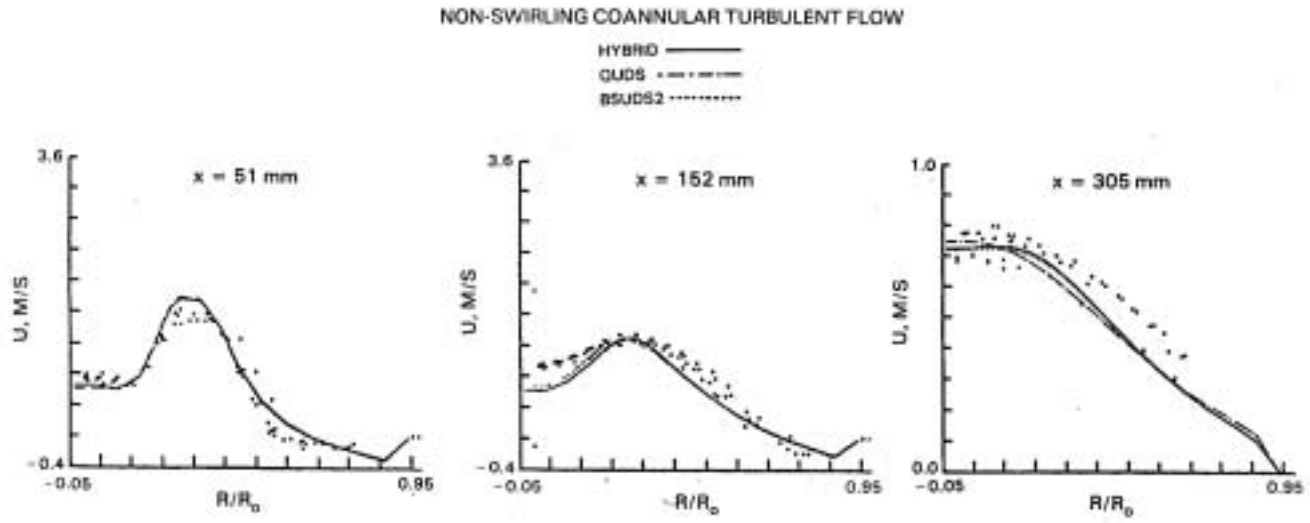

Figure 6-20 Comparison of Axial Velocity Profiles - Coarse Grid (R_0 = 61mm)

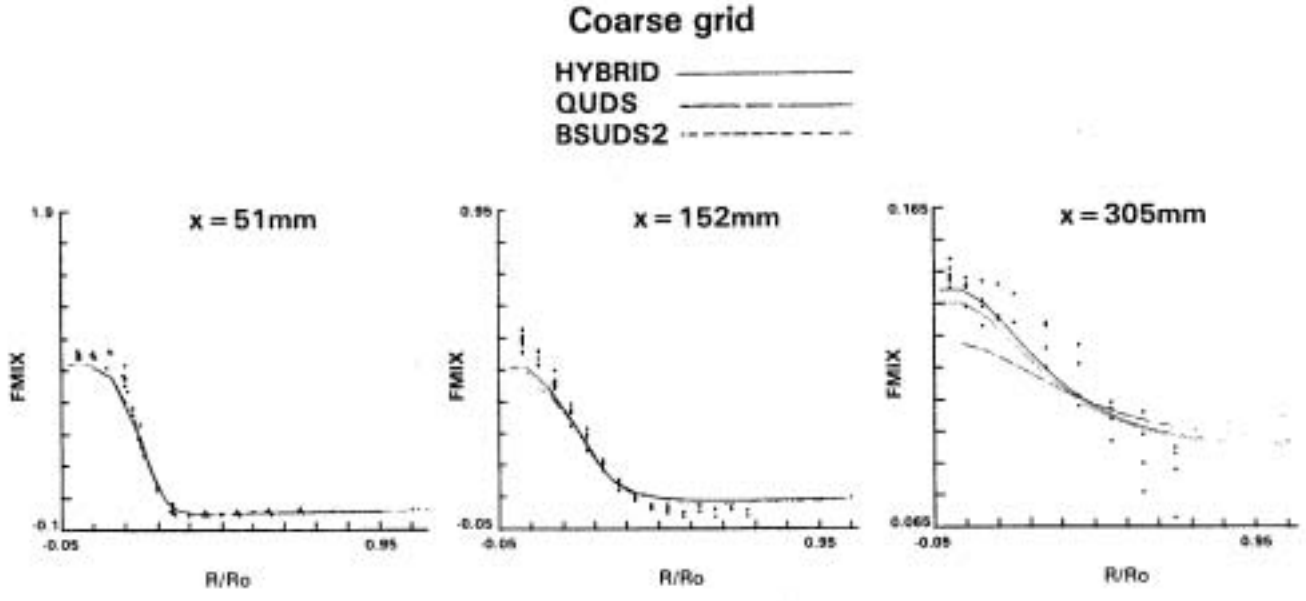

Figure 6-21 Comparison of Mixture Fraction Profiles - Coarse Grid (R_0 = 61mm)

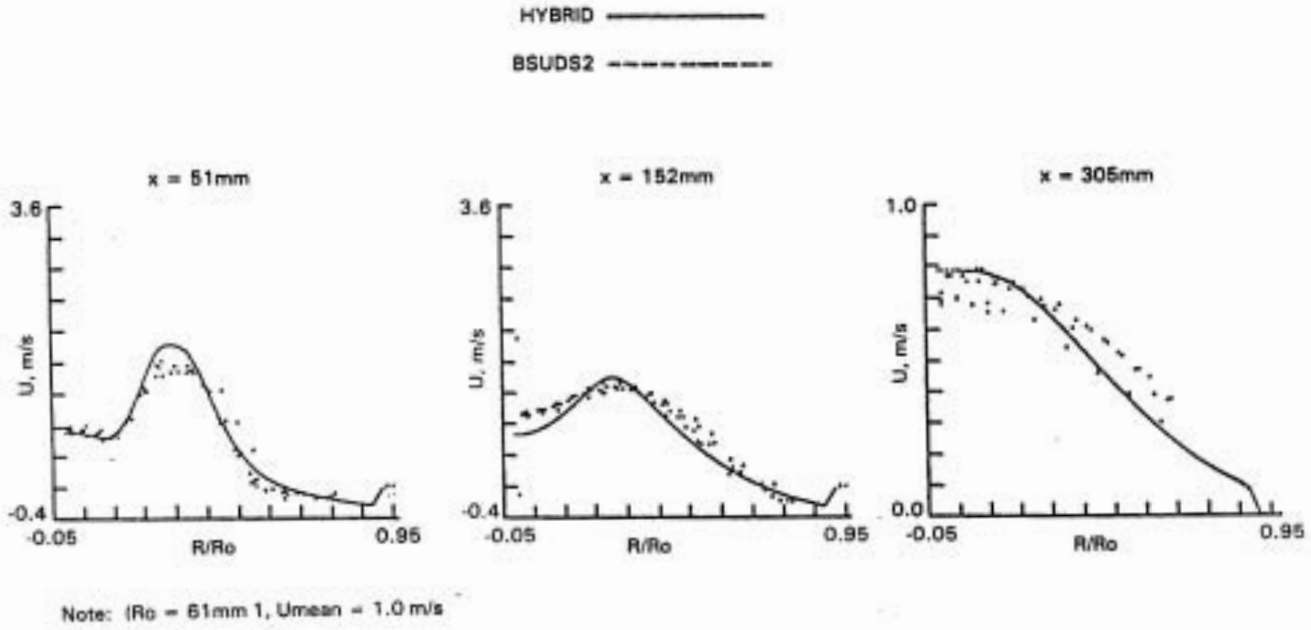

Figure 6-22 Comparison of Axial Velocity Profiles - Extra Fine Grid (R_0 = 61mm)

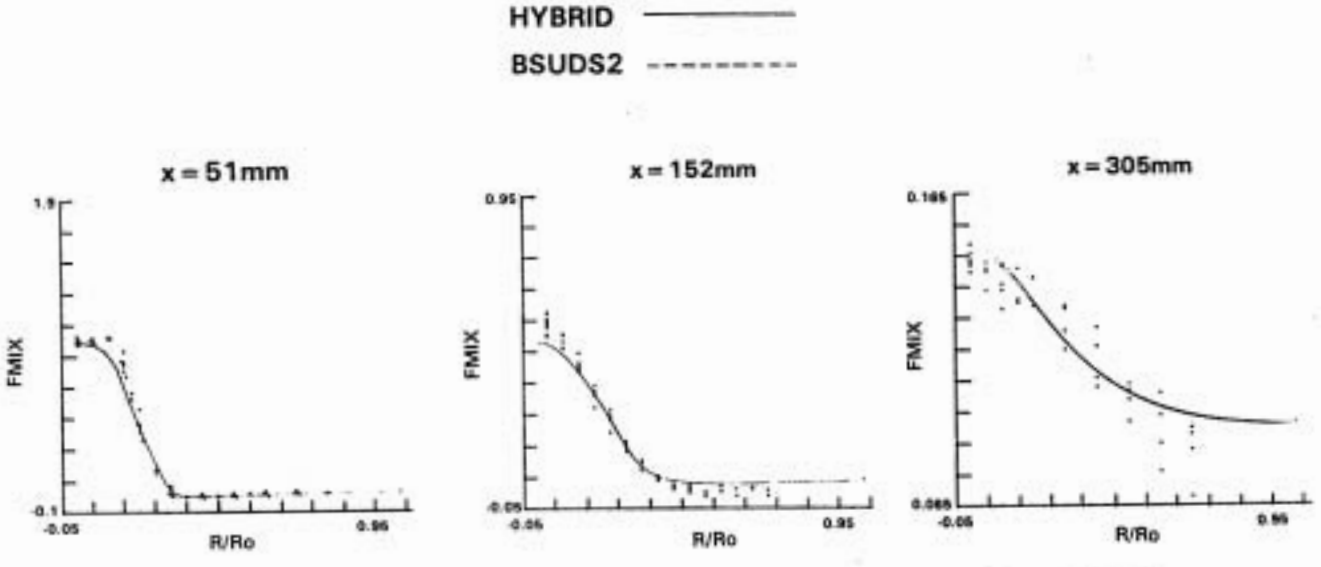

Figure 6-23 Comparison of Mixture Fraction Profiles - Extra Fine Grid (R_0 = 61mm)

The calculated and measured reattachment points are shown in Table 6-VII. The measured reattachment point was estimated from flow visualization data. It can be seen that the trend is the same as was seen for laminar flow over a rearward facing step, Figure 6-3. BSUDS2 seems to reach an asymptotic value more quickly than does hybrid differencing. But, as pointed out earlier the difference between BSUDS2 and hybrid differencing is not large. Since QUDS became unstable, its accuracy cannot be judged for this test case.

TABLE 6-VII

COMPARISON OF REATTACHMENT LENGTH FOR THE CORNER RECIRCULATION ZONES FOR COANNULAR NONSWIRLING FLOW MEASURED 200-225mm

MESH	CALCULATED REATTACHMENT LENGTH		
	HYBRID mm	BSUDS2 mm	QUDS mm
COARSE	239	241	234
FINE	243	254	UNSTABLE
EXTRA FINE	252	257	UNSTABLE

For completeness, additional information about the grid system used and the number of iterations required to achieve convergence is summarized in Table 6-VIII.

TABLE 6-VIII

ADDITIONAL GRID SYSTEM INFORMATION

Case	Grid	Iterations to Convergence*		
		HYBRID	BSUDS2	QUDS
COARSE	21 x 20	357	300	1911
FINE	21 x 38	1395	1228	Unstable
EXTRA FINE	40 x 38	1506	1430	Unstable

* Convergence defined as maximum residual source (normalized) 0.005

6.2.3 Coannular Swirling Turbulent Flow

The test case for swirling flow is based upon the data reported by Johnson and Roback (Ref. 30) for the experimental apparatus which was used for the coannular nonswirling flow. An extensive number of comparisons between experimental and analytical results have been reported previously under the HOST/Aerothermal Modelling Program - Phase I (Ref. 1) using the hybrid differencing scheme.

Since very limited data are currently available at the end of the annular region, the following assumptions were made to establish the boundary conditions for the inlet in the swirling flow case. The calculations were started at the first plane of measurement, 0.51 cm from the expansion plane, using the measured quantities as inlet boundary conditions. At this plane all variables, except the dissipation rate, required for the 2D-TEACH code were measured and can be specified. To specify the dissipation rate, it was assumed that the inner portion of the flow originated from the inner tube and the outer portion originated from the concentric outer tube; turbulence length scales were assigned accordingly, using 3 percent of the passage heights, and the dissipation rate was calculated from these length scales.

Four cases, each using a different grid system, were calculated using the same set of inlet conditions. The first case used the relatively coarse grid shown in Figure 6-24 and has been designated COARSE grid test case. The second case, designated ADJUSTED COARSE grid, used the same number of grid lines as coarse grid but with a greater concentration of grid lines in the axial direction near the entrance region. The third case, designated FINE grid, used a greater number of grid lines in the axial direction than either coarse grid or adjusted coarse grid; again, the grid lines were concentrated near the entrance region. The fourth case used the same axial grid line distribution as FINE grid together with more grid lines in the radial direction; this case has been designated EXTRA FINE grid. EXTRA FINE grid is shown in Figure 6-25. The number of grid lines for all cases in both the axial and radial directions, together with the number of iterations necessary to achieve a converged solution, are listed in Table 6-IX.

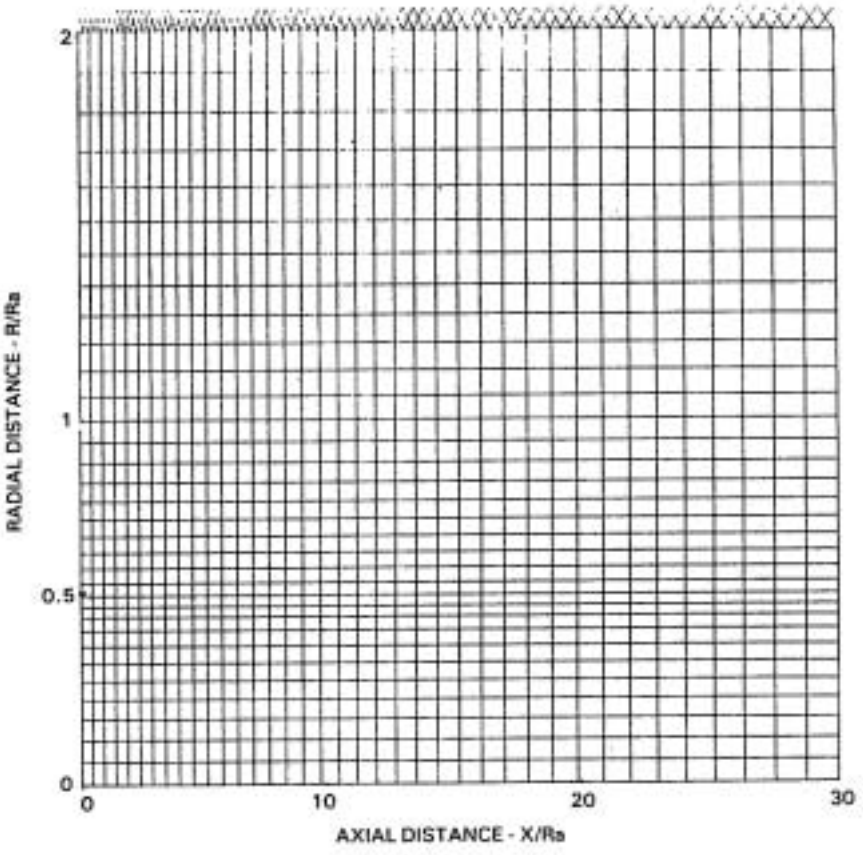

Note: (X and Y axis are not on same scale)

Figure 6-24 Grid System for Coarse Grid Test Case

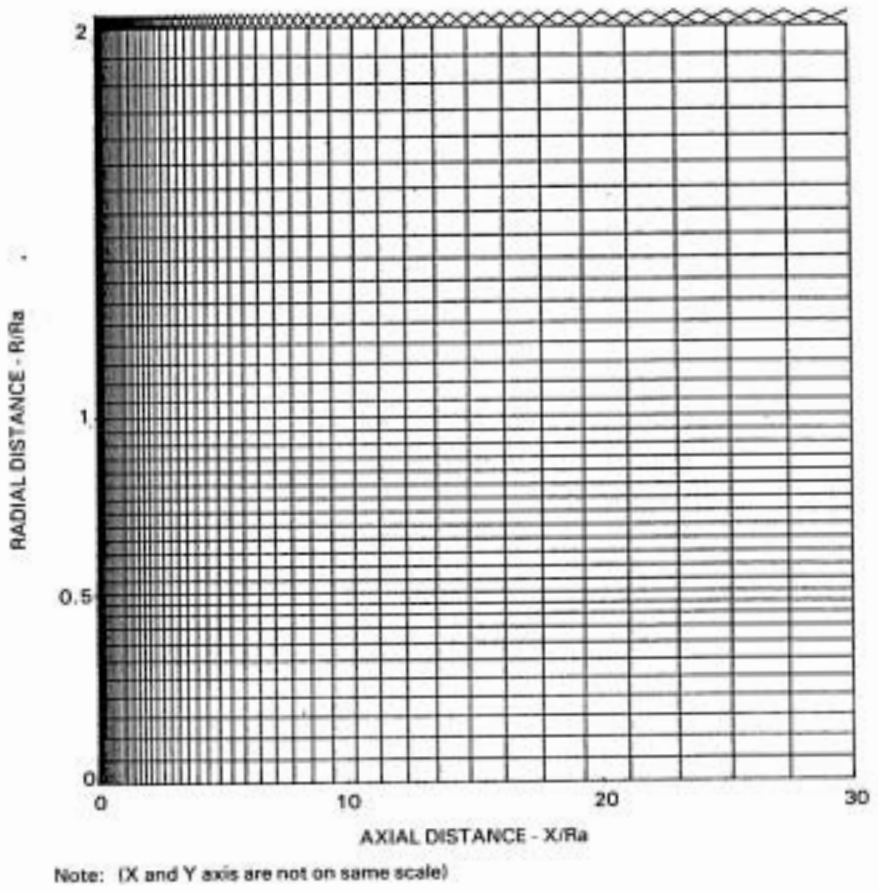

Figure 6-25 Grid System for Extra Fine Grid Test Case

TABLE 6-IX

COANNULAR SWIRLING TURBULENT FLOW
ADDITIONAL GRID SYSTEM AND CONVERGENCE INFORMATION

Case	Grid	Iterations to Convergence		
		HYBRID	BSUDS2	QUDS
COARSE	40 x 35	955	1186	3616
COARSE ADJUSTED	40 x 35	2594	1340	1579
FINE	47 x 35	1539	1422	1240
EXTRA FINE	47 x 43	2221	364*	1676

*Run with FAST Algorithm, which is the PWA version of PISO (Pressure-Implicit Split Operator) Algorithm - Ref. 40.

Contour plots for the east-west Peclet number distributions obtained using the baseline computer program are shown for COARSE grid and EXTRA FINE grid cases in Figures 6-26 and 6-27, respectively. There were very few differences between the ADJUSTED COARSE, FINE and EXTRA FINE results; hence, only the EXTRA FINE grid results are being shown. These contours show the region for which the absolute value of the Peclet number is 10 or less. Generally, the hybrid differencing procedure can be used for Peclet numbers less than 10, but in flow regions with strong gradients in flow properties such as the entrance region and corner recirculation region in the present case, the Peclet numbers should be less than 2 to ensure the use of central differencing and resulting solution accuracy. Inspection of Figures 6-26 and 6-27 shows that these criteria are not met for even the finest grid. However, it can be seen that, as the grid is refined in the axial direction, the east-west Peclet numbers are reduced to more acceptable values in both the entrance region and the corner recirculation region.

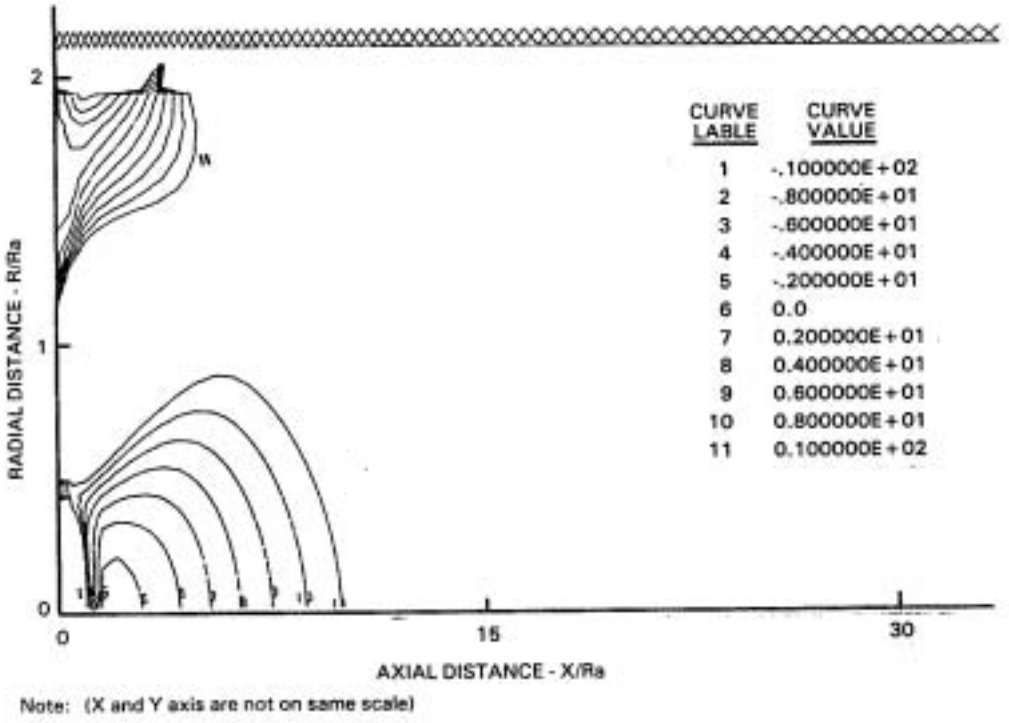

Figure 6-26 East-West Peclet Number Distribution for Coannular Swirling Flow - Coarse Grid

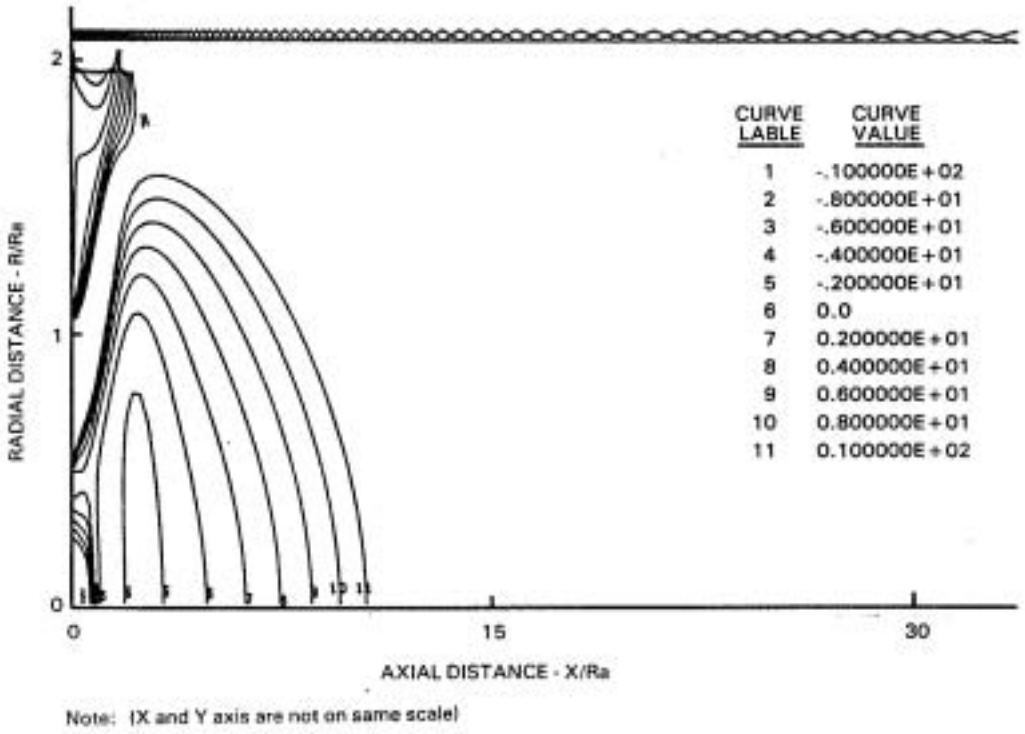

Figure 6-27 East-West Peclet Number Distribution for Coannular Swirling Flow - Extra Fine Grid

Contour plots for the north-south Peclet number distributions are shown in Figures 6-28 and 6-29. Generally, the radial velocity components are small relative to the axial velocity components, and, therefore, the north-south Peclet numbers are smaller than the east-west values. It is interesting to note that north-south Peclet numbers change significantly from the coarse grid to EXTRA FINE grid, Figure 6-28 and 6-29. The reason for the change in north-south Peclet numbers is that increasing the grid density in the axial direction modifies the flow field significantly, producing much larger radial velocities. These increased radial velocities are reflected in the change in north-south Peclet numbers. The north-south Peclet numbers, as was the case for east-west Peclet numbers, do not change significantly for the last three grids, and their magnitude is such that the grid in the radial direction is probably adequate.

Before detailed profile comparisons are made for this flow, it is instructive to compare the predicted reattachment lengths of the corner and central recirculation regions. These lengths are defined as the distance between the inlet and reattachment point Figure 6-30. The length of the corner recirculation region is given in Table 6-X. It can be seen that for hybrid differencing and BSUDS2 the predicted length is reduced by almost a factor of two between the coarse and adjusted coarse grids; further refinement does not bring about a significant change in this length. However, for QUDS, it can be seen that this length is reduced only by about 10 percent between the coarse and EXTRA FINE grid. Since QUDS seems to reach an asymptotic value sooner than does BSUDS2 and hybrid differencing, the implication is that for this case QUDS seems to be more accurate than BSUDS2 and hybrid differencing.

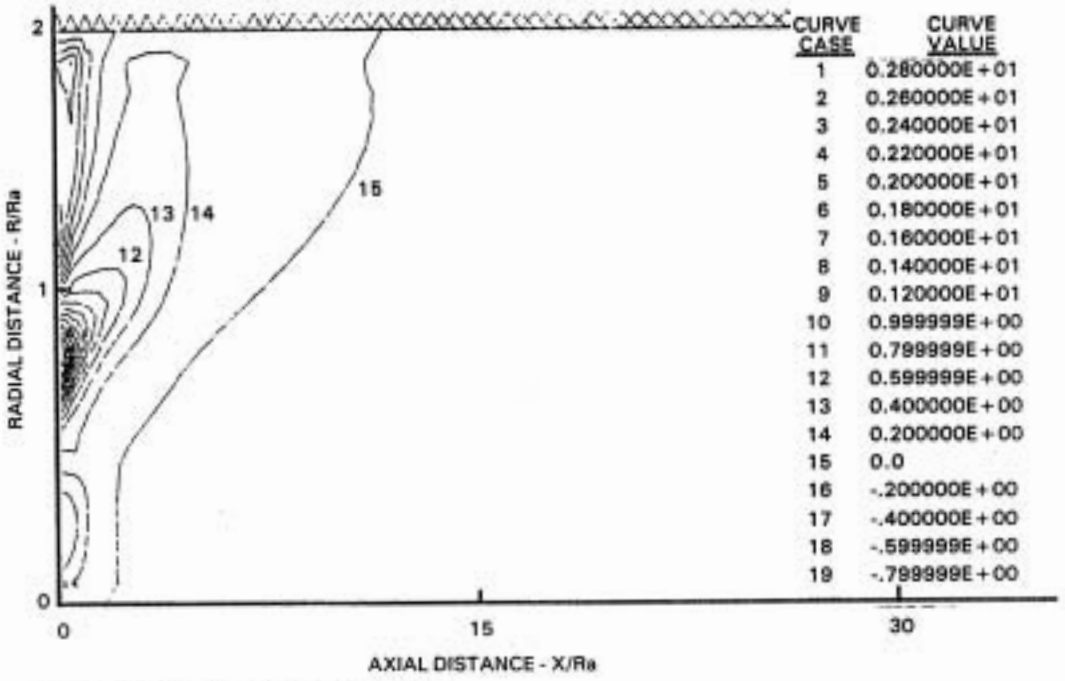

Note: (X and Y axis are not on same scale)

Figure 6-28 North-South Peclet Number Distribution for Coannular Swirling Flow - Coarse Grid

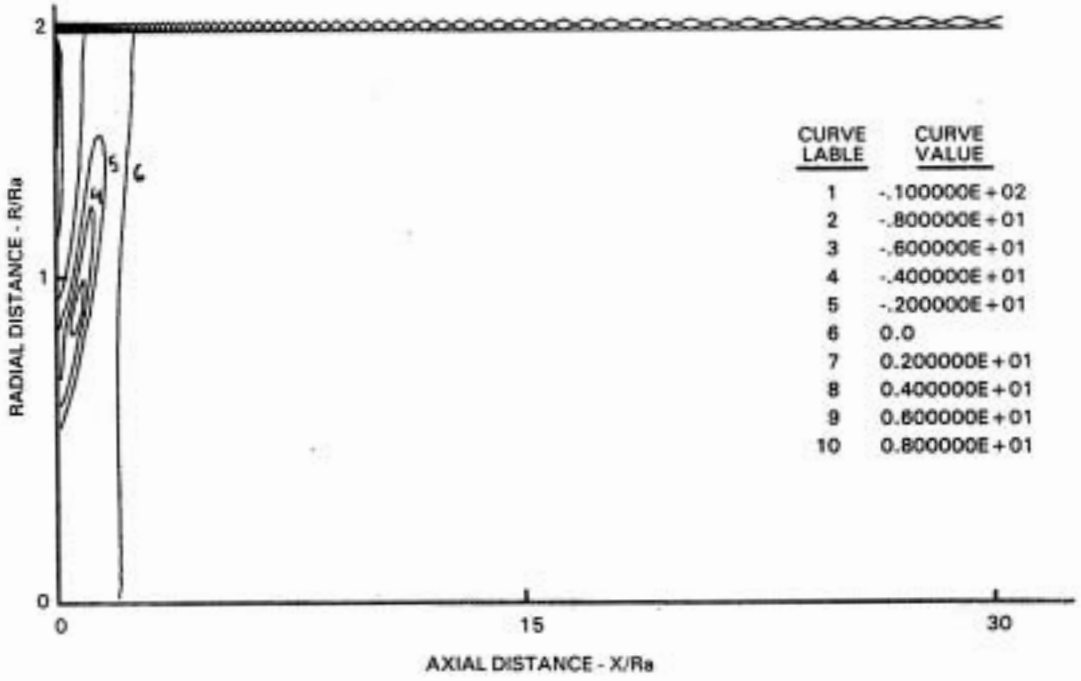

Note: (X and Y axis are not on same scale)

Figure 6-29 North-South Peclet Number Distribution for Coannular Swirling Flow - Extra Fine Grid

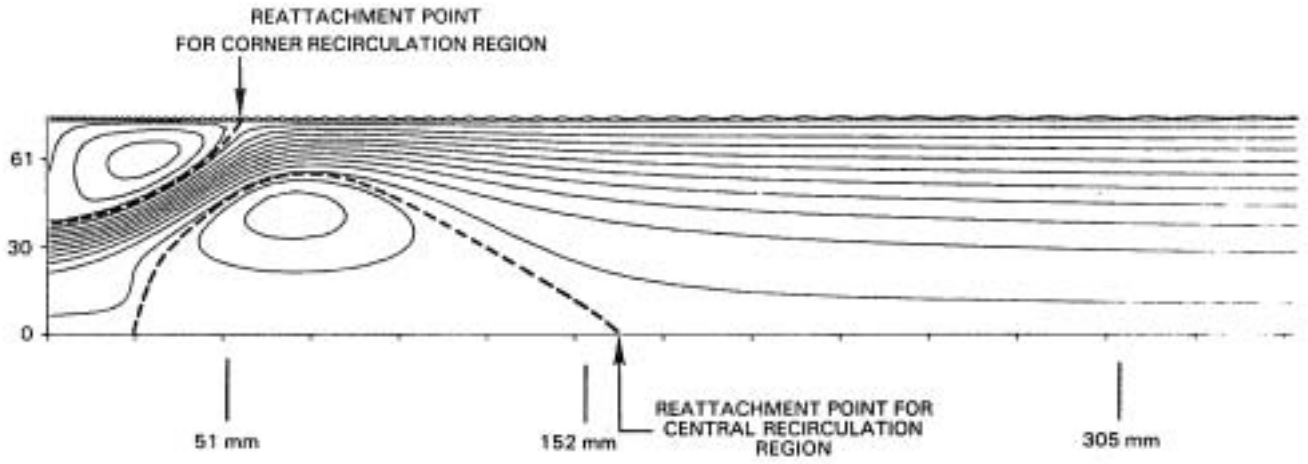

Figure 6-30 Streamlines for Coannular Swirling Flow

TABLE 6-X

COMPARISON OF REATTACHMENT LENGTH FOR THE CORNER RECIRCULATION REGION FOR COANNULAR NONSWIRLING FLOW

MESH	SCHEME		
	HYBRID	BSUDS2	QUDS
	mm	mm	mm
COARSE	113	102	58
COARSE ADJUSTED	54	56	50
FINE	49	54	51
EXTRA FINE	50	53	52

Table 6-XI gives the reattachment length for the central recirculation region, and again QUDS seems to be attaining an asymptotic value more quickly than BSUDS2 or hybrid differencing. In fact, hybrid differencing does not approach an asymptotic value even for the finest mesh. The superiority of QUDS is confirmed when the centerline velocity profiles, Figures 6-31 and 6-32, and radial profiles of axial and tangential velocities, Figures 6-33 to 6-36, are examined. It can be seen that for the coarse grid, QUDS agrees best with the experimental results. When the mesh is refined, there is no significant improvement in QUDS; however, both HYBRID and BSUDS2 show significant improvement and come close to QUDS results. It was also found that BSUDS2 was unstable for the finest mesh; an improved pressure algorithm, FAST, was used to achieve convergence. It is possible that QUDS has reached grid independence because its results did not change when the mesh was refined. However, the grid refinement was not sufficient to state this with confidence.

TABLE 6-XI

COMPARISON OF REATTACHMENT LENGTH OF THE CENTRAL RECIRCULATION REGION FOR COANNULAR NONSWIRLING FLOW

MESH	SCHEME		
	HYBRID	BSUDS2	QUDS
	mm	mm	mm
COARSE	129	134	126
COARSE ADJUSTED	129	146	155
FINE	139	153	158
EXTRA FINE	142	156	157

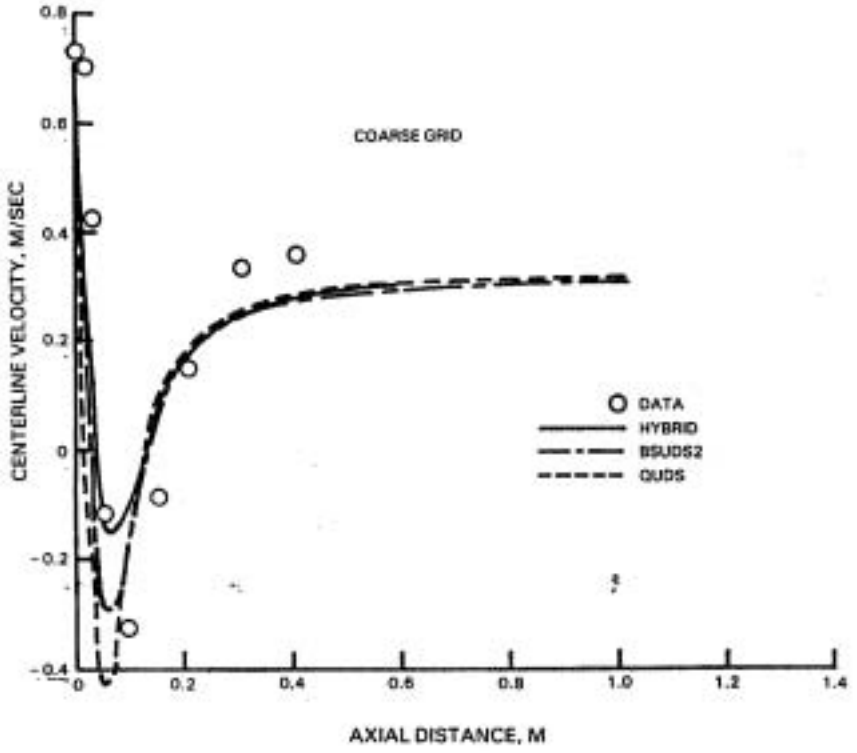

Figure 6-31 Axial Velocity Distribution - Third Turbulent Flow Test Case

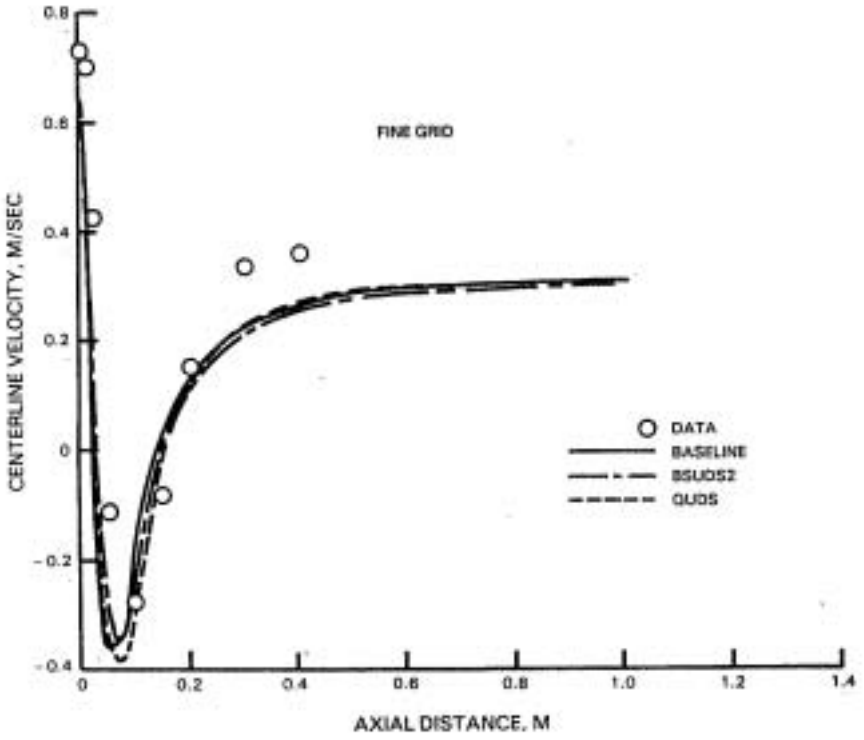

Figure 6-32 Axial Velocity Distribution - Third Turbulent Flow Test Case

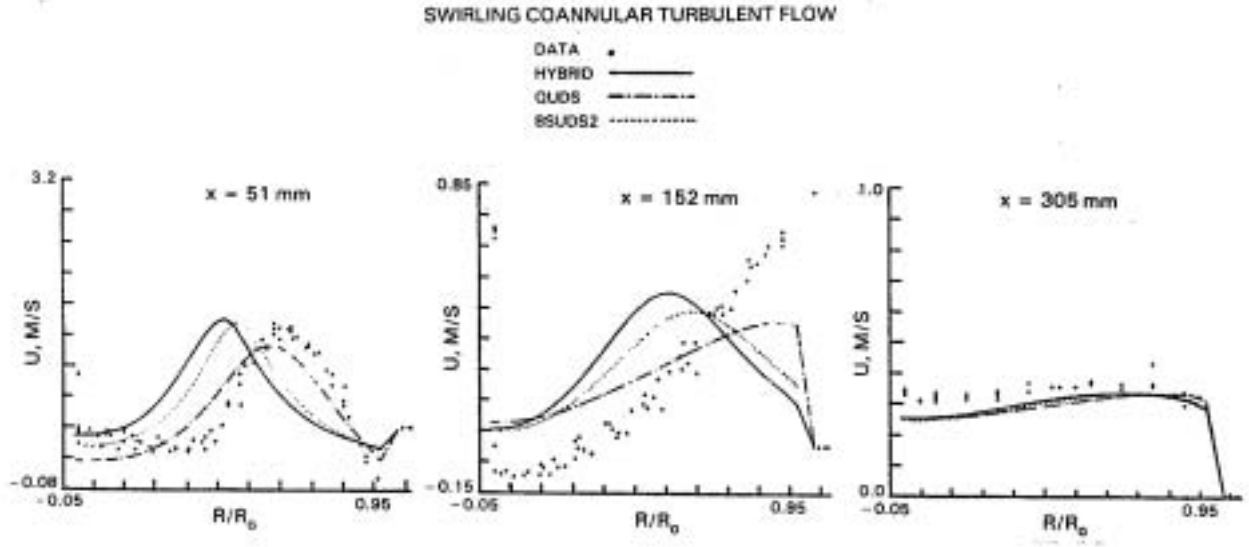

Figure 6-33 Comparison of Axial Velocity Profiles - Coarse Grid

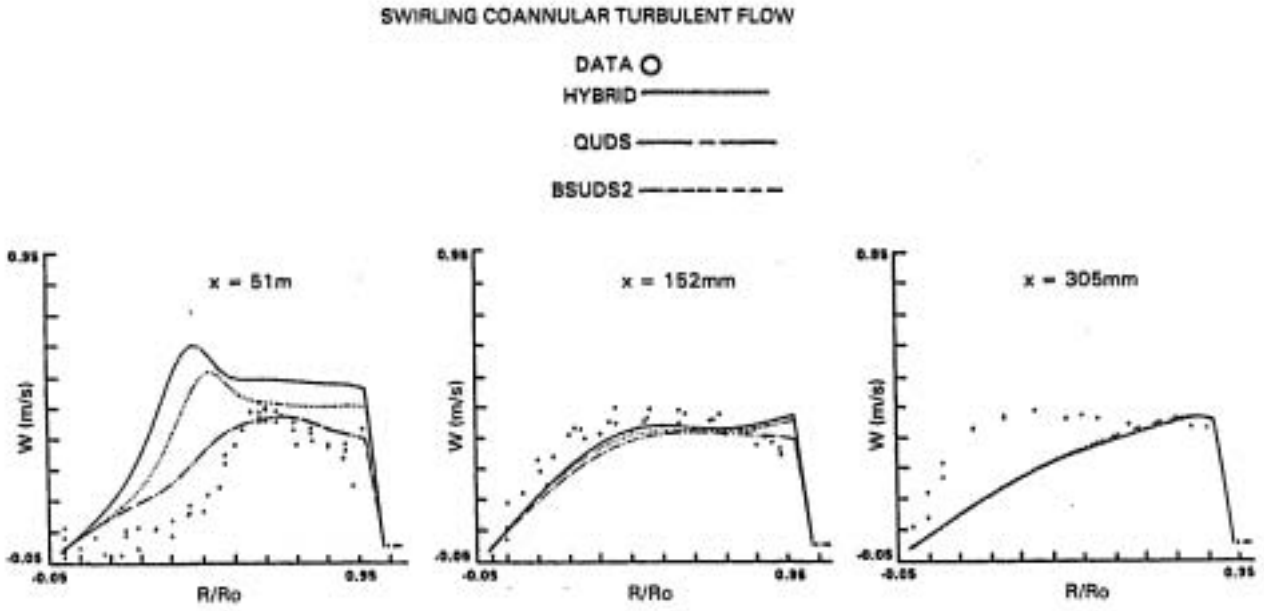

Figure 6-34 Comparison of Tangential Velocity Profiles - Coarse Grid

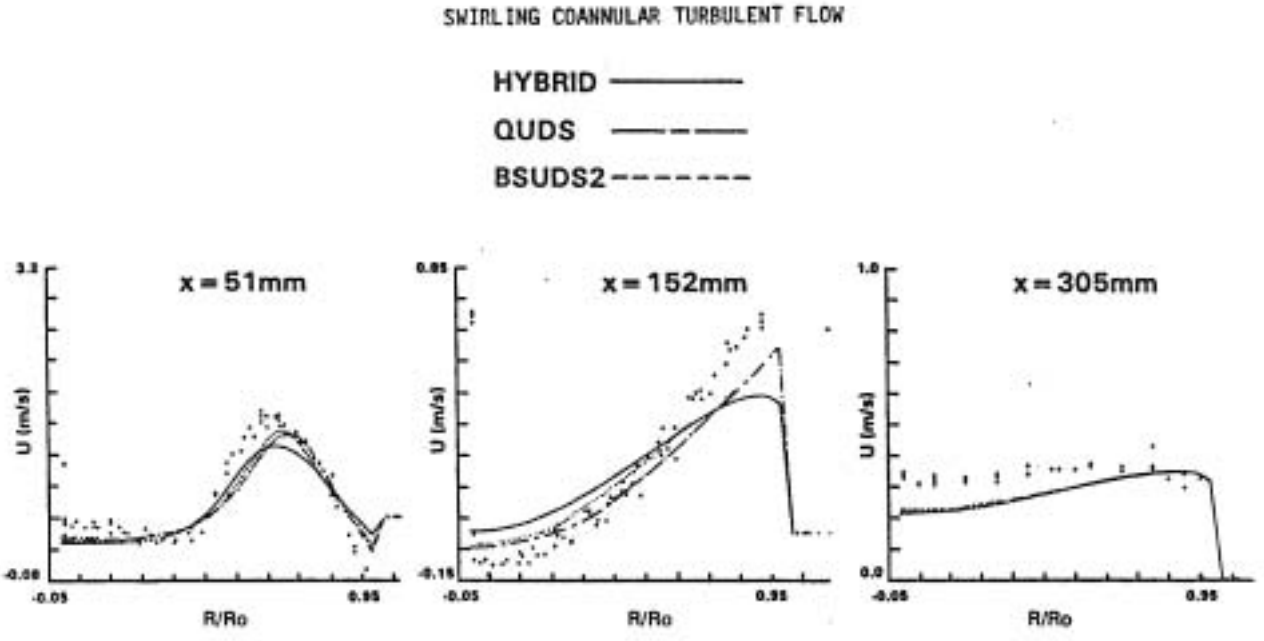

Figure 6-35 Comparison of Axial Velocity Profiles - Extra Fine Grid

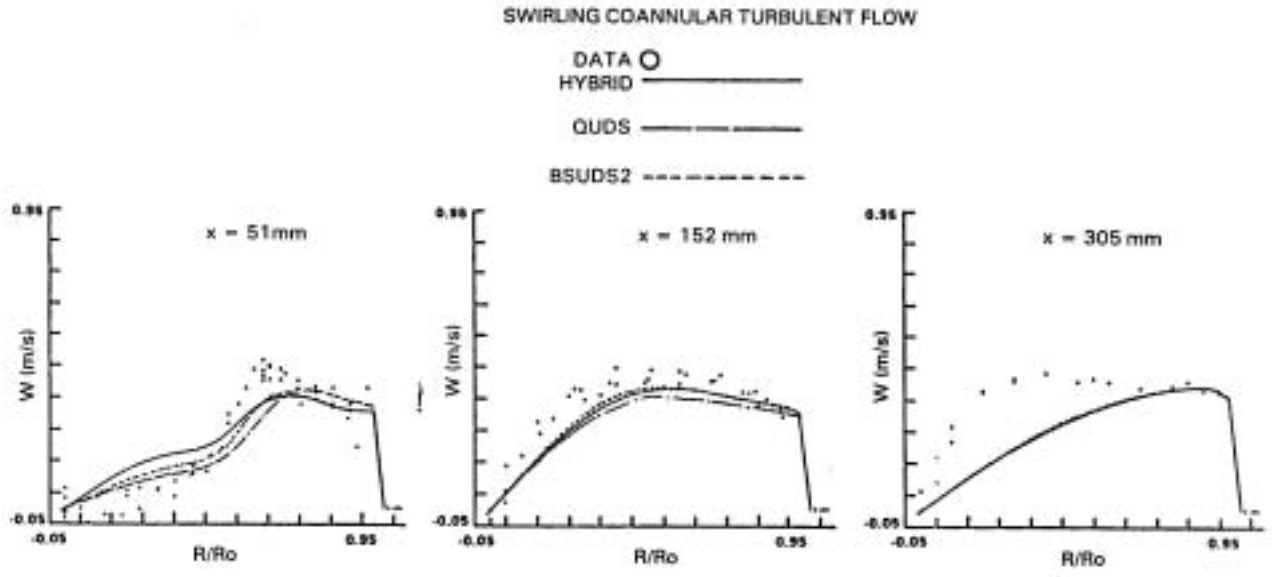

Figure 6-36 Comparison of Tangential Velocity Profiles - Extra Fine Grid

6.3 SUMMARY OF 2D-TEST CASES

Two laminar flow test cases and three turbulent flow test cases were calculated and compared against experimental data where such data were available. For laminar flow, the results confirmed the findings of the model problem studies; both schemes were markedly superior to the hybrid differencing scheme. BSUDS2 seemed to be more accurate at large flow angles, whereas QUDS was more accurate at small angles. For turbulent flows, especially for the first two test cases, hybrid differencing turned out to be almost as accurate as the two improved accuracy schemes. This behavior was unexpected and warrants further investigation. Also, QUDS became unstable for the first and the second turbulent flow test cases. This instability of QUDS was expected. For the third turbulent flow test case, QUDS was superior to both BSUDS2 and hybrid differencing for the coarse mesh. It was found that BSUDS2 was unstable for the third turbulent flow test case and the improved pressure algorithm, FAST, was used to achieve convergence. This behavior of BSUDS2 was also unexpected and needs further investigation. The unexpected behavior of the differencing schemes in turbulent flow emphasizes the importance of using realistic test cases for the final evaluation of the differencing schemes.

6.4 SELECTION OF DIFFERENCING SCHEME FOR 3D-TEACH

It was found from the computation of 2D-test cases that QUDS was prone to instability. Since in 3D, this tendency is bound to increase, there was little choice but to select the more stable BSUDS2 for incorporation into 3D-TEACH.

6.5 THREE-DIMENSIONAL TURBULENT FLOW TEST CASE

The baseline (hybrid differencing) and BSUDS2 versions of the three-dimensional computer program were used to analyze the three-dimensional test cases. This test case is based on the experiments conducted by Khan (Ref. 37) in which rows of jets were injected normal to the main flow in a duct with a rectangular cross-section. For the test condition simulated, a single row of

2.54-cm diameter jets with a pitch (jet centerline-to-centerline distance) to jet diameter ratio of four was used; the test section height to jet diameter ratio also was four. A schematic diagram of the flow geometry in the test section is shown in Figure 6-37.

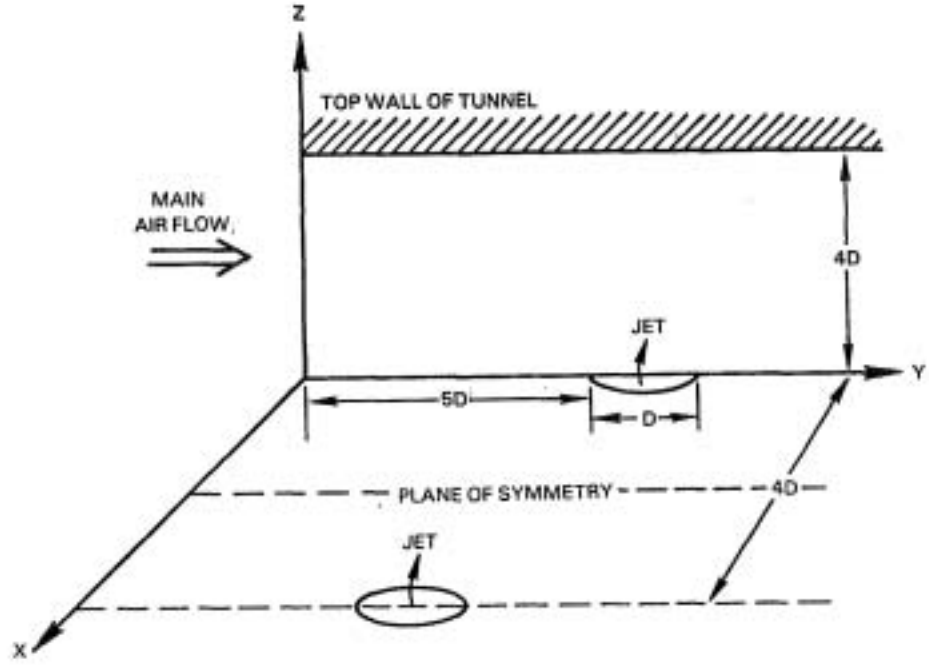

Figure 6-37 Test Case Flow Geometry for Base-Line Computer Program.

In the axial (x) direction, the simulation extends from a plane five jet diameters upstream of the leading edge of the jet to a point 24 jet diameters downstream of the trailing edge of the jet; that is, for 30 jet diameters. In the vertical direction, the calculation extends from the floor of the wind tunnel to the roof, a distance of four jet diameters. In the lateral direction the computational domain covers the distance through the jet centerline to the plane of symmetry between the jets, a distance of two jet diameters. Kahn verified that the flow was symmetric about the latter plane.

The grid system for each plane is shown in Figures 6-38 through 6-40, respectively. The jet was simulated using the relatively fine, rectangular grid in the injection plane, as shown schematically in Figure 6-41. The number of grid nodes in the x, y, and z directions were 34, 10, and 15, respectively. For later reference, this grid system has been designated as the COARSE grid.

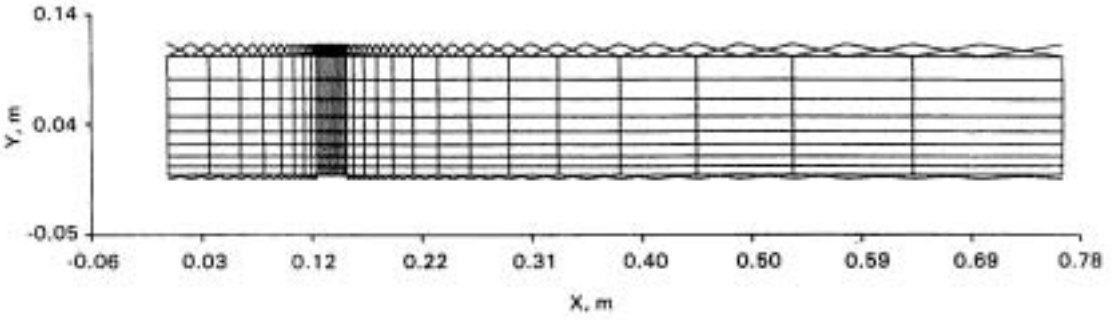

Figure 6-38 Coarse Mesh for the Test Case in X-Y Plane

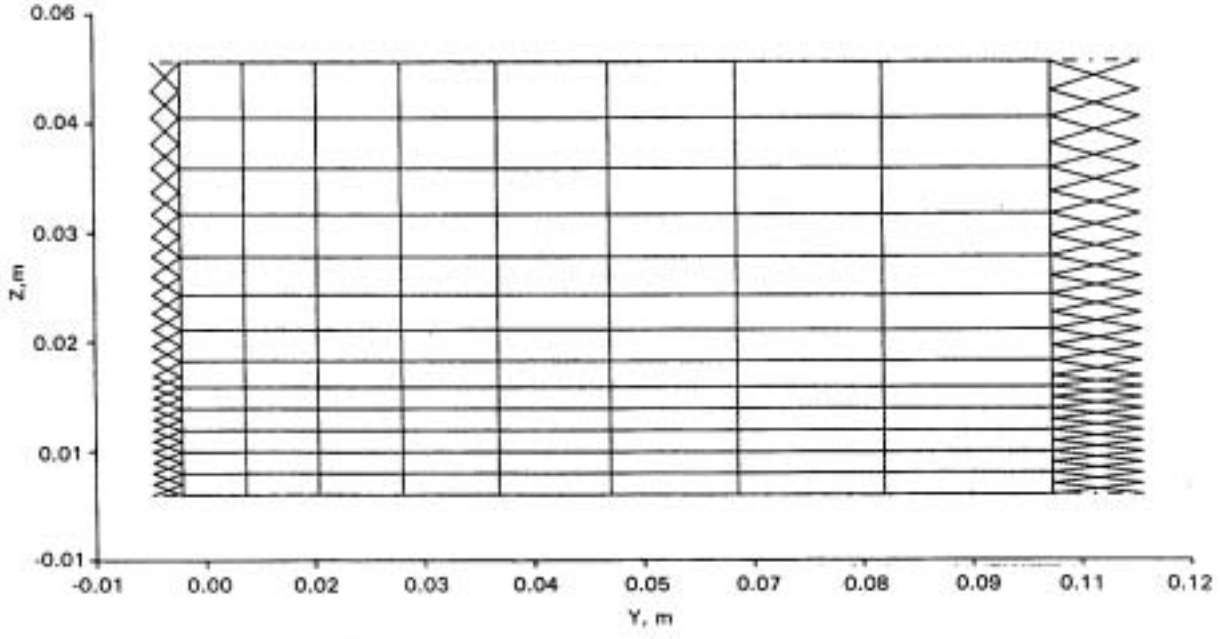

Figure 6-39 Coarse Mesh for the Test Case in Z-Y Plane

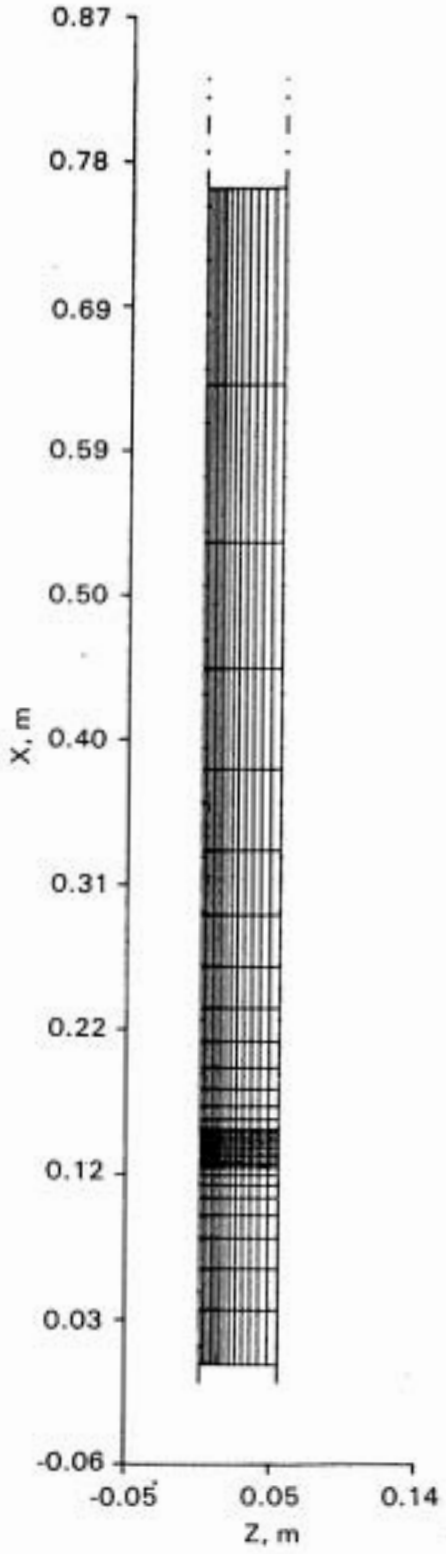

Figure 6-40 Coarse Mesh for the Test Case in X-Z Plane

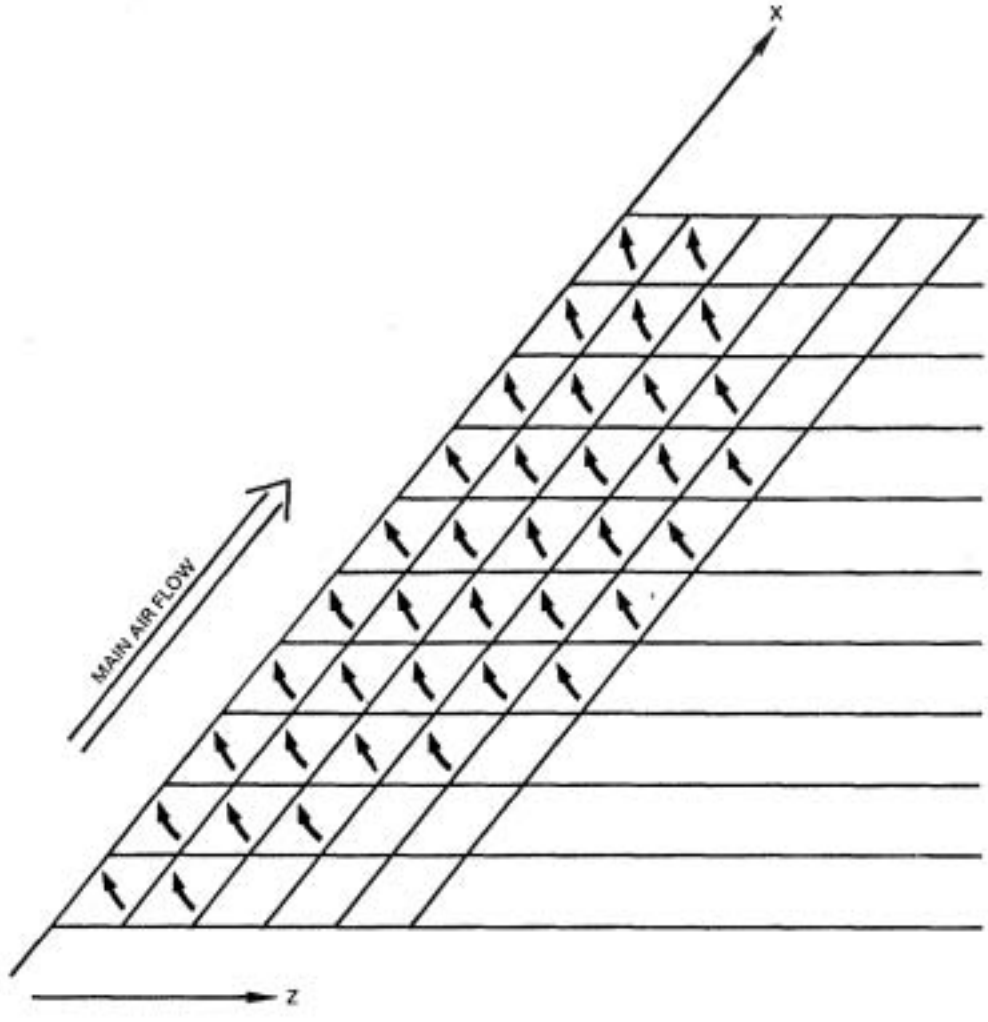

Figure 6-41 Grid Definition in Vicinity of Jet Exit.

The ratio of jet to mainstream velocity was approximately 2.3. Experimental data, Reference 38, were used to establish the initial velocity of the jet. These data, which were for a jet to mainstream velocity ratio of 2, are shown in Figure 6-42, together with the assumed jet velocity distribution used in the test case. For other calculationsin this flow system, see Ref. 1

For the baseline computer program with hybrid differencing, calculations were continued for 141 iterations until the maximum residual error was less than 5 percent. Selected calculations were continued to a lower level of maximum residual; the computed flow field did not change significantly.

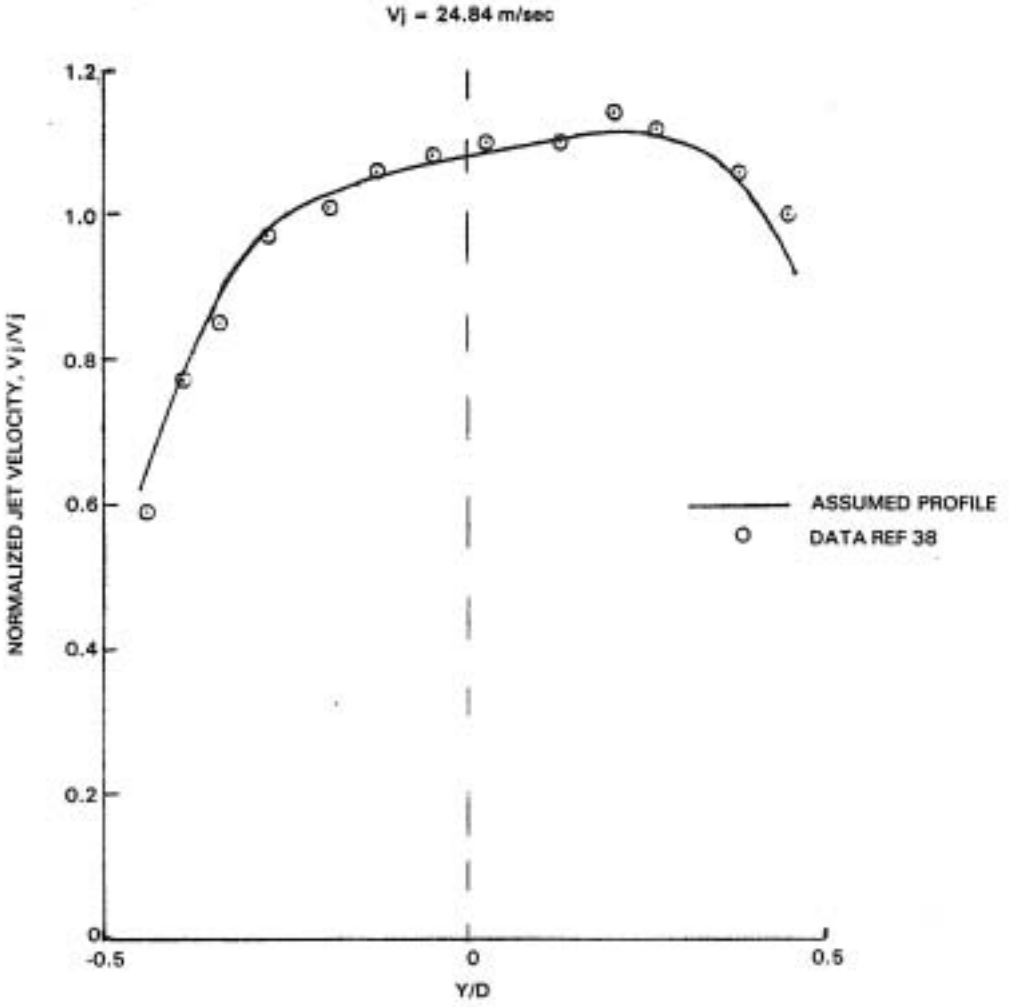

Figure 6-42 Jet Axial Velocity Profile.

Both BSUDS2 and Skew-Upwind Differencing (SUD) without bounding were used. The number of iterations required to achieve comparable levels of convergence were as follows:

Differencing	No. of Iteration
Hybrid	141
BSUDS2	222
SUD (No Bounding)	244

The BSUDS2 calculations were run with the blending factor initialized to unity.

Calculation time per iteration for BSUDS2 was approximately twice that for hybrid differencing. This large increase is probably due to the time required to assemble the additional finite-difference coefficients required for BSUDS2 and to the bounding procedure, as noted earlier.

The streakline plots for the coarse mesh are shown in Figure 6-43 to 6-45. These figures do not show significant differences between the hybrid and BSUDS2 calculations.

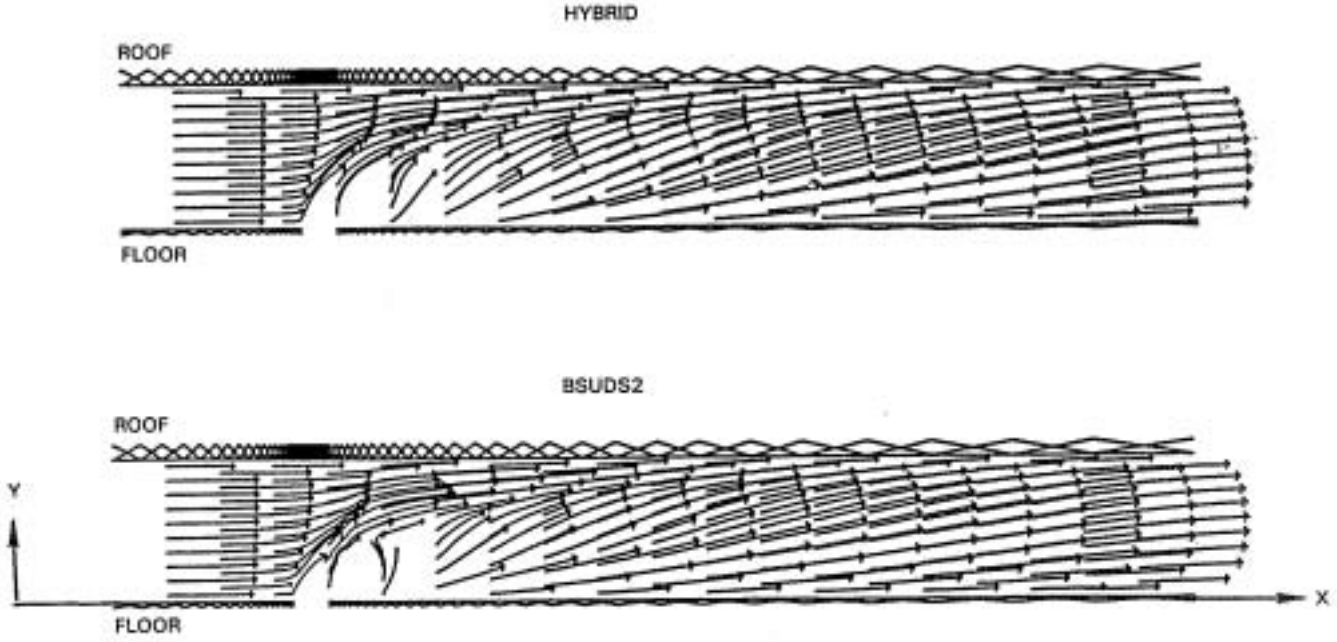

Figure 6-43 Comparison of Streakline Plots for BSUDS2 and HYBRID in the X-Y Plane through the Center of the Jet - Coarse Grid

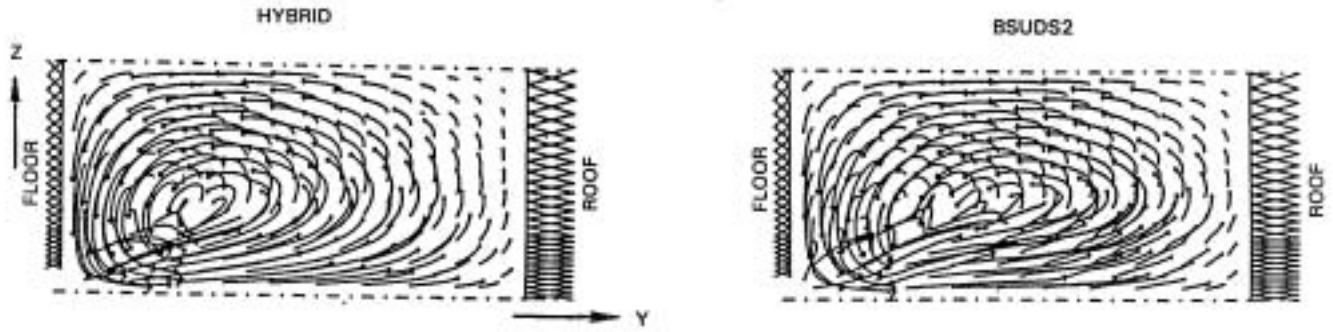

Figure 6-44 Comparison of Streakline Plots for BSUDS2 and HYBRID in the Y-Z Plane at Y/D = 0.5 - Coarse Grid

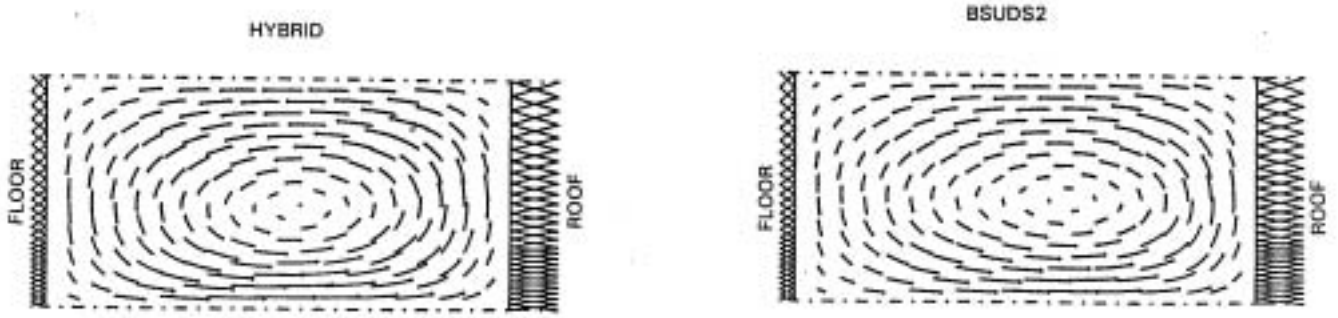

Figure 6-45 Comparison of Streakline Plots for BSUDS2 and HYBRID in the X-Z Plane at Y/D = 20 - Coarse Grid

Comparisons of calculated results with data at four axial locations are shown in Figures 6-46 to 6-49. As expected, calculations without bounding appear to contain less numerical diffusion than the bounded calculations. However, the difference between the two predictions is not significant. Also, either skew method is successful in reducing numerical diffusion, as can be seen from Figure 6-46 where peaked profiles are calculated by the skew schemes where as numerical diffusion smears out the peaks for hybrid. There are, however, significant differences between the experimental data and the predictions, and grid refinement is required to ascertain if the discrepancy is due to the coarseness of the mesh or inaccuracies of the turbulence model.

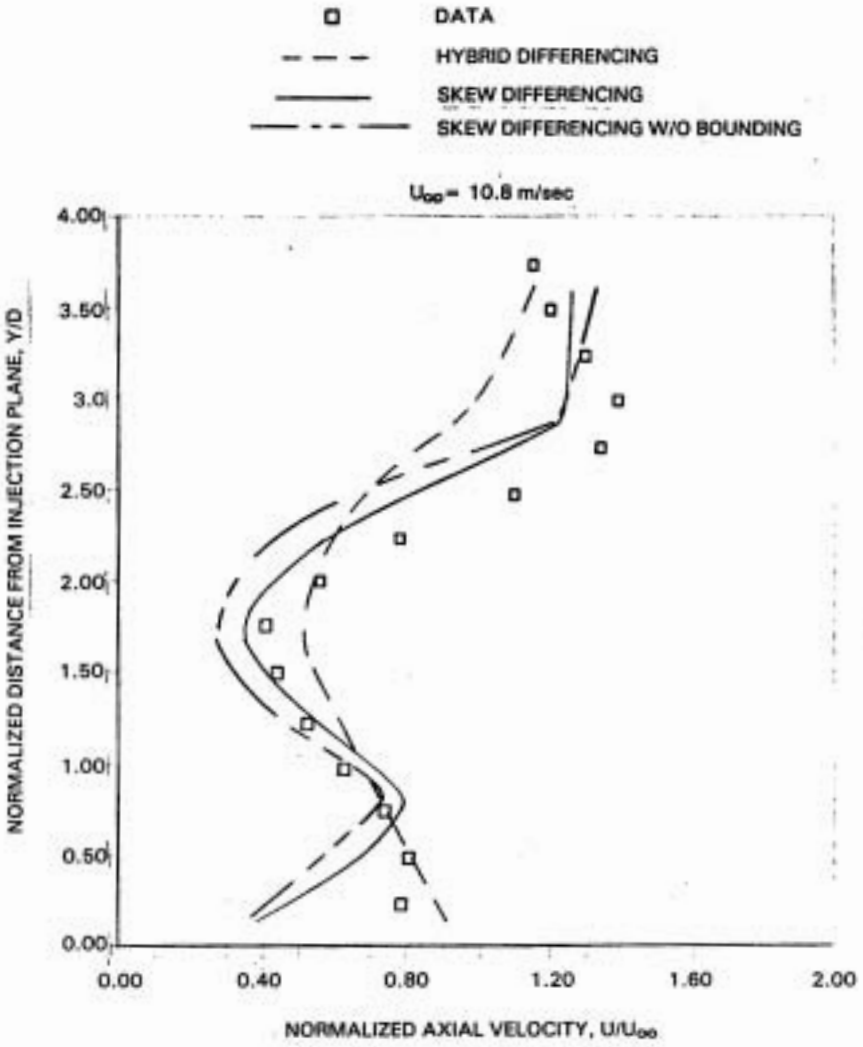

Figure 6-46 Comparison of Calculated and Measured Axial Velocity Profiles at X/D = 4 from Jet Centerline and Z /D = 0 Using Coarse Grid

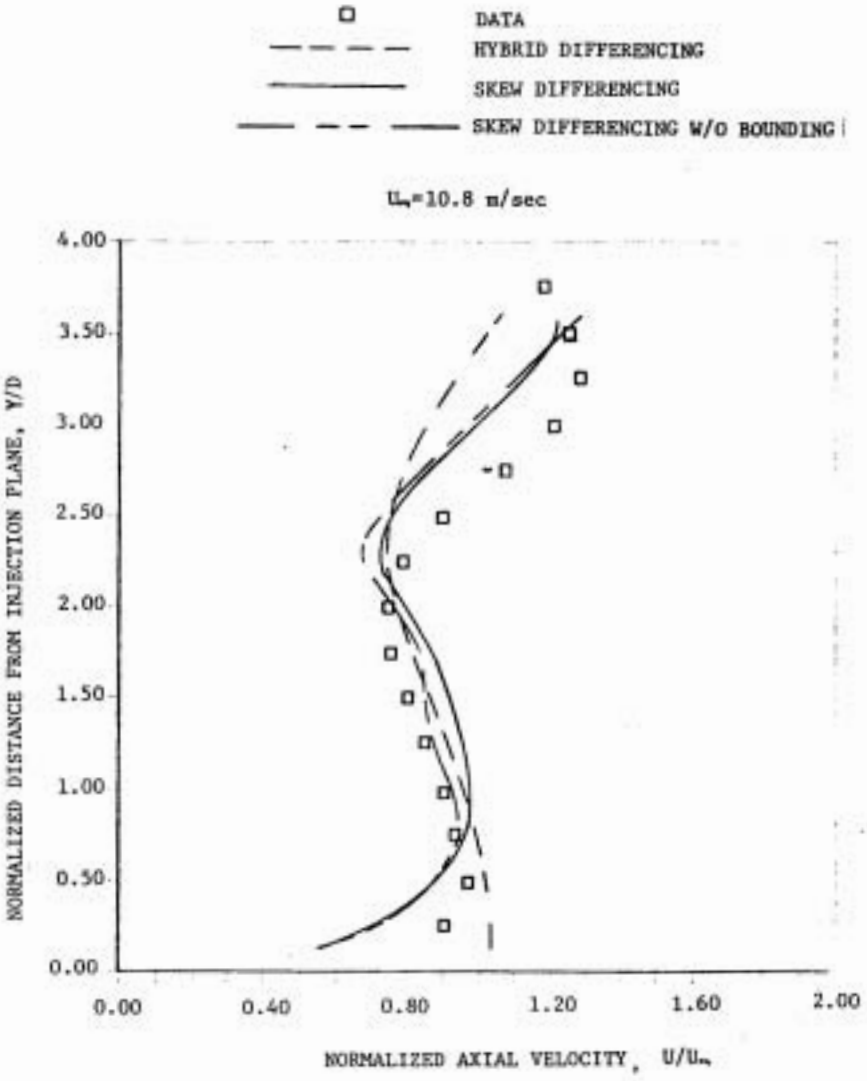

Figure 6-47 Comparison of Calculated and Measured Axial Velocity Profiles at X/D = 6 from Jet Centerline and Z /D = 0 Using Coarse Grid

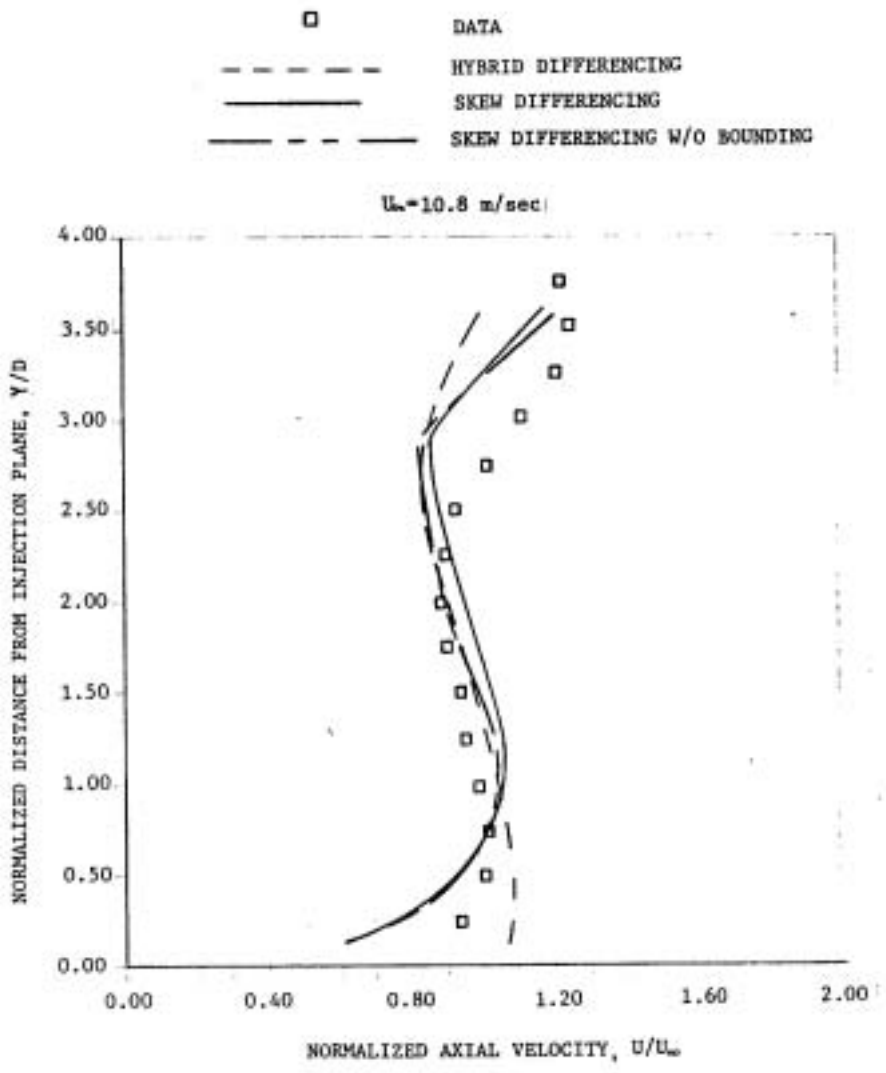

Figure 6-48 Comparison of Calculated and Measured Axial Velocity Profiles at X/D = 8 from Jet Centerline and Z /D = 0 Using Coarse Grid

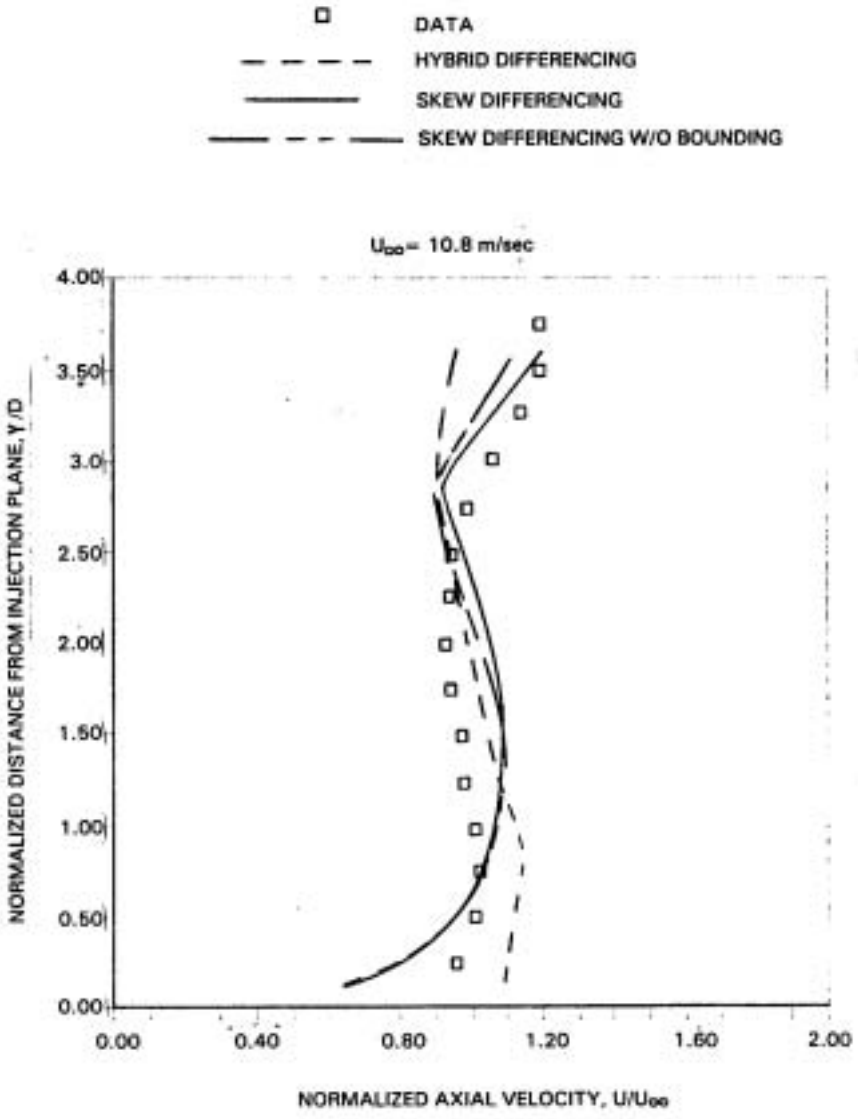

Figure 6-49 Comparison of Calculated and Measured Axial Velocity Profiles at X/D = 10 from Jet Centerline and Z /D = 0 Using Coarse Grid

The mesh used for the fine grid calculations used 40, 20, and 17 nodes in the x, y z direction, respectively. (Figures 6-50 to 6-52) It can be seen that the major difference between the coarse and fine meshes is the grid density in the vertical direction, which has doubled.

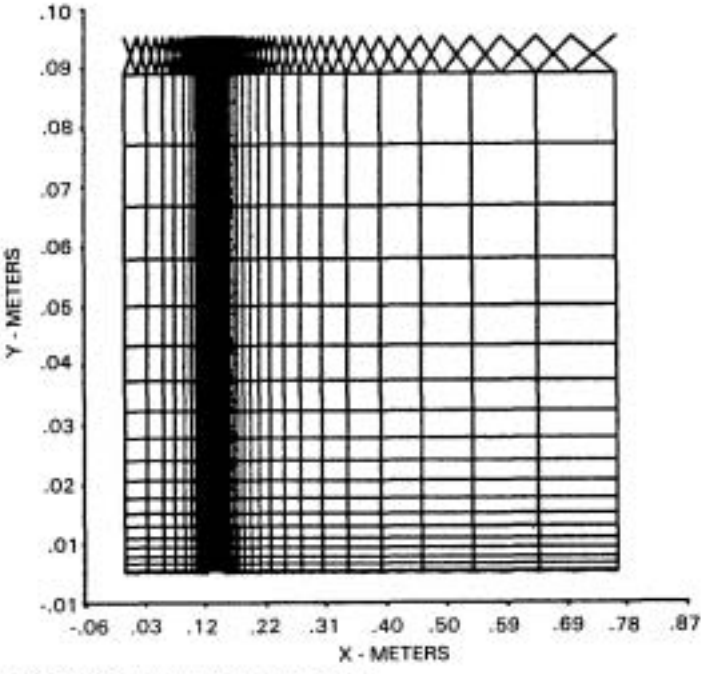

Note: (X and Y axis are not on the same scale)

Figure 6-50 Fine Grid System for Test Case in X-Y Plane.

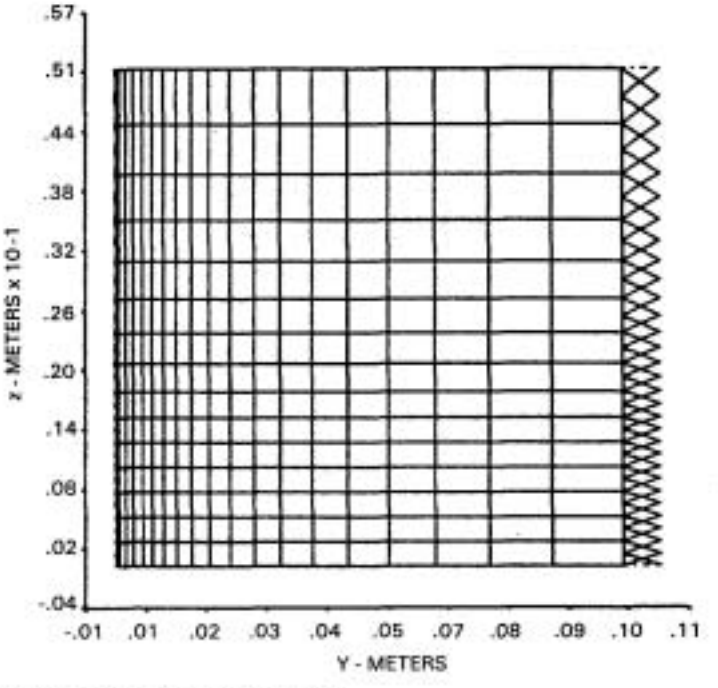

Note: (Y and Z axis are not on the same scale)

Figure 6-51 Fine Grid System for Test Case in Y-Z Plane.

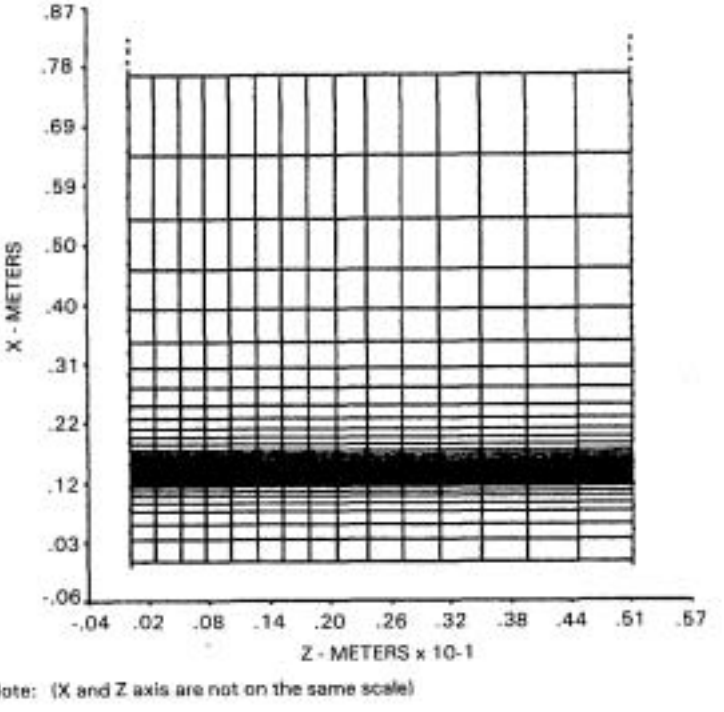

Figure 6-52 Fine Grid System for Test Case in X-Z Plane.

For FINE mesh calculations, the blending factor was initialized to 0.75. The reason for initializing the blending factor to 0.75 was that, when this factor was initialized to 1.0, (as is usually the case), severe convergence problems were encountered. These problems persisted even when a converged hybrid differencing solution was used as the initial guess for the BSUDS2 scheme. Since the initialized blending factor is not altered at a given node if the solution remains within bounds, reducing the initial blending factor by 25 percent has the effect of introducing some extra numerical diffusion. This diffusion seems to be sufficient to damp out the oscillations and to enable the solution to converge. Increasing the blending factor beyond 0.75 made the solution unstable. It was later found that the computer program was not computing the blending factors properly in some cases and the above instability could be due to the error in the code. Since it was ensured that the blending factors were in bound, the final solution is not in error. It may have more than the minimum amount of numerical diffusion required by the BSUDS2 scheme. However, as will be seen later, it has significantly less numerical diffusion than hybrid.

Comparisons of calculated results with data are shown in the Figures 6-53 to 6-56. It can be seen that as compared to the COARSE grid calculation, the predicted profile shapes have been modified, and the hybrid differencing and BSUDS2 predictions approach each other; however, there are still significant differences between the predictions and the data. Examination of the streakline plots, Figures 6-57 to 6-59, confirms the findings of the profile plots. The differences between the flow fields predicted by the two schemes are less pronounced than they were for the coarse grid.

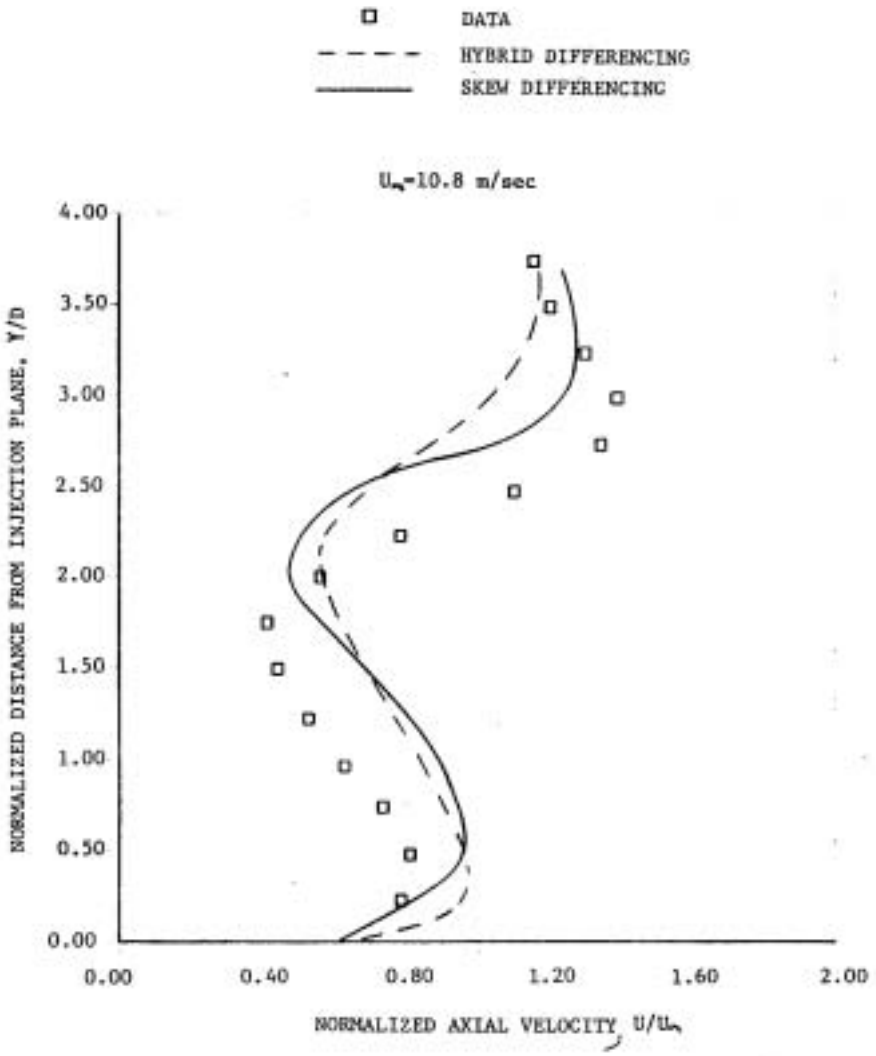

Figure 6-53 Comparison of Calculated and Measured Axial Velocity Profiles at X/D = 4 from Jet Centerline and Z/D = 0 Using Fine Grid

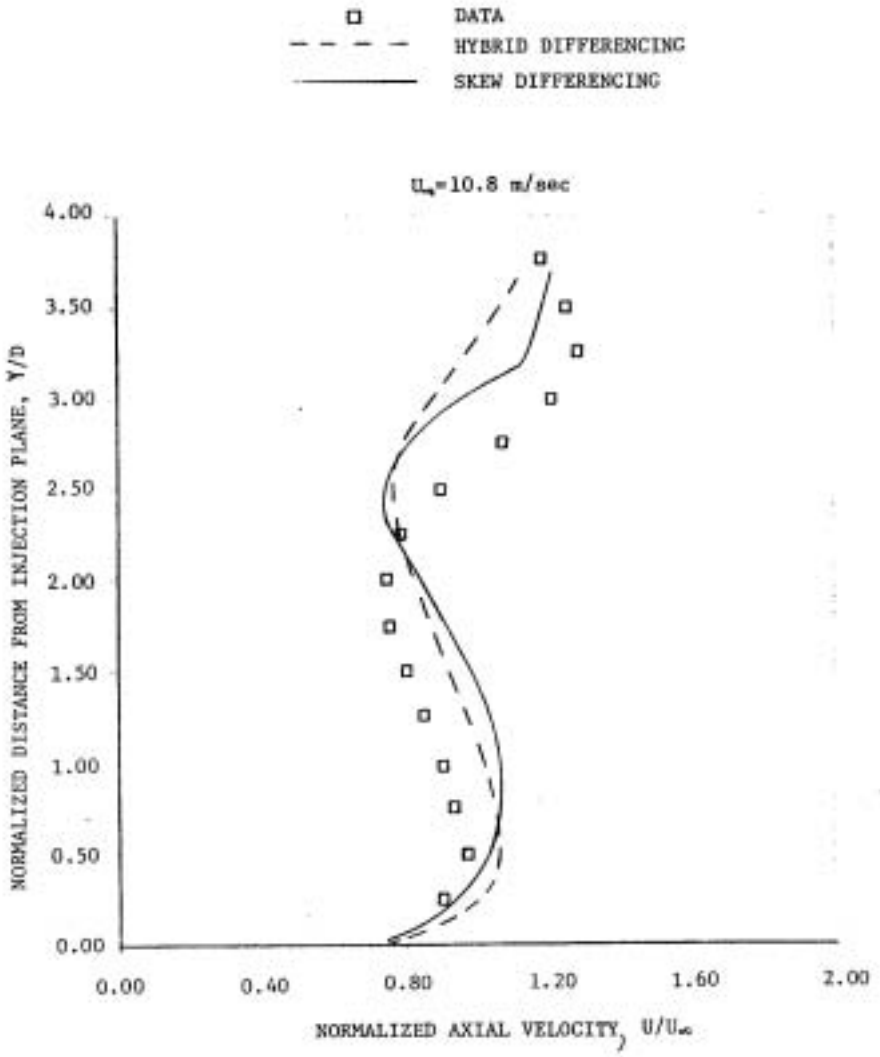

Figure 6-54 Comparison of Calculated and Measured Axial Velocity Profiles at X/D = 6 from Jet Centerline and Z/D = 0 Using Fine Grid

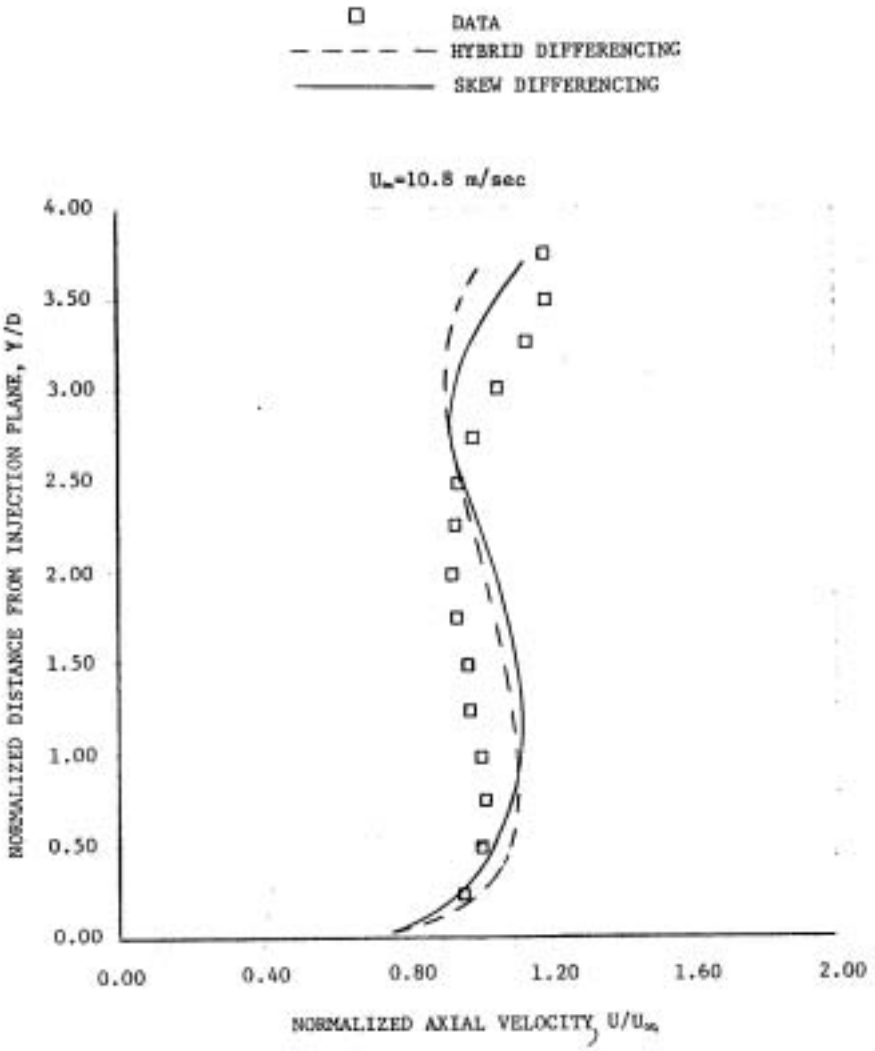

Figure 6-55 Comparison of Calculated and Measured Axial Velocity Profiles at X/D = 8 from Jet Centerline and Z/D = 0 Using Fine Grid

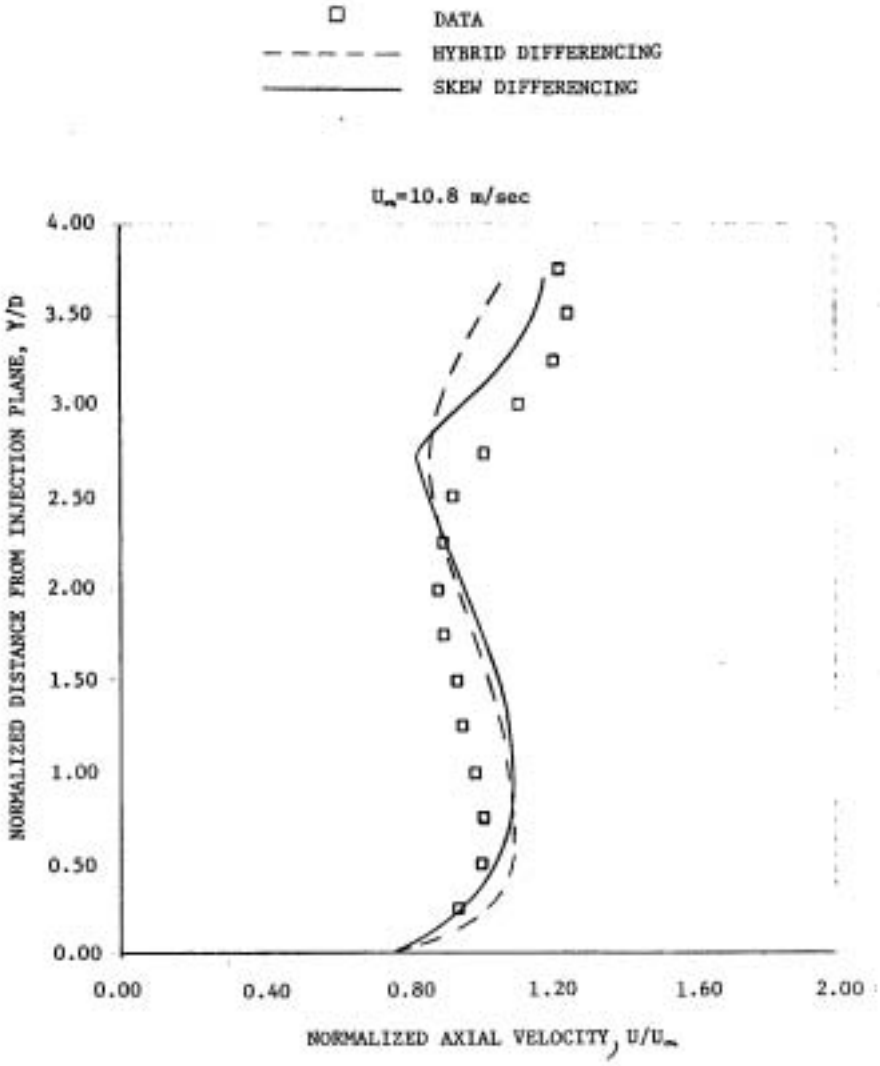

Figure 6-56 Comparison of Calculated and Measured Axial Velocity Profiles at X/D = 10 from Jet Centerline and Z/D = 0 Using Fine Grid

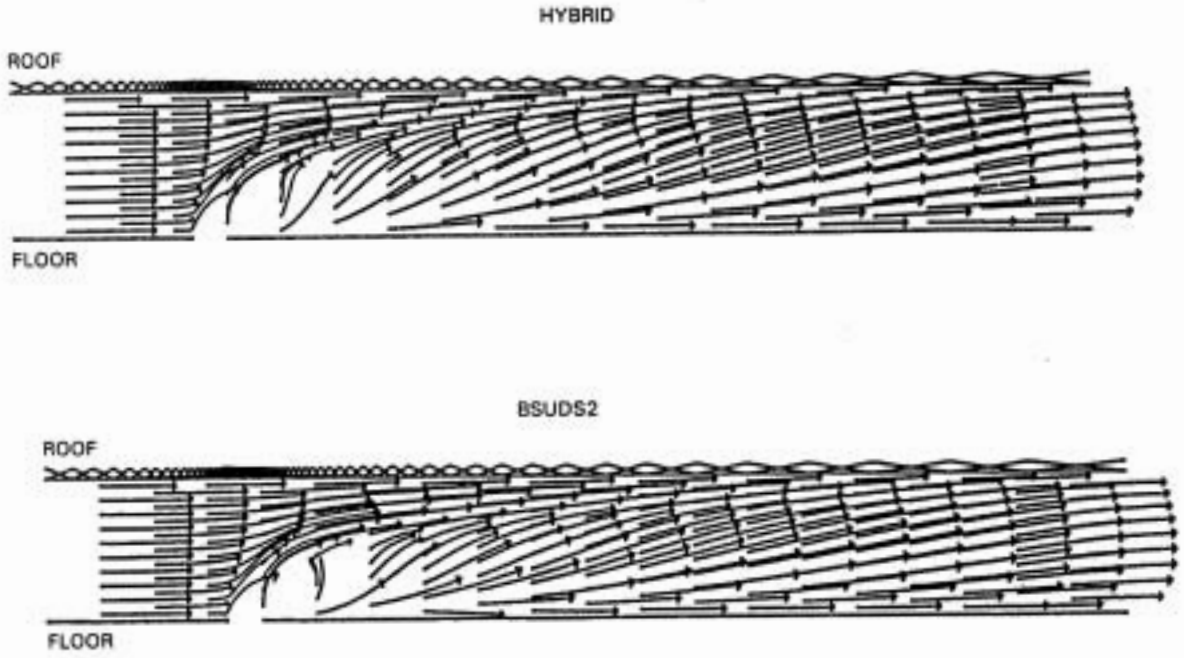

Figure 6-57 Comparison of Streakline Plots for BSUDS2 and HYBRID in the X-Y Plane through the Center of the Jet - Fine Grid

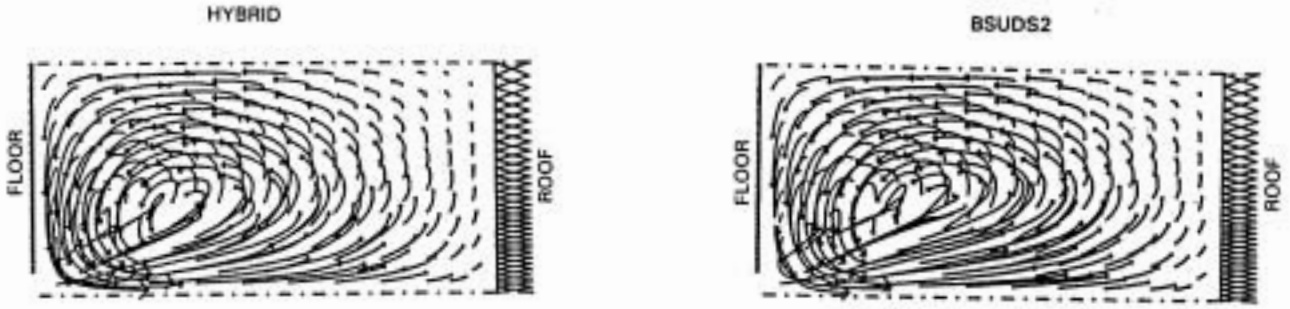

Figure 6-58 Comparison of Streakline Plots for BSUDS2 and HYBRID in the X-Z Plane at Y/D = 0.5 - Fine Grid

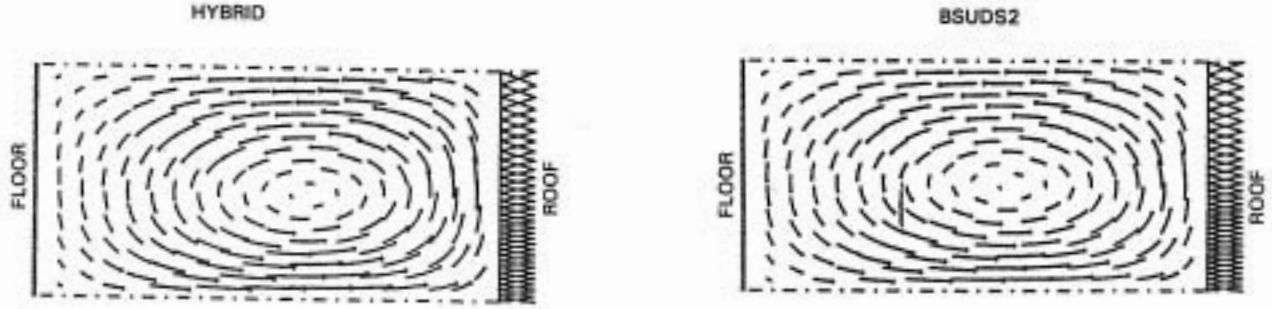

Figure 6-59 Comparison of Streakline Plots for BSUDS2 and HYBRID in the Y-Z Plane at X/D = 20 - Fine Grid

Figure 6-60 shows a comparison of COARSE and FINE mesh predictions for BSUDS2 and hybrid differencing. It can be seen that the predicted profiles have changed significantly near the floor of the tunnel but not near the roof. A comparison of the COARSE and FINE meshes in the y-z plane, Figure 6-61, shows that although the mesh was refined considerably near the floor its density was not increased sufficiently near the roof. Since the measured profile near the roof is also peaked and the gradients near the roof are as large as those near the floor, it can be inferred that a significant amount of numerical diffusion is still present in the FINE grid calculation. To ensure that a mesh independent solution has been achieved, the mesh density near the roof must be increased. Unfortunately, the cost of making such a run during present contract was prohibitive.

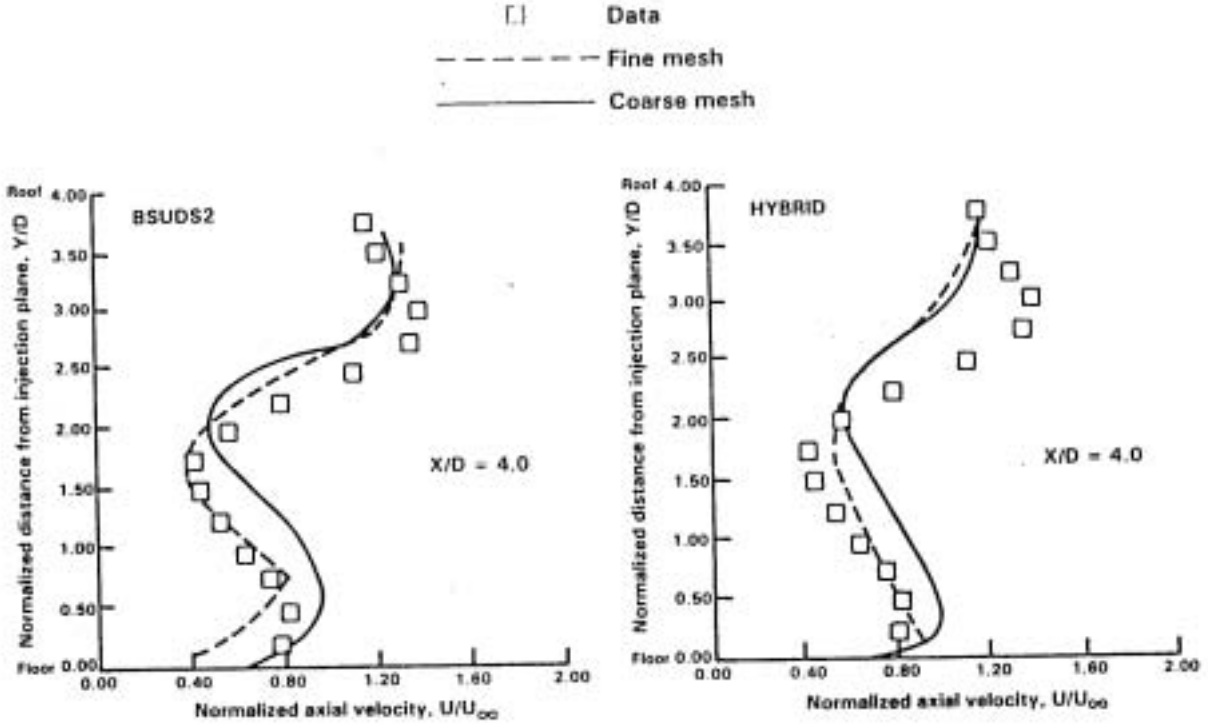

Figure 6-60 3D Test Case 1 - Comparison of Axial Velocity Profiles for Coarse and Fine Meshes

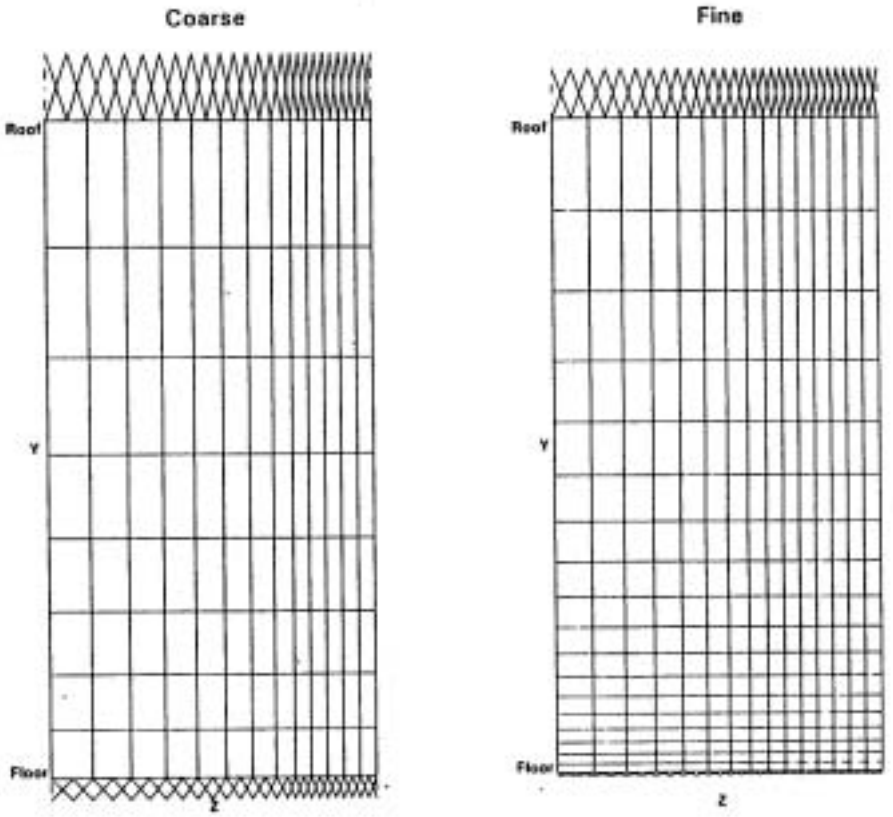

Figure 6-61 3D Test Case 1 - Comparison of Coarse and Fine Meshes in the Y-Z Plane

6.6 SUMMARY OF 3D-TEST CASE

One turbulent flow three-dimensional test case, a row of jets in cross flow, was calculated using hybrid differencing and BSUDS2. Two mesh sizes, COARSE (34 x 10 x 15) and FINE (40 x 20 x 17) were used. It was found that BSUDS2 was able to reduce numerical diffusion when compared to hybrid differencing. There remained a considerable discrepancy between the data and predictions. Because of budget limitations, a finer mesh, which would have been able to resolve the velocity near the roof of the tunnel, could not be used. Hence, it could not be ascertained if this discrepancy is due to the turbulence model or to an insufficient number of grid nodes.

6.7 SUMMARY OF TEST CASES

The improved accuracy finite-difference schemes, QUDS and BSUDS2, were evaluated in 2D-TEACH by computing laminar and turbulent flow test cases. These computations were compared with experimental data where such data were available. Every test case was calculated using successively finer grids in an effort to obtain grid independent solutions. Grid independence was obtained in most cases, but in some turbulent flow test cases, limitations of computer size or instability in the solution prevented achievement of this goal.

For the laminar flow test cases, the flow over a backward facing step and swirling flow into a sudden expansion were analyzed. For laminar flow, the results confirmed the predictions of the model problem studies described in Section 4.0. Both schemes were markedly superior to the hybrid differencing scheme; and, BSUDS2 was more accurate at large flow angles and QUDS was more accurate at small angles. Three turbulent flow test cases were considered: flow over a backward-facing step, nonswirling flow in a sudden expansion, and swirling flow in a sudden expansion. For the first two test cases the accuracy of hybrid differencing was the same as that of the two improved accuracy schemes. This behavior was unexpected and warrants further investigation. Also, QUDS became unstable for the first and second turbulent flow test cases. This instability of QUDS was expected. BSUDS2 became unstable for the third turbulent flow test case; this behavior was also unexpected and needs further investigation. The unexpected behavior of the performance of the differencing schemes for the turbulent flow test cases demonstrated the inadequacy of relying only upon model problem studies for selecting a scheme and emphasizes the importance of using realistic test cases.

One three dimensional, turbulent flow test case, a row of jets in cross flow, was calculated using hybrid differencing and BSUDS2 with two mesh sizes. Because of computer storage and budget limitations, a grid-independent solution could not be achieved for either scheme. It was found that BSUDS2 was more accurate than Hybrid differencing for this test case.

7.0 CONCLUDING REMARKS

This study has contributed significantly to the effort of reducing numerical error in computational fluid mechanics codes. One of the most important developments has been the establishment of a frame work by which future schemes can be judged. This frame work did not exist prior to this study. In this study, not only were the criteria for evaluation established, but a number of schemes were evaluated using these criteria and the procedure was successful in identifying the most suitable scheme for 3D-codes. In addition, the assessment methods developed during this study were able to predict most of the deficiencies of the selected scheme which were later exhibited in the 3D-code. Another important outcome of this study was the realization that an improved accuracy scheme cannot be completely divorced from the solution algorithm. It was because of the incompatibility of QUDS with the present solution algorithm, and the resulting instability, that it was not incorporated into 3D-TEACH, although it has significant advantages over BSUDS2.

This effort has resulted in the improvement of the accuracy of 2D as well as 3D-codes based on the TEACH concept. Although accuracy improvement is dependent on the flow field, it is expected that for practical applications, where some portion of the flow makes a large angle with the grid lines, this improvement will be more than sufficient to justify the increased cost. Since the selected scheme is never less accurate than hybrid differencing, there is no danger of the improved code giving less accurate answers than the baseline version.

This study should be looked upon as a first step in the process of reducing numerical error from combustor performance codes. More work is required, especially for the 3D code, to ensure that the selected scheme is performing with optimum accuracy.

The reasons for the poor performance of BSUDS2 in some of the 2D-test cases also need to be investigated more throughly. At present, it is conjectured that the sensitivity of each scheme to flow angle is responsible for this behavior. It is quite possible that this may not be the only reason. For example, all model problem studies were conducted on meshes of uniform size with cell aspect ratio of unity whereas the 2D turbulent flow test cases used a non-uniform mesh with large aspect ratio cells. Hence poor performance of BSUDS2 in 2D cases could also be attributed to large cell aspect ratio. In principle, modifications to the scheme can be made to take account of the cell aspect ratio. The scheme can also be modified to account for the pressure gradient in the flow field which, as discussed earlier, leads to inaccuracies. It is suggested that the test cases be rerun with the above modifications to the scheme to assess the improvement in performance. It is anticipated that the performance of BSUDS2 will improve significantly after these modifications.

The blending procedure used in BSUDS2 suffers from the disadvantage that the final solution is not path independent. It is even conceivable that different initial values of the blending factor may produce different convergedsolutions where convergence is measured by the level of residual source error which in practice is always nonzero; that is, the solution may not be unique

computationally. Path dependency may cause difficulties when this code is used in a production environment. Several schemes can be formulated to reduce or eliminate this path dependence. One scheme would be to always start with a converged hybrid solution. The other would be to recalculate the blending factors at every iteration and use their latest value without under relaxing them with their value of the previous iteration.

8.0 RECOMMENDATIONS

There are two type of recommendations that can be made based on this work. Recommendations of the first type are related to the use of current codes for optimum accuracy. Recommendations of the second kind are concerned with further developments of the code.

It is recommended that BSUDS2 be used for production running of 2D- and 3D-TEACH codes. Since flows commonly encountered in gas turbine combustors are complex, and since some portion of the flow makes a large angle with the grid lines, BSUDS2 will yield more accurate results than will hybrid differencing. It is also recommended that during grid selection account be taken of property gradients present in the flow field. Indiscriminate refinement is not feasible in three-dimensional calculations with present day computers.

Since the accuracy QUDS as well as that of BSUDS2 is dependent on flow angle, it is desirable to develop differencing schemes that are less sensitive to the direction of the velocity vector. It is not necessary to abandon present methods completely in the pursuit of flow angle independence. Since QUDS and SUDS are accurate at different flow angles, it may be feasible to combine these two schemes in such a manner that the resulting scheme is more accurate than either of the schemes at all flow angles. This possibility should be investigated. It was found that the model problem based on single cell calculations was successful in predicting the flow angle sensitivity of the schemes tested. Hence, it is recommended that this problem be used to screen the candidate schemes in future.

Incorporation of the more implicit pressure algorithm, FAST, into the 3D-TEACH code is recommended. It is expected that the stability of BSUDS2 will improve with this algorithm as demonstrated in the 2D-Code. In order to improve the stability of QUDS and other schemes, whose computational molecule is not compatible with the ADI method, a more compatible matrix solver must be developed.

Alternatively, instead of developing further the 3D-TEACH code, an entirely new computer program based (say) on a time-marching procedure which does not need a matrix solver. Since the time-step size necessary for stability of an explicit algorithm is extremely small, it is expected that a higher-order differencing scheme, such as QUDS, will be stable in this framework. However, considering that the time required to bring a new code to production status is about ten years and the expenditure of resources is considerable, any improvements to the present code in the interim are highly desirable.

References

1. Sturgess, G. J., "Aerothermal Modeling, Phase I - Final Report". NASA Report CR 168202, May 27, 1983.

2. Libby, P. A. and Williams, F. A., (Editors) Turbulent Reacting Flows, Topics in Applied Physics, Vol. 44, Apringer-Verlag, New York, 1980.

3. Spalding, D. B., "The Two-Fluid Model of Turbulence Applied to Combustion Phenomena". Paper No. AIAA-84-0476, AIAA 22nd Aerospace Sciences Meeting, Reno, Nevada, January 9-12, 1984.

4. Roach, P. J., "Computational Fluid Dynamics", Hermosa Publishers, New Mexico, 1976.

5. Leonard, B. P., "A Survey of Finite-Differences of Opinion on Numerical Muddling of the Incomprehensible Defective Confusion Equation". Applied Mechanics Division, ASME Winter Annual Meeting, New York, December 1979.

6. Boni, A. A., "Comments on the Computational Aspects of Turbulent Combustion". Acta Astronautical, Vol. 6, pp. 991-995, 1979.

7. Spalding, D. B., "A Novel Finite-Difference Formulation for Differential Expressions Involving Both First and Second Derivatives". Intl. J. Numerical Methods in Engineering, Vol. 4, p. 551, 1972.

8. Jones, W. P. and J. J. McGuirk, "Mathematical Modeling of Gas-Turbine Combustion Chambers". AGARD Conference Proceedings No. 275, Combustor Modeling, AGARD, pp. 4,1-4,11, 1980.

9. Jones, W. P. and J. H. Whitelaw, "Calculation Methods for Reacting Turbulent Flows. Proc. Panel Discussion, Prediction of Turbulent Reacting Flows in Practical Systems". Edit. T. Morel, ASME Fluids Engineering Conference, Boulder, Colorado, pp. 9-22, June 22-24, 1981.

10. Leonard, B. P., "A Stable and Accurate Convective Modeling Procedure Based on Quadratic Upstream Interpolation". Computer Methods in Applied Mechanics and Engineering, Vol. 19, pp. 59-98, 1979.

11. Raithby, G. D., Skew Upstream Differencing Schemes for Problems Involving Fluid Flow". Computer Methods in Applied Mechanics and Engineering, Vol. 9, pp. 153-164, 1976.

12. McDonald, H., Combustion Modeling in Two- and Three-Dimensions - Some Numerical Considerations", Prog. Energy Combus. Sci., Vol. 5, pp. 97-122, 1979.

13. Gosman, A.D. and Lai, K.Y. "Finite Difference and Other Approximations for the Transport and Navier Stokes Equations", Fluids Section, Mechanical Engineering Department, Imperial College, London, SW7 FS/82/18

14. Agarwal, R.K. "A Third-Order-Accurate Upwind Scheme for Navier-Stokes Solutions at High Reynolds Numbers", AIAA-81-0112 Presented at AIAA 19th Aerospace Sciences Meeting Jan. 12-15, 1981 - St. Louis, Missouri.

15. Leonard, B.P., "A Stable and Accurate Convectaive Modeling Procedure Based on Quadratic Upstream Interpolation", Computer Methods in Applied Mechanics and Engineering , Vol 19, pp. 59-98, 1979.

16. Raithby, G.D., "Skew-Upstream Differencing Schemes for Problems Involving Fluid Flow", Comp. Methods in Applied Mechanics and Engineering, 9, 151-162, 1976.

17. Rubin, S.G. and Graves, R.A. Jr. "Viscous Flow Solutions with a Cubic Spline Approximation", Computers and Fluids, Vol. 3, pp. 1-36, 1975.

18. Vacca, G., Werle, M.J. and Polak, A. "Application of Fourth Order Spline Collocation Procedure to Boundary Layer Like Flows", Department of Aerospace and Applied Mechanics, University of Cincinnati, AFL-77-12-37, 1977.

19. Kumar, A., "Convective Transport Analysis Using Spline Techniques", M.Sc Thesis, Mechanical Engineering Department, Imperial College London SW7, 1981.

20. Glass, J. and Rodi, W., "A Higher Order Numerical Scheme for Scalar Transport", Computer Methods in Applied Mechanics and Engineering, Vol. 31, pp. 337-358, 1982.

21. Boris, J.P. and Book, D.L., "Flux-Corrected Transport I: Shasta - A Fluid Transport Algorithm That Works", J. Comp. Phys. 11, 38, 1973.

22. Gosman, A.D. and Peric, M., "A Flux Blending Scheme for Reducing Numerical Diffusion in Convective Transport", Mechanical Engineering Department Report - Imperial College, London, 1985.

23. Lai, K.Y., "Numerical Analysis of Fluid Transport Phenomena", Ph.d Thesis, Mechanical Engineering Department, Imperial College, London SW7.

24. Schlichting, H., "Boundary Layer Theory", McGraw Hill, New York, 1979.

25. Castro, I.P. "Numerical Difficulties in the Calculation of Complex Turbulent Flows", Turbulent Shear Flows, Vol. I, Edit. Durst, F., Launder, B.E., Schmidt, F. and Whitelaw, T.H., Springer-Verlag, 1979.

26. Leschzeiner, M.A. and Rodi, W., "Calculation of Annular and Twin Parallel Jets Using Various Discretization Schemes and Turbulence - Model Variations", ASME Journal of Fluids Engineering Vol. 103, pp. 352-360, 1981.

27. Han, T., Humphrey, J.A.C. and Launder, R.E. "A Comparison of Hybrid and Quadratic-Upstream Differencing in High Reynolds Number Elliptic Flows", Computer Methods in Applied Mechanics and Engineering, Vol. 29, pp. 81-95, 1981.

28. Leschzeiner, M.A. and Launder, B.E., Private Communication, 1982.

29. Benadecker, R.W., Goddard, A.T.H., Gosman, A.D. and Issa, R.I., "Numerical Prediction of Turbulent Flow Over Rearface Mounted Ribs", ASME, 83-FE-13.

30. Leonard, B. P., "A Stable and Accurate Convective Modeling Procedure Based on Quadratic Upstream Interpolation. Computer Methods in Applied Mechanics and Engineering", Vol. 19, pp. 59-98, 1979.

31. Leonard, B. P., Leschziner, M. A. and McGuirk, J., Third-Order Finite-Difference Method for Steady Two-Dimensional Convection, Proceedings of the First International Conference on Numerical Methods in Laminar and Turbulent Flow. Editors: C. Taylor et al, Pentech Press, London, pp. 807-819, 1978.

32. Armaly, B. F. and Durst, F. "Reattachment Length and Recirculation Regions Downstream of a Two-Dimensional Single Backward Facing Step", Symposium on Momentum and Heat Transfer Processes in Recirculating Flows, HTD-Vol. 13, ASME 101st Winter Annual Meeting, Chicago, November, pp. 1-9, 1980.

33. Yoon, H. K. and Lilley, D. G., "Five-Hole Pilot (sic) Probe Time Mean Velocity Measurements in Confined Swirling Flows", Paper No. AIAA-83-0315, AIAA 21st Aerospace Sciences Meeting, Reno, Nevada, January 10-13, 1983.

34. Kim, J., Kline, S. J., and Johnston, J. P., "Investigation and Separation of a Turbulent Shear Layer Flow Over a Backward-Facing Step", Report MD-37, Thermosciences Division, Department of Mechanical Engineering, Stanford University, Stanford, CA, April 1978.

36. Johnson, B. V. and Bennett, J. C., "Mass and Momentum Turbulent Transport Experiments with Confined Coaxial Jets", NASA CR-165574, November 1981.

36. Johnson, B. V. and Roback, R., "Mass and Momentum Turbulent Transport Experiments with Confined Coaxial Jets", United Technologies Research Center, to be Published in 1983.

37. Khan, Z. A., "Opposed Jets in Crossflow", Doctoral Dissertation; Mechanical Engineering Department, Imperial College, London University, 1982.

38. Andreopoulos, J., "Measurements in a Pipe-Flow Issuing Perpendicularly into a Cross Stream", ASME Paper 80-WA/HT-24, 1980.

39. Syed, S. A. and Sturgess, G. J., "Velocity and Concentration Characteristics and Their Cross-Correlation for Co-Axial Jets in a Confined Sudden Expansion, Part II: Predictions, "Proc. Symp. Fluid Mechanics of Comoustion Systems, Edit. T. Morel, R. P. Lohmann and J. M. Rackley, ASME Fluids Engineering Conference, Boulder, Colorado, pp. 150-167 June 22-23, 1981.

40. Issa, R. I., "Solution of Implicitly Discretized Fluid Flow Equations by Operator-Splitting", Int. Rep. Dept. Mineral Resources Engineering, Imperial College, London, 1982.

Page intentionally left blank

APPENDIX A

APPENDIX A - THE THREE DIMENSIONAL BOUNDED SKEW-UPWIND DIFFERENCING SCHEME

In this section, the three dimensional Bounded Skew-Upwind Differencing Scheme (BSUDS) is described. First, a brief review of the flux form of the equations of motion is presented. Second, a detailed description of the finite-difference form of the flux contribution to a representative face of a typical control volume is given; the derivation of the flux contributions to the other five faces is then outlined. Third, the resulting co-efficients for the finite-difference equations representing the total flux (and sources) are presented. Fourth, the results of applying the boundary conditions in a manner consistent with the foregoing flux representation are shown. Fifth, the bounding scheme for the coefficients is detailed.

This section is an extension of the two-dimensional scheme presented in Section 5.0

A.1 - Flux Form of the Equations of Motion

The equations of motion for both laminar flow and (time-averaged) turbulent flow can be written in similar fashion for all of the dependent variables:

Cartesian Co-ordinates

$$\frac{\partial}{\partial x}(\rho u\phi) + \frac{\partial}{\partial y}(\rho v\phi) + \frac{\partial}{\partial z}(\rho w\phi)$$

$$= \frac{\partial}{\partial x}\left(\Gamma_\phi \frac{\partial \phi}{\partial x}\right) + \frac{\partial}{\partial y}\left(\Gamma_\phi \frac{\partial \phi}{\partial y}\right) + \frac{\partial}{\partial z}\left(\Gamma_\phi \frac{\partial \phi}{\partial z}\right) + S_\phi \qquad \text{(A1.1a)}$$

Cylindrical Coordinates

$$\frac{\partial}{\partial x}(\rho u\phi) + \frac{1}{r}\frac{\partial}{\partial r}(r\rho v\phi) + \frac{1}{r}\frac{\partial}{\partial \theta}(\rho w\phi)$$

$$= \frac{\partial}{\partial x}\left(\Gamma_\phi \frac{\partial \phi}{\partial x}\right) + \frac{1}{r}\frac{\partial}{\partial r}\left(r\,\Gamma_\phi \frac{\partial \phi}{\partial r}\right) + \frac{1}{r}\frac{\partial}{\partial \theta}\left(\frac{1}{r}\Gamma_\phi \frac{\partial \phi}{\partial \theta}\right) + S_\phi \qquad \text{(A1.1b)}$$

The variable ϕ represents any of the dependent variables (e.g., the velocity components u, v, w, mixture fraction, turbulent kinetic energy and turbulent energy dissipation). The exchange coefficient, Γ_ϕ, represents the sum of both laminar and turbulent contributions and is interpreted as the effective viscosity for ϕ = u, v, w, the effective diffusivity for ϕ = mixture fraction, etc. S_ϕ is a generalized source term.

Eqs. (A1.1) are integrated over a control volume appropriate for each dependent variable ϕ and, after some manipulation, the finite-difference equivalent forms of Eqs. (A1.1) are obtained. The control volumes are defined using an orthogonal grid formed by the intersection of co-ordinate lines in each axial, radial, and lateral co-ordinate direction. The intersection of the grid lines form the grid nodes at which all flow properties except the axial (u), radial (v), and lateral (w) velocities are calculated; i.e., all scalars. The axial velocity is calculated using a second grid with grid nodes located midway between the scalar grid nodes in the axial direction and co-incident with the scalar grid nodes in both radial and lateral positions. The radial velocity is calculated using a third grid with grid nodes located midway between the scalar grid nodes in the radial direction and co-incident with the scalar grid nodes in both axial and lateral position. The lateral velocity (or azimuthal velocity in cylindrical co-ordinates) is calculated using a fourth grid with

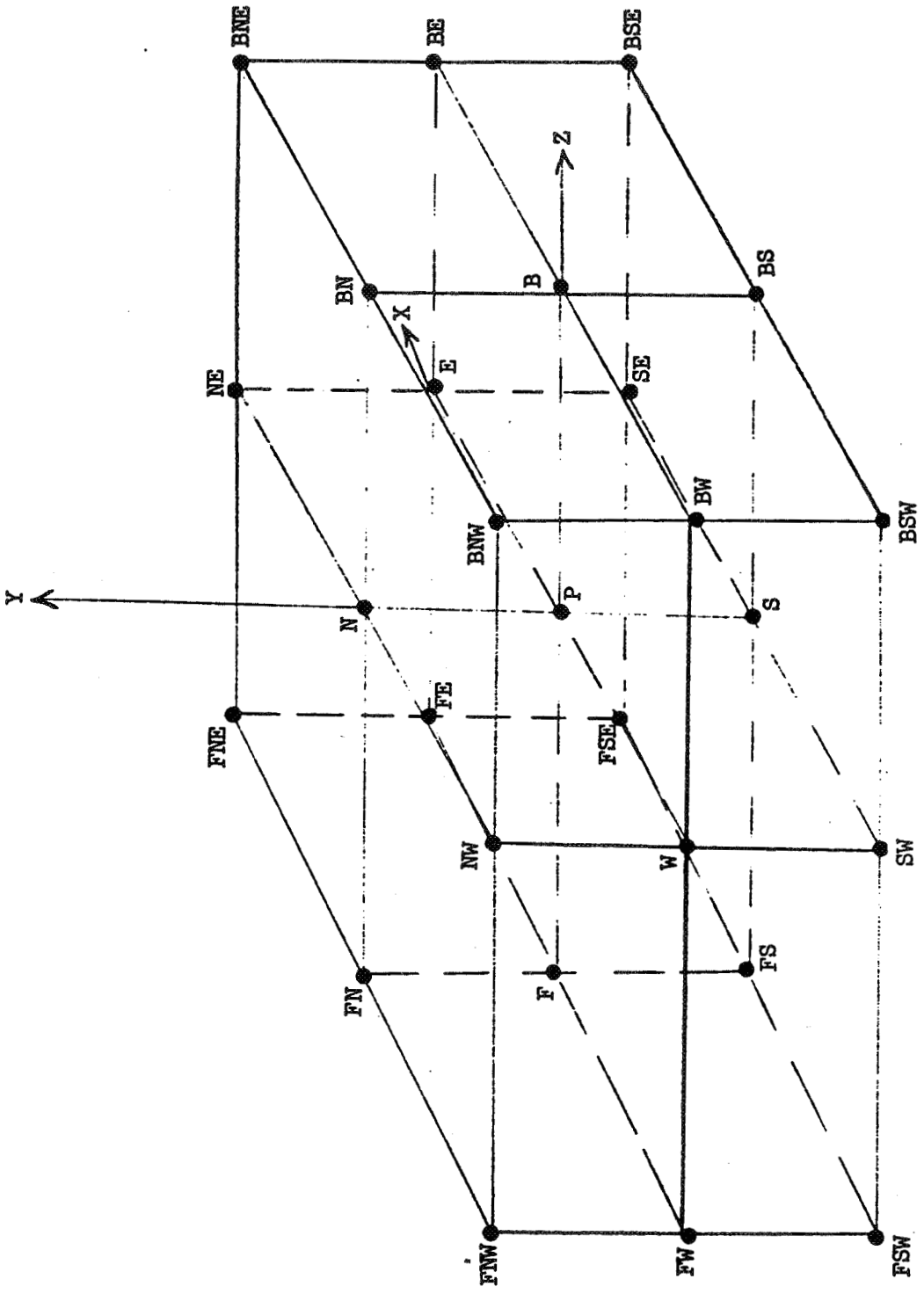

FIG. A-1 THREE-DIMENSIONAL GRID AND NODE SYSTEM

grid nodes located midway between the scalar grid nodes in the lateral (z or θ) direction and co-incident with the scalar grid nodes in both axial and radial position. Directions in the grids are identified as north, south, east, west, back and front. Nodes are identified as shown in Fig. A-1 where P is the node at the center of the control volume. For hybrid (upwind and central) differencing, the principal nodes are designated N, S, E, W, B, F and P. For the bounded skew-upwind differencing scheme, twenty additional nodes are used as shown in Fig. A-1.

The relative positions of the various grid systems can be illustrated by considering the grid systems in the x-y plane only. Then, the grid system for the scalars is shown in Fig. A-2 and the control volume for the scalars is shown in Fig. A-3. The relative positions of the axial and radial velocity control volumes is depicted in Fig. A-4. Similarly, in the y-z plane, the radial and lateral velocity control volumes are displaced relative to the scalar control volumes. Finally, in the x-z plane, the axial and lateral velocity control volumes are displaced relative to the scalar control volumes.

The faces of the control volumes for each scalar are defined by planes located midway between the scalar grid nodes as shown in Fig. A-3. Thus, the location of the east or west faces of a scalar control volume is co-incident with the axial locations of the axial velocity components, etc., so that normal velocity components lie along the boundaries of the control volumes. (Generally, boundaries for the u, v or w control volumes include scalar grid-lines and are not necessarily located midway between velocity grid lines.) For the scalars, the grid systems defined above provide some computational convenience. Since the u, v and w velocities are stored midway between the scalar grid nodes, the convective fluxes for each face can be calculated without recourse to averaging any of these velocities. Also, the pressure gradient driving the flow can be computed without averaging pressures.

The finite-difference forms of Eqs. (A1.1) are derived by integrating these equations over the appropriate control volume. In performing the integration over the control volume for each term in Eq. (A1.1), the mean-value theorem is employed and the source term is linearized in the vicinity of the center of the control volume (point P). After some manipulation, the finite-difference form of Eqs. (A1.1) is obtained

$$C_E\phi_e - C_W\phi_w + C_N\phi_n - C_S\phi_s + C_B\phi_b - C_F\phi_f$$

$$= D_E\,(\phi_E-\phi_P) - D_W\,(\phi_P-\phi_W)$$

$$+ D_N\,(\phi_N-\phi_P) - D_S\,(\phi_P-\phi_S)$$

$$+ D_B\,(\phi_B-\phi_P) - D_F\,(\phi_P-\phi_F) + S_U + S_P\phi_P \qquad \text{(A1.2)}$$

where C_E, C_W, etc. are "convective coefficients" as defined below

$$C_E = (\rho u)_e\, a_e$$

$$C_W = (\rho u)_w\, a_w$$

$$C_N = (\rho v)_n\, a_n$$

$$C_S = (\rho v)_s\, a_s$$

$$C_B = (\rho w)_b\, a_b$$

$$C_F = (\rho w)_f\, a_f \qquad \text{(A1.3)}$$

where a_e, a_w, a_n, a_s, a_b, a_f are the areas of the faces of the control volumes. The "diffusion coefficients" are given by

$$D_E = \left(\frac{\Gamma_\phi}{\Delta x}\right)_e a_e$$

$$D_W = \left(\frac{\Gamma_\phi}{\Delta x}\right)_w a_w$$

$$D_N = \left(\frac{\Gamma_\phi}{\Delta y}\right)_n a_n$$

$$D_S = \left(\frac{\Gamma_\phi}{\Delta y}\right)_s a_s$$

$$D_B = \left(\frac{\Gamma_\phi}{\Delta z}\right)_b a_b$$

$$D_F = \left(\frac{\Gamma_\phi}{\Delta z}\right)_f a_f \qquad \text{(A1.4)}$$

where the convective and diffusive coefficients are shown in terms of the cartesian co-ordinate system. Since Eq. (A1.2) has the same form for both cartesian and cylindrical co-ordinates, it is only necessary to define the geometric parameters used in the convective and diffusive fluxes in a manner appropriate for each coordinate system. These definitions are given in Appendix B. If a consistent set of geometric parameters is used, then the equations for the bounded skew-upwind differencing scheme developed below are identical in both cartesian and cylindrical co-ordinates. For convenience, the nomenclature for cartesian co-ordinates will be used.

It is important to note that Eq. (A1.2) applies to all of the dependent variables although the appropriate grid must be used in each case to define the geometric parameters used in the calculation. Also, Eq. (A1.2) can be used with any of the difference procedures considered in the program since each scheme is simply an alternative method for defining (interpolating for) the fluxes at the face of the control volume (e.g., ϕ_e, ϕ_w, ϕ_n, ϕ_s, ϕ_b, ϕ_f). However, the diffusion terms are always represented by central differences.

It is convenient to define a total flux for each face of the control volume as the sum of a convective flux and a diffusive flux such that

$$F_e - F_w + F_n - F_s + F_b - F_f = S_u + S_p\phi_p \qquad \text{(A1.5)}$$

where

$$\begin{aligned}
F_e &= C_E\phi_e - D_E\,(\phi_E - \phi_P)\\
F_w &= C_W\phi_w - D_W\,(\phi_P - \phi_W)\\
F_n &= C_N\phi_n - D_N\,(\phi_N - \phi_P)\\
F_s &= C_S\phi_s - D_S\,(\phi_P - \phi_S)\\
F_b &= C_B\phi_b - D_B\,(\phi_B - \phi_P)\\
F_f &= C_F\phi_f - D_F\,(\phi_P - \phi_F) \qquad \text{(A1.6)}
\end{aligned}$$

In the following section, the skew differencing procedure will be used to calculate the values of the dependent variables at the faces of the control volume. As a result, Eq. (A1.5) will include not only the values of ϕ at the "normal," or main, grid node locations (E, W, N, S, B, F and P) but also at the corner locations. The finite-difference

form for Eq. (A1.5) is then

$$A_P\phi_P = A_E\phi_E + A_W\phi_W + A_N\phi_N + A_S\phi_S + A_B\phi_B + A_F\phi_F + A_{NE}\phi_{NE}$$
$$+ A_{SE}\phi_{SE} + A_{NW}\phi_{NW} + A_{SW}\phi_{SW} + A_{BNE}\phi_{BNE} + A_{BSE}\phi_{BSE}$$
$$+ A_{BNW}\phi_{BNW} + A_{BSW}\phi_{BSW} + A_{BN}\phi_{BN} + A_{BS}\phi_{BS} + A_{BE}\phi_{BE}$$
$$+ A_{BW}\phi_{BW} + A_{FNE}\phi_{FNE} + A_{FSE}\phi_{FSE} + A_{FNW}\phi_{FNW} + A_{FSW}\phi_{FSW}$$
$$+ A_{FN}\phi_{FN} + A_{FS}\phi_{FS} + A_{FE}\phi_{FE} + A_{FW}\phi_{FW} + S_u + S_P\phi_P \qquad \text{(A1.7)}$$

A.2 - Calculation of the Fluxes

Recall that the equations of motion, Eqs. (A1.1), can be written in terms of fluxes to each face of the control volume, Eq. (A1.5). In this section, a procedure will be described to calculate fluxes, F_e, F_w, F_n, F_b and F_f. The derivation of F_w, the flux to the west face, of a typical scalar control volume is given in detail. The derivation of the other fluxes and of the fluxes of the u, v, and w velocity components are outlined.

Consider the control volume used to determine the value of a scalar variable at the point P. A portion of this control volume is shown in Fig. A-5 for the case in which the u and v components of velocity are non-negative and the w component is negative. For all velocity vectors located at the center of the west face of the control volume (point w), the flux to the west face is given by:

$$F_w = C_W\phi_w - D_W (\phi_P - \phi_W) \tag{A2.1}$$

Furthermore, for central-differencing (CD), the value of the dependent variable at the west face, ϕ_w, is always given by linear interpolation between ϕ at the W and P grid nodes:

$$\phi_w = (1 - \alpha_w) \phi_W + \alpha_w\phi_P \tag{A2.2}$$

where the interpolating factor is

$$\alpha_w = \frac{X_w - X_W}{X_P - X_W} \tag{A2.3}$$

In the 3D-TEACH computer program, $\alpha = 0.5$ for each face of the control volume for each scalar variable since the control volume faces are located midway between scalar grid nodes. For the axial, radial and lateral velocity components, however, the α for each face may assume other values. The central difference form of the flux at the west face is then:

$$\frac{F_{w_{CD}}}{D_W} = \left[P_{e_w} (1 - \alpha_w) + 1 \right] \phi_W + (\alpha_w P_{e_w} - 1) \phi_P \tag{A2.4}$$

where the Peclet number at this face is given by:

$$P_{e_w} = C_W/D_W \tag{A2.5}$$

The central difference form of the flux at all faces of the control volume for point P are presented in Table A-1.

The upwind difference (UD) form for the flux at the west face is defined by:

$$\frac{F_{w_{UD}}}{D_W} = P_{e_w}\phi_W \tag{A2.6}$$

for a non-negative value of axial component of velocity, u_w, and

$$\frac{F_{w_{UD}}}{D_W} = P_{e_w}\phi_P \tag{A2.7}$$

for a negative value of u_w. Essentially, the upwind differences are derived from the central difference by setting α_w equal to zero or unity, respectively, and by neglecting diffusion.

It is convenient to define the velocity switches

$$\sigma^u = \tfrac{1}{2}\left(1 + \frac{u}{|u|}\right)$$

$$\sigma^v = \tfrac{1}{2}\left(1 + \frac{v}{|v|}\right)$$

$$\sigma^w = \tfrac{1}{2}\left(1 + \frac{w}{|w|}\right) \tag{A2.8}$$

for the axial, radial, and lateral velocity components and to adopt the convention that the value of a switch is unity if the velocity component is non-negative and it is zero otherwise. Then, the upwind difference form of the flux at the west face of the control voluem is:

$$\frac{F_{w_{UD}}}{D_W} = P_{e_w}\left[\sigma_w^u\,\phi_W + (1 - \sigma_w^u)\,\phi_P\right] \tag{A2.9}$$

The upwind difference forms at all of the faces are summarized in Table A-2.

Equation (A2.1) is also the starting point for developing the flux equations for the skew-upwind differencing (SUD) procedure. The value of ϕ at the west face of

the control volume, ϕ_w, is determined by extrapolating the velocity vector upstream of the face. For the case shown in Fig. A-5, this point lies in the plane formed by the nodes W, SW, BW and BSW. The value of w''' is determined by linear interpolation. First, the projection of the velocity vector in the x-y plane is extrapolated upstream to the point w' which lies along the grid line between the nodes W and SW. The interpolation factor k_1 is defined by:

$$k_1 = \frac{(w'W)}{\Delta y} = \frac{1}{2} \frac{\Delta x}{\Delta y} \left| \frac{V_w}{U_w} \right| \tag{A2.10}$$

where (w'W) is the distance between point w' and the node W and Δy is the distance between nodes W and SW. Then,

$$\begin{aligned} \phi_{w'} &= k_1 (\phi_{SW} - \phi_W) + \phi_W \\ &= k_1 \phi_{SW} + (1 - k_1) \phi_W \end{aligned} \tag{A2.11}$$

For very large flow angles (skewing) relative to the co-ordinate directions, k_1 will exceed unity and w' will be defined in terms of ϕ at the SW and S nodes; however; it is known that for two-dimensional flows this approach can yield negative coefficients at corner nodes which can in turn produce oscillations in the solution; it is assumed that the same situation will prevail for three-dimensional flows. To assure that the coefficients for the corner nodes are non-negative, then:

$$k_1 = \min \left(1, \frac{1}{2} \left| \frac{V_w}{U_w} \right| \frac{\Delta x}{\Delta y} \right) \tag{A2.12}$$

The use of absolute values in Eq. (A2.12) permits this equation to be used to define k_1 for all velocity components at the west face. Similarly, the value of ϕ at the point w'' along the gridline connecting nodes BW and BSW is given by:

$$\phi_{w''} = k_1 \phi_{BSW} + (1 - k_1) \phi_{BW} \tag{A2.13}$$

where the same interpolation factor is used as in Eq. (A2.11). The value of ϕ at the point w''' is obtained by linear interpolation between $\phi_{w'}$ and $\phi_{w''}$. The interpolation factor is obtained by extrapolating the projection of the velocity vector in the x-z plane to the point 3 along the gridline connecting nodes W and BW:

$$\phi_{w'''}^{++-} = k_3 \, \phi_{w''} + (1 - k_3) \, \phi_{w'} \tag{A2.14}$$

with

$$k_3 = \min \left(1, \tfrac{1}{2} \, \frac{\Delta x}{\Delta z} \left| \frac{W_w}{U_w} \right| \right) \tag{A2.15}$$

The superscript ++- indicates $U_w \geq 0$, $V_w \geq 0$, $W_w < 0$.

Consequently,

$$\phi_{w'''}^{++-} = k_3 \left[k_1 \, \phi_{BSW} + (1 - k_1) \, \phi_{BW} \right] + (1 - k_3) \left[k_1 \, \phi_{SW} + (1 - k_1) \, \phi_{W} \right] \tag{A2.16}$$

For two-dimensional flow, $k_3 = 0$ and it can be seen that Eq. (A2.16) has the correct limiting value.

Equation (A2.16) was derived for the case of $U_w \geq 0$, $V_w \geq 0$, $W_w < 0$. For the case of $U_w \geq 0$, $V_w \geq 0$ and $W_w \geq 0$, the appropriate equation can be derived by rotating the velocity vector into the positive z direction and (referring to Fig. A-1) replacing the subscripts BSW by FSW and BW by FW. As a result, one obtains:

$$\phi_{w'''}^{+++} = k_3 \left[k_1 \, \phi_{FSW} + (1 - k_1) \, \phi_{FW} \right] + (1 - k_3) \left[k_1 \, \phi_{SW} + (1 - k_1) \, \phi_{W} \right] \tag{A2.17}$$

Then, for $U_w \geq 0$, $V_w \geq 0$, and <u>all</u> W_w

$$\phi_{w'''}^{++} = \sigma_w^w \, \phi_{w'''} \left[\text{Eq. (A2.17)} \right] + (1 - \sigma_w^w) \, \phi_{w'''} \left[\text{Eq. (A2.16)} \right] \tag{A2.18}$$

or

$$\phi_{w'''}^{++} = \sigma_w^w \, k_3 \left[k_1 \, \phi_{FSW} + (1 - k_1) \, \phi_{FW} \right] + (1 - \sigma_w^w) \, k_3 \left[k_1 \, \phi_{BSW} + (1 - k_1) \, \phi_{BW} \right] + (1 - k_3) \left[k_1 \, \phi_{SW} + (1 - k_1) \, \phi_{W} \right] \tag{A2.19}$$

where the superscript ++ indicate that U_w and V_w are both non-negative.

A similar expression can be derived from Eq. (A2.19) for the case $U_w \geq 0$, $V_w < 0$, and all W_w by replacing the subscripts FSW by FNW, BSW by BNW, and SW by NW to obtain

$$\phi_{w'''}^{+-} = \sigma_w^w k_3 [k_1 \phi_{FNW} + (1 - k_1) \phi_{FW}]$$
$$+ (1 - \sigma_w^w) k_3 [k_1 \phi_{BNW} + (1 - k_1) \phi_{BW}]$$
$$+ (1 - k_3) [k_1 \phi_{NW} + (1 - k_1) \phi_W] \qquad \text{(A2.20)}$$

Then, one can combine Eqs. (A2.19) and (A2.20) to obtain an expression for $\phi_{w'''}$ for $U_w \geq 0$, all V_w, all W_w from:

$$\phi_{w'''}^{+} = \sigma_w^v \phi_{w'''}^{++} + (1 - \sigma_w^v) \phi_{w'''}^{+-} \qquad \text{(A2.21)}$$

For the case in which $U_w < 0$, $V_w \geq 0$, and all W_w, an expression for $\phi_{w'''}^{-+}$ can be obtained from Eq. A(2.19) by replacing the subscripts as follows

FSW becomes FS

FW becomes F

W becomes P

SW becomes S

BW becomes B

BSW becomes BS

Hence

$$\phi_{w'''}^{-+} = \sigma_w^w k_3 [k_1 \phi_{FS} + (1 - k_1) \phi_F]$$
$$+ (1 - \sigma_w^w) k_3 [k_1 \phi_{BS} + (1 - k_1) \phi_B]$$
$$+ (1 - k_3) [k_1 \phi_S + (1 - k_1) \phi_P] \qquad \text{(A2.22)}$$

Finally, for the case of $U_w < 0$, $V_w < 0$ and all W_w, an expression for $\phi_{w'''}^{--}$ can be obtained from Eq. (A2.20) by replacing the subscripts as follows:

FNW becomes FN

FW becomes F

BNW becomes BN

BW becomes B

NW becomes N

W becomes P

Hence

$$\phi_{w'''}^{--} = \sigma_w^w \, k_3 \, [\, k_1 \, \phi_{FN} + (1 - k_1) \, \phi_F \,]$$

$$+ (1 - \sigma_w^w) \, k_3 \, [\, k_1 \, \phi_{BN} + (1 - k_1) \, \phi_B \,]$$

$$+ (1 - k_3) \, [\, k_1 \, \phi_N + (1 - k_1) \, \phi_P \,] \qquad \text{(A2.23)}$$

Then for $U_w \leq 0$, all V_w and all W_w

$$\phi_{w'''}^{-} = \sigma_w^v \, \phi_{w'''}^{-+} + (1 - \sigma^v) \, \phi_{w'''}^{--} \qquad \text{(A2.24)}$$

and for all U_w, all V_w and all W_w:

$$\phi_{w'''} = \sigma_w^u \, \phi_{w'''}^{+} + (1 - \sigma_w^u) \, \phi_{w'''}^{-} \qquad \text{(A2.25)}$$

In analogous fashion, interpolated values for ϕ at the other faces of the control volume can be derived. Equations for $\phi_{e'''}$, $\phi_{n'''}$, and $\phi_{b'''}$ can be derived immediately from the expressions for $\phi_{w'''}$, $\phi_{s'''}$, and $\phi_{f'''}$, respectively, by shifting nodal subscripts in each case in the positive co-ordinate direction (i.e., toward the opposite face of the control volume). Tables A-4 through A-9 present the equations corresponding to Eqs. (A2.19) through (A2.25) for each of the faces.

Since the grid is not uniform, the geometric parameters Δx, Δy, Δz, used in the calculation of k_1 and k_3 differ for each face of the control volume and for each orientation of the velocity vector at each face. A summary of the geometric parameters is presented in Table A-3. Only the definitions for the parameters used for the east, north and back faces are shown in Table A-3. Since the fluxes at only these faces are actually computed as indicated in the next section; the flux at the west face for the control volume at node (I, J, K) is the flux at the east face of node (I-1, J, K), etc.

In his original development of the skew upwind differencing procedure for two-dimensional flow, Raithby(Ref. A-1)assumed that the value of the dependent variable at (say) the west face of the control volume is equal to the interpolated value. In the present development, this is equivalent to assuming that $\phi_w = \phi_{w'''}$ so that--using Eq. (A1.6) and the definition of Peclet number--

$$\frac{F_{w_{SUD}}}{D_W} = P_{e_w}\,\phi_{w'''} - D_W\,(\phi_P - \phi_W) \tag{A2.26}$$

It is desirable to use the central-difference procedure for small values of the grid Peclet number and the skew upwind differencing method for large values of the grid Peclet number. It is also desirable that these two formulations produce a continuous transition at the transition Peclet number which in the case of $U_w \geq 0$ at the west face of the control volume becomes:

$$P^*_{e_w} = \frac{1}{\alpha_w} \tag{A2.27}$$

For the scalar grid system used in the 2D-TEACH computer program, $P_e^* = 2$. At the transition Peclet number, the central difference result using (Eq. A2.4) is:

$$\frac{F_{w_{CD}}}{D_W} = \frac{\phi_W}{\alpha_w} \tag{A2.28}$$

while the skew upwind differencing method (Eq. (A2.26)) yields:

$$\frac{F_{w_{SUD}}}{D_W} = \frac{\phi_{w'''}}{\alpha_w} - (\phi_P - \phi_W) \tag{A2.29}$$

From Eqs. (A2.18) through (A2.25), it is clear that these two results are not equal. (Note: At present, $\phi_{w'''} = \phi_w^{++}$.)

The fluxes at the transition Peclet number can be made equal by noting (contrary to the assumption made by Raithby) that ϕ_w and $\phi_{w'''}$ are related by:

$$\phi_{w'''} = \phi_w - \left(\frac{\partial \phi}{\partial s}\right)_w \Delta s + \ldots \tag{A2.30}$$

so that Eq. (A2.26) becomes

$$\frac{F_{w_{SUD}}}{D_W} = P_{e_w}\phi_w - P_{e_w}\left(\frac{\partial\phi}{\partial s}\right)_w \Delta s - (\phi_P - \phi_W) \tag{A2.31}$$

where Δs is defined in Fig. A-5. Writing the central differencing result in terms of the flux definition, Eq. A2.1, then:

$$\frac{F_{w_{CD}}}{D_W} = P_{e_w}\phi_w - (\phi_P - \phi_W) \tag{A2.32}$$

Clearly, these two fluxes will be equal at the transition Peclet number if a correction $P^*_{e_w}\left(\frac{\partial\phi}{\partial s}\right)_w \Delta s$ is added to the skew upwind differencing flux, Eq. (A2.26), to obtain:

$$\frac{F_{w_{SUD}}}{D_W} = P_{e_w}\phi_w''' + P^*_{e_w}\left(\frac{\partial\phi}{\partial s}\right)_w \Delta s - (\phi_P - \phi_W) \tag{A2.33}$$

The derivative $(\partial\phi/\partial s)_w$ can be computed by

$$\frac{\partial\phi}{\partial s} = \frac{\phi_w - \phi_w'''}{\Delta s} \tag{A2.34}$$

To provide a continuous variation in flux at the transition Peclet number, the derivative in Eq. (A2.34) is approximated further as:

$$\frac{\partial\phi}{\partial s} = \frac{(\phi_w)_{CD} - \phi_w'''}{\Delta s} \tag{A2.35}$$

where $(\phi_w)_{CD}$ is given by Eq. (A2.2). Then, after using Eqs. (A2.2) and (A2.35) and some rearrangement, Eq. (A2.23) becomes:

$$\frac{F_{w_{SUD}}}{D_W} = (P_{e_w} - P^*_{e_w})\,\phi_w''' + [\,P_e^*\,(1 - \alpha_w) + 1\,]\,\phi_W + (\alpha_w P^*_{e_w} - 1)\,\phi_P \tag{A2.36}$$

This last result is valid for all U_w, V_w, W_w (i.e., for all ϕ_w''') provided that the transition Peclet number is given by:

$$P^*_{e_w} = \frac{1}{\sigma^u_w - (1 - \alpha_w)} \tag{A2.37}$$

At the transition Peclet number, the flux given by both central differencing and skew upwind differencing are:

$$\underline{U_w \geq 0} \qquad \frac{F_w}{D_W} = \frac{\phi_W}{\alpha_w} \tag{A2.38}$$

$$\underline{U_w < 0} \qquad \frac{F_w}{D_W} = \frac{\phi_P}{\alpha_w - 1} \tag{A2.39}$$

Results similar to Eqs. (A2.36) and (A2.37) for all faces of the control volume are summarized in Table A-10.

In the hybrid differencing procedure, the more accurate central differencing formulation (see Table A-1) is used when the Peclet number is less than the transition value while the less accurate, but stable, upwind differencing result (see Table A-2) is used when the Peclet number is greater than the transition value. In the development of the equations for two-dimensional flow, it was believed at first that a similar hybrid differencing method could be formulated using central differencing for $P_e < P_e^*$ and skew-upwind differencing for $P_e > P_e^*$. However, this approach proved to be unworkable since some of the coefficients derived from this hybrid formulation could be negative. As an alternative, a flux blending scheme was used in which a weighted average of the upwind differencing fluxes is used. The weighting (blending) factor, γ, was chosen to assure boundedness (i.e., all co-efficients of the difference equations are non-negative). It is assumed that a similar flux blending procedure can be utilized for the three-dimensional case. The Bounded Skew-Upwind Differencing (BSUD) scheme is defined by

$$F_{\Pi_{BSUD}} = \gamma_\Pi F_{\Pi_{SUD}} + (1 - \gamma_\Pi) F_{\Pi_{UD}} \tag{A2.40}$$

where Π represents one of the six faces of the control volume. The weighting factor γ_Π is restricted to the range $0 \leq \gamma_\Pi \leq 1$ and is calculated as described in Section A.5.

A.3 - Calculation of the Co-efficients for the Finite-Difference Form of the Equations of Motion

The finite-difference form of the equations of motion (e.g., Eq. (A1.7)), can be derived directly from the flux information presented in Tables A-1, A-2, A-4 through A-10 and Eq. (A2.40). The resulting expressions will contain the unknown blending factor, γ. The blending strategy requires that the terms in the equations for the coefficients responsible for producing negative co-efficients be isolated so that appropriate values for γ can be determined. Furthermore, the coefficients for the control volumes adjacent to the physical boundaries of the flow may require modification to incorporate the effect of the boundary conditions. Thus, to simplify manipulation and modification, some additional notation will be defined.

Let the center of the control volume (point P) be located at the Ith axial position, Jth radial position, and Kth lateral position. The flux contributions (the components of the total flux) to the east face are denoted as E1(I,J,K), E2(I,J,K), E3(I,J,K,L); the flux contributions to the north face are denoted as N1(I,J,K), N2(I,J,K), N3(I,J,K,L), and the flux contributions at the back face are denoted as B1(I,J,K), B2(I,J,K), B3(I,J,K,L) where L = 1,2,3,4 as indicated below. The flux contributions are defined as follows:

Central Differencing

$$E1(I,J,K) = D_E - \alpha_e C_E$$
$$E2(I,J,K) = E1(I,J,K) + C_E$$
$$E3(I,J,K,L) = 0 \qquad L = 1,2,3,4 \tag{A3.1}$$

$$N1(I,J,K) = D_N - \alpha_n C_N$$
$$N2(I,J,K) = N1(I,J,K) + C_N$$
$$N3(I,J,K,L) = 0 \qquad L = 1,2,3,4 \tag{A3.2}$$

$$B1(I,J,K) = D_B - \alpha_b C_B$$
$$B2(I,J,K) = B1(I,J,K) + C_B$$
$$B3(I,J,K,L) = 0 \qquad L = 1,2,3,4 \tag{A3.3}$$

Bounded Skew-Upwind Differencing

$$E1(I,J,K) = (\sigma_e^u - 1)\, C_E$$
$$E2(I,J,K) = E1(I,J,K) + C_E$$
$$E3(I,J,K,1) = D_E(Pe_e - Pe_e^*)(k_3 k_1)_e$$
$$E3(I,J,K,2) = D_E(Pe_e - Pe_e^*)\,[\, k_3\,(1 - k_1)\,]_e$$
$$E3(I,J,K,3) = D_E(Pe_e - Pe_e^*)\,[\,(1 - k_3)\,k_1\,]_e$$
$$E3(I,J,K,4) = D_E(Pe_e - Pe_e^*)\,[\,(1 - k_3)\,(1 - k_1) - 1\,]_e \qquad \text{(A3.4)}$$

$$N1(I,J,K) = (\sigma_n^v - 1)\, C_N$$
$$N2(I,J,K) = N1(I,J,K) + C_N$$
$$N3(I,J,K,1) = D_N(Pe_n - Pe_n^*)\,(k_3 k_1)_n$$
$$N3(I,J,K,2) = D_N(Pe_n - Pe_n^*)\,[\, k_3\,(1 - k_1)\,]_n$$
$$N3(I,J,K,3) = D_N(Pe_n - Pe_n^*)\,[\,(1 - k_3)\,k_1\,]_n$$
$$N3(I,J,K,4) = D_N(Pe_n - Pe_n^*)\,[\,(1 - k_3)\,(1 - k_1) - 1\,]_n \qquad \text{(A3.5)}$$

$$B1(I,J,K) = (\sigma_b^w - 1)\, C_B$$
$$B2(I,J,K) = B1(I,J,K) + C_B$$
$$B3(I,J,K,1) = D_B(Pe_b - Pe_b^*)\,(k_3 k_1)_b$$
$$B3(I,J,K,2) = D_B(Pe_b - Pe_b^*)\,[\, k_3\,(1 - k_1)\,]_b$$
$$B3(I,J,K,3) = D_B(Pe_b - Pe_b^*)\,[\,(1 - k_3)\,k_1\,]_b$$
$$B3(I,J,K,4) = D_B(Pe_b - Pe_b^*)\,[\,(1 - k_3)\,(1 - k_1) - 1\,]_b \qquad \text{(A3.6)}$$

The use of central vs. bounded skew-upwind differencing is determined by the value of the Peclet number at each face. The parameters, C_E, D_E, α_e, k_1, . . . are local values; the subscripts (I,J,K) have been omitted in the interest of readability. The corresponding flux contributions at the west face are given immediately by E1(I-1,J,K), E2(I-1,J,K), . . ., the flux contributions at the south face are N1(I,J-1,K), N2(I,J-1,K) . . ., and the flux contributions at the front face are B1(I,J,K-1), B2(I,J,K-1), . . .

The coefficients of the finite-difference form of the equations of motion may then be defined in terms of these flux contributions. The results are presented in Table A-11. The notation used in Table A-11 can be explained by examining, for example, the second term, exclusive of the blending factor, in the equation for A_B at the node (I,J,K): $[\ \sigma_e^u\ (1 - \sigma_e^w)\ E3\ ]\ (I,J,K,2)$. The subscripts I,J,K indicate the node at which σ_e^u, σ_e^w, and E3 are evaluated; the fourth subscript refers to the flux contribution E3(I,J,K,L) with L equal to 2--see Eq. (A3.1) or Eq. (A3.4).

For the two-dimensional case, it is relatively easy to demonstrate that A_p is equal to the sum of the other eight co-efficients when use is made of the mass continuity equation. It is assumed in the three-dimensional case that A_p is now equal to the sum of the other 26 co-efficients in Table A-11 when use is made of the mass continuity equation:

$$C_E - C_W + C_N - C_S + C_B - C_F = 0 \qquad \text{(A3.7)}$$

The boundary conditions (Section A.4) and the blending scheme (Section A.5) can be applied directly to the flux contributions so that the results shown in Table A-11 are general.

A.4 - Boundary Conditions

The boundary conditions are applied to the flux contributions as defined by Eqs. (A3.1) through (A3.6) so that the set of coefficients (e.g., Table A-11) for each dependent variable is the same throughout the computational domain. This consistency simplifies the application of both (1) the algorithm for solving the set of simultaneous equations for each variable and (2) the bounding procedure (see Section A.5).

Scalars

It will be recalled that the axial velocities are stored midway between the scalar gridlines in the axial direction; therefore, the axial velocities are stored at the midpoint of the east and west faces of the scalar control volumes. Similarly the radial velocities are stored at the midpoint of the north and south faces of the scalar control volumes and the lateral velocities are stored at the midpoint of the front and back faces of the scalar control volumes.

Physical boundaries are located midway between scalar gridlines in the appropriate direction. In the following discussion, the boundary conditions are applied to the various faces of the control volume for an interior node (I,J,K) to produce modified east-west flux contributions (E1, E2, E3), north-south flux contributions (N1, N2, N3), or back-front flux contributions (B1, B2, B3) for use in calculating the co-efficients of the finite-difference equations for the scalars (e.g., Table A-11).

There are five types of boundary conditions to be considered; these types are:

(1) specified wall,
(2) axis of symmetry, planes of symmetry,
(3) unspecified opening,
(4) specified inlet, and
(5) periodicity.

The application of these boundary conditions to modify the flux contributions used to determine the finite-difference coefficients for a node (I,J,K) having a physical boundary on the west face of its control volume will be described in detail. The modifications to the co-efficients due to the other physical boundaries are similar and will be summarized.

a) West Face

For a specified wall, the value of the scalar at the wall may be either known (e.g., turbulence kinetic energy = 0) or unknown (e.g., turbulence dissipation). Since the

variation of the scalar from its wall value to the value at the node (I,J) is (generally) non-linear, it is prudent in every case to decouple the wall values from the system of equations. The influence of the wall can be reflected by using appropriate wall functions to compute the source terms for the scalars. From Table A-11, it can be seen that the (known or unknown) wall values of the scalar can be excluded if the co-efficients A_{BNW}, A_{BSW}, A_{BW}, A_{FNW}, A_{FSW}, A_{FW}, A_{NW}, A_{W} and A_{SW} are set to zero. These coeffiicents will vanish if the following flux contributions are set accordingly:

$$\begin{aligned} &E2(I-1,J,K) = 0 \\ &E3(I-1,J,K,L) = 0 \qquad L = 1,2,3,4 \\ &\left.\begin{aligned} &N3(I,J,K,L) = 0 \\ &N3(I,J-1,K,L) = 0 \\ &B3(I,J,K,L) = 0 \\ &B3(I,J,K-1,L) = 0 \end{aligned}\right\} \quad L = 1,2 \end{aligned} \tag{A4.1}$$

If the west face of the control volume for the node (I,J,K) is a plane of symmetry, then the flux normal to this face is zero. By definition, the unknown values of the scalar at the nodes (I-1,J,K) and (I,J,K) are equal; the gradient of the scalar normal to the axis vanishes there. Thus, an axis of symmetry is mathematically identical to a specified wall boundary condition with zero gradient (source) at the wall. The modifications to the flux contributions are given by Eq. (A4.1).

For an unspecified opening, it is assumed that (1) the flow is exiting through the opening, (2) the streamlines are parallel in the vicinity of the opening, and (3) the cell Peclet number exceeds the transition value. By the third assumption, the skew differencing formulae, Eqs. (A3.4) through (A3.6) are used but by the second assumption the flux contributions E3, N3 and B3 used in the calculation of the nine co-efficients are zero. By the first assumption, the flow direction switch σ_e^u at the node (I-1,J,K) is zero so that E2(I-1,J,K) is zero. As a result, the conditions in Eq. (A4.1) are satisfied and all nine coefficients are zero. Thus, the unknown values of the scalars at the unspecified opening are decoupled from the system of equations.

It is seen that the modifications to the flux contributions for the specified wall, axis of symmetry, and unspecified opening boundary condition are identical.

For a specified opening, the value of the scalar is known at the west face of the control volume for the node (I,J,K) since, as noted above, the physical boundary in this case is located at the west face of the scalar control volume. In general, the cell Peclet number is greater than the transition value whenever the boundary represents a specified opening. Therefore, the flux contributions E1, E2 and E3 at the node (I-1,J,K) are computed using the skew upwind differencing formulae, Eq. (A3.4). However, since the boundary is coincident with the west face of the control volume for the node (I,J,K), there is no skewing of the flow at this face and, therefore, all E3 at (I-1,J,K) are set to zero.

The determination of the co-efficients for the node (I,J,K) in this case also requires the computation of north, south, back and front contributions. Since the specified opening is coincident with the west face of the control volume for the node (I,J,K) and since this face is located midway between the nodes (I-1,J,K) and (I,J,K), it is necessary to double the value of the skewing interpolation factors used in calculating these flux contributions. Thus, for the specified opening:

$$
\begin{aligned}
&E3(I-1,J,K,L) = 0 \qquad L = 1,2,3,4 \\
&(K_3)_n = \min\left[\, 1,\ 2(K_3)_n \,\right] \\
&(K_3)_s = \min\left[\, 1,\ 2(K_3)_s \,\right] \\
&(K_3)_b = \min\left[\, 1,\ 2(K_3)_b \,\right] \\
&(K_3)_f = \min\left[\, 1,\ 2(K_3)_f \,\right]
\end{aligned}
\qquad \text{(A4.2)}
$$

The analysis of the modifications to the flux contributions for a physical boundary at other faces of the control volume is similar and the results are summarized as follows.

b) East Face

(1) For a specified wall, axis of symmetry, or unspecified opening:

$$
\begin{aligned}
&E1(I,J,K) = 0 \\
&E3(I,J,K,L) = 0 \qquad L = 1,2,3,4 \\
&\left.\begin{aligned}
&N3(I,J,K,L) = 0 \\
&N3(I,J-1,K,L) = 0 \\
&B3(I,J,K,L) = 0 \\
&B3(I,J,K-1,L) = 0
\end{aligned}\right\} \quad L = 1,2
\end{aligned}
\qquad \text{(A4.3)}
$$

(2) For a specified opening:

$$E3(I,J,K,L) = 0 \qquad L = 1,2,3,4$$
$$(K_3)_n = \min [\ 1,\ 2(K_3)_n\ ]$$
$$(K_3)_s = \min [\ 1,\ 2(K_3)_s\ ]$$
$$(K_3)_b = \min [\ 1,\ 2(K_3)_b\ ]$$
$$(K_3)_f = \min [\ 1,\ 2(K_3)_f\ ] \qquad \text{(A4.4)}$$

c) South Face

(1) For a specified wall, axis of symmetry, or unspecified opening:

$$N2(I,J-1,K) = 0$$
$$N3(I,J-1,K,L) = 0 \qquad L = 1,2,3,4$$
$$\left.\begin{aligned} &E3(I,J,K,L) = 0 \\ &E3(I-1,J,K,L) = 0 \\ &B3(I,J,K,L) = 0 \\ &B3(I,J,K-1,L) = 0 \end{aligned}\right\} \quad L = 1,3 \qquad \text{(A4.5)}$$

(2) For a specified opening:

$$N3(I,J-1,K,L) = 0 \qquad L = 1,2,3,4$$
$$(K_1)_e = \min [\ 1,\ 2(K_1)_e\ ]$$
$$(K_1)_w = \min [\ 1,\ 2(K_1)_w\ ]$$
$$(K_1)_b = \min [\ 1,\ 2(K_1)_b\ ]$$
$$(K_1)_f = \min [\ 1,\ 2(K_1)_f\ ] \qquad \text{(A4.6)}$$

d) North Face

(1) For a specified wall, axis of symmetry, or unspecified opening:

$$N1(I,J,K) = 0$$
$$N3(I,J,K,L) = 0 \qquad L = 1,2,3,4$$
$$\left.\begin{aligned} &E3(I,J,K,L) = 0 \\ &E3(I-1,J,K,L) = 0 \\ &B3(I,J,K,L) = 0 \\ &B3(I,J,K-1,L) = 0 \end{aligned}\right\} \quad L = 1,3 \qquad \text{(A4.7)}$$

(2) For a specified opening:

$$N3(I,J,K,L) = 0 \qquad L = 1,2,3,4$$
$$(K_1)_e = \min [\ 1,\ 2(K_1)_e\ ]$$
$$(K_1)_w = \min [\ 1,\ 2(K_1)_w\ ]$$
$$(K_1)_b = \min [\ 1,\ 2(K_1)_b\ ]$$
$$(K_1)_f = \min [\ 1,\ 2(K_1)_f\ ] \qquad \text{(A4.8)}$$

e) Front Face

(1) For a specified wall, axis of symmetry, or unspecified opening:

$$B2(I,J,K-1) =)$$
$$B3(I,J,K-1,L) = 0. \qquad L = 1,2,3,4$$
$$\left.\begin{aligned} E3(I,J,K,L) &= 0 \\ E3(I-1,J,K,L) &= 0 \end{aligned}\right\} \quad L = 1,2$$
$$\left.\begin{aligned} N3(I,J,K,L) &= 0 \\ N3(I,J-1,K,L) &= 0 \end{aligned}\right\} \quad L = 1,3 \qquad \text{(A4.9)}$$

(2) For a specified opening:

$$B3(I,J,K-1,L) = 0 \qquad L = 1,2,3,4$$
$$(K_3)_e = \min [\ 1,\ 2(K_3)_e\ ]$$
$$(K_3)_w = \min [\ 1,\ 2(K_3)_w\ ]$$
$$(K_1)_n = \min [\ 1,\ 2(K_1)_n\ ]$$
$$(K_1)_s = \min [\ 1,\ 2(K_1)_s\ ] \qquad \text{(A4.10)}$$

f) Back Face

(1) For a specified wall, axis of symmetry, or unspecified opening:

$$B1(I,J,K) = 0$$
$$B3(I,J,K,L) = 0 \qquad L = 1,2,3,4$$
$$\left.\begin{aligned} E3(I,J,K,L) &= 0 \\ E3(I-1,J,K,L) &= 0 \end{aligned}\right\} \quad L = 1,2$$
$$\left.\begin{aligned} N3(I,J,K,L) &= 0 \\ N3(I,J-1,K,L) &= 0 \end{aligned}\right\} \quad L = 1,3 \qquad \text{(A4.11)}$$

(2) For a specified opening:

$$B3(I,J,K,L) = 0 \qquad L = 1,2,3,4$$

$$(K_3)_e = \min [\ 1,\ 2(K_3)_e\ ]$$

$$(K_3)_w = \min [\ 1,\ 2(K_3)_w\ ]$$

$$(K_1)_n = \min [\ 1,\ 2(K_1)_n\ ]$$

$$(K_1)_s = \min [\ 1,\ 2(K_1)_s\ ] \qquad \text{(A4.12)}$$

Axial Velocity

The east and west faces of the axial velocity control volumes are co-incident with the vertical scalar gridlines. The axial storage locations of physical boundaries are the same as the axial locations of the axial velocities; the inverse is, of course, not true. The radial and lateral locations of the u velocity and scalar control volumes are identical.

a) West Face

Assume that a physical boundary is located to the west of the axial velocity control volume. If the physical boundary represents either a specified wall or an axis of symmetry, then the axial velocity at this face is zero; if it represents a specified opening, then the axial velocity is a known, specified value. If the physical boundary represents an unspecified opening, then it is assumed that the axial velocity is known from the previous iteration. In every case, it is seen that the axial velocity is known at the west face of the axial velocity control volume. Therefore, the axial velocity at the west face of the control volume can be computed in the same manner as is used for any axial velocity interior node.

The radial and lateral velocities for the west face of the axial velocity control volume are interpolated in the same manner as they are for the west face of a scalar control volume since the radial and lateral grid line locations for the scalars and axial velocity are identical. Thus, one can obtain the values of u, v and w and the flux contributions can be computed using Eqs. (A3.1) through (A3.6) in the usual manner. Thus, it is seen, that the application of the boundary conditions requires no modification to the computation of the flux contributions.

b) East Face

A similar analysis leads to the conclusion that no modifications are made to the computation of the flux contributions.

c) South, North, Front and Back Faces

Since the radial and lateral positions are identical for both the axial velocity and scalars, the modifications of the flux contributions for these faces of the axial velocity control volume are the same as those required for the corresponding face of the scalar control volume.

Radial Velocity

The radial velocity control volumes have radial and lateral positions identical to those for the scalar control volumes.

a) South and North Faces

No modifications are necessary. (See discussion for west and east faces of axial velocity control volumes.)

b) West, East, Front and Back Faces

Use modifications for corresponding face of the scalar control volume.

Lateral Velocity

The lateral velocity control volumes have axial and radial positions identical to those for the scalar control volumes.

a) Front and Back Faces

No modifications are necessary. (See discussion for west and east faces of axial velocity control volumes.)

b) West, East, South and North Faces

Use modifications for corresponding face of scalar control volumes.

Special Treatment for Corner Regions

At a corner, it is necessary to compute the flux contributions as a weighted average of the fluxes in the vicinity of both a wall and a fluid boundary (unspecified opening or specified opening). The weighting is equal to the fraction of the face of the control volume adjacent to the solid boundary. Since this procedure is not peculiar to the bounded skew-upwind differencing procedure, but is part of the general procedures used for all finite-difference schemes in the TEACH computer program, it will not be described further.

A.5 - The Bounding Scheme

The calculation of the bounded skew-upwind differencing fluxes and, therefore, the determination of the coefficients to the finite-difference form of the equations of motion requires that the blending factor, γ, be determined. The blending factor specifies the relative proportions of the flux computed using skew and upwind differencing. For example, at the west face of the typical control volume, Eq. (A2.40) states:

$$F_{w_{BSUD}} = \gamma_w F_{w_{SUD}} + (1 - \gamma_w) F_{w_{UD}} \qquad (A5.1)$$

The co-efficients including the local blending factors are listed in Table A-11. The blending factors are limited to the range $0 \leq \gamma \leq 1$. Examination of the terms in each of the co-efficients in Table A-11 lead to the following general conclusions:

(1) For the principal co-efficients (those with a single subscript such as A_B, A_E, etc.), the term without a blending factor γ is unconditionally non-negative and the five terms containing blending factors are unconditionally non-positive.

(2) For the edge co-efficients (those with two subscripts such as A_{BE}, A_{NW}, etc.), two terms are unconditionally non-negative and two terms are unconditionally non-positive.

(3) The corner co-efficients (those with three subscripts such as A_{BSE}, A_{FSW}, etc.) are unconditionally non-negative.

Therefore, it is possible that some of the coefficients in Table A-11 will be negative.

It is desirable that all of the co-efficients of the finite-difference form of the equations of motion (Eq. (A1.7)) be non-negative for in this case the value of the dependent variable ϕ at the node P is simply a weighted average of the values of ϕ at the surrounding nodes exclusive of (the somewhat complicating) effects of local sources. A bounding scheme is a procedure to limit the values of the co-efficients of the finite-difference equations in such a manner as to produce this physically realistic result. Its principal computational advantage is to exclude under- and overshoots of the solution during the iterative procedure; these oscillations can produce severe numerical instability.

The bounding procedure used herein is based upon the following sequence:

(1) for each iteration, the solution for the distribution of the dependent variable ϕ is obtained using the blending factors γ determined during the previous iteration; the blending factors are set to unity for the first iteration;

(2) for each point P in the variable field, the maximum and minimum values for ϕ are determined from the 26 neighbors:

$$\phi_{max} = \max (\phi_k) \tag{A5.2}$$

$$\phi_{min} = \min (\phi_k) \tag{A5.3}$$

where ϕ_k is the value of ϕ at any of the 26 neighboring nodes and $k \neq P$.

It should be noted that the effects of sources are not included explicitly in calculating ϕ_{max} or ϕ_{min} since the explicit result is difficult to perform while avoiding double counting of the source effect. In any case, the results obtained will be no worse than to force the use of upwind differencing by making $\gamma = 0$. According to Professor A. D. Gosman, consultant to this project, the determination of ϕ_{max} and ϕ_{min} is an area for which further research is needed.

It should also be noted that one or more ϕ may be excluded from the determination of ϕ_{max} or ϕ_{min} when the control volume under consideration is adjacent to certain types of physical boundaries. For example, if the x-axis is an axis of symmetry, then ϕ_S is excluded since it is identical to ϕ_P and its use could yield an inappropriate range of permissible values.

(3) if $\phi_{min} < \phi_P < \phi_{max}$, then the local value of the blending factor is unaltered from its current value. However, if ϕ_P is outside of this range, then a new value of γ must be determined. For this purpose each of the co-efficients in Table A-11 is written in the form:

$$A_k = A_k' + \gamma A_k'', \quad k = N, S, NE, SE \ldots \tag{A5.4}$$

where it has been assumed that the blending factors for each of the faces of the local control volume are equal. Then Eq. (A1.7) can be written as:

$$\phi_P \left[\Sigma A_k' + \gamma \Sigma A_k'' \right] - S_P\phi_P = \Sigma A_k'\phi_k + \gamma \Sigma A_k''\phi_k + S_u \tag{A5.5}$$

Now, if $\phi_p < \phi_{min}$, then from this equation,

$$\gamma > \frac{\Sigma A'_k\phi_k - \phi_{min} \Sigma A'_k + S_u + S_p\phi_{min}}{\phi_{min} \Sigma A''_k - \Sigma A''_k\phi_k} \qquad \text{(A5.6)}$$

but if $\phi_p > \phi_{max}$, then

$$\gamma < \frac{\Sigma A'_k\phi_k - \phi_{max} \Sigma A'_k + S_u + S_p\phi_{max}}{\phi_{max} \Sigma A''_k - \Sigma A''_k\phi_k} \qquad \text{(A5.7)}$$

Of course, in practice the value of γ is determined by use of the appropriate equality for Eq. (A5.6) or Eq. (A5.7).

(4) In this fashion, the local value of $\gamma(I,J,K)$ is determined. The co-efficients in Table A-11 are then recomputed using the blending factors and the new distribution of ϕ is determined. For each face of the control volume at the point (I,J,K) there are two values of γ as determined for the two control volumes sharing the common face. Thus, a sufficient condition for assigning local values of the blending factors is given by:

$$\gamma_w = \min [\ \gamma(I-1,J,K),\ \gamma(I,J,K)\ ]$$

$$\gamma_e = \min [\ \gamma(I,J,K),\ \gamma(I+1,J,K)\ ]$$

$$\gamma_s = \min [\ \gamma(I,J-1,K),\ \gamma(I,J,K)\ ]$$

$$\gamma_n = \min [\ \gamma(I,J,K),\ \gamma(I,J+1,K)\ ]$$

$$\gamma_f = \min [\ \gamma(I,J,K-1),\ \gamma(I,J,K)\ ]$$

$$\gamma_b = \min [\ \gamma(I,J,K),\ \gamma(I,J,K+1)\ ] \qquad \text{(A5.7)}$$

This procedure for determining the blending factors effectively limits the value of the dependent variable range to values of its immediate neighbors. However, it is still possible that some of the main co-efficients will be negative. More restrictive schemes can be formulated that guarantee that all co-efficients of the finite-difference equations are non-negative but these procedures achieve this result by reducing the blending factor toward zero; the greater relative contribution of upwind differencing in this case produces larger amounts of numerical diffusion. Thus, the selection of a blending scheme represents a compromise between the undesirable effects of numerical instability and numerical diffusion.

The final blending factor field determines the ratio of the UDS solution present in the final solution. Since at present it is not possible to ensure that the blending factor field is unique for a given problem the solution generated by BSUDS2 is also not unique. Although it lies between UDS and SUDS. The reason for non-unique blending factor field is the following.

The calculation of blending factors depends on the value of the coefficients. These coefficients are calculated on the basis of the flow field that existed in the previous iteration. Hence the initial blending factor field strongly depends on the first guess. If, due to a bad guess, for example, at some nodes in the first iterations some of the factors are set to zero, the following iteration will produce a solution for those nodes which will be in inbounds. Hence the blending factors will never be increased from zero subsequently, and the final solution will be nearer to UDS. On the contrary a good first guess will not cause these factors to be set to zero at the final solution would be nearer to SUDS. In short if a bad guess forces the introduction of more than the minimum required numerical diffusion in the solution, there is no mechanism for diffusion to be taken out in the final stages of the solution. In the present code this adverse effect is minimized by under-relaxing the blending factor. But this practice can some times cause a minor problem. In some cases it is possible to obtain convergence with the solution being unbounded at some nodes. This problem can be completely avoided by checking for the undershoots and overshoots after convergence has been obtained. If an unbounded solution is detected iterations can be continued until a bounded solution is obtained. The above approach to achieving a unique solution from BSUDS2 is only one of a number of options that can be used. Another approach would be to update the blending factor at every iteration and not under-relax them at all.

APPENDIX A - REFERENCES

A-1 Raithby, G. D.: Skew Upwind Differencing for Problems Involving Fluid Flow, Computational Methods in Applied Mechanics and Engineering, Vol. 9, 1976, pp. 153-164.

Nomenclature

A	Coefficient in finite-difference equations (Eq. A1.7)
a	Flow area
B1,B2,B3	Flux contributions, back face of control volume
C	Convective flux
D	Diffusive flux
E1,E2,E3	Flux contributions, east face of control volume
F	Flux
I	Index for nodes - axial direction
J	Index for nodes - radial location
K	Index for nodes - lateral direction
k_1,k_3	Skewing interpolation factors
L	Flux contribution index for B3, E3 or N3
N1,N2,N3	Flux contributions, north face of control volume
Pe	Peclet number
r	Radial coordinate
S	Source
s	Distance along streamline (e.g., see Fig. A-5)
u	Axial velocity
v	Radial (or vertical) velocity
w	Lateral velocity
x	Axial co-ordinate
y	Vertical (or radial) co-ordinate
z	Lateral co-ordinate
α	Interpolation factor
Γ	Exchange co-efficient
γ	Blending factor
$\Delta x,\Delta y,\Delta z$	Internodal distances
θ	Azimuthal or co-ordinate
ϕ	Dependent variable
ρ	Density

$\sigma^u, \sigma^v, \sigma^w$	Flow velocity direction switches

Subscripts

B	Back node - see Fig. A-1
b	Back face
BE,BN,BS,BW	Back edge nodes - see Fig. A-1
BNE,BNW,BSE,BSW	Back corner nodes - see Fig. A-1
BSUD	Bounded skew-upwind differencing
CD	Central differencing
E	East node - see Fig. A-1
e	East face
F	Front node - see Fig. A-1
f	Front face
FE,FN,FS,FW	Front edge nodes - see Fig. A-1
FNE,FNW,FSE,FSW	Front corner nodes - see Fig. A-1
k	Dummy index
max	Maximum value
min	Minimum value
N	North node - see Fig. A-1
n	North face
NE	Northeast node - see Fig. A-1
NW	Northwest node - see Fig. A-1
P	Node at center of control volume - see Fig. A-1
S	South node - see Fig. A-1
s	South face
SE	Southeast node - see Fig. A-1
SW	Southwest node - see Fig. A-1
SUD	Skew upwind differencing
u	Value not dependent on ϕ_P
UD	Upwind differencing
W	West node - see Fig. A-1
w	West face

π	Dummy node indicator
ϕ	Dependent variable
$'$, $''$, $'''$	Interpolated value

Superscripts

$(\ )^{u}$	Axial velocity
$(\ )^{v}$	Radial or vertical velocity
$(\ )^{w}$	Lateral velocity
$(\ )^{*}$	Transition
$(\ )'$	For co-efficients, value not associated with γ
$(\ )''$	For coefficients, value associated with γ
$(\ )^{+}$, $(\ )^{++}$, etc.	Intermediate values of interpolated result for assumed velocity components

TABLE A-1

Central Differencing Fluxes

West

$$\frac{F_{w_{CD}}}{D_W} = \left[Pe_w (1-\alpha_w) + 1 \right] \phi_W + (\alpha_w Pe_w - 1) \phi_P$$

East

$$\frac{F_{e_{CD}}}{D_E} = \left[Pe_e (1-\alpha_e) + 1 \right] \phi_P + (\alpha_e Pe_e - 1) \phi_E$$

South

$$\frac{F_{s_{CD}}}{D_S} = \left[Pe_s (1-\alpha_s) + 1 \right] \phi_S + (\alpha_s Pe_s - 1) \phi_P$$

North

$$\frac{F_{n_{CD}}}{D_N} = \left[Pe_n (1-\alpha_n) + 1 \right] \phi_P + (\alpha_n Pe_n - 1) \phi_N$$

Front

$$\frac{F_{f_{CD}}}{D_F} = \left[Pe_f (1-\alpha_f) + 1 \right] \phi_F + (\alpha_f Pe_f - 1) \phi_P$$

Back

$$\frac{F_{b_{CD}}}{D_B} = \left[Pe_b (1-\alpha_b) + 1 \right] \phi_P + (\alpha_b Pe_b - 1) \phi_B$$

TABLE A-2

Upwind Difference Fluxes

West

$$\frac{F_{w_{UD}}}{D_W} = P_{e_w}\left[\ \sigma_w^u\ \phi_W + (1-\sigma_w^u)\ \phi_P\ \right]$$

East

$$\frac{F_{e_{UD}}}{D_E} = P_{e_e}\left[\ \sigma_w^u\ \phi_P + (1-\sigma_e^u)\ \phi_E\ \right]$$

South

$$\frac{F_{s_{UD}}}{D_S} = P_{e_s}\left[\ \sigma_w^v\ \phi_S + (1-\sigma_s^v)\ \phi_P\ \right]$$

North

$$\frac{F_{n_{UD}}}{D_N} = P_{e_n}\left[\ \sigma_n^v\ \phi_P + (1-\sigma_n^v)\ \phi_N\ \right]$$

Front

$$\frac{F_{f_{UD}}}{D_F} = P_{e_f}\left[\ \sigma_f^w\ \phi_F + (1-\sigma_f^w)\ \phi_P\ \right]$$

Back

$$\frac{F_{b_{UD}}}{D_B} = P_{e_b}\left[\ \sigma_b^w\ \phi_P + (1-\sigma_b^w)\ \phi_B\ \right]$$

TABLE A-3

Geometric Parameters Used in Interpolation Factors

Face	u	v	w	Nodes Used to Calculate: Δx	Δy	Δz
East	≥ 0	≥ 0	≥ 0	P to E	P to S	P to F
	≥ 0	≥ 0	< 0	P to E	P to S	P to B
	≥ 0	< 0	≥ 0	P to E	P to N	P to F
	≥ 0	< 0	< 0	P to E	P to N	P to B
	< 0	≥ 0	≥ 0	P to E	P to S	P to F
	< 0	≥ 0	< 0	P to E	P to S	P to B
	< 0	< 0	≥ 0	P to E	P to N	P to F
	< 0	< 0	< 0	P to E	P to N	P to B
North	≥ 0	≥ 0	≥ 0	P to W	P to N	P to F
	≥ 0	≥ 0	< 0	P to W	P to N	P to B
	≥ 0	< 0	≥ 0	P to W	P to N	P to F
	≥ 0	< 0	< 0	P to W	P to N	P to B
	< 0	≥ 0	≥ 0	P to E	P to N	P to F
	< 0	≥ 0	< 0	P to E	P to N	P to B
	< 0	< 0	≥ 0	P to E	P to N	P to F
	< 0	< 0	> 0	P to E	P to N	P to B
Back	≥ 0	≥ 0	≥ 0	P to W	P to S	P to B
	≥ 0	≥ 0	< 0	P to W	P to S	P to B
	≥ 0	< 0	≥ 0	P to W	P to N	P to B
	≥ 0	< 0	< 0	P to W	P to N	P to B
	< 0	≥ 0	≥ 0	P to E	P to S	P to B
	< 0	≥ 0	< 0	P to E	P to S	P to B
	< 0	< 0	≥ 0	P to E	P to N	P to B
	< 0	< 0	< 0	P to E	P to N	P to B

TABLE A-4

INTERPOLATED VALUE FOR ϕ - WEST FACE

$U_w \geq 0$, $V_w \geq 0$, all W_w

$$\phi_{w'''}^{++} = \sigma_w^w \, k_3 \, [k_1\phi_{FSW} + (1-k_1)\,\phi_{FW}] + (1-\sigma_w^w)\, k_3\, [k_1\phi_{BSW} + (1-k_1)\,\phi_{BW}]$$
$$+ (1-k_3)\, [k_1\phi_{SW} = (1-k_1)\,\phi_W]$$

$U_w \geq 0$, $V_w < 0$, all W_w

$$\phi_{w'''}^{+-} = \sigma_w^w \, k_3 \, [k_1\phi_{FNW} + (1-k_1)\,\phi_{FW}] + (1-\sigma_w^w)\, k_3\, [k_1\phi_{BNW} + (1-k_1)\,\phi_{BW}]$$
$$+ (1-k_3)\, [k_1\phi_{NW} + (1-k_1)\,\phi_W]$$

$U_w < 0$, $V_w \geq 0$, all W_w

$$\phi_{w'''}^{-+} = \sigma_w^w \, k_3 \, [k_1\phi_{FS} + (1-k_1)\,\phi_F\,] + (1-\sigma_w^w)\, k_3\, [k_1\phi_{BS} + (1-k_1)\,\phi_B]$$
$$+ (1-k_3)\, [k_1\phi_S + (1-k_1)\,\phi_P]$$

$U_w < 0$, $V_w < 0$, all W_w

$$\phi_{w'''}^{--} = \sigma_w^w \, k_3 \, [k_1\phi_{FN} + (1-k_1)\,\phi_F] + (1-\sigma_w^w)\, k_3\, [k_1\phi_{BN} + (1-k_1)\,\phi_B]$$
$$+ (1-k_3)\, [k_1\phi_N + (1-k_1)\,\phi_P]$$

Then

$$\phi_{w'''}^{+} = \sigma_w^v \, \phi_{w'''}^{++} + (1-\sigma_w^v)\, \phi_{w'''}^{+-}$$
$$\phi_{w'''}^{-} = \sigma_w^v \, \phi_{w'''}^{-+} + (1-\sigma_w^v)\, \phi_{w'''}^{--}$$
$$\phi_{w'''} = \sigma^u \, \phi_{w'''}^{+} + (1-\sigma_w^u)\, \phi_{w'''}^{-}$$

$$k_1 = \min\left[\, 1,\ \frac{1}{2}\,\frac{\Delta x}{\Delta y}\,\left|\frac{V_w}{U_w}\right| \,\right]$$

$$k_2 = \min\left[\, 1,\ \frac{1}{2}\,\frac{\Delta x}{\Delta z}\,\left|\frac{W_w}{U_w}\right| \,\right]$$

TABLE A-5

INTERPOLATED VALUE FOR ϕ-EAST FACE

Ue $\geq$ 0, Ve $\geq$ 0, all We

$$\phi_e^{++}{}''' = \sigma_e^w K_3 [K_1\phi_{FS} + (1-K_1)\phi_F] + (1-\sigma_e^w) K_3 [K_1\phi_{BS} + (1-K_1)\phi_B]$$

$$+ (1-K_3) [K_1\phi_S + (1-K_1)\phi_P]$$

Ue $\geq$ 0, Ve $\geq$ 0, all We

$$\phi_e^{+-}{}''' = \sigma_e^w K_3 [K_1\phi_{FN} + (1-K_1)\phi_F] + (1-\sigma_e^w) K_3 [K_1\phi_{BN} + (1-K_1)\phi_B]$$

$$+ (1-K_3) [K_1\phi_N + (1-K_1)\phi_P]$$

Ue $<$ 0, Ve $\geq$ 0, all We

$$\phi_e^{-+}{}''' = \sigma_e^w K_3 [K_1\phi_{FSE} + (1-K_1)\phi_{FE}] + (1-\sigma_e^w) K_3 [K_1\phi_{BSE} + (1-K_1)\phi_{BE}]$$

$$+ (1-K_3) [K_1\phi_{SE} + (1-K_1)\phi_E]$$

Ue $<$ 0, Ve $<$ 0, all We

$$\phi_e^{--}{}''' = \sigma_e^w K_3 [K_1\phi_{FNE} + (1-K_1)\phi_{FE}] + (1-\sigma_e^w) K_3 [K_1\phi_{BNE} + (1-K_1)\phi_{BE}]$$

$$+ (1-K_3) [K_1\phi_{NE} + (1-K_1)\phi_E]$$

Then

$$\phi_e^{+}{}''' = \sigma_e^v \phi_e^{++}{}''' + (1-\sigma_e^v) \phi_e^{+-}{}'''$$

$$\phi_e^{-}{}''' = \sigma_e^v \phi_e^{-+}{}''' + (1-\sigma_e^v) \phi_e^{--}{}'''$$

$$\phi_e''' = \sigma_e^u \phi_e^{+}{}''' + (1-\sigma_e^u) \phi_e^{-}{}'''$$

$$K_1 = \min\left[1, \frac{1}{2}\frac{\Delta x}{\Delta y}\left|\frac{Ve}{Ue}\right|\right]$$

$$K_3 = \min\left[1, \frac{1}{2}\frac{\Delta x}{\Delta z}\left|\frac{We}{Ue}\right|\right]$$

TABLE A-6

INTERPOLATED VALUE FOR ϕ-SOUTH FACE

All Us, Vs $\geq$ 0, Ws $\geq$ 0

$$\phi_{s'''}^{++} = \sigma_s^u K_3 [K_1\phi_{FSW} + (1-K_1)\phi_{SW}] + (1-\sigma_s^u) K_3 [K_1\phi_{FSE} + (1-K_1) \phi_{SE}] + (1-K_3) [K_1\phi_{FS} + (1-K_1)\phi_S]$$

All Us, Vs $\geq$ 0, Ws $<$ 0

$$\phi_{s'''}^{+-} = \sigma_s^u K_3 [K_1\phi_{BSW} + (1-K_1)\phi_{SW}] + (1-\sigma_s^u) K_3 [K_1\phi_{BSE} + (1-K_1) \phi_{SE}] + (1-K_3) [K_1\phi_{BS} + (1-K_1)\phi_S]$$

All Us, Vs $<$ 0, Ws $\geq$ 0

$$\phi_{s'''}^{-+} = \sigma_s^u K_3 [K_1\phi_{FW} + (1-K_1)\phi_W] + (1-\sigma_s^u) K_3 [K_1\phi_{FE} + (1-K_1) \phi_E] + (1-K_3) [K_1\phi_F + (1-K_1)\phi_P]$$

All Us, Vs $<$ 0, Ws $<$ 0

$$\phi_{s'''}^{--} = \sigma_s^u K_3 [K_1\phi_{BW} + (1-K_1)\phi_W] + (1-\sigma_s^u) K_3 [K_1\phi_{BE} + (1-K_1) \phi_E] + (1-K_3) [K_1\phi_B + (1-K_1)\phi_P]$$

Then

$$\phi_{s'''}^{+} = \sigma_s^w \phi_{s'''}^{++} + (1-\sigma_s^w)\phi_{s'''}^{+-}$$

$$\phi_{s'''}^{-} = \sigma_s^w \phi_{s'''}^{-+} + (1-\sigma_s^w)\phi_{s'''}^{--}$$

$$\phi_{s'''} = \sigma_s^v \phi_{s'''}^{+} + (1-\sigma_s^v)\phi_{s'''}^{-}$$

$$K_1 = \min \left[1, \frac{1}{2} \frac{\Delta y}{\Delta z} \left|\frac{Ws}{Vs}\right|\right]$$

$$K_3 = \min \left[1, \frac{1}{2} \frac{\Delta y}{\Delta x} \left|\frac{Us}{Vs}\right|\right]$$

TABLE A-7

INTERPOLATED VALUE FOR ϕ-NORTH FACE

All U_n, $V_n \geq 0$, $W_n \geq 0$

$$\phi^{++}_{n'''} = \sigma^u_n K_3 [K_1\phi_{FW} + (1-K_1)\phi_W] + (1-\sigma^u_n) K_3 [K_1 \phi_{FE} + (1-K_1) \phi_E]$$
$$+ (1-K_3) [K_1\phi_F + (1-K_1) \phi_P]$$

All U_n, $V_n \geq 0$, $W_n < 0$

$$\phi^{+-}_{n'''} = \sigma^u_n K_3 [K_1 \phi_{BW} + (1-K_1) \phi_W] - (1-\sigma^u_n) K_3 [K_1 \phi_{BE} + (1-K_1) \phi_E]$$
$$+ (1-K_3) [K_1 \phi_B + (1-K_1) \phi_P]$$

All U_n, $V_n < 0$, $W_n \geq 0$

$$\phi^{-+}_{n'''} = \sigma^u_n K_3 [K_1 \phi_{FNW} + (1-K_1) \phi_{NW}] + (1-\sigma^u_n) K_3 [K_1 \phi_{FNE} + (1-K_1) \phi_{NE}]$$
$$+ (1-K_3) [K_1 \phi_{FN} + (1-K_1) \phi_N]$$

All U_n, $V_n < 0$, $W_n < 0$

$$\phi^{--}_{n'''} = \sigma^u_n K_3 [K_1 \phi_{BNW} + (1-K_1) \phi_{NW}] + (1-\sigma^u_n) K_3 [K_1 \phi_{BNE} + (1-K_1) \phi_{NE}]$$
$$+ (1-K_3) [K_1 \phi_{BN} + (1-K_1) \phi_N]$$

Then

$$\phi^{+}_{n'''} = \sigma^w_n \phi^{++}_{n'''} + (1-\sigma^w_n) \phi^{+-}_{n'''}$$
$$\phi^{-}_{n'''} = \sigma^w_n \phi^{-+}_{n'''} + (1-\sigma^w_n) \phi^{--}_{n'''}$$
$$\phi_{n'''} = \sigma^v_n \phi^{+}_{n'''} + (1-\sigma^v_n) \phi^{-}_{n'''}$$

$$K_1 = \min \left[1, \frac{1}{2} \frac{\Delta y}{\Delta z} \left|\frac{W_n}{V_n}\right|\right]$$
$$K_3 = \min \left[1, \frac{1}{2} \frac{\Delta y}{\Delta x} \left|\frac{U_n}{V_n}\right|\right]$$

TABLE A-8

INTERPOLATED VALUE FOR ϕ-FRONT FACE

$U_f \geq V_f \geq 0$, all W_f

$$\phi_{f'''}^{++} = \sigma_f^w \{K_3[K_1\phi_{FSW} + (1-K_1)\phi_{FW}] + (1-K_3)[K_1\phi_{FS} + (1-K_1)\phi_F]\}$$

$$+ (1-\sigma_f^w)[K_1\phi_{SW} + (1-K_1)\phi_W] + (1-K_3)[K_1\phi_S + (1-K_1)\phi_P]\}$$

$U_f \geq 0$, $V_f < 0$, all W_f

$$\phi_{f'''}^{+-} = \sigma_f^w \{K_3[K_1\phi_{FNW} + (1-K_1)\phi_{FW}] + (1-K_3)[K_1\phi_{FN} + (1-K_1)\phi_F]\}$$

$$+ (1-\sigma_f^w)\{K_3[K_1\phi_{NW} + (1-K_1)\phi_W] + (1-K_3)[K_1\phi_N + (1-K_1)\phi_P]\}$$

$U_f < 0$, $V_f \geq 0$, all W_f

$$\phi_{f'''}^{-+} = \sigma_f^w \{K_3[K_1\phi_{FSE} + (1-K_1)\phi_{FE}] + (1-K_3)[K_1\phi_{FS} + (1-K_1)\phi_F]\}$$

$$+ (1-\sigma_f^w)\{K_3[K_1\phi_{SE} + (1-K_1)\phi_E] + (1-K_3)[K_1\phi_S + (1-K_1)\phi_P]\}$$

$U_f < 0$, $V_f \leq 0$, all W_f

$$\phi_{f'''}^{--} = \sigma_f^w \{K_3[K_1\phi_{FNE} + (1-K_1)\phi_{FE}] + (1-K_3)[K_1\phi_{FN} + (1-K_1)\phi_F]\}$$

$$+ (1-\sigma_f^w)\{K_3[K_1\phi_{NE} + (1-K_1)\phi_E] + (1-K_3)[K_1\phi_N + (1-K_1)\phi_P]\}$$

Then

$$\phi_{f'''}^{+} = \sigma_f^v \phi_{f'''}^{++} + (1 - \sigma_f^v)\phi_{f'''}^{+-}$$

$$\phi_{f'''}^{-} = \sigma_f^v \phi_{f'''}^{-+} + (1 - \sigma_f^v)\phi_{f'''}^{--}$$

$$\phi_{f'''} = \sigma_f^u \phi_{f'''}^{+} + (1 - \sigma_f^u)\phi_{f'''}^{-}$$

$$K_1 = \min\left[1,\ 1/2\ \frac{\Delta z}{\Delta y}\left|\frac{V_f}{W_f}\right|\right]$$

$$K_3 = \min\left[1,\ 1/2\ \frac{\Delta z}{\Delta x}\left|\frac{U_f}{W_f}\right|\right]$$

TABLE A-9

INTERPOLATED VALUE FOR ϕ-BACK FACE

$U_b \geq 0$, $V_b \geq 0$, all W_b

$$\phi_{b'''}^{++} = \sigma_b^w \{K_3 [K_1 \phi_{SW} + (1-K_1) \phi_W] + (1-K_3) [K_1 \phi_S + (1-K_1) \phi_P]\}$$
$$+ (1-\sigma_b^w) \{K_3 [K_1 \phi_{BSW} + (1-K_1) \phi_{BW}] + (1-K_3) [K_1 \phi_{BS} + (1-K_1) \phi_B]\}$$

$U_b \geq 0$, $V_b < 0$, all W_b

$$\phi_{b'''}^{+-} = \sigma_b^w \{K_3 [K_1 \phi_{NW} + (1-K_1) \phi_W] + (1-K_3) [K_1 \phi_N + (1-K_1) \phi_P]\}$$
$$+ (1-\sigma_b^w) \{K_3 [K_1 \phi_{BNW} + (1-K_1) \phi_{BW}] + (1-K_3) [K_1 \phi_{BN} + (1-K_1) \phi_B]\}$$

$U_b < 0$, $V_b \geq 0$, all W_b

$$\phi_{b'''}^{-+} = \sigma_b^w \{K_3 [K_1 \phi_{SE} + (1-K_1) \phi_E] + (1-K_3) [K_1 \phi_S + (1-K_1) \phi_P]\}$$
$$+ (1-\sigma_b^w) \{K_3 [K_1 \phi_{BSE} + (1-K_1) \phi_{BE}] + (1-K_3) [K_1 \phi_{BS} + (1-K_1) \phi_B]\}$$

$U_b < 0$, $V_b < 0$, all W_b

$$\phi_{b'''}^{--} = \sigma_b^w \{K_3 [K_1 \phi_{NE} + (1-K_1) \phi_E] + (1-K_3) [K_1 \phi_N + (1-K_1) \phi_P]\}$$
$$+ (1-\sigma_b^w) \{K_3 [K_1 \phi_{BNE} + (1-K_1) \phi_{BE}] + (1-K_3) [K_1 \phi_{BN} + (1-K_1) \phi_B]\}$$

Then

$$\phi_{b'''}^{+} = \sigma_b^v \phi_{b'''}^{++} + (1-\sigma_b^v) \phi_{b'''}^{+-}$$
$$\phi_{b'''}^{-} = \sigma_b^v \phi_{b'''}^{-+} + (1-\sigma_b^v) \phi_{b'''}^{--}$$
$$\phi_{b'''} = \sigma_b^u \phi_{b'''}^{+} + (1-\sigma_b^u) \phi_{b'''}^{-}$$

$$K_1 = \min \left[1, \frac{1}{2} \frac{\Delta z}{\Delta y} \left|\frac{V_b}{W_b}\right|\right]$$
$$K_3 = \min \left[1, \frac{1}{2} \frac{\Delta z}{\Delta x} \left|\frac{U_b}{W_b}\right|\right]$$

TABLE A-10

SKEW UPWIND DIFFERENCING FLUXES

West

$$\frac{F_{w_{SUD}}}{D_W} = (Pe_w - Pe_w^*)\ \phi_{w'''} + [Pe_w^*\ (1-\alpha_w) + 1]\ \phi_W + (\alpha_w\ Pe_w^* - 1)\ \phi_P$$

$$Pe_w = \frac{D_W}{C_W}\ ,\quad Pe_w^* = \frac{1}{\sigma_w^u - (1-\alpha_w)}$$

East

$$\frac{Fe_{SUD}}{D_E} = (Pe_e - Pe_e^*)\ \phi_{e'''} + [Pe_e^*\ (1-\alpha_e) + 1]\ \phi_P + (\alpha_e Pe_e^* - 1)\ \phi_E$$

$$Pe_e = \frac{D_E}{C_E}\ ,\ Pe_e^* = \frac{1}{\sigma_e^u - (1-\alpha_e)}$$

South

$$\frac{F_{s_{SUD}}}{D_S} = (Pe_s - Pe_s^*)\ \phi_{s'''} + [Pe_s^*\ (1-\alpha_s) + 1]\ \phi_S + (\alpha_s\ Pe_s^* - 1)\ \phi_P$$

$$Pe_s = \frac{D_S}{C_S}\ ,\ Pe_s^* = \frac{1}{\sigma_s^v - (1-\alpha_s)}$$

North

$$\frac{F_{n_{SUD}}}{D_N} = (Pe_n - Pe_n^*)\ \phi_{n'''} + [Pe_n^*\ (1-\alpha_n) + 1]\ \phi_P + (\alpha_n Pe_n^* - 1)\ \phi_N$$

$$Pe_n = \frac{D_N}{C_N}\ ,\ Pe_n^* = \frac{1}{\sigma_n^v - (1-\alpha_n)}$$

Front

$$\frac{F_{f_{SUD}}}{D_F} = (Pe_f - Pe_f^*)\ \phi_{f'''} + [Pe_f^*\ (1-\alpha_f) + 1]\ \phi_F + (\alpha_f\ Pe_f^* - 1)\ \phi_P$$

$$Pe_f = \frac{D_F}{C_F}\ ,\ Pe_f^* = \frac{1}{\sigma_f^w - (1-\alpha_f)}$$

Back

$$\frac{F_{b_{SUD}}}{D_B} = (Pe_b - Pe_b^*)\ \phi_{b'''} + [Pe_b^*\ (1-\alpha_b) + 1]\ \phi_P + (\alpha_b\ Pe_b^* - 1)\ \phi_B$$

$$Pe_b = \frac{D_B}{C_B}\ ,\ Pe_b^* = \frac{1}{\sigma_b^w - (1-\alpha_b)}$$

TABLE A-11

COEFFICIENTS OF THE FINITE-DIFFERENCE EQUATION

$$A_B(I,J,K) = B1(I,J,K)$$
$$- \gamma_e [\sigma_e^u (1-\sigma_e^w) E3] (I,J,K,2)$$
$$- \gamma_b [(1-\sigma_b^w) B3] (I,J,K,4)$$
$$- \gamma_n [\sigma_n^v (1-\sigma_n^w) N3] (I,J,K,3)$$
$$- \gamma_w [(1-\sigma_e^u)(1-\sigma_e^w) E3] (I-1,J,K,2)$$
$$- \gamma_s [(1-\sigma_n^v)(1-\sigma_n^w) N3] (I-1,J-1,K,3)$$

$$A_{BE}(I,J,K) = -\gamma_e [(1-\sigma_e^u)(1-\sigma_e^w) E3] (I,J,K,2)$$
$$- \gamma_b [(1-\sigma_b^u)(1-\sigma_b^w) B3] (I,J,K,2)$$
$$- \gamma_n [(1-\sigma_n^u) \sigma_n^v (1-\sigma_n^w) N3] (I,J,K,1)$$
$$+ \gamma_s [(1-\sigma_n^u) (1-\sigma_n^v) (1-\sigma_n^w) N3] (I,J-1,K,1)$$

$$A_{BN}(I,J,K) = -\gamma_e [\sigma_e^u (1-\sigma_e^v) (1-\sigma_e^w) E3] (I,J,K,1)$$
$$- \gamma_b [(1-\sigma_b^v)(1-\sigma_b^w) B3] (I,J,K,3)$$
$$- \gamma_n [(1-\sigma_n^v)(1-\sigma_n^w) N3] (I,J,K,3)$$
$$+ \gamma_w [(1-\sigma_e^u)(1-\sigma_e^v)(1-\sigma_e^w) E3] (I-1,J,K,1)$$

TABLE A-11 (Cont'd)

COEFFICIENTS OF THE FINITE-DIFFERENCE EQUATION

$$A_{BNE}(I,J,K) = - \gamma_e[(1-\sigma_e^u)\ (1-\sigma_e^v)(1-\sigma_e^w)\ E3]\ (I,J,K,1)$$

$$- \gamma_b[(1-\sigma_b^u)\ (1-\sigma_b^v)(1-\sigma_b^w)\ B3]\ (I,J,K,1)$$

$$- \gamma_n[(1-\sigma_n^u)\ (1-\sigma_n^v)(1-\sigma_n^w)\ N3]\ (I,J,K,1)$$

$$A_{BNW}(I,J,K) = - \gamma_b[\sigma_b^u(1-\sigma_b^v)\ (1-\sigma_b^w)\ B3]\ (I,J,K,1)$$

$$- \gamma_n[\sigma_n^u(1-\sigma_n^v)\ (1-\sigma_n^w)\ N3]\ (I,J,K,1)$$

$$+ \gamma_w[\sigma_e^u(1-\sigma_e^v)\ (1-\sigma_e^w)\ E3]\ (I-1,J,K,1)$$

$$A_{BS}(I,J,K) = - \gamma_e[\sigma_e^u\ \sigma_e^v\ (1-\sigma_e^w)\ E3](I,J,K,1)$$

$$- \gamma_b[\sigma_b^v(1-\sigma_b^w)\ B3]\ (I,J,K,3)$$

$$+ \gamma_w[(1-\sigma_e^u)\ \sigma_e^v(1-\sigma_e^w)\ E3]\ (I-1,J,K,1)$$

$$+ \gamma_s[\sigma_n^v(1-\sigma_n^w)\ N3]\ (I,J-1,K,3)$$

$$A_{BSE}(I,J,K) = - \gamma_e[(1-\sigma_e^u)\ \sigma_e^v(1-\sigma_e^w)\ E3]\ (I,J,K,1)$$

$$- \gamma_b[(1-\sigma_b^u)\ \sigma_b^v(1-\sigma_b^w)\ B3]\ (I,J,K,1)$$

$$+ \gamma_s[(1-\sigma_n^u)\ \sigma_n^v\ (1-\sigma_n^w)\ N3]\ (I,J-1,K.1)$$

TABLE A-11 (Cont'd)

COEFFICIENTS OF THE FINITE-DIFFERENCE EQUATION

$$A_{BSW}(I,J,K) = -\gamma_b[\sigma_b^u\ \sigma_b^v(1-\sigma_b^w)\ B3]\ (I,J,K,1)$$

$$+\gamma_w[\sigma_e^u\ \sigma_e^v(1-\sigma_e^w)\ E3]\ (I-1,J,K,1)$$

$$+\gamma_s[\sigma_n^u\ \sigma_n^v\ (1-\sigma_n^w)\ N3]\ (I,J-1,K,1)$$

$$A_{BW}(I,J,K) = -\gamma_b[\sigma_b^u(1-\sigma_b^w)\ B3]\ (I,J,K,2)$$

$$-\gamma_n[\sigma_n^u\ \sigma_n^v\ (1-\sigma_n^w)\ N3]\ (I,J,K,1)$$

$$+\gamma_w[\sigma_e^u\ (1-\sigma_e^w)\ E3]\ (I-1,J,K,2)$$

$$+\gamma_s[\sigma_n^u\ (1-\sigma_n^v)\ (1-\sigma_n^w)N3]\ (I,J-1,K,1)$$

$$A_E(I,J,K) = E1(I,J,K)$$

$$-\gamma_e[(1-\sigma_e^u)\ E3]\ (I,J,K,4)$$

$$-\gamma_b[(1-\sigma_b^u)\ \sigma_b^w\ B3]\ (I,J,K,2)$$

$$-\gamma_n[(1-\sigma_n^u)\ \sigma_n^v\ N3]\ (I,J,K,2)$$

$$+\gamma_f[(1-\sigma_b^u)\ (1-\sigma_b^w)\ B3]\ (I,J,K-1,2)$$

$$+\gamma_s[(1-\sigma_n^u)\ (1-\sigma_n^v)\ N3]\ (I,J-1,K,2)$$

TABLE A-11 (Cont'd)

COEFFICIENTS OF THE FINITE-DIFFERENCE EQUATION

$$A_F(I,J,K) = B2(I,J,K-1)$$

$$- \gamma_e[\sigma_e^u \sigma_e^w E3] \ (I,J,K,2)$$

$$- \gamma_n[\sigma_n^v \sigma_n^w N3] \ (I,J,K,3)$$

$$- \gamma_w[(1-\sigma_e^u) \sigma_e^w E3] \ (I-1,J,K,2)$$

$$+ \gamma_f[\sigma_b^w B3] \ (I,J,K-1,4)$$

$$+ \gamma_s[1-\sigma_n^v) \sigma_n^w N3] \ (I,J-1,K,3)$$

$$A_{FE}(I,J,K) = - \gamma_e[(1-\sigma_e^u) \sigma_e^w E3] \ (I,J,K,2)$$

$$- \gamma_n[(1-\sigma_n^u) \sigma_n^v \sigma_n^w N3] \ (I,J,K,1)$$

$$+ \gamma_f[(1-\sigma_b^u) \sigma_b^w B3] \ (I,J,K-1,2)$$

$$+ \gamma_s[(1-\sigma_n^u) (1-\sigma_n^v) \sigma_n^w N3] \ (I,J-1,K,1)$$

$$A_{FN}(I,J,K) = - \gamma_e[\sigma_e^u(1-\sigma_e^v) \sigma_e^w E3] \ (I,J,K,1)$$

$$- \gamma_n[(1-\sigma_n^v) \sigma_n^w N3] \ (I,J,K,3)$$

$$+ \gamma_w[(1-\sigma_e^u) (1-\sigma_e^v) \sigma_e^w E3] \ (I-1,J,K,1)$$

$$+ \gamma_f[(1-\sigma_b^v) \sigma_b^w B3] \ (I,J,K-1,3)$$

TABLE A-11 (Cont'd)

COEFFICIENTS OF THE FINITE-DIFFERENCE EQUATION

$$A_{FNE}(I,J,K) = - \gamma_e[(1-\sigma_e^u)\ (1-\sigma_e^v)\ \sigma_e^w\ \ E3]\ (I,J,K,1)$$

$$- \gamma_n[(1-\sigma_n^u)\ (1-\sigma_n^w)\ \sigma_n^w\ \ N3]\ (I,J,K.1)$$

$$+ \gamma_f[(1-\sigma_b^u)\ (1-\sigma_b^v)\ \sigma_b^w\ \ B3]\ (I,J,K-1,1)$$

$$A_{FNW}(I,K,K) = - \gamma_n[\sigma_n^u\ (1-\sigma_n^v)\ \sigma_n^w\ \ N3]\ (I,J,K,1)$$

$$+ \gamma_w[\sigma_e^u\ (1-\sigma_e^v)\ \sigma_e^w\ \ E3]\ (I-1,J,K,1)$$

$$+ \gamma_f[\sigma_b^u\ (1-\sigma_b^v)\ \sigma_b^w\ \ B3]\ (I,J,K-1,1)$$

$$A_{FS}(I,J,K) = - \gamma_e[\sigma_e^u\ \sigma_e^v\ \sigma_e^w\ \ E3]\ (I,J,K,1)$$

$$+ \gamma_w[(1-\sigma_e^u)\ \sigma_e^v\ \sigma_e^w\ E3]\ (I,J,K-1,1)$$

$$+ \gamma_f[\sigma_b^v\ \sigma_b^w\ B3]\ (I,J,K-1,3)$$

$$+ \gamma_s[\sigma_n^v\ \sigma_n^w\ N3]\ (I,J-1,K,3)$$

$$A_{FSE}(I,J,K) = - \gamma_e[(1-\sigma_e^u)\ \sigma_e^v\ \sigma_e^w\ E3]\ (I,J,K,1)$$

$$- \gamma_f[(1-\sigma_b^u)\ \sigma_b^v\ \sigma_b^w\ B3]\ (I,J,K-1,1)$$

$$- \gamma_s[(1-\sigma_n^u)\ \sigma_n^v\ \sigma_n^w\ N3]\ (I,J-1,K,1)$$

TABLE A-11 (Cont'd)

COEFFICIENTS OF THE FINITE-DIFFERENCE EQUATION

$$A_{FSW}(I,J,K) = \gamma_w[\sigma_e^u \sigma_e^v \sigma_e^w E3] \ (I-1,J,K,1)$$

$$+ \gamma_f[\sigma_b^u \sigma_b^v \sigma_b^w B3] \ (I,J,K-1,1)$$

$$+ \gamma_s[\sigma_n^u \sigma_n^v \sigma_n^w N3] \ (I,J-1,K,1]$$

$$A_{FW}(I,J,K) = - \gamma_n[\sigma_n^u \sigma_n^v \sigma_n^w N3] \ (I,J,K,1)$$

$$+ \gamma_w[\sigma_e^u \sigma_e^w E3] \ (I-1,J,K,2)$$

$$+ \gamma_f[\sigma_b^u \sigma_b^w B3] \ (I,J,K-1,2)$$

$$+ \gamma_s[\sigma_n^u (1-\sigma_n^v) \sigma_n^w N3] \ (I,J-1,K,1)$$

$$A_N(I,J,K) = N1 \ (I,J,K)$$

$$- \gamma_e [\sigma_e^u(1-\sigma_e^v) E3] \ (I,J,K,3)$$

$$- \gamma_b [(1-\sigma_b^v) \sigma_b^w B3] \ (I,J,K,3)$$

$$- \gamma_n [(1-\sigma_b^v) N3] \ (I,J,K,4)$$

$$+ \gamma_w [(1-\sigma_e^u) (1-\sigma_e^v) E3] \ (I-1,J,K,3)$$

$$+ \gamma_f [(1-\sigma_b^v) (1-\sigma_b^w) B3] \ (I,J,K-1,3)$$

TABLE A-11 (Cont'd)

COEFFICIENTS OF THE FINITE-DIFFERENCE EQUATION

$$A_{NE}(I,J,K) = - \gamma_e[(1-\sigma_e^u)\ (1-\sigma_e^v)\ E3]\ (I,J,K,3)$$

$$- \gamma_b[(1-\sigma_b^u)\ (1-\sigma_b^v)\ \sigma_b^w\ B3]\ (I,J,K,1)$$

$$- \gamma_n[(1-\sigma_n^u)\ (1-\sigma_n^v)\ N3]\ (I,J,K,2)$$

$$+ \gamma_f[(1-\sigma_b^u)(1-\sigma_b^v)\ (1-\sigma_b^w)\ B3]\ (I,J,K-1,1)$$

$$A_{NW}(I,J,K) = - \gamma_b[\sigma_b^u\ (1-\sigma_b^v)\ \sigma_b^w\ B3]\ (I,J,K,1)$$

$$- \gamma_n[\sigma_n^u\ (1-\sigma_n^v)\ N3]\ (I,J,K,2)$$

$$- \gamma_w[\sigma_e^u\ (1-\sigma_e^v)\ E3]\ (I-1,J,K,3)$$

$$+ \gamma_f[\sigma_b^u\ (1-\sigma_b^v)\ (1-\sigma_b^w)\ B3]\ (I,J,K-1,1)$$

$$A_S(I,J,K) = N2(I,J-1,K)$$

$$- \gamma_e[\sigma_e^u\ \sigma_e^v\ E3]\ (I,J,K,3)$$

$$- \gamma_b[\sigma_b^v\ \sigma_b^w\ B3]\ (I,J,K,3)$$

$$+ \gamma_w[(1-\sigma_e^u)\sigma_e^v\ E3]\ (I-1,J,K,3)$$

$$+ \gamma_f[\sigma_b^v\ (1-\sigma_b^w)\ E3]\ (I,J,K-1,3)$$

$$+ \gamma_s[\sigma_n^v\ N3]\ (I,J-1,K,4)$$

TABLE A-11 (Cont'd)

COEFFICIENTS OF THE FINITE-DIFFERENCE EQUATION

$$A_{SE}(I,J,K) = -\gamma_e[1-\sigma_e^u)\ \sigma_e^v\ E3]\ (I,J,K,3)$$

$$-\gamma_b[(1-\sigma_b^u)\sigma_b^v\ \sigma_b^w\ B3]\ (I,J,K,1)$$

$$+\gamma_f[(1-\sigma_b^u)\ \sigma_b^v\ (1-\sigma_b^w)\ B3]\ (I,J,K-1,1)$$

$$+\gamma_s[(1-\sigma_n^u)\ \sigma_n^v\ N3]\ (I,J-1,K,2)$$

$$A_{SW}(I,J,K) = -\gamma_b[\sigma_b^u\ \sigma_b^v\ \sigma_b^w\ B3]\ (I,J,K,1)$$

$$+\gamma_w[\sigma_e^u\ \sigma_e^v\ E3]\ (I-1,J,K,3)$$

$$+\gamma_f[\sigma_b^u\ \sigma_b^v\ (1-\sigma_b^w)\ B3]\ (I,J,K-1,1)$$

$$+\gamma_s[\sigma_n^u\ \sigma_n^v\ N3]\ (I,J-1,K,2)$$

$$A_W(I,J,K) = E2(I-1,J,K)$$

$$-\gamma_b[\sigma_b^u\ \sigma_b^w\ B3]\ (I,J,K,2)$$

$$-\gamma_n[\sigma_n^u\ \sigma_n^v\ N3]\ (I,J,K,2)$$

$$+\gamma_w[\sigma_e^u\ E3]\ (I-1,J,K,4)$$

$$+\gamma_f[\sigma_b^u\ (1-\sigma_b^w)\ B3]\ (I,J,K-1,2)$$

$$+\gamma_s[\sigma_n^u\ (1-\sigma_n^v)\ N3]\ (I,J-1,K,2)$$

FIG. A-1 THREE-DIMENSIONAL GRID AND NODE SYSTEM

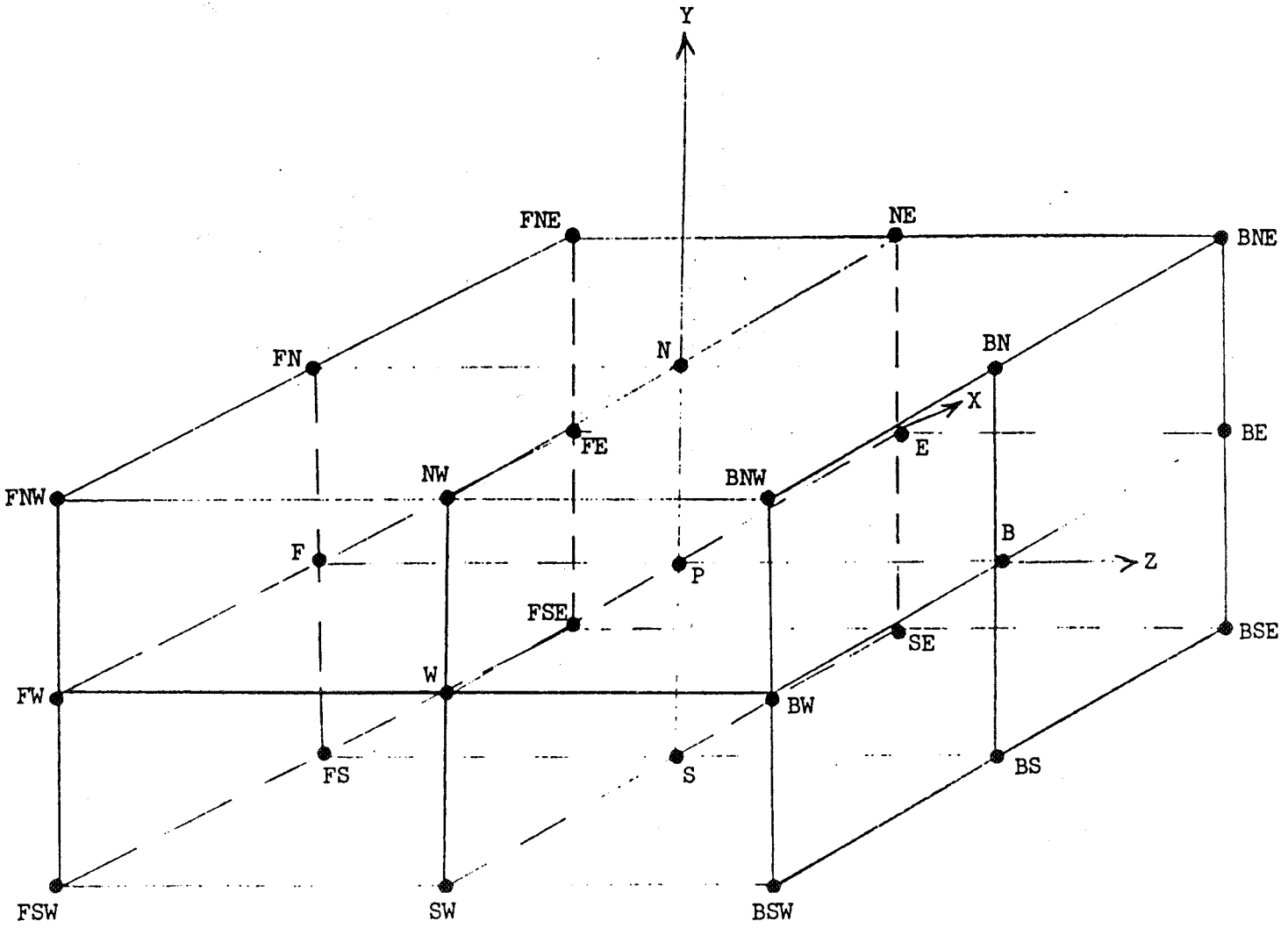

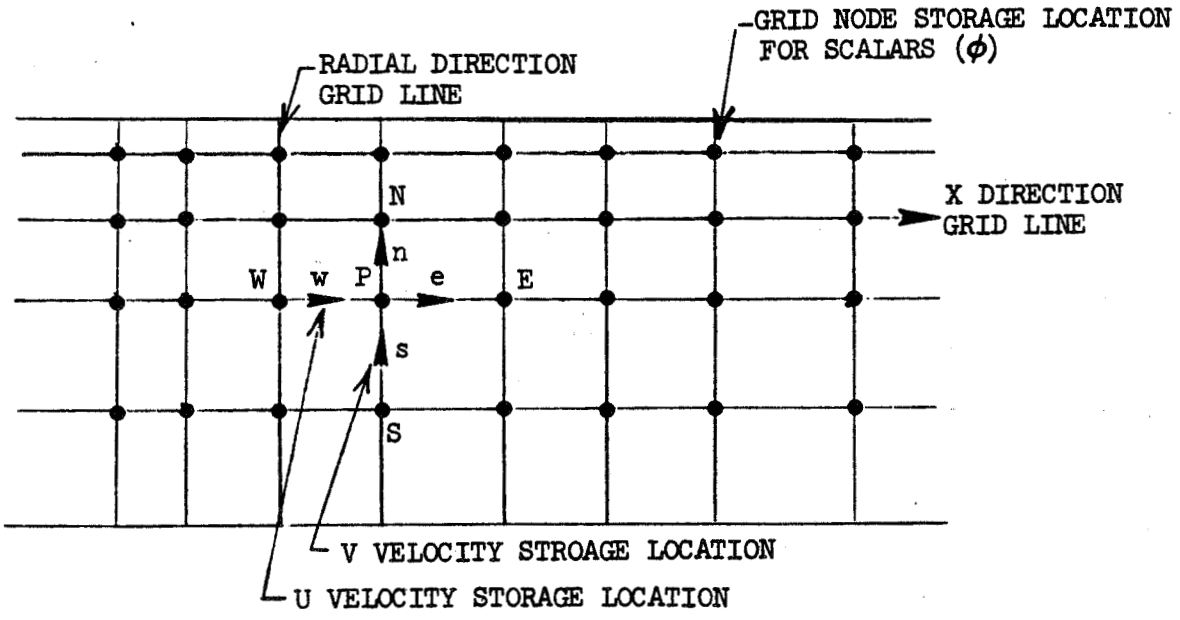

FIG. A-2 GRID SYSTEM FOR SCALARS IN X-Y PLANE

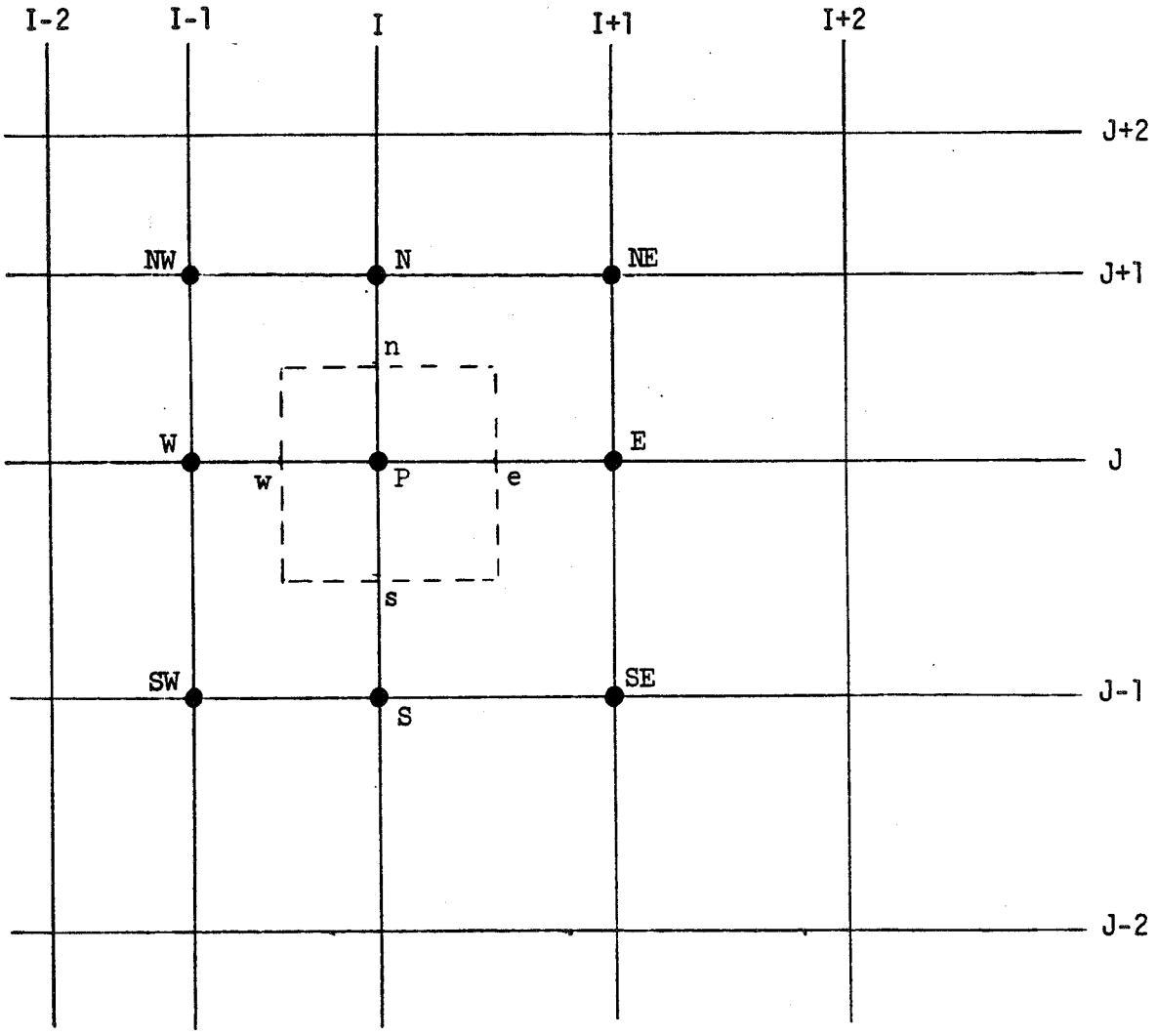

FIG. A-3 SCALAR CONTROL VOLUME IN X-Y PLANE

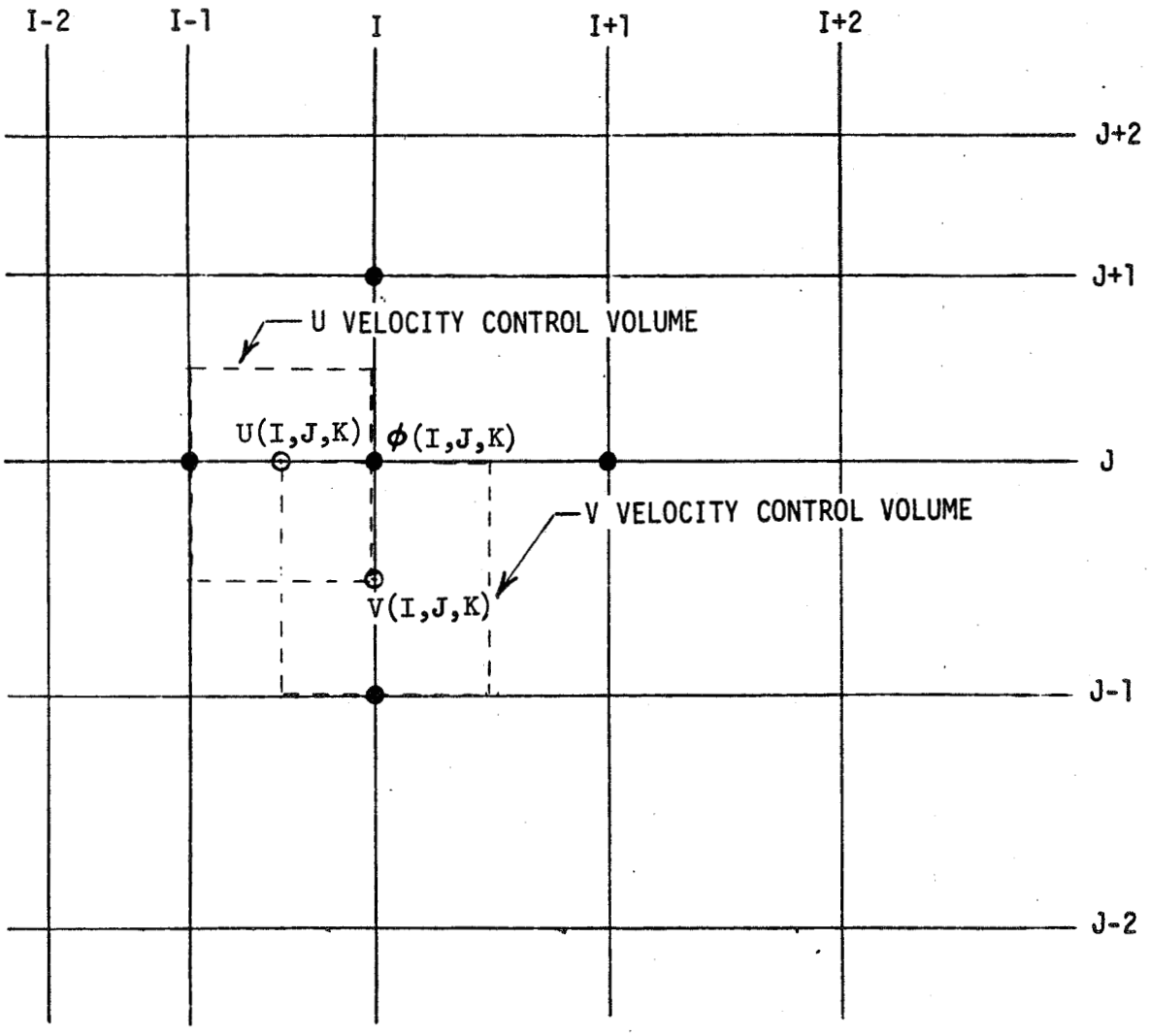

FIG. A-4 STORAGE LOCATIONS FOR AXIAL (U) AND RADIAL (V) VELOCITIES RELATIVE TO SCALAR (ϕ) GRID SYSTEM IN X-Y PLANE

APPENDIX B

DESCRIPTION OF 3D-TEACH

B.1 Description of Aerothermal Model

3D-TEACH is a computer code that can solve fully three-dimensional fluid dynamics problems. It can handle axisymmetric, planar, or three-dimensional, elliptic, turbulent flows. It is one of a family of such codes with titles 2D-TEACH, 2D(C)-TEACH, 3D-TEACH and, 2D-PREACH.

The input to all of these codes is generalized such that different problems can be run without the need for Fortran programming between problems. Also, the physical models used can be turned on or off by input command. These collective features result in an extremely flexible system.

The codes form a family in that:

a) As computer codes they are written with the same format, menus and commands such that an operator trained to run 2D-TEACH can easily run 3D-TEACH.

b) All codes have an interactive nature using the IBM Conversational Monitor System (CMS), and use prompts and cautions to ensure smooth execution of a case. The operator has the choice of either CMS or Batch running. The recommended procedure is to set up a case and get it running on CMS, then switch it to Batch to complete execution. File modification and selection of running mode is identical for all codes.

c) The same basic equations are solved and the same physical models are used, together with solution algorithms, in all codes such that regression is possible. This means that the same two-dimensional problem can be solved on 2D-TEACH and 3D-TEACH, and the same results will be achieved. The only difference between the 2D-TEACH and 3D-TEACH is the additional dimension available in the three-dimensional code. Also, the post-processors available with 3D-TEACH are necessarily more comprehensive than those with 2D-TEACH, in order to adequately display the results.

The acronym TEACH (Teaching Elliptic Axisymmetric Characteristics Heuristically) represents a generic solution technique and these codes represent current production state-of-the-art calculations in terms of equations solved, physical models used, discretization of the equations, and solution algorithms. They are not perfect, but are a marked advance on one-dimensional flow calculations and global modeling that formed the previous capability. The structure of the codes has been made such that modular replacement can be carried out as better models and solution algorithms are developed, while the basic framework and operational features remain.

The 2D-PREACH code is similar in concept to the others, but uses different solution procedures. It is not considered further here.

B.2 Outline of Calculation Procedure

B.2.1 Equations to Be Solved

The combustion process is an extremely complex turbulent flow. It is a somewhat daunting task to describe such a random flow of chemically active eddy structures in terms that can be currently solved and can provide useful answers for the designer of practical equipment.

Currently, the most practical approach is to stay within the framework of continuum mechanics and to use a statistical description of the turbulence, coupled with the accepted Eulerian description provided by the Navier-Stokes equations of motion. Hence, an instantaneous quantity is described as the sum of a time-averaged value and a random, fluctuating value.

When the statistical description of an instantaneous quantity is substituted into the Navier-Stokes equations (Reference B-1) and time averaged, the resulting equation set is known as the Reynolds equations (Reference B-2). These equations are similar to the Navier-Stokes equations except that time-averaged quantities are used, and for the appearance of time-averaged correlations of fluctuating quantities.

Turbulent motions increase the apparent viscosity of a fluid by some orders of magnitude since there is a continuous transfer of energy from the mean flow into large eddies and thence, cascading down through progressively smaller eddies, to the molecular level where the energy is dissipated as heat. If laminar diffusion terms are therefore very much smaller than turbulent diffusion terms, then neglect of fluctuations in laminar viscosity is permissible. This results in simplification of the Reynolds equations. It is a frequently used practice (Reference B-3) to also neglect terms involving fluctuating density, although this implies that temperature differences in the flow are not large. This practice also results in simplification of the Reynolds equations.

The simplified Reynolds equations are expressed in terms of time-mean quantities and also cross-correlations of fluctuating velocities such as $u_i'u_j'$. These terms are known as the Reynolds stresses, and result in a closure problem. Turbulence modeling provides the necessary descriptions of the Reynolds stresses in known or determinable quantities. When the flow consists of more than one chemical species, modeling is required also for the turbulent mass flux $u_j'm_l'$. These terms arise from applying the statistical treatment of turbulence to an instantaneous species transport equation. The instantaneous energy equation is given the same treatment.

To model the turbulent mass fluxes it was assumed that, similar to molecular Schmidt and Prandtl numbers, there are turbulent Schmidt and Prandtl numbers that relate turbulent mass and heat diffusivities to momentum diffusivity. Closure to the Reynolds equations was provided by a particular turbulence model known as the two-equation or K- model. It relies on the eddy viscosity concept. Finally, the modeled equations were algebraically manipulated into a general form in cylindrical coordinates:

$$\frac{\partial}{\partial x}(\bar{\rho}\bar{u}\bar{\phi}) + \frac{\partial}{r\partial r}(r\bar{\rho}\bar{v}\bar{\phi}) + \frac{\partial}{r\partial\theta}(\bar{\rho}\bar{w}\bar{\phi}) - \frac{\partial}{\partial x}\left(\Gamma_{eff,\phi}\frac{\partial\bar{\phi}}{\partial x}\right) - \frac{\partial}{r\partial r}\left(r\,\Gamma_{eff,\phi}\cdot\frac{\partial\bar{\phi}}{\partial r}\right) - \frac{\partial}{r\partial\theta}\left(\frac{1}{r}\,\Gamma_{eff,\phi}\,\frac{\partial\bar{\phi}}{\partial\theta}\right) = S_{\phi} \qquad \text{B.1}$$

where:

ϕ = any of the independent variables

$\Gamma_{eff,\phi}$ = an appropriate turbulent exchange coefficient, depending on what ϕ represents

S_{ϕ} = a so-called "source term" which lumps together all other terms in a given equation not included in the first four terms of Equation B.1.

The equation given is for steady state flow. Reynolds averaging does result in the equations retaining time-dependent terms, but these have been dropped. This was done for two reasons: (1) compatibility with the present design system and (2) time averaging precludes dynamic behavior other than that induced deliberately through one of the independent variables.

By way of example, Figure B-1 gives the values of some of the items in Equation B-1.

EQUATION	ϕ	$\Gamma_{Eff,\phi}$	S_ϕ
CONTINUITY	1	0	0
x-MOMENTUM	$\bar{u}$	μ_{Eff}	$\bar{\rho}g_x - \frac{\partial \bar{p}}{\partial x} + \frac{\partial}{\partial x}\left(\mu_{Eff}\frac{\partial \bar{u}}{\partial x}\right) + \frac{\partial}{r\partial r}\left(\mu_{Eff} r \frac{\partial \bar{v}}{\partial x}\right) - \frac{2}{3}\frac{\partial}{\partial x}(\mu_{Eff}\nabla\cdot\vec{v}) + \frac{\partial}{r\partial\theta}\left(\mu_{Eff}\frac{\partial \bar{w}}{\partial x}\right)$
r-MOMENTUM	$\bar{v}$	μ_{Eff}	$\frac{-\partial \bar{p}}{\partial r} + \bar{\rho}g_r + \frac{\partial}{\partial x}\left(\mu_{Eff}\frac{\partial \bar{u}}{\partial r}\right) + \frac{\partial}{r\partial r}\left(r\mu_{Eff}\frac{\partial \bar{v}}{\partial r}\right) - \frac{\partial}{\partial r}\left(\frac{2}{3}\mu_{Eff}\nabla\cdot\vec{v}\right) + \frac{\partial}{r\partial\theta}\left(\mu_{Eff}\frac{\partial \bar{w}}{\partial r}\right) + \frac{\bar{\rho}\bar{w}^2}{r} - \frac{2\mu_{Eff}\bar{v}}{r^2} - \frac{2\mu_{Eff}}{r^2}\frac{\partial \bar{w}}{\partial\theta} - \frac{1}{r}\frac{\partial}{r\partial\theta}(\mu_{Eff}\bar{w})$
θ-MOMENTUM	$\bar{w}$	μ_{Eff}	$\frac{-\partial \bar{p}}{r\partial\theta} + \frac{\partial}{r\partial\theta}\left(\mu_{Eff}\frac{\partial \bar{w}}{\partial\theta}\right) + \frac{\partial}{\partial x}\left(\mu_{Eff}\frac{\partial \bar{u}}{r\partial\theta}\right) + \frac{\partial}{\partial r}\left(\mu_{Eff}\frac{\partial \bar{v}}{r\partial\theta}\right) - \frac{2}{3}\frac{\partial}{r\partial\theta}(\mu_{Eff}\nabla\cdot\vec{v}) + \frac{2\mu_{Eff}}{r}\frac{\partial \bar{v}}{r\partial\theta} - \frac{\bar{\rho}\bar{v}\bar{w}}{r} - \frac{\bar{w}}{r^2}\frac{\partial}{\partial r}(\mu_{Eff} r)$
TURBULENCE ENERGY	K	μ_{Eff}/σ_K	$\mu_{Eff}\left[2\frac{\partial \bar{v}}{r\partial\theta}\frac{\partial \bar{w}}{\partial r} + 2\frac{\partial \bar{w}}{\partial x}\frac{\partial \bar{u}}{r\partial\theta} + \left(\frac{\partial \bar{u}}{r\partial\theta}\right)^2 + \left(\frac{\partial \bar{v}}{r\partial\theta}\right)^2 + 2\left(\frac{\partial \bar{w}}{r\partial\theta}\right)^2\right] + \mu_{Eff}\left[2\left(\frac{\partial \bar{w}}{r\partial\theta}\frac{\bar{v}}{r} - \frac{\partial \bar{v}}{r\partial\theta}\frac{\bar{w}}{r}\right) + 2\frac{\bar{v}}{r}\frac{\partial \bar{w}}{r\partial\theta}\right]$
ENERGY DISSIPATION	ϵ	$\mu_{Eff}/\sigma_\epsilon$	$C_{\epsilon 1}\frac{\epsilon}{K}\mu_{Eff}\left[2\frac{\partial \bar{v}}{r\partial\theta}\frac{\partial \bar{w}}{\partial r} + \left(\frac{\partial \bar{u}}{r\partial\theta}\right)^2 + 2\frac{\partial \bar{w}}{\partial x}\frac{\partial \bar{u}}{r\partial\theta} + \left(\frac{\partial \bar{v}}{r\partial\theta}\right)^2\right] + C_{\epsilon 3}\frac{\epsilon}{K}\left[2\mu_{Eff}\left(\frac{\partial \bar{w}}{r\partial\theta}\right)^2 - \frac{2}{3}\nabla\cdot\vec{v}(\mu_{Eff}\nabla\cdot\vec{v} + \bar{\rho}K)\right] + C_{\epsilon 1}\frac{\epsilon}{K}\mu_{Eff}\left[2\left(\frac{\partial \bar{w}}{r\partial\theta}\right)\frac{\bar{v}}{r} - \left(\frac{\partial \bar{v}}{r\partial\theta}\right)\frac{\bar{w}}{r} + 2\left(\frac{\partial \bar{w}}{r\partial\theta}\right)\frac{\bar{v}}{r} + (\nabla\cdot\vec{v})k\right] - C_{\epsilon 2}\bar{\rho}\frac{\epsilon^2}{K}$

where $\nabla\cdot\vec{v} = \frac{\partial \bar{u}}{\partial x} + \frac{1}{r}\frac{\partial(r\bar{v})}{\partial r} + \frac{\partial \bar{w}}{r\partial\theta}$

C_{ε_3} is an additional constant, presently taken as being equal to C_{ε_1}.

Figure B-1 Summary of Some of the Equations Solved in 3D-TEACH

B.2.2 Numerical Approach to Equation Solution

The simultaneous set of main and auxiliary equations to be solved in a turbulent reacting flow with a liquid-fuel spray contains a significant number of individual equations, most of which are either ordinary or partial differential equations, and which are nonlinear. Numerical solution of these equations is necessary. Rearrangement into the general form represented by Equations B-1 and B-2 enables one solution algorithm to be used for all equations.

Conventional numerical methods available to solve equations of these types can be broadly divided into finite difference and finite element methods, although the dividing line is not distinct. Finite differences have a considerable background, and most solution approaches utilize this method.

The finite difference analog of the differential equations is obtained by overlaying a computational mesh on the flow domain, and obtaining the basic finite difference form of the partial derivatives for every node of the mesh from a control volume approach (Reference B-4). The finite difference expressions, when substituted back into the differential equations, yield a set of linearized, algebraic equations for every node of the mesh. Thus, there are as many sets of equations as there are nodes in the calculation domain. These sets, along with the problem boundary conditions, can then be solved to give solutions for the entire flow field.

Standard numerical techniques can be employed to solve the finite difference forms of the differential equations (Reference B-5). A steady-state implicit solution method is often used (Reference B-6); an initial guess is made of the field variables, and these guesses are iteratively updated until the solutions have converged. Convergence is deemed to have been obtained when the absolute sums of the residuals of each variable over the whole grid goes below a specified value.

The relevant equations describing the flow motions, the physical models, and the solution techniques are assembled into the computer codes to carry out direct flow simulations on high-speed, large-core digital computers. Figure B-2 presents a flow diagram describing the calculation procedure, showing the assembly of the equations, the utilization of physical modeling, the computer solution, and the output for design use. The 3D-TEACH code conforms to this organization.

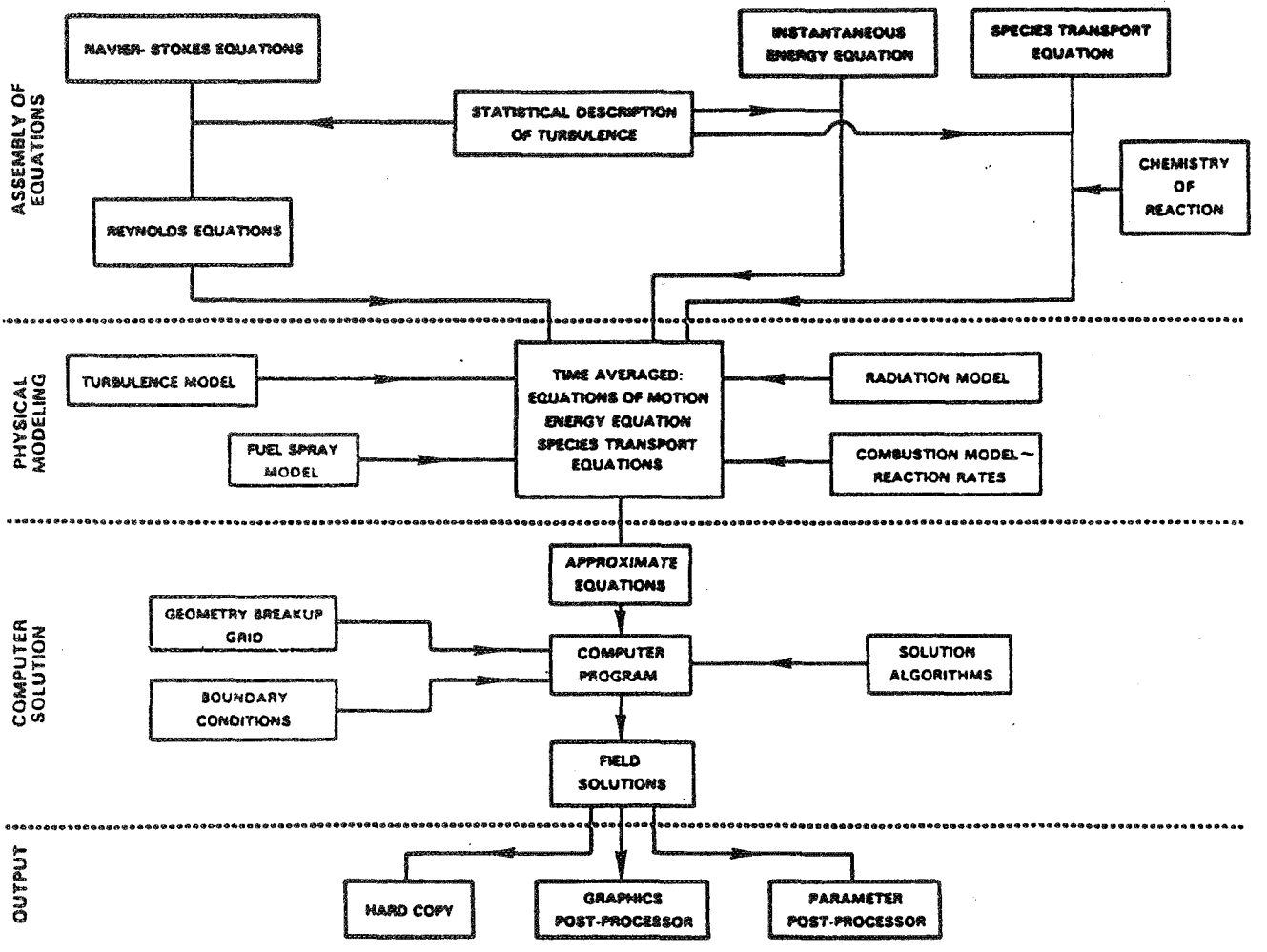

Figure B-2 Flow Diagram of Calculation Procedure

B.3 Solution Procedure

With reference to Figure B-2, assembly of the equations governing the problem has been briefly described. The details of the computer solution of the resulting equation sets are to be described.

Rearrangement of the equations into the general form represented by Equation B-1 enables one solution algorithm to be used for all equations. The equation set is solved using a steady state, implicit, finite difference numerical procedure. Initial guesses are made of the field variables, and these guesses are iteratively updated until the solutions have converged. Convergence is deemed to have been obtained when the absolute sum of the residuals over the whole grid of each variable goes below a specified value.

B.3.1 Discretization of the Equations

The finite difference analog of the difference equations is obtained by overlaying a computational mesh on the flow domain to be calculated, and obtaining the basic finite difference form of the partial derivatives for every node of the mesh from a control volume approach, (Reference B-4). The finite difference expressions, when substituted back into the differential equations, yield a set of linearized, algebraic equations for every node of the mesh. To demonstrate, first in two-dimensions, Figure B-3 illustrates the mesh and the control volume established about a considered node, P. The control volume approach is based on the satisfaction of macroscopic physical laws such as conservation of mass, momentum and energy. The conservation property is essential when combustion is taking place.

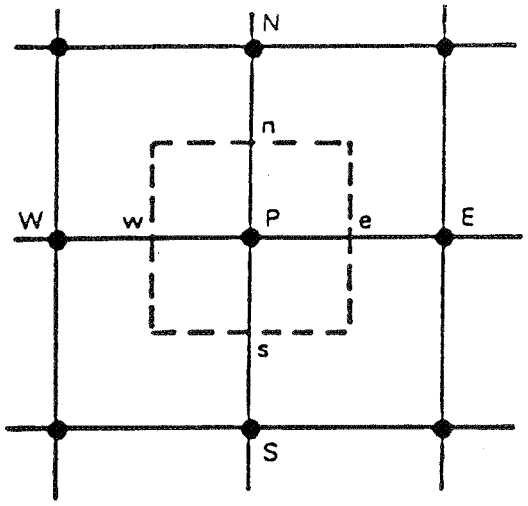

Figure B-3 Control Volume for the Finite Difference Scheme

The code is written in both cylindrical and cartesian coordinates. The grid system consists of a set of coordinate lines intersecting in the x-r, x-Θ and r-Θ planes for the cylindrical system. In the cartesian system the grid is formed by the intersection of x-y, x-z, and y-z plane lines. The intersections of these lines form the grid nodes at which all scalar properties are stored. Vector quantities are stored midway between nodes. Figure B-4 gives the finite difference grid control volumes for the scalar quantities and storage locations for the velocities in both coordinate systems. Note that compared to Figure B-3, there are two additional neighboring nodes, F and B, denoting Front and Back nodes in the z or Θ direction. The faces of the scalar control volume are denoted by lower case letters. Figure B-5 shows typical scalar control volumes in perspective and gives the face areas and volume. Since the velocity components are located midway between the grid nodes, the control volumes for velocity components are formed by planes passing through the grid lines. Note that since the control volumes for the velocity components are staggered (Figure B-6) the areas and volumes for these control volumes will be different from those of the scalar control volume.

The finite difference form of the general partial differential equation is derived by supposing that each variable is enclosed in its own control volume, as illustrated in Figures B-3-6. The general ϕ transport equation has a source term . This is expressed in linearized form and integrated over the control volume. The remainder of the transport equation is also integrated over the control volume, and added to the integrated source term. This yields,

$$C_E \phi_e - C_W \phi_w + C_N \phi_n - C_S \phi_s + C_B \phi_b - C_F \phi_f = D_E (\phi_E - \phi_p) - D_W(\phi_p - \phi_W)$$
$$+D_N (\phi_N - \phi_p) - D_S (\phi_p - \phi_S) + D_B (\phi_B - \phi_p) - D_F (\phi_p - \phi_F) + (S_u + S_p \phi_p)$$

B2.

In the above equation the convection coefficients are defined as,

$$C_E = (\bar{\rho}\,\bar{u})_e\, a_e \quad ; \quad C_F = (\bar{\rho}\,\bar{w})_f\, a_f \qquad \text{etc.,}$$

and the diffusion coefficients are defined as:

$$D_E = \left(\frac{\Gamma_{eff,\phi}}{\Delta x}\right)_e \cdot a_e \quad ; \quad D_F = \left(\frac{\Gamma_{eff,\phi}}{r\,\Delta\,\theta}\right) \cdot a_f \qquad \text{etc.}$$

a_e, a_f etc. are the areas of the cell faces

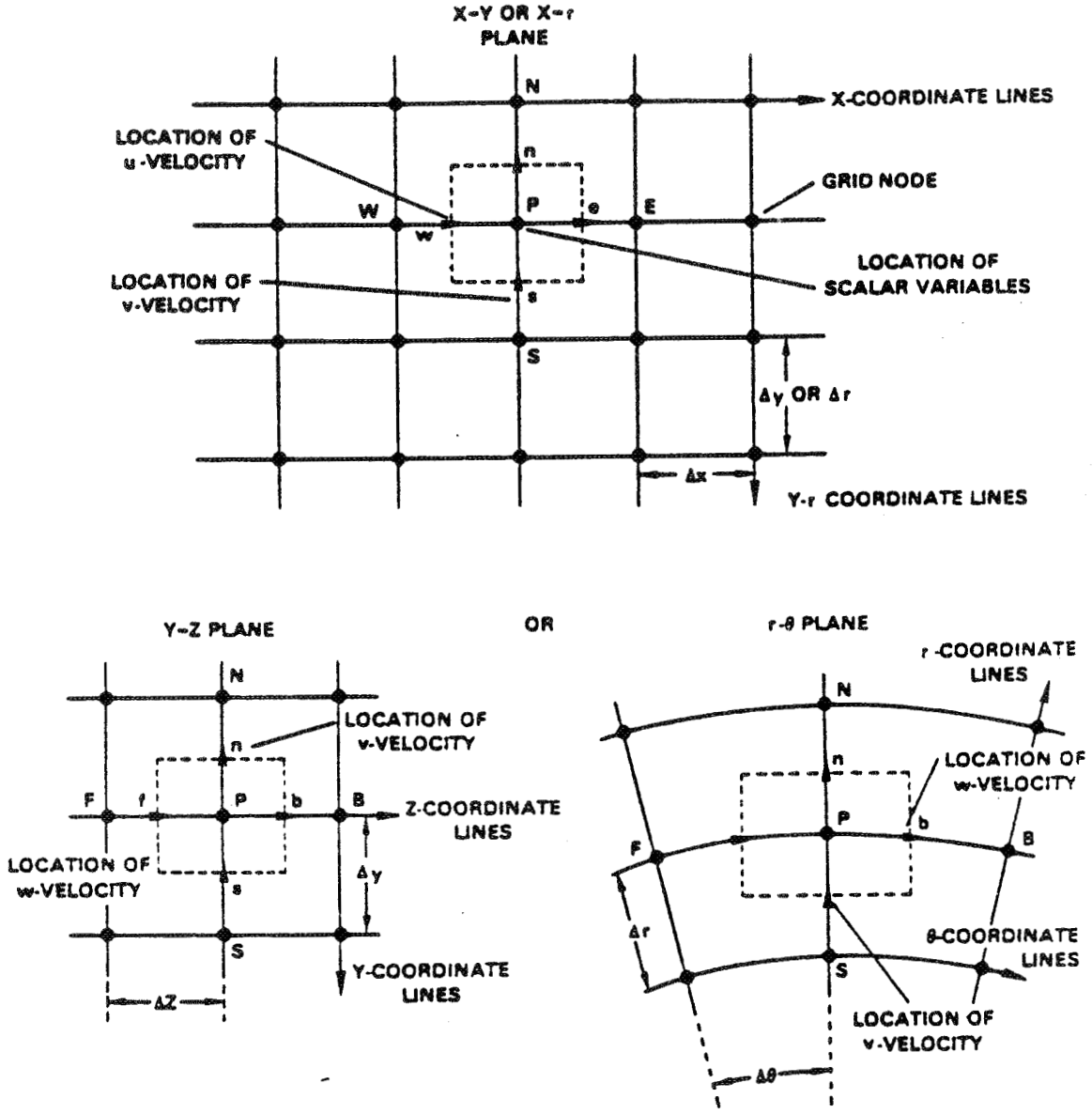

Figure B-4 3-D TEACH: Finite Difference Grid in Cylindrical and Cartesian Coordinate Systems

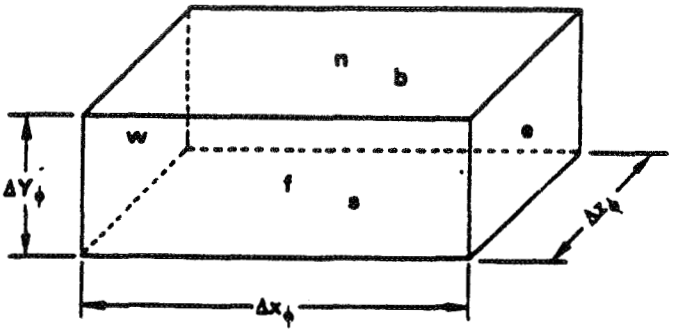

CONTROL VOLUME IN THE CARTESIAN SYSTEM

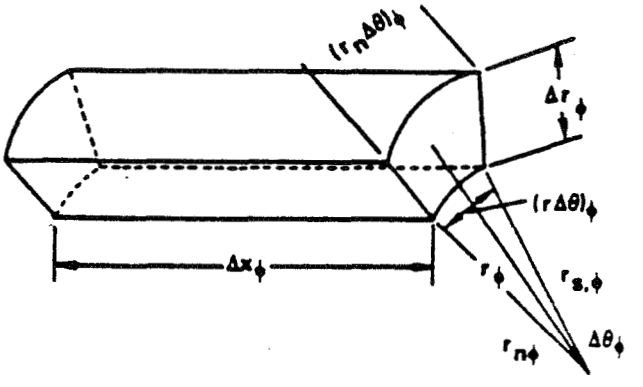

CONTROL VOLUME IN THE CYLINDRICAL SYSTEM

AREA	CARTESIAN	CYLINDRICAL	REMARKS
$a_{w\phi}$ -	$(\Delta Y \Delta Z)_\phi$	$(\Delta r \Delta\theta r)_\phi$	Cartesian system can be obtained from cylindrical system by putting r = 1. $\Delta\theta = \Delta Z$.
$a_{e\phi}$ -	$(\Delta Y \Delta Z)_\phi$	$(\Delta r \Delta\theta r)_\phi$	
$a_{n\phi}$ -	$(\Delta X \Delta Z)_\phi$	$(\Delta r \Delta\theta r_n)_\phi$	
$a_{s\phi}$ -	$(\Delta X \Delta Z)_\phi$	$(\Delta x \Delta\theta r_s)_\phi$	
$a_{f\phi}$ -	$(\Delta X \Delta Y)_\phi$	$(\Delta x \Delta r)_\phi$	
$a_{b\phi}$ -	$(\Delta X \Delta Y)_\phi$	$(\Delta x \Delta r)_\phi$	
Vol_ϕ -	$(\Delta X \Delta Y \Delta Z)_\phi$	$(\Delta x \Delta r \Delta\theta r)_\phi$	

Figure B-5 Perspective View of Scalar Control Volume, Giving Face Areas and Volume

c) X-Z PLANE

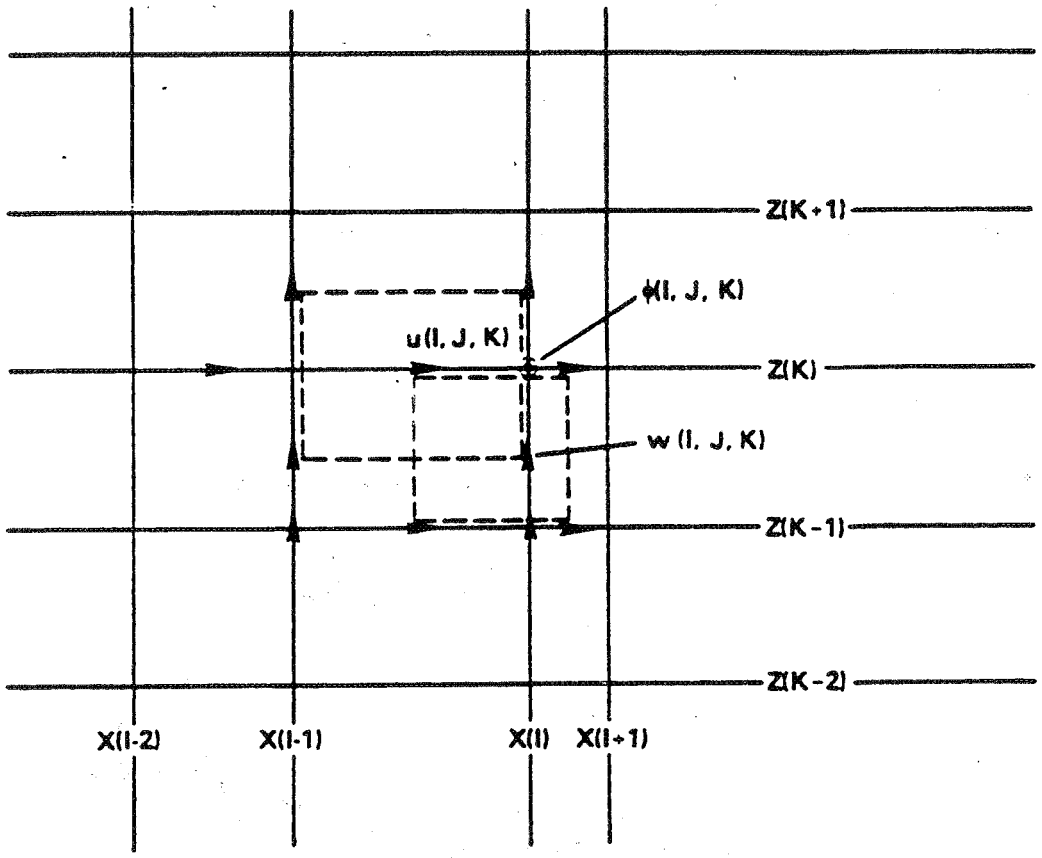

Figure B-6 Control Volumes for Velocity Components

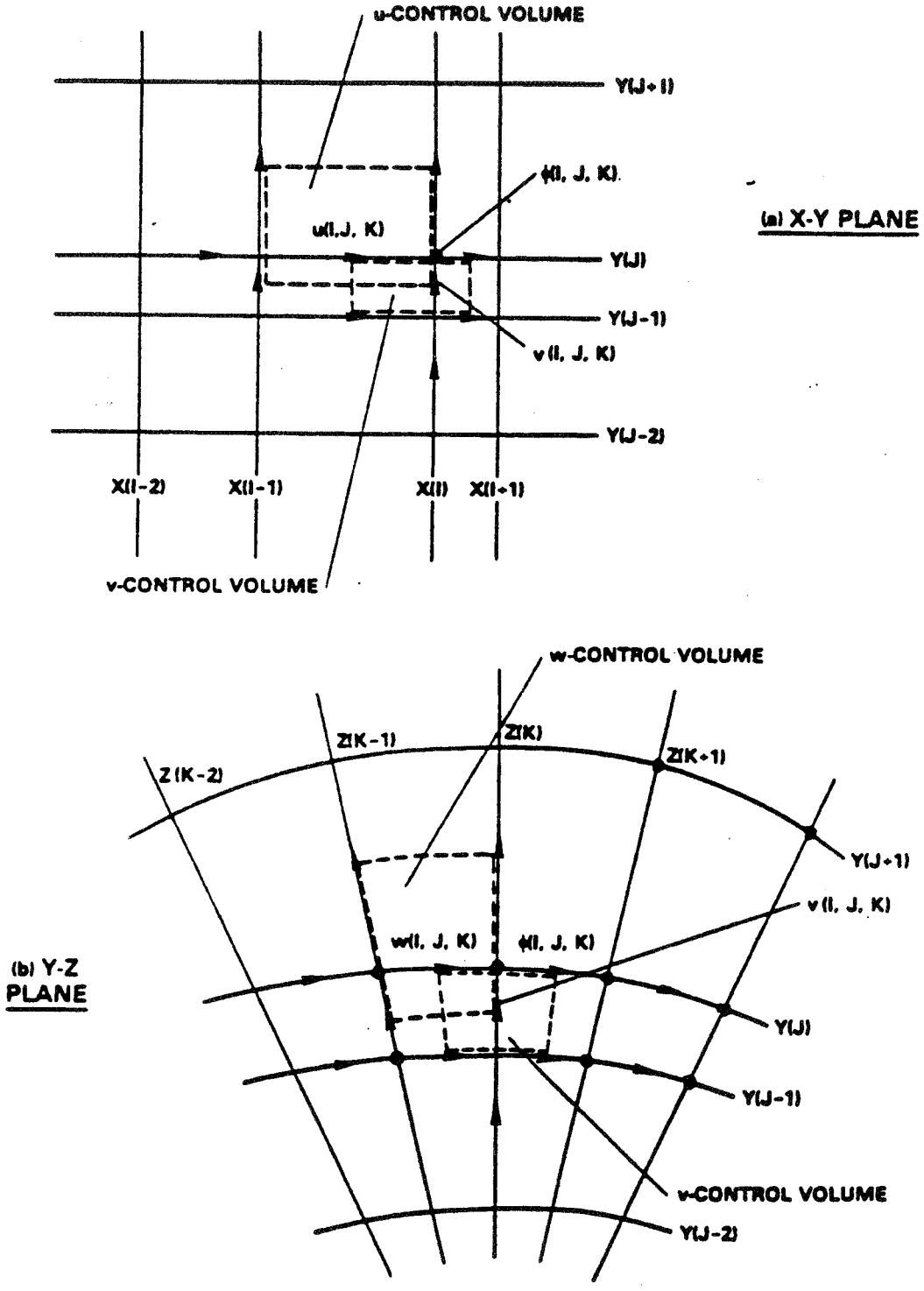

Figure B-6 Control Volumes for Velocity Components (Cont'd)

Certain weighting factors are introduced into the variation of ϕ , the variable being calculated, and with the help of continuity, Equation B-2 can be manipulated and normalized to give the form,

$$A_P \phi_P = A_N \phi_N + A_S \phi_S + A_N \phi_W + A_E \phi_E + A_F \phi_F + A_B \phi_B + S_u$$

where, B-3.

$$A_P = A_N + A_S + A_E + A_N + A_F + A_B - S_P$$

and Equation B-3 is the finite difference equation for ϕ , and the main coefficients are defined as,

$$A_N = 0 \text{ when } P_{e_N} < -2$$

$$A_N = D_N - \frac{C_N}{2} \text{ when } -2 \leq P_{e_N} \leq 2$$

$$A_N = C_N \quad \text{when} \quad P_{e_N} > 2$$

Similarly for A_S. A_E etc., where the cell Peclet number is defined as,

$$P_{e_N} = C_N/D_N \quad \text{etc.}$$

There are several differencing schemes that can be used to evaluate the weighting factors. The values of the coefficients A_N, A_S etc. above were obtained using Spaldings Hybrid Differencing Scheme (HDS), of Reference B-7.

The hybrid differencing scheme is unconditionally stable and the solution is bounded. It uses second order central differencing for convection and diffusion fluxes when the absolute value of cell Peclet number is less than or equal to two. When Peclet number is greater than two, first order upwind differencing is used for convection fluxes, and diffusion fluxes are neglected altogether. The switch of differencing is done both locally and directionally in the computational grid. Peclet number defines the relative importance of convective and diffusive transport.

The finite difference Equation B-3, derived in the previous section could be used to obtain the velocity if the pressure field were known a priori. Since the pressure field is unknown, an iterative solution procedure, SIMPLE (Reference B-8) is used. SIMPLE is an acronym for Semi Implicit Method for Pressure Linked Equations.

The essence of SIMPLE is that a pressure field is guessed, velocities are calculated from their finite difference equations, then the pressure and velocity fields are updated using a "pressure correction" equation which satisfies continuity. The procedure is repeated until the momentum and the continuity equations are adequately and simultaneously satisfied. The pressure correction equation can be derived from the continuity and momentum equations; the procedure is described below.

The finite difference form of the continuity equation can be written as:

$$(\bar{\rho}\ \bar{u})_e\, a_e - (\bar{\rho}\ \bar{u})_w\, a_w + (\bar{\rho}\ \bar{v})_n\, a_n - (\bar{\rho}\ \bar{v})_s\, a_s + (\bar{\rho}w)_f\, a_f - (\bar{\rho}w)_b\, a_b = 0 \qquad \text{B-4}$$

The momentum equations can be written as:

$$A_p\, v_p^* = A_N\, v_N^* + A_S\, v_S^* + A_E\, v_E^* + A_W\, v_W^* + A_F\, v_F^* + A_B\, v_B^* + a_s\,(P_S^* - P_p^*)$$

$$A_p\, u_p^* = A_N\, u_N^* + A_S\, u_S^* + A_E\, u_E^* + A_W\, u_W^* + A_F\, u_F^* + A_B\, u_B^* + a_w\,(P_W^* - P_p^*)$$

$$A_p w_p^* = A_N w_N^* + A_S w_S^* + A_E\, w_E^* + A_W w_W^* + A_F w_F^* + A_B w_B^* + a_b\,(P_F^* - P_p^*)$$

In the above equations the pressure term has been separated from the source term and the (*) superscript denotes the values obtained from solving the momentum equations using the guessed pressure. An incorrect guess will give rise to a "mass source", Mp, in each cell because the continuity equation will not be satisfied. The mass source can be found by using Equation B-4. Hence

$$Mp = (\bar{\rho}\ u^*)_e\, a_e - (\bar{\rho}\ u^*)_w\, a_w + (\bar{\rho}\ v^*)_n\, a_n - (\bar{\rho}\ v^*)_s\, a_s - (\bar{\rho}w)_f a_f + (\bar{\rho}w)_b a_b$$

If the above equation is subtracted from Equation B-4.,

$$-Mp = (\bar{\rho}\ u')_e a_e - (\bar{\rho}\ u')_w\, a_w + (\bar{\rho}\ v')_n\, a_n - (\bar{\rho}\ v')_s\, a_s - (\bar{\rho}w')_f a_f + (\bar{\rho}w')_b a_b$$

B-5.

where $u_e' = (\bar{u} - u^*)_e$ etc.

The above velocity corrections can be calculated from the linearized momentum equations.

$$Ap\ up' = a_w\,(P_W' - Pp')$$

B-6

Note that u_p' in the momentum equation control volume is u_w' for the continuity control volume and similarly for v_p' etc. On substitution of Equation B-6 in Equation B-5 and simplification,

$$A_P P_P' = A_N P_N' + A_S P_S' + A_W P_W' + A_E P_E' + A_F P_F' + A_B P_B' + S_u \qquad \text{B-7}$$

where

$$A_W = (a_W/A_P)$$

$$S_u = - M_P$$

$$A_P = A_N + A_S + A_W + A_E + A_F + A_B$$

Equation B-7 is called the pressure correction equation which is solved to obtain corrected velocities and pressures,

$$\bar{u}_e = u_e^* + u_e'$$

$$\bar{P}_e = P_e^* + P'$$

etc.

The difference equation for P' (Equation B-7) is in the same form as the difference equations for ϕ (Equation B-3) an d ence a single solution algorithm can be used to solve all difference equations embodied in the numerical method.

Since the SIMPLE procedure computes the variable fields successively it is highly flexible with respect to the methods of solution which it will admit for the difference equations. At present the following line by line iteration method is employed. This method is also known as Alternating Direction Implicit Method (Ref. B-9). The ADI methods were initially formulated for unsteady equations; their adaptation to steady state equations is sometimes also known as Alternating Direction Iterative Methods.

The finite difference Equation (B-3) to be solved is

$$A_P \phi_P = A_N \phi_N + A_S \phi_S + A_W \phi_W + A_E \phi_E + A_F \phi_F + A_B \phi_B + S_u$$

where ϕ stands for u, v, p, K, ε , and H successively. This equation can be recast in the following form

$$A_P \phi_P = A_N \phi_N + A_S \phi_S + C'$$

or

$$A_P \phi_j = A_N \phi_{j+1} + A_S \phi_{j-1} + C_j'$$

B-8.

To solve the equations for points on each line (e.g., N-S line) values on neighboring lines are assumed to be temporarily known. The equation for each point on the N-S line then reduces to one where only three values (ϕ_P, ϕ_N, ϕ_S in Equation B-8) are unknown. An equation of this type can then be solved by the Tri-Diagonal Matrix Algorithm (TDMA), which is explained below.

Equation B-8 can be rearranged for the j^{th} point as

$$\phi_j = B_j \phi_{j+1} + C_J \phi_{j-1} + D_j$$

where

$$B_j = A_N/A_P \quad , \quad C_j = A_S/A_P$$

$$D_j = (A_W \phi_W + A_E \phi_E + A_F\phi_F + A_B\phi_B + S_u)/A_P$$

The points on the computation grid range from 1 to Nj in the N-S direction with points 1 and Nj on the boundaries. Since the boundary values ϕ_1 and ϕ_{NJ} are known, equations for ϕ_2 to ϕ_{NJ-1} are solved. The set of equations then becomes:

$$\phi_2 = B_2 \phi_3 + C_2 \phi_1 + D_2$$

$$\phi_3 = B_3 \phi_u + C_3 \phi_2 + D_3$$

$$\vdots$$

$$\phi_{Nj-1} = B_{Nj-1} \phi_{Nj} + C_{Nj-1} \phi_{Nj-2} + D_{Nj-1}$$

B-9

Now, since ϕ_1 is known, ϕ_2 can be eliminated from Equation B-9 and so on, yielding a general recurrence relation

$$\phi_j = A_j \ \phi_{j+1} + D_j' \qquad \text{B-10}$$

To get the relation for A_j and D_j' Equation B-10 is written as

$$\phi_{j-1} = A_{j-1} \cdot \phi_j + D_{j-1}'$$

Now putting in the value of ϕ_j

$$\phi_j = \left(\frac{A_N}{A_P - A_S \cdot A_{j-1}} \right)_j \phi_{j+1} + \left[\frac{C_j' + A_S D_{j-1}'}{A_P - A_S A_{j-1}} \right]_j \qquad \text{B-11}$$

Comparing Equation B-10 and B-11 yields coefficients for the recurrence formula

where $$A_j = \left(A_N / (A_P - A_S A_{j-1}) \right)_j \qquad \text{B-12}$$

$$D_j' = \left((A_S D_{j-1}' + C_j') / (A_P - A_S A_{j-1}) \right)_j \qquad \text{B-13}$$

Using Equations B-12 and B-13, ϕ_j can be calculated from Equation B-10. Having solved for ϕ_j on one N-S ϕ_j's on the next N-S line are solved and so on until the entire solution domain is swept. The same treatment is then applied in the W-E direction and finally, in the F-B direction. It is usually necessary to sweep between 1 and 3 times per iteration for optimum solution time.

The coefficient matrix formed by the finite difference equation of ϕ should satisfy the stability condition,

$$A_P \geq \sum_n |A_n|$$

Now

$$A_P = \sum_n A_n - S_P$$

So if $S_p \leq 0$

the above criteria is satisfied. In the solution procedure care is taken so that Sp is always less than or equal to zero.

In the process of the computations, convergence is assessed at the end of each iteration on the basis of the "Residual Source" criterion. The residual source R_ϕ is defined as

$$R_\phi = A_p \phi_p - \sum_n A_n \phi_n - S$$

It is required that:

$$\Sigma | R_\phi | < \epsilon R_{\phi\,Ref}$$

for each finite difference equation.

$R_{\phi\,Ref}$ is the fixed flux of the relevant extensive property fed into the domain of calculation, and ε is of the order of 10^{-3}.

When it is the equations for mass fraction of species that are being solved an additional convergence criterion requires that the sum of the mass fractions at each node is $\leq (1 + \varepsilon)$.

When the flow is of variable density it is initially required that the change in density in one iteration at every node must also be less than ε

or

$$\left(\rho_{ij}^{new} - \rho_{ij}^{old} \right) / \rho_{ij}^{old} < \epsilon$$

Since the enthalpy values in the calculation domain do not conform with the species mass fractions during the first few iterations, temperature and density are not updated for the first 10 - 25 iterations. If the density gradients are steep, density is updated every second or third iteration after the first update.

A typical convergence plot is shown in Figure B-7.

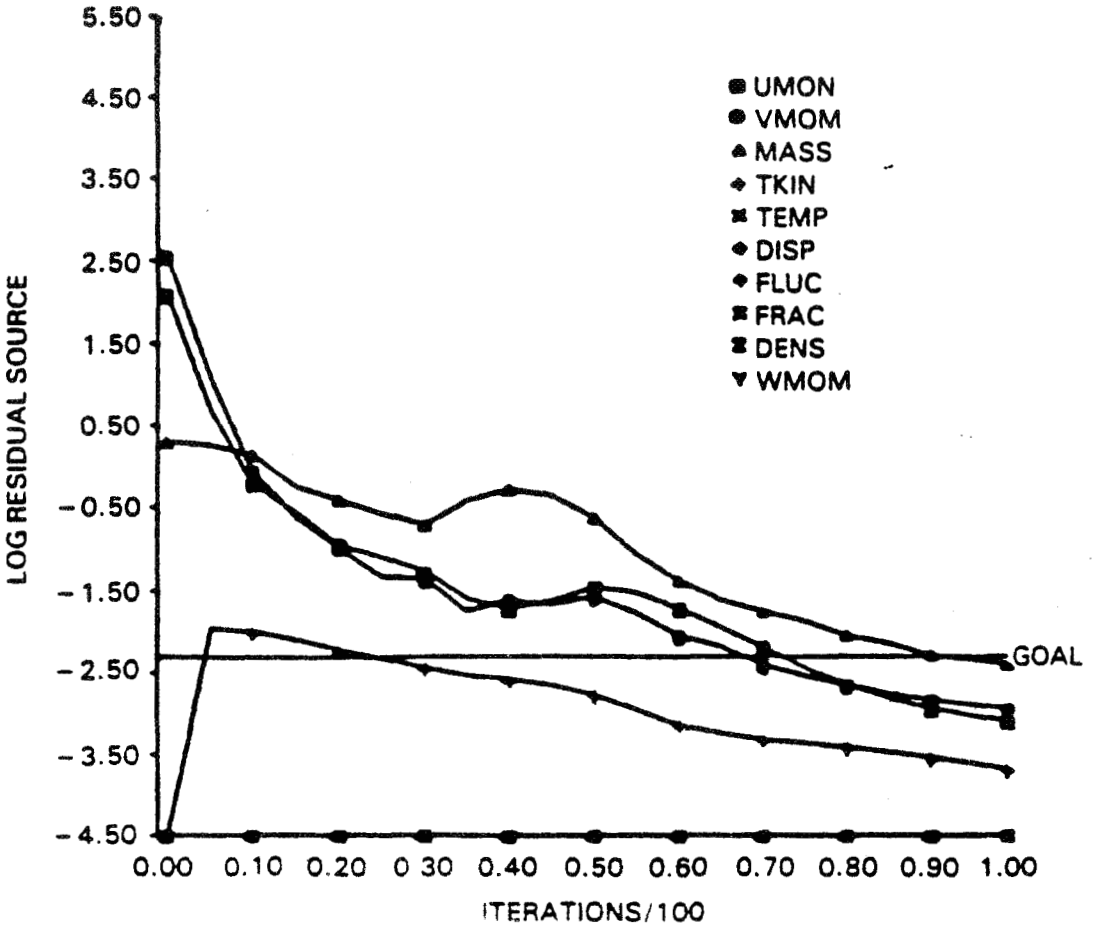

Figure B-7 Typical Convergence Plot

Since the finite difference equations are nonlinear in nature the convergence is facilitated and sometimes divergence is avoid e by under-relaxing the value of being calculated as:

$$\phi_p^R = F\phi_p^{New} + (1-F)\phi_p^{Old}$$

B-14

where F is an under-relaxation factor which is less than one.

The way in which the above relation is introduced into the numerical procedure is as follows:

$$A_p^R = A_p/F$$

$$S_u^R = S_u + (1 - F)\, A_p^R\, \phi^{Old}$$

B-15

It can easily be shown that the effect of introducing the above modifications is to under-relax ϕ_p according to Equation B-14. From Equation B-3 we have

$$\phi_p^{New} = \frac{\sum_n A_n \phi_n + S_u}{Ap} \qquad \text{B-16}$$

putting in the under-relaxation factors,

$$\phi_p^R = \frac{\sum_n A_n \phi_n + S_u^R}{A_p^R} \qquad \text{B-17}$$

putting the value of A_p^R and S_u^R from Equations B-14 and B-15 in B-16,

$$\phi_p^R = \frac{\sum_n A_n \phi_n + S_u + (1-F) A_p^R \phi_p^{Old}}{A_p^R} \qquad \text{B-18}$$

$$\phi_p^R = \left(\frac{\sum_n A_n \phi_n + S_u}{Ap} \right) F + (1-F) \phi_p^{Old} \qquad \text{B-19}$$

$$\phi_p^R = \phi_p^{New} F + (1-F) \phi_p^{Old} \qquad \text{B-19}$$

It should also be noted that the effect of under-relaxation is to make the coefficient matrix more diagonally dominant.

The various steps in the numerical procedure can now be summarized as follows:

1. Guess fields for all variables.

2. Assemble coefficients of momentum equations and solve for U* and V* using prevailing pressures.

3. Solve the pressure correction equation and update velocities and pressures.

4. Solve equations for other variables.

5. Update fluid properties such as viscosity and density.

6. Test for convergence. If not attained use prevailing fields as new guesses and repeat from step 2 until convergence is attained.

In general, it is necessary to specify ϕ or its gradient at the boundaries of the calculation domain. There are six types of boundaries that can be assigned to a fluid block:

1. Plane/axis of symmetry
2. Unspecified wall
3. Specified wall
4. Unspecified opening
5. Specified opening
6. Periodic

A specified boundary is one for which all boundary values such as velocities, temperatures, etc. are given. An unspecified boundary is one for which the boundary values are calculated by the code. If the flow structure is repeating, periodic can be used to compute only one segment.

On a plane/axis of symmetry the gradient of all ϕ's except v-velocity is put to zero; v-velocity itself is set to zero. It should be noted that the symmetry condition should be applied to all block faces which constitute the plane/axis of symmetry. Most walls are specified, with all velocities set to zero (no slip condition). A moving wall is modeled with the no slip condition by specifying nonzero velocities in the plane of the wall. A porous wall is modeled by specifying nonzero velocities normal to the plane of the wall. At the outflow, it is required that there be no negative axial velocity components. At high Reynolds numbers this requirement makes specification of boundary values of all ϕ except u redundant. The axial velocity is specified thus,

$$u_{ni,\,j} = u_{ni-1,\,j} + U_{INC} \qquad \text{B-21}$$

where ni is the outflow boundary and U_{INC} is calculated such that the total mass outflow is equal to mass inflow. Alternatively, if an exit velocity profile is known, it can be specified.

The calculation mesh is constrained by the coordinate system, which presently has been selected as orthogonal. Therefore, curvilinear geometries have to be represented in the form of discrete steps or "staircases." The specified blockage boundary condition permits this representation and allows inflow and outflow through elements of these staircases. In addition, the condition allows solid bodies to be placed inside the flowfield and to contain mass sources or sinks within them. This capability is written in generalized form and confers considerable geometric flexibility on the code without the need for interproblem reprogramming.

Adjacent to solid boundaries, the local Reynolds number of the flow based on local velocity and distance from the wall becomes very small and the two-equation turbulence model, which was developed for high Reynolds numbers, becomes inadequate. Although a version of the two equation model that can handle both high and very low local Reynolds numbers exists (Reference B-10), its application requires a large number of grid nodes (more than 30) in the wall layer. This is due to the steep gradients of properties in the wall region (Reference B-11).

To avoid these difficulties, it was argued that the flowfield in the calculation domain is not influenced to first order by the details of the flow at the walls (Reference B-12). Consequently, as a matter of computational efficiency and economy, the high Reynolds number version of the turbulence model was retained and a Couette-flow analysis was used to give an equilibrium boundary layer on all solid surfaces bounding the calculation domain. The resulting wall functions are used to link the walls to the near-wall nodes of the finite difference grid.

REFERENCES

B-1. Schlichting, H., Boundary Layer Theory, 7th Edition, McGraw-Hill, pp. 47-69, 1979.

B-2. Hinze, J. O., Turbulence, 2nd Edition, McGraw-Hill, 1975, pp. 20-24.

B-3. Gosman, A. D., Lockwood, F. C., and Syed, S. A., "Prediction of a Horizontal Free Turbulent Diffusion Flame", 16th Symposium (International) on Combustion, The Combustion Institute, pp. 1543-1555, 1976, (see discussion).

B-4. Roach, P. J., Computational Fluid Dynamics, Aermosa Publishers, New Mexico, 1976.

B-5. Carnahan, B., Luther, H. A., and Wilkes, J. O., Applied Numerical Methods, John Wiley a Sons, New York, 1969.

B-6. Richtmeyer, R. O., and Morton, K. W., Difference Methods for Initial Value Problems, Interscience Publishers Inc., New York, 1957.

B-7. Spalding, D. B., "A Novel Finite-Difference Formulation for Differential Expressions Involving Both First and Second Derivatives", Intl. J. Numerical Methods in Engineering, Vol. 4, pp. 551 1972.

B-8. Patankar, S. V. and Spalding, D. B., "A Calculation Procedure for Heat, Mass and Momentum Transfer in Three-Dimensional Parabolic Flows", Intl. J. Heat. Mass Transfer, Vol. 15, p. 1787, 1972

B-9. Paceman, D. W., and Rachford, H. H., Jr., "The Numerical Solution of Parabolic and Elliptic Differential Equations", J. Soc. Industrial Applied Math., Vol. 3, pp. 28-41, 1955.

B-10. Jones, W. P., and Launder, B. E., "The Prediction of Laminarization With a Two-Equation Model of Turbulence", Intl. J. Heat Mass Transfer, Vol. 15, pp. 301-319, 1969.

B-11. Launder, B. E., Priddin, C., and Sharma, B., "The Calculation of Turbulent Boundary Layers on Spinning and Curved Surfaces", Trans, ASME, J. Fluids Engineering, March, pp. 231-239, 1977.

B-12. Sturgess, G. J. and Syed, S. A., "Widely-Spaced Co-Axial Jet Diffusion Flame Combustor: Isothermal Flow Calculations Using the Two-Equation Turbulence Model", AIAA-20th Aerospace Sciences Meeting, Paper No. AIAA-82-0133, Orlando, Florida, January 1982.

DISTRIBUTION LIST

I. NASA	Copies
NASA Lewis Research Center 21000 Brookpark Road Cleveland, OH 44135	
Attn: Report Control Office MS 60-1	1
Technology Utilization MS 7-3	1
Library MS 60-3	1
D. Sokolowski MS 49-5	1
L. Schopen MS 501-11	1
P. Sockol MS 5-7	1
L. A. Diehl MS 501-6	2
R. Gaugler MS 6-10	1
R. E. Jones MS 6-11	1
E. J. Mularz MS 6-11	1
B. Miller MS 6-8	1
USAF Office MS 501-3	1
Propulsion Lab., USARTL (AVRADCOM) MS 302-2	2
Project Manager - Russ Claus MS 6-11	40
NASA Headquarters Attn: RTF/S. Wander 600 Independence Avenue, S.W. Washington, DC 20546	1
NASA Scientific & Technical Information Facility Attn: Accessioning Department P.O.. Box 8757 Baltimore/Washington International Airport MD 21240	25
NASA Langley Research Center Attn: Dr. H. Lee Beach Jr. MS 168 Hampton, VA 23665	1
NASA Ames Research Center Attn; Dr. H. Lee Beach Jr. NS-202A-1 Moffett Field, CA 94035	1

DISTRIBUTION LIST - Continued

II. OTHER GOVERNMENT AGENCIES	Copies
Air Force Office of Scientific Research Attn: Mr. Tischkoff Bolling AFB Washington, DC 20332	1
Sverdrup Corp. Attn: Library Arnold Air Force Station, TN 37389	1
Chief Army Research Office Attn: Dr. David M. Mann P.O. Box 12211 Research Triangle Park, NC 27709	1
Commander U.S. Army Aviation R&D Command Attn: DRDAV-EQP (Mr. Larry Bell) 4300 Goodfellow Blvd. St. Louis, MO 63120	1
Commander U.S. Army Fuels & Lubricants Research Lab. Southwest Research Institute Attn: Dr. C. Moses P.O. Drawer 28510 San Antonio, TX 78284	1
Defense Documentation Center Cameron Station 5010 Duke Street Alexandria, VA 22314	1
Director, Applied Tech. Laboratory Attn: DAVDL-ATL-AT (Mr. R. Bolton) U.S. Army Research & Tech. Lab. (AVRADCOM) Ft. Eustis, VA 23604	1
Director Applied Technology Laboratory Army Research & Technology Laboratory (AVRADCOM) ATTN: DAVDL-ATL-AT (Mr. John W. White) Fort Eustis, VA 23604	1
Environmental Protection Agency 2565 Plymouth Road Ann Arbor, MI 48105	1

DISTRIBUTION LIST - Continued

II. OTHER GOVERNMENT AGENCIES	Copies
Environmental Protection Agency Attn: Library Mail Drop 65 Research Triangle Park, NC 27111	1
Environmental Protection Agency Attn: W. S. Lanier Mail Drop 65 Research Triangle Park, NC 27111	1
Jet Propulsion Laboratory Attn: M. Clayton MS 125-224 4800 Oak Grove Drive Pasadena, CA 91103	1
Naval Air Propulsion Center Attn: Mr. Anthony Cifone PE-42 P.O. Box 7176 Trenton, NJ 08628	1
Naval Air Propulsion Center Attn: Mr. P. Karpovich, PE-71 P.O. Box 7176 Trenton, NJ 08628	1
Naval Ordnance Systems Command Attn: Mr. John W. Murrin Department of Navy Arlington, VA 20360	1
Wright-Patterson Air Force Base Attn: E. E. Bailey AFWAL/NASA-PO Wright-Patterson AFB, OH 45433	1
Wright-Patterson Air Force Base Attn: Charles R. Martel AFWAL/POSF Wright-Patterson AFB, OH 45433	1
FAA/NAFEC Attn: W. Westfield, ANA-310 Atlantic City, NJ 08405	1
United State Air Force Attn: Major John Slankas/AFESC/RDVC Tyndall Air Force Base, FL 32403	1

DISTRIBUTION LIST - Continued

II. OTHER GOVERNMENT AGENCIES	Copies
HQ AFSC/DL Andrews AFB, DC 20334	1
Naval Research Laboratory ATTN: Dr. Elaine Oran Code 4040 Washington, DC 20375	1
Office of Naval Research Attn: Dr. K. Ellingsworth 800 North Quency Arlington, VA 22217	1
National Bureau of Standards Attn: Dr. Robert S. Levine Center for Fire Research Washington, DC 20238	1

DISTRIBUTION LIST - Continued

III. UNIVERSITIES	Copies
Cornell University Attn: Prof. F. Gouldin Sibley School of Mechanical & Applied Engineering Upson & Grumman Halls Ithaca, NY 14850	1
Northwestern University Attn: Prof. C. K. Law Department of Mechanical Engineering & Astronautical Sciences Evanston, IL 60201	1
Pennsylvania State University Prof. G. M. Faeth Dept. of Mechanical Engineering 208 Mech. Eng. Bldg. University Park, PA 16802	1
Princeton University Attn: Prof. F. Bracco Dept. of Mechanical and Aerospace Engineering The Engineering Quadrangle Princeton, NJ 08544	1
Purdue University Attn: Prof. A. H. Lefebvre School of Mechanical Engineering West Lafayette, IN 47907	1
Department of Mechanical Engineering Attn: Prof. J. Odgers Laval University Quebec, CANADA Gik 7Pa	1
University of California Attn: Prof. R. F. Sawyer Department of Mechanical Engineering Berkeley, CA 94720	1
University of California Attn: Prof. G. Scott Samuelson Mechanical and Environmental Eng. Irvine, CA 92717	1
University of California - Berkeley Attn: Prof. A. K. Oppenheim Dept. of Mechanical Engineering Berkeley, CA 94720	1

DISTRIBUTION LIST - Continued

III. UNIVERSITIES	Copies
University of Illinois at Urbana-Champaign Attn: Prof. R. A. Strehlow Dept. of Aeronautical & Astronautical Engineering 101 Transportation Building Urbana, IL 61801	1
University of Michigan Attn: Prof. A. Nicholls Department of Aerospace Engineering Gas Dynamics Lab. North Campus Ann Arbor, MI 48105	1
Michigan State University Attn: Prof. J. F. Foss Dept. of Mechanical Engineering 201 Engineering Bldg. E. Lansing, MI 48824	1
University of Washington Attn: Prof. David Pratt Dept. of Mechanical Engineering Mail Stop FV-10 Seattle, WA 98125	1
Carnegie-Mellon University Attn: Prof. William Sirignano Department of Mechanical Engineering Pittsburgh, PA 15213	1
Case Western Reserve University Attn: Prof. Isaac Greber Department of Mechanical and Aerospace Eng. Cleveland, OH 44106	1
Case Western Reserve University Attn: Prof. J. T'ien Department of Mechanical and Aerospace Eng. Cleveland, OH 44106	1
Drexel University Attn: Prof. N. Cernansky Dept. of Mechanical Engineering and Mechanics Philadelphia, PA 19104	1

DISTRIBUTION LIST - Continued

III. UNIVERSITIES	Copies
California Institute of Technology Attn: Prof. Frank Marble Dept. of Mechanical Engineering 205-45 Pasadena, CA 91125	1
Oklahoma State University Attn: Prof. David Lilley Dept. of Mechanical and Aerospace Engineering Engineering North 218 Stillwater, OK 74074	1
Arizona State University Attn: Prof. R. So Dept. of Mechanical Engineering Tempe, AZ 85281	1
Stanford University Attn: Prof. R. Hanson Dept. of Mechanical Engineering Stanford, CA 94305	1
University of Connecticut Attn: Prof. John Bennett Department of Mechanical Engineering Storrs, CT 06268	1

IV. INDUSTRY

AVCO/Lycoming Division 1
Attn: Nicholas R. Marchionna
550 South Main Street
Stratford, CT 06497

AVCO/Lycoming Corp. 1
Attn: G. Opdyke
550 South Main Street
Stratford, CT 06497

AVCO Everett Research Labs 1
Attn: Dr. S. Piller
2385 Revere Beach Parkway
Everett, MA 02149

Allison GTO 1
Attn: J. Tomlinson
Speed Code T14
P.O. Box 420
Indianapolis, IN 46206-0420

AGTO 1
Attn: H. Mongia
Speed Code T14
P.O. Box 420
Indianapolis, IN 46202

AGTO Allison 1
Attn: S. Reider
Department 8882, Plant 8
Speed Code T14
P.O. Box 420
Indianapolis, IN 46206-0420

Exxon Research and Engineering Company 1
Attn: Dr. W. S. Blazowski
Government Research Laboratories
P.O. Box 8
Linden, NJ 07036

Electric Power Research Institute 1
Attn: L. E. Angello
Advanced Fossil Power Systems Dept.
3412 Hillview Avenue
P.O. Box 10412
Palo Alto, CA 94303

DISTRIBUTION LIST - Continued

IV. INDUSTRY	Copies
Garrett Turbine Engine Company A Division of the Garrett Corporation Attn: J. M. Haasis 111 So. 34th Street, P.O. Box 5217 Phoenix, AR 85010	1
Garrett Turbine Engine Company A Division of the Garrett Corporation Attn: Library 111 So. 34th Street, P.O. Box 5217 Phoenix, AR 85010	1
Garrett Turbine Engine Company A Division of the Garrett Corporation Attn: Dr. John Sanborn 111 So. 34th Street, P.O. Box 5217 Phoenix, AR 85010	1
General Electric Company Attn: D. Bahr K-64 Aircraft Engine Group Evendale, OH 45215	1
General Electric Company Attn: E. Ekstedt K-64 Aircraft Engine Group Evendale, OH 45215	1
General Electric Company Attn: T. Lyons, K-64 Aircraft Engine Group Evendale, OH 45215	1
General Electric Company Attn: Mr. J. Hoffman Main Combustor Design 1000 Western Avenue Lynn, MA 24067	1

DISTRIBUTION LIST - Continued

IV. INDUSTRY	Copies
General Electric Company Attn: Mr. Norman R. Dibelius Energy Systems & Technology Division Bldg. #53 Room 331 One River Road Schenectady, NY 12345	1
Dr. R. Mani, CB211 General Electric Research & Development Center P.O. Box 8 Schenectady, NY 12305	1
Solar Turbines Incorporated Attn: P. B. Roberts P.O. Box 80966 San Diego, CA 92138	1
Northern Research & Engineering Corp. Attn: Dr. George Smith 39 Olympia Avenue Woburn, MA 01801	1
Teledyne CAE Attn: Clifford L. Brackett 1330 Laskey Road P.O. Box 6971 Toledo, OH 43697	1
United Technologies Corporation Attn: H. Craig Pratt & Whitney Group Commercial Products Division 400 Main Street East Hartford, CT 06108	1
United Technologies Corporation Attn: R. Marshall Pratt & Whitney Group Commercial Products Division 400 Main Street East Hartford, CT 06108	1

DISTRIBUTION LIST - Continued

IV INDUSTRY	Copies
United Technologies Corporation Attn: I. Segalman Pratt & Whitney Group 400 Main Street East Hartford, CT 06108	1
United Technologies Corporation Attn: Dr. S. Mosier Pratt & Whitney Group Government Products Div. P.O. Box Z681 MS 713-43 West Palm Beach, FL 33402	1
United Technologies Corporation Attn: Mr. T. Dubell Pratt & Whitney Group Government Products Division Box 2691 West Palm Beach, FL 33402	1
United Technologies Research Center Attn: R. Pelmas Aero-Thermal Technology Silver Lane East Hartford, CT 06108	1
United Technologies Research Center Attn: M. Werle Aero-Thermal Technology Silver Lane East Hartford, CT 06108	1
United Technologies Research Center Attn: H. Couch Silver Lane East Hartford, CT 06108	1
Westinghouse Electric Corp. Attn: Mr. S. M. Decorso Combustion Turbine Systems Div. Mail Stop Lab 100 P.O. Box 251 Concordville, PA 19331	1
Westinghouse Electric Corp. Attn: Mr. Richard M. Chamberlain Research and Development Center Pittsburgh, PA 15235	1

DISTRIBUTION LIST - Continued

IV INDUSTRY	Copies
Williams International Corp. Attn: M. Bak 2280 West Maple Walled Lake, MI 48088	1
Mr. S. A. Lawton Research Scientist McDonnell Douglas Research Laboratories Box 516 St. Louis, MO 63166	1
Sandia Laboratories Attn: Dr. D. L. Hartley Combustion Sciences Department Livermore, CA 94055	1
General Electric Research & Development Lab. Attn: Dr. Robert G. Hantman P.O. Box 8, Bldg. K-1 Combustion Bldg. Schenectady, NY 12301	1
Mr. Henry McDonald Scientific Research Associates, Inc. P.O. Box 498 Glastonbury, CT 06033	1
Flow Research Company Attn: Dr. J. J. Riley 21414 - 68th Avenue, South Kent, WA 98031	1